*Center for Radiological Research – 630 W. 168th St., New York, NY 10032 – http://crr-cu.org*

# ANNUAL REPORT 2008


**David J. Brenner**
***Director***

**Howard B. Lieberman**
***Editor***

**Jinshuang Lu**
***Assistant Editor***

COLUMBIA UNIVERSITY

*College of Physicians and Surgeons*

# Table of Contents

# Collaborating Institutions

Individuals from the following institutions collaborated with the Center's faculty and staff in the research reports included in this year's publication (for individual attributions see specific reports):

*Collaborating Columbia University Departments:*

- College of Dental Medicine, Division of Oral & Maxillofacial Pathology
- Department of Biochemistry and Molecular Biophysics, Howard Hughes Medical Institute
- Department of Biomedical Engineering
- Department of Clinical Pathology
- Department of Environmental Health Sciences, Mailman School of Public Health
- Department of Mechanical Engineering
- Department of Obstetrics and Gynecology
- Department of Radiation Oncology
- Herbert Irving Comprehensive Cancer Center

*Collaborating Institutions:*

- Caritas St. Elizabeth's Medical Center, Tufts University School of Medicine, Boston, MA
- Department of Genetics and Complex Diseases Harvard School of Public Health, Boston, MA
- Departments of Mathematics and Physics, University of California, Berkeley, CA
- Department of Microtechnologies, Ecole Polytechnique de Lausanne, Switzerland
- Department of Radiation Oncology, The University of Texas Medical Branch, Galveston, TX
- Environmental and Radiological Health Sciences, Colorado State University, Fort Collins, CO
- Helmholtz Zentrum München - German Research Center for Environmental Health (GmbH), Neuherberg, Germany
- Institute for Advanced Research, Tarapaca University, Arica, Chile
- Laboratoire des lésions des Acides Nucléiques, LCIB (UMR-E 3 CEA-UJF), DRFMC CEA, Grenoble, France
- Laboratório de Citogenética e Mutagênese, Departa-mento de Genética, Faculdade de Medicina de Ribeirão Preto-USP, Brazil
- Medical College of Georgia, Institute of Molecular Medicine and Genetics, Augusta, GA
- National Institute of Radiological Sciences, Chiba, Japan
- National Laboratory of Biomacromolecules, Institute of Biophysics, Chinese Academy of Sciences, Beijing, China
- Nutritional Genomics and DNA Damage Diagnostics Laboratory, CSIRO Human Nutrition, Australia
- Physics and Life Sciences Directorate, LLNL, Livermore, CA
- School of Radiation Medicine and public health, Soochow University, Suzhou, China ■

# Acknowledgment of Support

In 2008 the Center for Radiological Research was supported by competitively awarded grants from the following agencies:

***State:***

- New York State Department of Health, Health Research Science Board

***Federal:***

- Department of Defense
  - Defense Threat Reduction Agency
- Department of Energy
  - Office of International Health Programs
  - Office of Science, Office of Biological and Environmental Research [Low Dose Radiation Research Program]
- Department of Health and Human Services
  - National Institutes of Health:
    - National Cancer Institute [Program Project (PO1) & Individual Research Grants (RO1s)]
    - National Center for Research Resources
    - National Institute of Biomedical Imaging and Bioengineering (P41)
    - National Institute of Allergy and Infectious Disease (U19)
    - National Institute of Environmental Health and Safety (RO1s)
    - National Institute of General Medical Sciences (RO1)
- National Aeronautics and Space Administration ■

# Web Sites

- **Center for Radiological Research** ..... **http://crr-cu.org**
- **Radiological Research Accelerator Facility** ..... **http://www.raraf.org**
- **Center for High-Throughput Minimally-Invasive Radiation Biodosimetry** ..... **http://www.cmcr.columbia.edu**
- **Mechanism of Bystander Effects** ..... **http://www.radiation-bystander.columbia.edu**
- **Web-Rad-Train** ..... **http://www.web-rad-train.org**
- **Department of Radiation Oncology** ..... **http://cpmcnet.columbia.edu/dept/radoncology**
- **Radiation Safety Office** ..... **http://rso.cumc.columbia.edu**

- **CRR Annual Reports *(1998–present)*** ..... **http://crr-cu.org/reports.htm**

# Introduction

This Introduction is intended to give the flavor of the recent directions of our Center for Radiological Research, and especially to give a brief overview of the principal research initiatives and academic activities.

Physically, the Center is in two locations, both at the Columbia University Medical Center, in Washington Heights, Manhattan and at our Radiological Research Accelerator Facility (RARAF) in Irvington, New York, 15 miles upstate.

As we have always been, we are very much a multidisciplinary center, and articles in this Annual Report cover the fields of radiation physics, radiation biology, molecular biology, radiation oncology and diagnostic radiology.

Broadly speaking the main areas of research within the center are:

- *Understanding and predicting the biological effects of low doses of ionizing radiation.*
- *High throughput biodosimetry for use after a large-scale radiological event.*
- *Using single-particle microbeams to investigate non-targeted phenomena such as the bystander effect and genomic instability.*
- *Defining the molecular mechanism by which radiation exposure caused DNA damage and mutagenesis that can lead to carcinogenesis.*
- *Research of relevance to radiotherapy, including the potential for hypofractionation in the treatment of prostate cancer, and the impact of new technologies on the incidence of radiation-induced second cancers.*
- *Research of relevance to diagnostic radiology, especially the radiological impact of the burgeoning use of techniques such as CT.*
- *The biological effect of the radiations encountered in space.*
- *Defining the mechanisms of other environmental carcinogens and their interactions with radiation at the molecular and tissue levels.*

One particular major milestone in 2008 was that one of our charged particle microbeams is now focused to a sub-micrometer target spot size.

Overall, the Center has 34 doctoral scientists, 17 technical support staff, 3 graduate students and 6 administrative staff. We are largely funded through research grants, and the CRR staffs together have a total of 27 grants, from the NIH, the DOE, NASA, and the DOD.

Our three biggest research grants support our Radiological Research Accelerator Facility (RARAF), our Columbia Center for High-Throughput Minimally-Invasive Radiation Biodosimetry, and our NCI Program Project grant on bystander responses.

Our parent department is the Department of Radiation Oncology, and we welcome the new Chairman, Dr. Clifford Chao, who brings a strong commitment to collaborative translational research. We have strong academic and teaching ties with the clinical department, which was cemented in the past year with the appointment of Dr. Tom Hei as the Vice-Chairman for Research in the Department of Radiation Oncology. In this role, he will foster closer ties between the clinical department and our Center.

The productivity of the Center continues at a high level, as evidenced by a steady stream of scientific papers in peer-reviewed high-profile journals, as well as continuing grant support. As described in the Staff News, members of the staff are regularly invited to participate in national and international meetings, and to serve as consultants and reviewers. We were particularly delighted that Eric Hall was awarded the Gold Medals of the American College of Radiology and the American Roentgen Ray Society.

The Center's teaching activities include radiation biology and radiation physics for undergraduates, medical students graduate students, and residents in Radiology and Radiation Oncology, as well as running a city-wide course for residents in Radiology.

As described elsewhere in this Report, our Center organized three major meetings in 2008:

- *Predicting Individual Radiation Sensitivity: Current and Evolving Technologies,*
- *Radiological Science in the Context of Radiological Terrorism,*
- *An International Symposium Celebrating the career of Eric Hall: "From Beans to Genes: A forty year odyssey in radiation biology".* ■


(L-r): Clifford Chao, Chair, Department of Radiation Oncology, Eric Hall (Former CRR Director), David Brenner (CRR Director), and Tom Hei (CRR Associate Director).

# Staff News

**Dr. David Brenner** has continued his work on the risk / benefit balance associated with radiological examinations. He was the G. William Morgan Lecturer on the Annual Health Physics Society Meeting in Pittsburgh, on this subject. He chaired the Organizing Committee of the International Workshop on "*Predicting Individual Radiation Sensitivity: Current and Evolving Technologies*", described elsewhere in this report. At the Annual NCRP meeting in Bethesda, he argued against the motion in a debate on the topic "*Does Scientific Evidence Support a Change from the LNT Model for Low-Dose Radiation Risk Extrapolation*?" He continues to Chair all three of the Columbia University Radiation Safety Committees.


At the 2008 NCRP Annual Meeting, and moderated by Eric Hall, David Brenner (right) debated Dietrich Averbeck of the Institute Curie, Paris, on the merits of a straight-line (linear) extrapolation of radiation-induced cancer risks to low doses.

**Dr. Tom Hei** has been appointed as the Vice-Chairman for Research in our parent department of Radiation Oncology to spearhead research training for clinical residents and to facilitate career development for junior faculty members. He has been appointed as the Deputy Director of the National Institute of Environmental Health Center in the Department of Environmental Health Sciences of the Mailman School of Public Health. He has been appointed the Distinguished Visiting Professor at the National Institute of Radiological Sciences in Chiba. In November 2008, he was honored by the Organization of Chinese Americans at a gala event and was presented with the Dynamic Achiever Award. His two Ph.D. students, Sarah Huang won the Best Poster Award at the International Mineral Fiber meeting in Cape Town in September, 2008 while Yunfei Chai was awarded Young Investigator to present his work at the Nagasaki University Center of Excellent Meeting in November, 2008.

Dr. Tom K. Hei, with his wife, after receiving the Dynamic Achievement Award in a gala event last November.

**Dr. Eric Hall** was awarded the Gold Medal of the American Roentgen Ray Society; the ARRS is the oldest radiological society in the United States. He also received the Gold Medal of the American College of Radiology. In 2008, Dr Eric Hall chaired the organizing committee of a workshop on "*Low Dose Epidemiology: What can it tell us?*", sponsored by the DOE Low Dose Program, and attended by scientists from Europe and Japan, as well as the United States. He has recently been appointed Operational Director of the the Columbia Kreitchman PET Center.

Dr. Eric Hall receiving the American College of Radiology Gold Medal at their 2008 meeting in Washington.

**Dr. Howard Lieberman** has been appointed Associate Editor of the Journal Radiation Research. He also has continued as an Ad Hoc reviewer for the NIH RTB Study Section.

**Dr. Sally Amundson** was awarded a grant from NASA to study "*HZE-induced mammary cancer development processes in murine and 'humanized' models, and their influence on radiation quality functions*." She gave the keynote address at the annual meeting of the Council on Ionizing Radiation Measurements and Standards (CIRMS). Her publication "*Integrating global gene expression and radiation survival parameters across the 60 cell lines of the National Cancer Institute Anticancer Drug Screen*" was featured on the cover of *Cancer Research.*

We will miss the staff members who have left the Center in the past year, for new adventures in new places, and we wish them all the very best:

Dr. Michael Partridge, Associate Research Scientist in Dr. Hei's lab, left the center for a position in pharmaceutical company. His good cheer and team spirit will be much missed. Dr. Chuanxin Huang, Post-Doctoral Research Scientist in Dr.Yin's lab, left the Center for new position elsewhere. Anne Sutthoff, the Administrator of our CMCR program since its inception, left the center to return to Europe. Ms. Marisol Cruz, who was our highly efficient Administrative Clerk, has left for a new position in Columbia University. Also leaving in 2008 were Staff Associates Jing Nie and Ling Han, and Technicians Jennifer Maerki and Bharat Patel.

The Center is delighted to welcome several new members: Three new Post-Doctoral Research Scientists joined us in 2008. They are: Dr. Antonella Bertucci in Dr. David Brenner's group, Dr. Thomas Templin in Dr. Smilenov's lab, and Dr. Ping Lu in Dr. Zhao's lab. In addition, Bo Shen, Tingting Gu and Ying Kong joined the Center as Staff Associates during 2008. Finally, the Center welcomes Ms. Lilian Oling as our CMCR Project Manager, and welcomes back Annerys Rodriguez as the CMCR Bookkeeper. ■

# Columbia Colloquium and Laboratory Seminars

At regular intervals during the year the Center for Radiological Research is pleased to welcome accomplished specialists from around the world to present formal seminars and/or spend time discussing ongoing research.

The seminars are attended by Center and RARAF professional staff, senior technical staff and graduate students, as well as doctors and scientists from other departments of the College of Physicians & Surgeons interested in collaborative research. Attention has focused on recent findings and future plans, with special emphasis on the interdisciplinary nature of our research effort.

The 2008 sessions included the following guest speakers (listed alphabetically):

- Dr. David A. Boothman, Ph.D., Professor in Oncology, Pharmacology and Radiation Oncology, University of Texas Southwestern Medical School: "Regulation of IGF-1-sCLU and Implications for Warburg Theory, Aging, and Cancer."
- Dr. Richard Britten, Ph.D., Associate Professor of Radiation Oncology, Eastern Virginia Medical School: "The Use of Proteomic Profiling to Assess Individual Susceptibility to Radiation-Induced Cognitive Impairment."
- Professor Clifford Chao, Chairman of Department of Radiation Oncology, College of Physicians & Surgeons, Columbia University: "Advances in Image-Guided Radiotherapy."
- Dr. Junjie Chen, Ph.D., Professor, Department of Therapeutic Radiology, Yale University School of Medicine: "DNA Damage Checkpoints and Tumorigenesis."
- Dr. Michael Fenech, Ph.D., Commonwealth Scientific and Industrial Research Organisation (CSIRO), Adelaide, South Australia, Australia: "Cytokinesis-Block and Buccal Micronucleus Cytome Assay."
- Dr. Sundeep Kalantry, Ph.D., Department of Genetics, University of North Carolina, School of Medicine: "Deconstructing Imprinted Mouse X-chromosome Inactivation."
- Dr. Toru Ouchi, Ph.D., Department of Medicine, Feinberg School of Medicine, Northwestern University: "DNA Stress Pathways and Mammary Carcinogenesis."
- Professor Regina Santella, Department of Environmental Health Sciences, Mailman School of Public Health, Columbia University: "Biomarkers of Oxidative Stress, DNA Repair and Methylation in Studies of Breast and Liver Cancer Risk."
- Dr. Gloria Su, Department of Otolaryngology / Head and Neck Surgery, Columbia University: "From Human Cancer Genetics to Mouse Modeling for Pancreatic Cancer."
- Anne L. Taylor, M.D., Vice Dean for Academic Affairs, College of Physicians & Surgeons, Columbia University Medical Center: "Mentoring for Faculty Success."
- Dr. Angela J. Yoon, College of Dental Medicine, Columbia University: "Exfoliative Oral Cell Based Cytogenetic Biodosimetry for Ionizing Radiation Exposure."
- Dr. Lydia B. Zablotska, Department of Epidemiology, Mailman School of Public Health, Columbia University: "Risk of Leukemia after Protracted Exposure to Low Doses of Ionizing Radiation: Scientific Research and Lessons Learned Twenty-One Years after Chernobyl."

Seminars were also conducted by professionals from our own Center staff:

- Dr. Adayabalam S. Balajee: "Role of Histone H2AX in Genomic Integrity: DSB Repair and More."
- Dr. Antonella Bertucci: "Small Animal Microbeam Facility at RARAF."
- Dr. Alan Bigelow: "Multiphoton Microscopy on a Microbeam Endstation."
- Yunfei Chai: "Study of radiation induced bystander effects *in vivo* using the *gpt* delta transgenic mouse model."
- Dr. Guy Garty: "A day in the life of a RABIT: the Rapid Automated Biodosimetry Imaging Tool."
- Dr. Peter Grabham: "Non-Cancer Effects of Space Radiation on 3D Vessel Models."
- Professor Tom K. Hei: "The Ying and the Yang of Low Dose Radiobiology."
- Professor Howard B. Lieberman: "Role of Rad9 in Prostate Cancer."
- Dr. Gerhard Randers-Pehrson: "Sub-micron Ion Beam at RARAF."
- Dr. Lubomir Smilenov: "Some Evidence on the Role of miRNA in Radiation Response." ■

# Center for Radiological Research Organized Meetings

## Predicting Individual Radiation Sensitivity: Current and Evolving Technologies

**Columbia University, New York, NY, March 17-18, 2008**

In 2005, the National Institute of Allergy and Infectious Diseases (NIAID) established a Radiation/Nuclear Program to develop radio-protectors, mitigators and therapeutic agents to facilitate an effective medical response against radiological and nuclear threats. This program also supports development of biomarker/biodosimetry techniques and devices for rapid triage and treatment of radiation-exposed individuals after any radiological event.

In support of this program, NIAID and the Center for Radiological Research jointly organized an International Workshop entitled, "Predicting Individual Radiation Sensitivity: Current and Evolving Technologies." The meeting was held at the Columbia University in New York on March 17-18, 2008, attended by 86 participants from 8 countries, and the proceedings were published in Radiation Research (*Rad. Res*. 170, 666–675, 2008).

The background to the Workshop relates to the need for mass biodosimetry and mitigation / therapy after a large-scale radiological event, both in regard to short-term sequelae, and also in terms of long-term endpoints such as carcinogenesis and heart disease. While retrospective dose estimates provide information about average risks, it is known from higher-dose radiotherapy studies that there is considerable person-to person variability in response to a given radiation dose. Thus the goals of this Workshop were to assess the significance of inter-individual radiation sensitivity in terms of the aftermath of a large-scale radiological event, and to assess whether the approaches used at clinical doses can be translated to lower doses, or whether different approaches will be needed.

Session themes were:

- Individual Radiation Sensitivity in the Context of Radiological Emergencies
- Candidate Genes for Radiosensitivity
- Genome-wide Approaches
- Bioinformatics
- Future Developments ■

## Radiological Science in the Context of Radiological Terrorism

**University of California, San Francisco, October 28, 2008**

This year, as a part of our goal to provide regularly scheduled courses entitled *Radiological Science in the Context of Radiological Terrorism* in a variety of locations, we held the fifth training course at the University of California, San Francisco on October 28. Registration was free, and CME accreditation was available to qualified students, sponsored by Columbia University Medical Center. The one-day course was attended by over 80 physicians, nurses, paramedics, hospital administrators, medical and health physicists, graduate students, and science communicators.

The training course covers a broad spectrum of topics to help participants understand 1) the nature of ionizing radiation; 2) how radiation is damaging to people; 3) how we know what we know about radiation risks; 4) potential radiological terrorist scenarios; and 5) emergency preparedness for a radiological event. We designed the course to serve as an introduction to the biological hazards of ionizing radiation, particularly in the context of radiological terrorism issues. The course is designed around a series of lectures with a question and answer session after each speaker. As an example, the faculty and topics for the most recent course were:

| | |
|---|---|
| **The nature of radiological terrorism**<br>Described a) the physical nature of radiation and b) the various possible scenarios, including "dirty bombs" that may be involved in a radiological incident. | **David Brenner**<br>Columbia University |
| **Basics of Radiation Biology**<br>This topic discussed the types of damage induced in DNA and other cellular compartments by ionizing radiation, how cells process this damage, and how to detect this resulting damage. | **Sally Amundson**<br>Columbia University |
| **Acute Somatic Effects of Radiation**<br>This topic described radiation-induced damage to the blood forming organs and gastrointestinal tract that can lead to serious injury or death at sufficiently high doses. | **John Little**<br>Harvard University |
| **Radiation Epidemiology**<br>This topic surveyed the information on radiation-induced cancer in human populations from high and low doses and described techniques to obtain risk estimates for radiation-induced cancer from population studies. | **Elaine Ron**<br>NCI |
| **Long-term Radiation Effects**<br>This topic discussed the long-term effects of radiation. Effects discussed included carcinogenesis, hereditary effects, cataractogenesis, and consequences to the developing embryo and fetus. | **Eric Hall**<br>Columbia University |
| **Anticipated Psychological Impact of Radiological Terrorism**<br>Psychological trauma is one of the greatest risk for individuals in a "dirty bomb" scenario. This topic highlighted the symptoms and treatment modalities in the context of a radiological terrorism event. | **Kathleen Ayers**<br>Uniformed Services University |
| **Emergency Preparedness**<br>This topic addressed the general aspects of preparedness for unexpected emergencies based on the "all-hazards" approach. The relationship between healthcare providers and public health, planning considerations, inter-organizational relationships, and the concept of incident command/incident management were discussed. | **Stephen Morse**<br>Columbia University |

## An International Symposium in honor of Professor Eric J. Hall: "From Beans to Genes: A Forty Year Odyssey in Radiation Biology"

**Columbia University, New York, October 13-14, 2008**

A major event for the Center for Radiological Research in 2008 was the Symposium honoring professor Eric Hall, celebrating his 25 years of leadership as Director of the Center, and his career of more than 50 years in Radiation Research. Organized by Drs Brenner and Hei, more than 120 colleagues and former students from around the world gathered at Columbia for two days in October, to participate in a series of scientific talks by leading proponents from the field, and to enjoy a Gala Dinner held in the Low Library Rotunda of Columbia University. The occasion was sponsored by the US Department of Energy Low Dose Program, NASA Space Radiation Program, Lippincott, Williams and Wilkins as well as by the Center for Radiological Research of Columbia University.

Session themes were:

- Tumor Hypoxia and Radiosensitizers
- Modulating Factors in Low Dose Radiation Response
- Radiobiology in the practice of Radiation Oncology
- Radiation Hazard in Space and genetic Predisposition to Cancer ■

# Faculty and Staff

***Faculty:***

**DAVID J. BRENNER**, Ph.D., D.Sc.
— ***Director***
— ***RARAF Director***
Higgins Professor of Radiation Biophysics
Professor of Radiation Oncology
Professor of Environmental Health Science
Chairman, Joint Radiation Safety Committee
Chairman, Radioactive Drug Research Committee

**TOM K. HEI**, Ph.D.
— ***Vice-Chairman, Dept. of Radiation Oncology***
— ***Associate Director***
Professor of Radiation Oncology
Professor of Environmental Health Sciences

**ERIC J. HALL**, D.Phil., D.Sc., FACR, FRCR, FASTRO
Higgins Professor of Radiation Biophysics
Professor of Radiology and Radiation Oncology

**CHARLES R. GEARD**, Ph.D.
Professor of Clinical Radiation Oncology

**HOWARD B. LIEBERMAN**, Ph.D.
Professor of Radiation Oncology
Professor of Environmental Health Sciences

**SALLY A. AMUNDSON**, Sc.D.
Associate Professor of Radiation Oncology

**YUXIN YIN**, M.D., Ph.D.
Associate Professor of Radiation Oncology

**LUBOMIR SMILENOV**, Ph.D.
Assistant Professor of Radiation Oncology

**YONGLIANG ZHAO**, Ph.D.
Assistant Professor of Radiation Oncology

***Research Staff:***

**GERHARD RANDERS-PEHRSON**, Ph.D.
Senior Research Scientist

**ADAYABALAM BALAJEE**, Ph.D.
Research Scientist

**VLADIMIR IVANOV**, Ph.D.
Research Scientist

**HONGNING ZHOU**, M.D.
Research Scientist

**ALAN BIGELOW**, Ph.D.
Associate Research Scientist

**GLORIA CALAF**, Ph.D.
Adj. Associate Research Scientist

**GUY GARTY**, Ph.D.
Associate Research Scientist

**PETER GRABHAM**, Ph.D.
Associate Research Scientist

**CORINNE LELOUP**, Ph.D.
Associate Research Scientist

**ALEXANDRE MEZENTSEV,** Ph.D.
Associate Research Scientist

**MICHAEL PARTRIDGE**, Ph.D.
Associate Research Scientist

**SUNIRMAL PAUL**, Ph.D.
Associate Research Scientist

**BRIAN PONNAIYA**, Ph.D.
Associate Research Scientist

**HELEN TURNER,** Ph.D.
Associate Research Scientist

**CARL ELLISTON**, M.S.
Senior Staff Associate

**KEVIN M. HOPKINS**, M.S.
Senior Staff Associate

**STEPHEN A. MARINO**, M.S.
Senior Staff Associate

**AIPING ZHU**, M.D.
Senior Staff Associate

**JING NIE**, B.S.
Staff Associate

**JINSHUANG LU**, M.S.
Junior Programmer

***Post-Doctoral Research Scientists:***

**ANTONELLA BERTUCCI**, Ph.D.
**SHANAZ GHANDHI**, Ph.D.
**ANDREW HARKEN,** Ph.D.
**MEI HONG,** Ph.D.
**BURONG HU**, Ph.D.
**CHUANXIN HUANG**, Ph.D.
**ALEXANDER KOFMAN**, Ph.D.
**PING LU**, Ph.D.
**JARAH MEADOR**, Ph.D.
**WENHONG SHEN,** Ph.D.
**THOMAS TEMPLIN**, Ph.D.
**GENYUN WEN**, Ph.D.
**YANPING XU**, Ph.D.

***Visiting Research Scientists:***

**LING HAN**, M.D.
**BO SHEN**, Ph.D.

***Design & Instrument Shop:***

**GARY W. JOHNSON**, A.A.S., Senior Staff Associate
— ***Design & Instrument Shop Director***
**DAVID CUNIBERTI**, B.A., Instrument Maker
**DENNIS KEAVENEY**, Instrument Maker
**ROBERT C. MORTON**, Instrument Maker

***Technical Staff:***

**XIAOJIAN WANG**, M.S., Research Worker
**JENNIFER MAERKI** B.S., Technician B
**BHARAT PATEL** B.S., Technician B
**BENJAMIN YAGHOUBIAN** B.S., Technician B
**CUI-XIA KUAN**, Technical Assistant

***Administrative & Secretarial Staff:***

**MONIQUE REY**, B.A., Center Administrator
**LILIAN OLING**, M.A., Project Manager
**MARGARET ZHU**, M.A., Business Manager
**YVETTE ACEVEDO**, Administrative Assistant
**ANGELA LUGO**, Junior Accountant
**ANNERYS RODRIGUEZ**, Bookkeeper

# Faculty and Staff


*Front row* (*l-r*): Dr. Gerhard Randers-Pehrson, Dr. Sally Amundson, Dr. Charles Geard, Dr. Tom Hei, Dr. David Brenner, Dr. Eric Hall, Dr. Howard Lieberman, Ms. Monique Rey.

*2nd row*: Mr. Gary Johnson, Dr. Wenhong Shen, Mr. Yunfei Chai, Ms. Sarah Huang, Mrs. Cui-Xia Kuan, Ms. Suping Zhang, Ms. Tingting Gu, Dr. Corinne Leloup, Ms. Lilian Oling, Dr. Bo Shen, Dr. Aiping Zhu, Dr. Jarah Meador, Ms. Sasha Lyulko, Ms. Margaret Zhu, Ms. Angela Lugo, Dr. Antonella Bertucci.

*3rd row*: Dr. Peter Grabham, Ms. Jinshuang Lu, Dr. Guy Garty, Dr. Ping Lu, Dr. Vladmir Ivanov.

*4th row*: Dr. Mei Hong, Mr. David Cuniberti, Dr. Sunirmal Paul, Dr. Hongning Zhou, Ms. Xiaojian Wang, Dr. Alexandre Mezentsev, Dr. Shanaz Ghandhi, Dr. Alan Bigelow, Ms. Yvette Acevedo, Mr. Dennis Keaveney.

*Back row*: Dr. Yongliang Zhao, Mr. Ying Kong, Mr. Stephen Marino, Dr. Lubomir Smilenov, Mr. Kevin Hopkins, Dr. Thomas Templin, Dr. Igor Shuryak, Dr. Andrew Harken, Mr. Robert Morton.

*Not pictured*: Dr. Yuxin Yin, Dr. Adayabalam Balajee, Dr. Gloria Calaf, Dr. Helen Turner, Dr. Brian Ponnaiya, Dr. Gengyun Wen, Dr. Yanping Xu, Dr. Alexander Kofman, Mr. Carl Elliston, Mr. Benjamin Yaghoubian.

# Under-Dish Detector for the Microbeam at Columbia University

*Guy Garty, Andrew D. Harken, Gerhard Randers-Pehrson and David J. Brenner*

## Introduction

Currently the RARAF microbeam irradiator delivers a precise number of particles by irradiating the sample and counting the particles traversing it, using a gas-based ionization chamber placed immediately above the cells. This method was found to be inadequate for the thicker samples (either tissue or medium-covered cells) now required by RARAF users, where the projectile particles are fully absorbed and do not reach the gas counter. To alleviate this problem we need to be able to detect the irradiating particles **before** they enter the sample.

For this reason, we are developing an upstream particle detector, termed LD$^2$ (Lumped Delay Line Detector). The LD$^2$ does not scatter particles at all, and can thus be used in sub-micron irradiations.

## LD$^2$ structure

The LD$^2$ detector, shown schematically in Figure 1, consists of a 1 meter long string of 250 cylindrical pickup electrodes. Each projectile particle passing through a pickup electrode induces a mirror charge, identical in magnitude and opposite in polarity to its own, on the inside of each pickup electrode[1]. The electrodes are connected by surface mount inductors and capacitively coupled to a ground electrode, forming a lumped delay line with a time constant that can be matched to the velocity of the projectile, by tuning the capacitor values. As all capacitors need to have the same value, while maintaining a tuning range of 40% (allowing tuning for 5-10 MeV He ions), we have decided to build the LD$^2$ as a string of pickup electrodes embedded in a dielectric, capacitively coupled to a movable ground electrode, extending its entire length.

The structure of the LD$^2$ is shown in Figure 2. The ground electrode pivots around the dielectric giving a 40% variation in capacitance. This was seen both in finite element analysis simulations and in measurements (Fig. 3b).

We built and tested two short LD$^2$ prototypes using Rexolite and Macor as the dielectric and using 50 electrodes connected by 100 nH inductors.

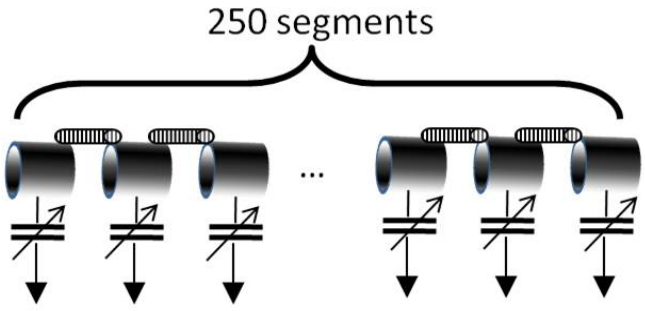


**Fig. 1.** Schematic layout of the LD$^2$. See text for details.

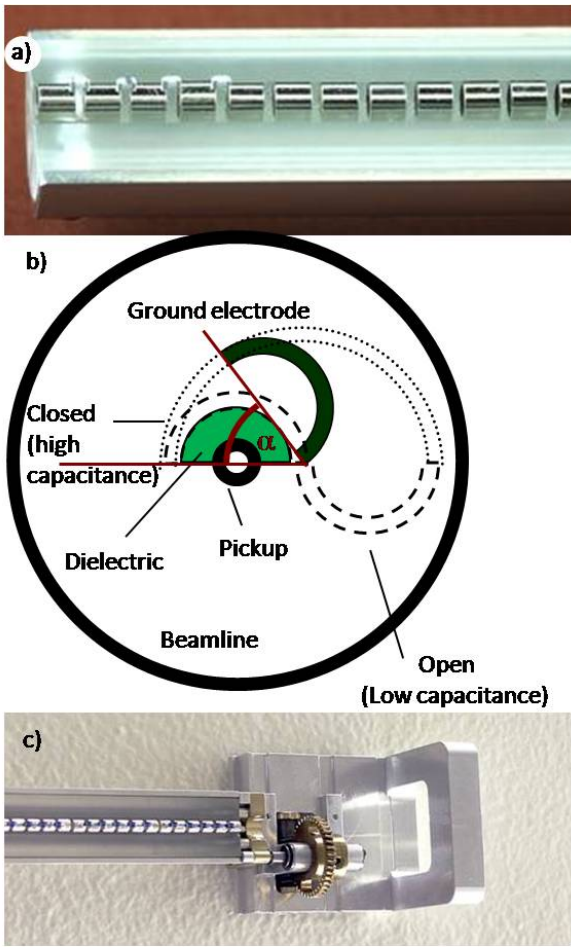


**Fig. 2. a)** A close-up photo of the final LD$^2$ prototype. **b)** A sketch of the tuning mechanism. A grounded electrode is pivoted between the closed position (high capacitance – low speed) and the open position (low capacitance – high speed). **c)** Photo of the tuning mechanism.

The propagation times were measured in both prototypes in the open and closed configurations (Fig. 3a). We have seen that both prototypes have roughly the same ratio of pulse propagation velocity in the open and closed configurations (1.4 for the Rexolite and 1.45 for the Macor) and so decided to make the full length LD$^2$ out of Rexolite, to simplify production efforts. Furthermore, we have measured the angular dependence of the pulse propagation time in the Rexolite prototype and compared with that obtained from finite element analysis, using Ansys. Figure 3b shows the good agreement between the measurements and simulations. Based on the results of these tests we

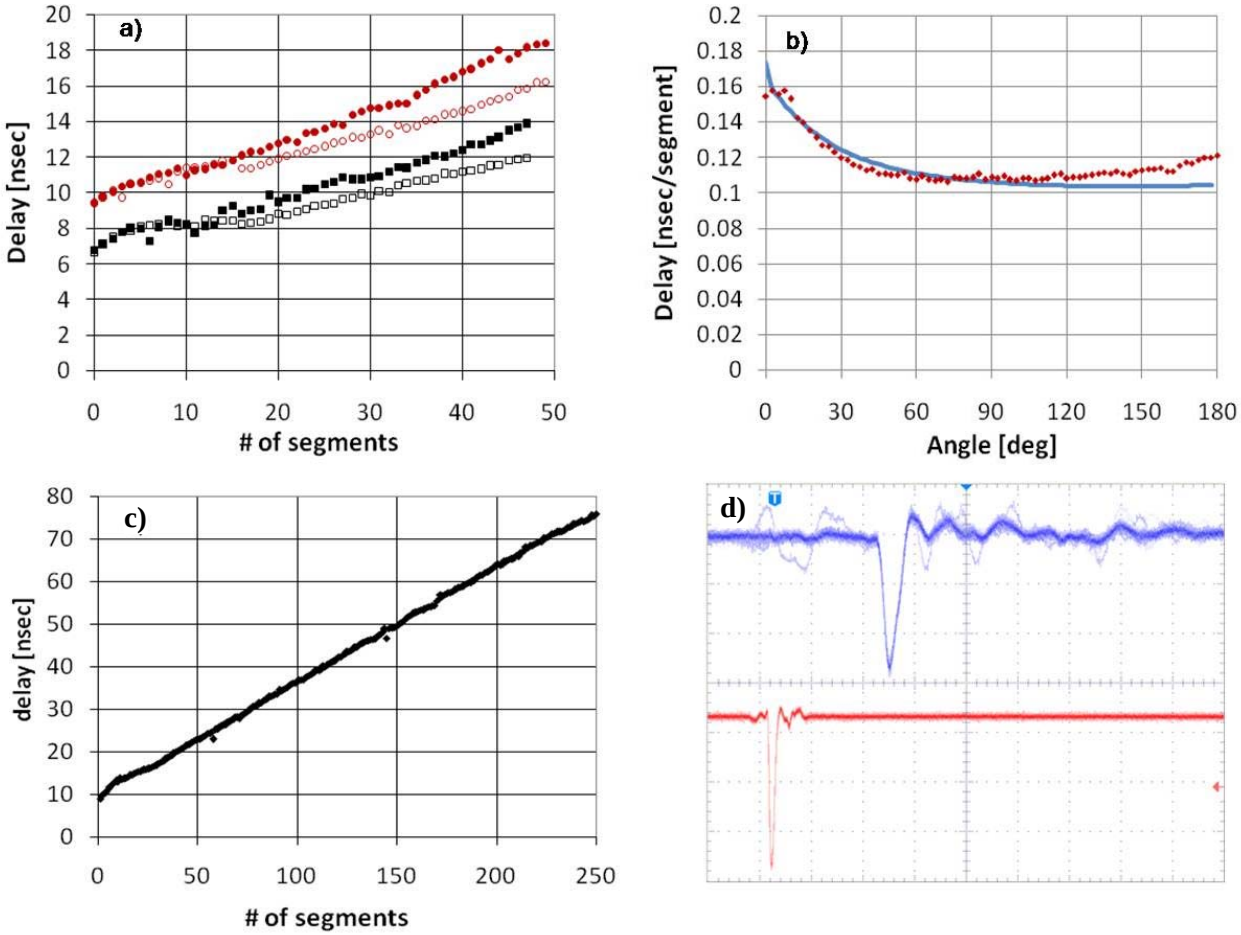


**Fig. 3.** The measured pulse propagation times. **a)** as a function of segment number for the two short prototypes. The black squares correspond to the Rexolite prototype; the red circles correspond to the Macor prototype. The open and closed symbols correspond to the open and closed configurations respectively. **b)** as a function of the pivot angle in the short rexolite prototype. The symbols are measurements, the line is simulation. **c)** In the full length LD$^2$. This pulse propagation velocity corresponds to 4.6 MeV He$^{++}$. **d)** sample pulses in the full length LD$^2$. The bottom waveform was injected into the first element of the LD$^2$, the top waveform was read off the last element. The time scale is 40 nsec/division.

elected to build the LD$^2$ from Rexolite and to use 330nH inductors providing velocity matching to protons of 1.2- 2.3 MeV and Helium ions of 4.6-9 MeV.

Figure 3c shows the pulse delay as a function of the number of segments in the full length LD$^2$. This corresponds to a pulse propagation velocity of $1.5 \times 10^7$ m/sec, corresponding to 4.6 MeV helium nuclei. Figure 3d shows sample pulses, generated by a pocket pulser (Phillips) on the first element of the LD$^2$.

**Noise in the LD$^2$**

Currently the LD$^2$ is mounted on one of the RARAF beam lines where it, and its associated electronics, are undergoing testing and calibrations using a collimated He$^{++}$ ion beam. Since the signal obtained from the LD$^2$ is predicted to be small (250 electrons), we have developed a custom preamplifier based on an A250 preamplifier (Amptek). The A250 features a minimal noise of significantly less than 200 electrons when coupled to a 2SK152 input FET (Field Effect Transistor). To further minimize noise, we have physically mounted the input FET and feedback components on the LD$^2$.

Although our preliminary modeling had indicated that we would have an acceptable signal to noise ratio,[2] our measurements show that we are currently not sensitive enough to reliably see our detection signal above the intrinsic noise levels in the system. Our next logical step is to use a liquid-nitrogen cooled HEMT (high electron mobility transistor)[3] as our input FET, which will significantly reduce the thermal noise from the signal acquisition electronics.

We are also currently planning tests of the LD$^2$ using a pulsed ion beam at the Edwards Accelerator laboratory at Ohio University. The use of a pulsed beam allows simulating particles, having the correct propagation velocity but very high (>1000) charge state. At such high charge states we are guaranteed to see signals high above the noise level, which will allow better diagnostics of the LD$^2$.

**References**

1. Weinheimer AJ. The charge induced on a conducting cylinder by a point charge and its application to the measurement of charge on precipitation. *J Atmos.*

*Ocean. Tech.* **5**:298-304, 1988.
2. Tuinenga PW. *SPICE: a guide to circuit simulation and analysis using PSpice.* (Prentice Hall, Englewood Cliffs, N.J., 1995).
3. Pospiezalski MW, Weinreb S, Norrod RD and Harris R. FETs and HEMTs at cryogenic temperatures-their properties and use in low-noise amplifiers. *IEEE T Microw Theory* **36**:552-60, 1988. ■

# The Permanent Magnet Microbeam At Columbia University

*Guy Garty, Andrew D. Harken, Yanping Xu, Gerhard Randers-Pehrson and David J. Brenner*

## Introduction

The permanent magnet microbeam (PMM), at RARAF,[1-4] presents an alternative approach to microbeam design. Instead of focusing the ion beam using electromagnetic or electrostatic lenses, this system uses permanent magnets, which require no power supplies or water cooling and yet provides comparable if not better optical properties.[2]

## PMM Layout

The layout of the PMM is shown in Figure 1:

$^4$He ions from the accelerator are focused using a compound magnetic lens consisting of two quadrupole triplets. The first triplet is placed 2m above the object aperture, with a second (identical) triplet placed 2m above the focal plane of the first. Each triplet consists of 3 sets of 4 permanent magnets on micrometric screws. The magnets can be extended or retracted in a steel yoke, forming an adjustable quadrupole.[5] Since each triplet does not have identical demagnifications in the x and y axes, the two lenses are rotated by 90° in the x-y plane so that a circular beam spot is obtained (Russian Symmetry).

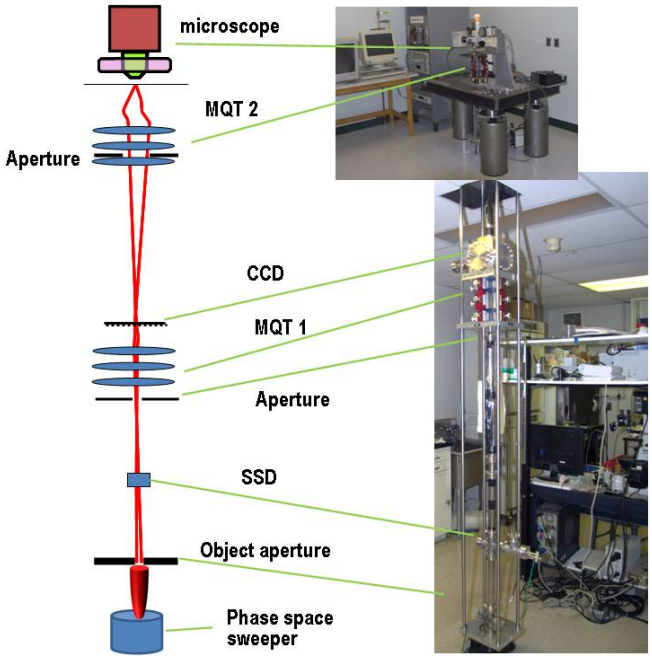


**Fig. 1.** A scheme (left) and photos (right) of the PMM. See text for details. The two red lines are theoretical predictions of the beam profile in the X and Y directions.

Limiting apertures are placed before the first triplet and inside the second triplet to reject ions which have very large aberrations.

In order to homogenize the beam, preventing spot size instability due to beam fluctuations, the object aperture was initially covered with a 1.8µm Al scattering foil. The foil had been removed and a magnetic phase space sweeper has been installed just before the object aperture. The phase space sweeper traces the beam in a Lissajous figure over the area of the first limiting aperture just below the first triplet. By directing the beam through all possible transmission angles through the object aperture, the object appears to the focusing system to be an isotropic source.

The cells to be irradiated are placed at the image plane of the compound lens. The PMM is mounted on the original microbeam endstation consisting of a microscope with a particle detector mounted on one of the objective lenses and a stepping motor stage. Details of the microbeam end-station are given elsewhere.[6, 7]

## Beam Tests

At the end of 2007, we had obtained a spot size of approximately 8µm in diameter (a demagnification of x60, compared to the theoretically attainable x100).[8]

Following intensive Monte Carlo calculations of the beam transport through the MQTs, we have found that our theoretical limit of an 8µm diameter beam comes from the large acceptance of the MQTs. By reducing the aperture below MQT1, we reduce the theoretical limit to 3.5µm diameter. With the new limiting aperture (0.3mm in diameter) and some minor adjustments to the tuning of the focusing magnets, the beam spot has reached a focused spot size guaranteed 5µm diameter or less.

Due to the use of a permanent magnet lens, the PMM requires no daily tuning and indeed we have seen that the spot size reproduces from day to day, provided that the beam energy is maintained to within 4 keV.

The PMM endstation, consisting of an XY stepping

motor stage, a fluorescence microscope, with a particle detector mounted on one of the objective lenses and all required electronics, has been reassembled and tested and the PMM is currently ready to take its place as a second microbeam irradiator at RARAF.

### References


1. Garty G, Ross GJ, Bigelow AW, Randers-Pehrson G and Brenner DJ. Testing the stand-alone microbeam at Columbia University. *Radiat Prot Dosimetry* **122**:292-6, 2006.
2. Ross GJ, Garty G, Randers-Pehrson G and Brenner DJ. A single-particle/single-cell microbeam based on an isotopic alpha source. *Nuclear Instruments & Methods in Physics Research Section B-Beam Interactions with Materials and Atoms* **231**: 207-11, 2005.
3. Garty G, Ross GJ, Bigelow AW, Schettino G, Randers-Pehrson G and Brenner DJ. Status of the Stand-Alone Microbeam at Columbia University. *Radiation Research* **166**: 656, 2006.
4. Garty G, Ross GJ, Bigelow AW, Schettino G, Randers-Pehrson G and Brenner DJ. Tuning the Stand-Alone Microbeam at Columbia University. *CRR Annual Report* 10-11, 2005.
5. Gottschalk SC, Dowell DH and Quimby DC. Permanent magnet systems for free-electron lasers. *Nuclear Instruments and Methods in Physics Research Section A: Accelerators, Spectrometers, Detectors and Associated Equipment* **507**: 181-5, 2003.
6. Bigelow AW, Ross GJ, Randers-Pehrson G and Brenner DJ. The Columbia University microbeam II endstation for cell imaging and irradiation. *Nuclear Instruments & Methods in Physics Research Section B-Beam Interactions with Materials and Atoms* **231**: 202-6, 2005.
7. Randers-Pehrson G, Geard CR, Johnson G, Elliston CD and Brenner DJ. The Columbia University single-ion microbeam. *Radiat Res* **156**:210-4, 2001.
8. Garty G, Harken A, Randers-Pehrson G and Brenner DJ. The Permanent Magnet Microbeam at Columbia University. *CRR Annual Report* 10-11. 2007. ■


# Application for the Microbeam-Integrated Multiphoton Imaging System at RARAF

*Alan W. Bigelow, Charles R. Geard, Gerhard Randers-Pehrson and David J. Brenner*

RARAF microbeam[1] users are increasingly employing 3-D tissue samples and small organisms.[2] To image their 3-D samples, our users require the multiphoton microscope[3] that we developed and fully integrated into our main electrostatic-lens Microbeam II endstation at RARAF. A custom-design for the multiphoton microscope was necessary, given the geometrical constraints of the pre-existing microscope fitted at the terminus of the vertical ion beamline. Intended for detecting and observing short-term molecular kinetics of radiation responses in living tissue and in cell-culture samples, the multiphoton microscope at RARAF is the first of its kind to be assembled and implemented onto a microbeam cell-irradiation platform.

### Image Acquisition

Image acquisition in laser-scanning microscopy relies on correlating the laser multiphoton excitation position with the photon yield from the sample. Light emitted from the specimen enters the microscope objective vertically and is reflected laterally by a dichroic element mounted in a specially-designed filter cube. This deflected signal then enters a custom-built, light-tight photomultiplier tube (PMT) housing shown in Figure 1, where an additional dichroic mirror assigns signal towards one of two H5783 PMTs, each followed by a C7319 preamplifier unit (Hamamatsu, Japan). An emission filter placed before each PMT designates the wavelength range of detected signal. For samples with multiple fluorophores, color images can be produced using appropriate dichroic mirrors and emission filters. Two potentiometers mounted to the side of the PMT housing provide independent signal gain control.

The resolution of raw, multiphoton microscopy images is limited by the size of the point spread function (PSF) of the

**Fig. 1.** Fluorescent signal detector housing attachment.

illuminating laser beam.[3] To remove the out-of-focus haze introduced by the PSF in 3D image stacks, we have acquired AutoQuant deconvolution software, which applies a computational technique for debluring images.

**Laser Upgrade**

Our collaborators often use red fluorescent protein (RFP). However, the original Ti:S laser on our multiphoton microscope did not produce the wavelengths needed for RFP excitation. Following up with user requests, we purchased and installed a laser upgrade (Chameleon Ultra II), which covers a wavelength range of 680-1080 nm. At this new laser's focal point, the two-photon process effectively provides (340-540 nm), enabling us to excite RFP.

**User Applications of the Microbeam-Integrated Multi-photon Imaging System**

The system is now fully operational, and some brief descriptions of its current uses follow below:

**1. Particle-Induced Foci Formation**

One of our collaborators (David Chen, University of Texas Southwestern, Dallas, TX) is using the microbeam to examine particle-induced single strand breaks in DNA within single cells. They are using human HT1080 fibrosarcoma cells that have been transfected with a GFP-tagged XRCC1 DNA single-strand break repair protein. Figure 2 shows multiphoton images of one cell (a) before irradiation and (b) 4 minutes after exposure to 400 3-MeV alpha particles at a predetermined position within a cell nucleus. Four minutes after irradiation, the region of enhanced GFP signal corresponds to the XRCC1 focus and the irradiation position. In this example, ion-beam targeting was deliberate to avoid areas deficient in GFP (likely nucleoli). This clear response demonstrates that the multiphoton microscope was successful at recording high-resolution, time-lapse images of particle-induced focus formation within a single cell in real time. As an additional capability, projections of 3D z-stacks can quantify focus track volume to correlate with the amount of radiation (number of particles) delivered to the cell nucleus.

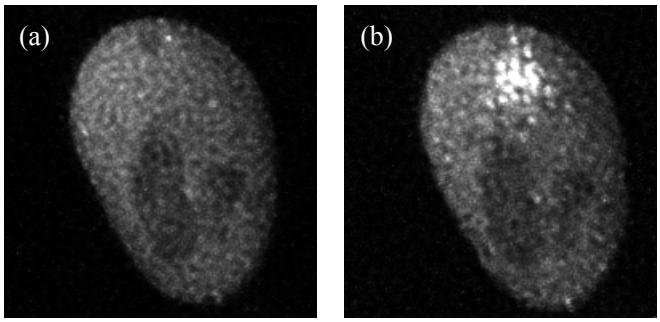


**Fig. 2.** Multiphoton microscopy images of a HT1080 cell nucleus with GFP-tagged XRCC1 **(a)** prior to irradiation and **(b)** 4 minutes after microbeam exposure to 400 alpha particles with energy 3 MeV. The ion beam diameter was nominally 2 microns. These views are max projections with intensity normalization after deconvolution using the AutoQuant software package.

**2. Three-Dimensional Tissue Imaging, *In Vitro***

As radiation experiments move more towards tissue samples and small organisms, the necessity to image optical sections within 3-D tissue was a driving factor in developing a multiphoton microscope into the endstation of the RARAF microbeam. RARAF user, Peter Grabham, planned a microbeam irradiation of a 3-D construct derived from human umbilical vein endothelial cells (HUVEC), which in intial studies, were optically sectioned using our multiphoton system. Derived from the walls of the umbilical vein, HUVEC cells were seeded onto a collagen matrix, a disk approximately 200 μm thick by 4 mm in diameter. While these cells "tunneled" through the matrix, forming a 3D structure similar to the capillaries of the blood circulatory system, collagen was displaced by cell growth and was degraded by cell enzyme action. A series of optical sections through these tissue samples (z-stacks) were compiled as movies to effectively transport the observer through the tissue slice. Figure 3 shows frames from these z-stack movies. In addition to using the nuclear stain YOYO-1, two non-stain imaging modes were used to capture the cytoplasm and the collagen matrix: autofluorescence (AF) and second harmonic generation (SHG). These two non-stain imaging modes require less sample preparation and allow structural imaging in 3D. With the capacity for optical sectioning, the multiphoton microscope at RARAF offers a mode for observing radiation-induced effects, such as foci formation, within tissue.

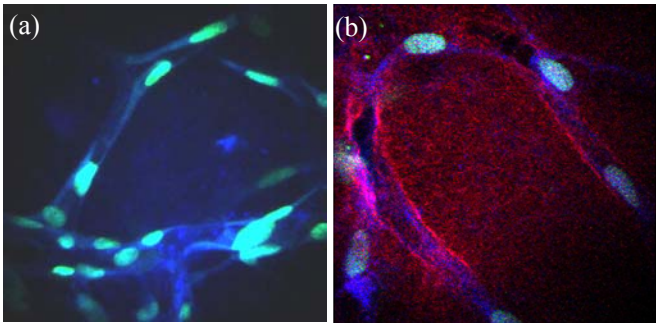


**Fig. 3.** Multiphoton microscopy images of HUVEC tissue samples. The cell nuclei, are stained with YOYO-1. Imaging modes: **(a)** Cell nuclei imaged by YOYO-1 (green) and cell cytoplasm imaged with autofluorescence (AF) (blue); **(b)** Cell nuclei imaged by YOYO-1 (green), cell cytoplasm imaged with AF (blue), and collagen imaged by SHG (red).

**3. Three-Dimensional Tissue Imaging, *In Vivo***

Researchers at RARAF are now irradiating small, living organisms, such as the *C. elegans* nematode. With its genome fully characterized in the literature, this organism offers an ideal model for particle-irradiation effects. The worms undergo anesthesia prior to microbeam irradiation. Immobilization of the worms is important for multiphoton microscopy, where image exposure can range from 0.5 seconds to 2 seconds. Figure 4 shows cross-sectional multiphoton images of GFP expression in live *C. elegans* under anesthesia. Following the anesthesia period and the multiphoton imaging process, the *C. elegans* specimen regained normal motion and health. This is a testament to the

non-damaging quality of multiphoton microscopy. By successfully imaging optical sections within a live, small organism, the microbeam-integrated multiphoton imaging system at RARAF offers users an array of imaging modes for 3D samples.

In radiation experiments using wild type *C. elegans,* imaging modes that do not require added fluorescent markers are required. AF and SHG offer two non-stain imaging modes available with the multiphoton microscope at RARAF. Figure 5 demonstrates this capacity through a composite image of the pharynx section of a wild type *C. elegans* specimen. The red components were imaged using SHG and the blue portions originate from AF signal. Light with an incident wavelength of 780 nm is used, while both SHG and AF signals are gathered simultaneously.

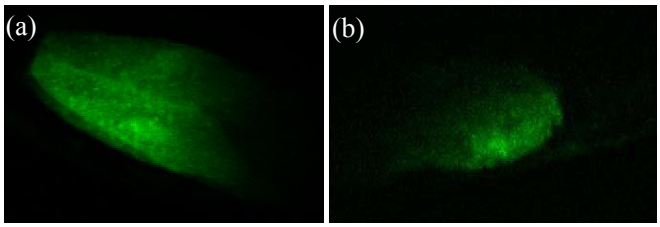


**Fig. 4.** Multiphoton microscope images of GFP expression in *C. elegans*: **(a)** pharynx, **(b)** tail.

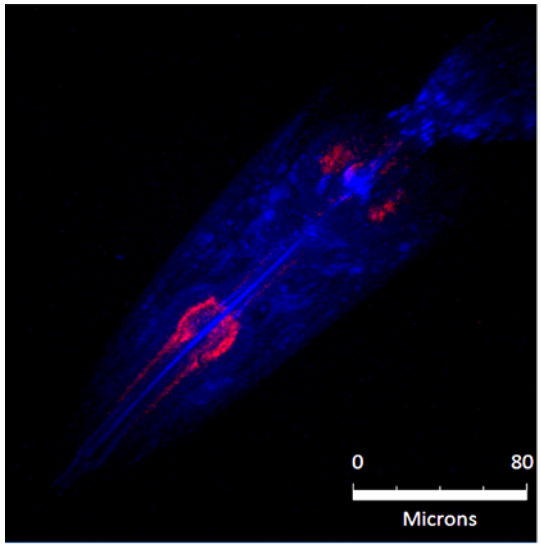


**Fig. 5.** Multiphoton microscope images of the pharynx section of a wild-type *C. elegans* specimen. SHG (red) and AF (blue) were used to produce this image. This view is a max projection after deconvolution using the AutoQuant software package.

## 4. Sub-Cellular Targeting

Typical examples of sub-cellular targets for the RARAF microbeam have been: (1) the cell nucleus or (2) the cell cytoplasm. Now that a focused charged-particle beam with a sub-micron diameter is routinely available using the compound electrostatic quadrupole triplet lens on the RARAF microbeam, additional targets within cellular systems are accessible. For instance, preliminary radiation experiments that target mitochondira have been conducted on small airway epithelial cells. In these experiments, the multiphoton microscope was used to image GFP-tagged mitochondria sites and position them over the ion beam for irradiation. Figure 6 shows a multiphoton microscope image of mitochondria (green) within small airway epithelial cells. For this image and for post-irradiation time-lapse images of mitochondria behavior, Hoechst was used to counter stain the nuclei.

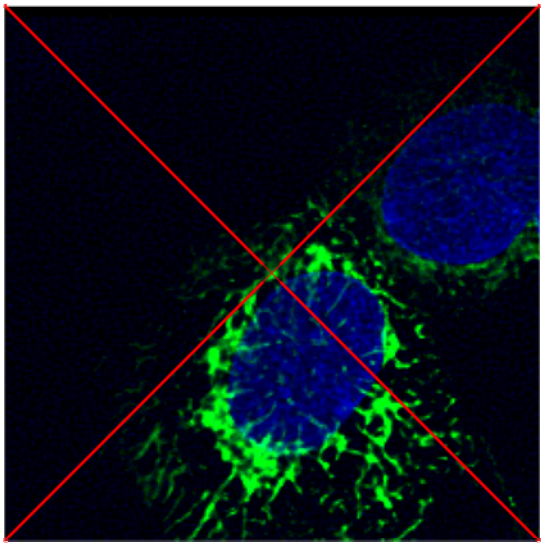

**Fig. 6.** Multiphoton microscope image acquired during an irradiation experiment using mitochondria sites (green) as targets. The cross-hairs (red) mark the center of the image, which coincides with the position of the ion beam. This view is a max projection after deconvolution using the AutoQuant software package.

## References

1. Bigelow AW, Brenner DJ, Garty G and Randers-Pehrson G. Single-particle/single-cell ion microbeams as probes of biological mechanisms. *IEEE Transactions on Plasma Science* **36**:1424-31, 2008.
2. Belyakov OV, Mitchell SA, Parikh D, Randers-Pehrson G, Marino SA, Amundson SA, Geard CR and Brenner DJ. Biological effects in unirradiated human tissue induced by radiation damage up to 1 mm away. *Proc Natl Acad Sci USA* **102**:14203-8, 2005.
3. Bigelow AW, Geard CR, Randers-Pehrson G and Brenner DJ. Microbeam-integrated multiphoton imaging system. *Rev Sci Instrum* **79**:123707, 2008. ■

# Immersion Mirau Interferometry Developments

*Oleksandra V. Lyulko, Gerhard Randers-Pehrson and David J. Brenner*

Immersion Mirau Interferometry (IMI) is a non-stain imaging technique that is based on the principles of phase-shifting interferometry.[1, 2] Several interference images are acquired at different heights with quarter-wavelength phase shifts between their interference patterns. As an interferometric technique, IMI does not require fluorescent staining of the cells, which eliminates potential damage induced by fluorescent stains. It operates at 540 nm (green light), therefore does not induce UV-exposure of the cells. Lastly, immersion mode allows the experimenter to keep the cells in cell medium during the irradiation experiment and minimize cell death due to dehydration.

To facilitate the immersion operation mode, a custom interferometric attachment has been previously built at RARAF (Fig. 1).[3]

In case of interferometric imaging, even a fraction-of-a-wavelength shift in the vertical direction lowers the image quality. Thus, despite the fact that the microbeam is mounted on a 27" thick concrete floor, the IMI system is still sensitive to unpredictable low-amplitude vibrations.

In 2008 we have tried a variety of passive and active vibration reduction techniques to build a vibration-free environment for IMI. The tests included isolating the microscope with sorbothane (shock-absorbing material) and using active vibration isolation units (the Vario Basic-40 units were loaned to RARAF by Halcyonics, Inc.). We also built a feed-back loop with a capacitive sensor (Fig. 1) measuring the position of the stage, sending analog signal to a PID controller which, in turn, was sending processed signal to the Nano-Drive. All these techniques resulted in only limited improvement.

Eventually, we have developed an approach to overcome the vibration problem based on Simultaneous Immersion Mirau Interferometry (SIMI) and have demonstrated its feasibility.

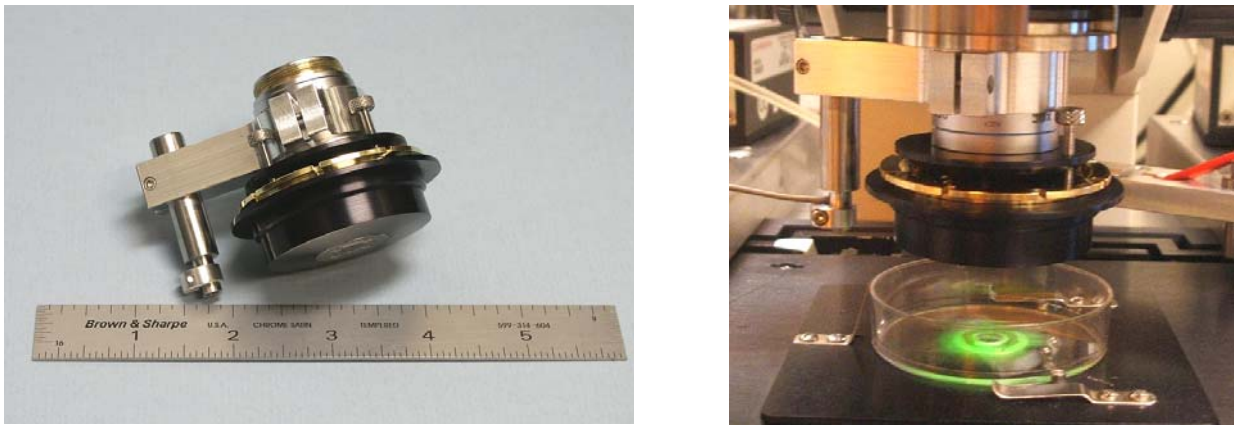


**Fig. 1.** Custom-built interferometric attachment. The shape is designed to fit the microbeam dish. Two adjustment screws regulate the inclination of the optics with respect to the sample. Aluminum surface is anodized to protect corrosion by the medium. The optics holders are interchangeable. Also attached to the objective is the holder for capacitive sensor.

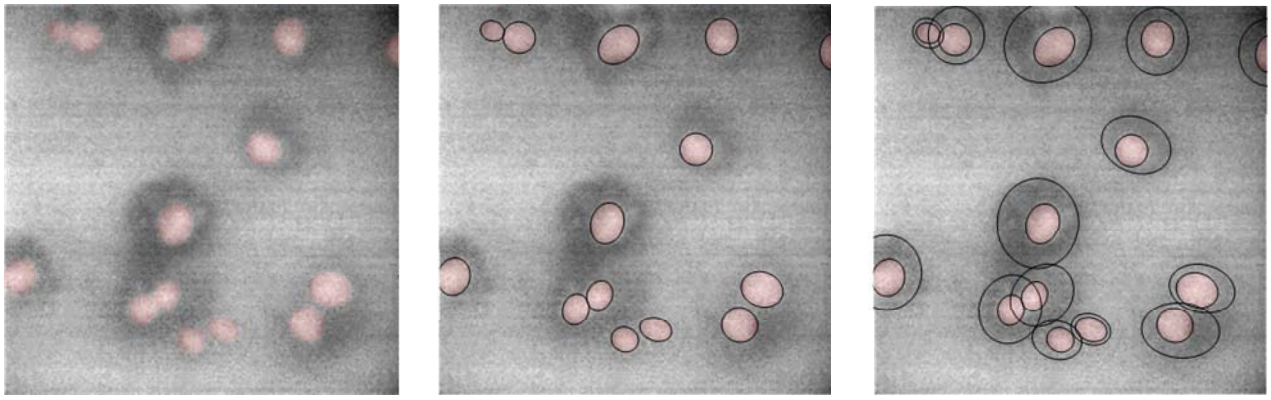

**Fig. 2.** Epi-illumination false-color images human cells using IMI, which involves no stain and no UV illumination (left panel). The data are sufficient to identify both nuclei (middle panel) and cytoplasm (right panel). In this case the nuclear and cytoplasmic boundaries were estimated using a genetic algorithm for fast ellipse detection.[4]

We have adapted the dynamic imaging concept described in reference 5 to the Mirau interferometer with some modifications (Fig. 3). A linear polarizer (**P**) is inserted on the output of the mercury light source (**LS**) and is oriented so that the light becomes linearly polarized at a 45° angle with respect to the x and y axes. A neutral beamsplitter (**BS**) directs the light into the objective with the interferometric attachment. A λ/8 waveplate is introduced between the lower window of the interferometric attachment and the sample. The waveplate creates a 90° phase difference between the x and y components of the test beam. Therefore, the output of the interferometer contains two interferograms with a relative phase shift of 90°. A polarization beam splitter (**PBS**) is placed after the Mirau attachment and the neutral beam splitter to split the x and y components of both beams. The outputs of the polarization beam splitter form two interferograms on two separate CMOS sensors. The image processing algorithm was modified so that only two interferograms and the background intensity are used.

Figures 4 and 5 demonstrate the results of our work using a two-camera simultaneous Mirau imaging system (left panels), with a comparison to corresponding fluorescent images of the same samples (right panels). The unstained cells were fixed and imaged with the simultaneous Mirau interferometric system on glass slides. The same samples were subsequently stained with DAPI and Red Counterstain C and imaged with a fluorescent microscope (Zeiss Imager Z1). On the Mirau interference images, cell structures can be seen, such as nuclei, cytoplasm, nucleoli and micronuclei.

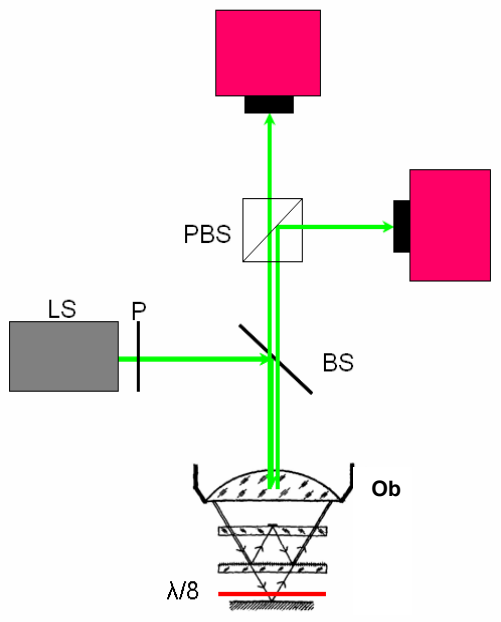


**Fig. 3.** Simultaneous Mirau Interferometer: abbreviations as in text.

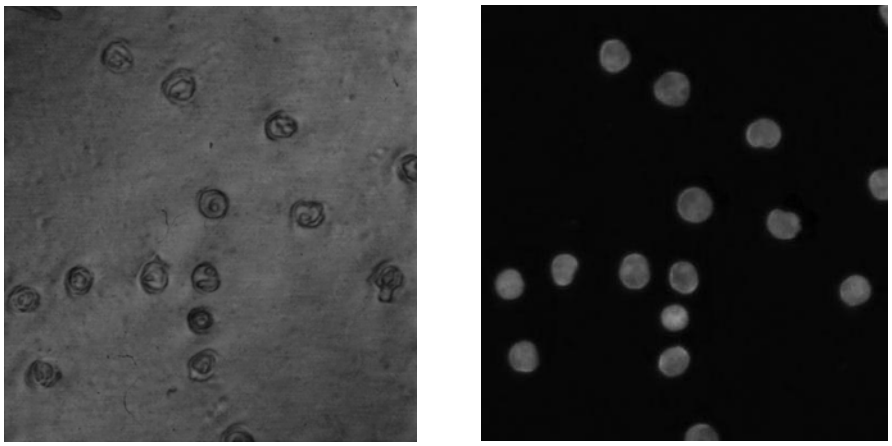

**Fig. 4.** WISH cells – note the cytoplasm in these cells is very thin. **Left:** No-stain, no-UV Simultaneous Mirau interferometric image shows cell nuclei and nucleoli; **Right:** Corresponding fluorescent image.

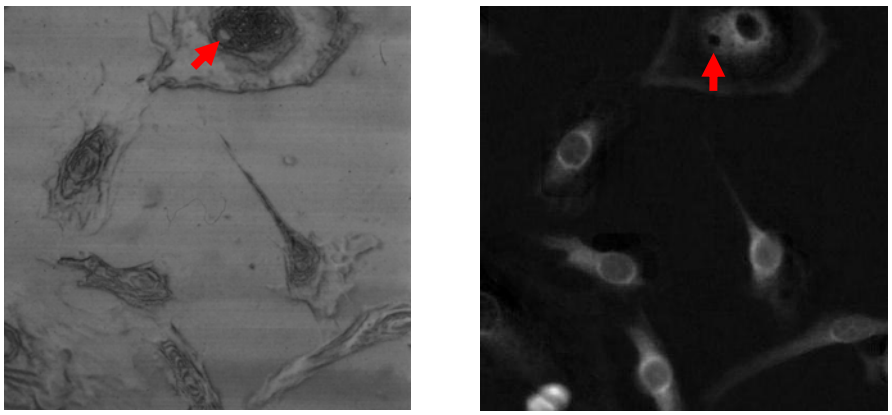

**Fig. 5.** 3T3 cells: **Left**: No stain / no UV Simultaneous Mirau Interferometric image shows cytoplasm and a micronucleus. **Right:** Corresponding fluorescent image. The red arrows indicate the micronucleus on each image.

**References**

1. Creath, K. Phase-measurement interferometry techniques. Progress in Optics XXVI, 349-93, 1988.
2. Ross GJ, Bigelow AW, Randers–Pehrson G, Peng CC and Brenner DJ. Phase-based cell imaging techniques for microbeam irradiations. *Nuclear Instruments and Methods in Physics Research B* 241: 387–91, 2005.
3. Lyulko O, Randers-Pehrson G and Brenner DJ. Immersion Mirau Interferometry. *CRR Annual Report* 80-1, 2007.
4. Yao J, Kharma N and Grogono P. A multi-population genetic algorithm for robust and fast ellipse detection. *Pattern Analysis & Applications* **8**:149-62, 2005.
5. Brock N, Hayes J, Kimbrough B, Millerd J, North-Morris M, Novak M and Wyant JC. Dynamic interferometry. *Novel Optical Systems Design and Optimization* VIII. San Diego, CA, USA: SPIE, 58750F-10, 2005. ■


# Point-and-Shoot: Charged-Particle Microbeam Irradiation Targeting through Beam Deflection

*Andrew D. Harken, Gerhard Randers-Pehrson and David J. Brenner*

During irradiation, targets to be exposed are moved to the beam position using a high-resolution three-axis piezoelectric stage. When a collimated microbeam was being used, this was a necessary but relatively time-consuming method to position targets for irradiation. Unlike a collimated microbeam, a focused microbeam is not restricted to a single location on the exit window. Therefore, the beam can be deflected to any position in the field of view of the microscope (pointing) and the target at that position irradiated (shooting). Moving the beam to the cell position magnetically or electrostatically can be performed much faster than moving the stage allowing us to "Point-and-Shoot" targets faster than currently capable.

We have developed a Point-and-Shoot targeting system for microbeam irradiation based on the wide-field magnetic split-coil deflector system from Technisches Büro Fischer (Ober Ramstadt, Germany). The deflector, shown in Figure 1, consists of four interlaced coils in a set of ferrite rings. The coils are paired to create two axes that are orthogonal to each other. When wired in series, a pair on opposite sides will create a temporary dipole magnetic field, which deflects the beam. It is possible to "scan" the beam into a rectangular area in the microscope view by using the two pairs of coils independently. The amount of current needed in each coil to deflect the beam to a specific location can be mapped and this mapping used as a look-up table for the target locations. The irradiation would then proceed by rapidly switching through the required sets of coil currents to steer the beam to the targets, irradiating each target with the time limited only by the beam shutter speed and beam current. The selection and purchase of two KEPCO BOP power supplies (KEPCO, INC., Flushing, New York) allows us to switch between samples 5 times faster than the current mechanical stage.

**Fig. 1.** A picture of the interlaced magnetic split-coil deflector.

We have performed preliminary testing of the system on our permanent magnet microbeam (PMM) endstation using 5.2 MeV $^4$He ions. Results shown in Figure 2 demonstrate that we can deflect the beam accurately in both directions

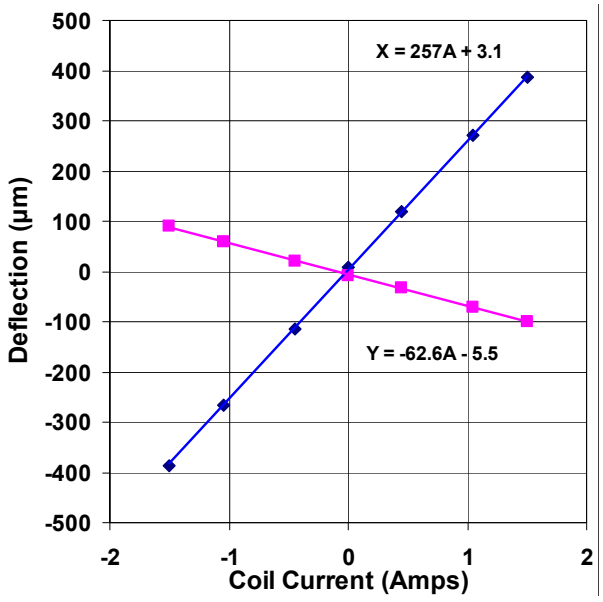


**Fig. 2.** Graph of beam deflection versus current in the deflection coils. Note the linearity of the deflection through the range of applied current.

with a good linear correlation between applied coil current and deflection distance. Since the Point-and-Shoot system is located below the upper focusing quadrupole triplet, the deflection in the two directions is reduced by the demagnification of the focusing lens. The PMM system was designed for a demagnification ratio of 3 between the two directions in a single lens. As seen from the slopes of the linear fit lines in the graph, we measured a demagnification ratio of 4. The ideal system would be able to position the particle beam at any location in the image. The KEPCO power supplies source currents that will allow complete coverage of the microscope field of view on the microbeam endstation.

With the preliminary tests completed on the PMM, the Point-and-Shoot deflector was recently installed on our charge particle microbeam endstation. Initial beam tests are being performed and we will be using this system for accelerating microbeam irradiations. ■

# Proton Induced Soft X-Ray Microbeam at RARAF

*Andrew D. Harken, Gerhard Randers-Pehrson and David J. Brenner*

## Introduction

The development of the soft x-ray microbeam for low-LET ionization of single cells and sub-cellular organelles is moving forward. The x-ray microbeam endstation has been constructed. It is currently undergoing beam tests to bring it on-line for irradiation experiments.

## Endstation Design

The x-rays are generated by proton induced x-ray emission (PIXE). The target we have chosen is titanium (Kα, 4.5keV) for its combination of low energy to avoid Compton scattering and ability to penetrate (1/e depth of 146μm) enough to irradiate into tissue specimens. The target will be a small titanium slug ¼ inch in diameter embedded in a cooled copper rod that will extend to outside the vacuum system. The target position will be manipulated through screws that finely adjust the copper rod position. The copper rod/titanium target will be electrically isolated from the vacuum housing to assist in proton beam assessment measurements and x-ray generation calibration. The titanium target face will be cut at a 70 degree angle to the proton incidence to emit x-rays in the vertical direction.

A micropositioning stage (MicroStage with a Nano-Z200, Mad City Labs, Madison, WI) has been integrated with a fluorescence microscope (Nikon FN1 Eclipse, Nikon USA, Melville, NY) for imaging, targeting and moving a specimen. This stage and microscope combination, based upon our previous endstation designs for particle microbeam systems, will be positioned above the beam line using a vertical x-ray beam. This orientation allows the use of current biological specimen dishes with medium still on the cells, reducing the exposure of the samples to the room environment.

A Fresnel zone plate (Zoneplates, Inc., London, UK) has been purchased for focusing the x-rays. The zone plate is

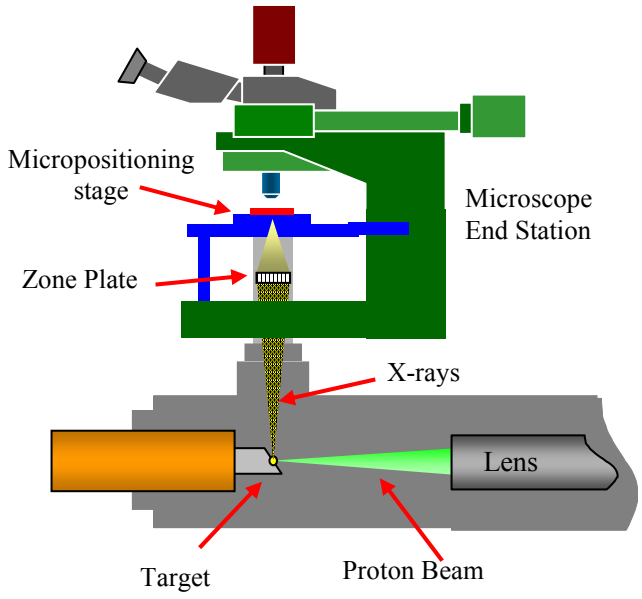


**Fig. 1.** Schematic layout diagram of the x-ray microbeam endstation.

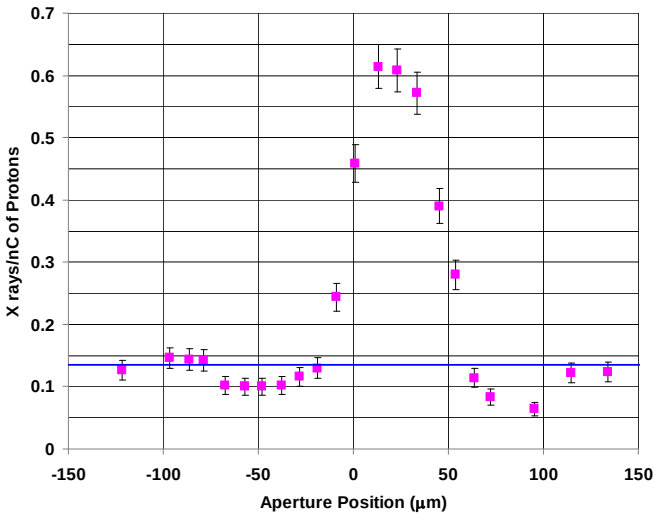


**Fig. 2.** Test configuration: x rays per nC of protons incident on the titanium target, vs. aperture position in the zone-plate focal plane.

held in a helium filled chamber separated from the proton target with a beryllium window, which allows x-rays to pass through while maintaining the vacuum of the particle system. The endstation is mounted on a kinetic system allowing the distance between the zone plate and proton target to be adjusted for best focusing characteristics.

**Zone Plate Testing**

We have performed a preliminary test of the zone plate using the charged-particle microbeam endstation. The charge-particle beam was focused to a 10μm spot on a 60μm thick titanium foil to create a small x-ray source. Figure 2 shows number of x-rays detected per nanocoulomb of protons at a given location obtained by scanning a 50μm aperture through the zone plate focal point. Note that there is a slight decrease in the background before the sharp increase for the focal peak; this is due to the zeroth order diffraction and is expected for this geometry. The focused x-ray spot size can be determined from the increasing transitions around the 0μm and 50μm points in the data plot. The spot size for this test is ~14μm in diameter which was expected for the testing geometry. This verification of the zone plate optics correlates with our calculations for the final x-ray system to deliver 5mGy/sec with an irradiation spot size of 2μm.

**Conclusions**

Testing of the system will be completed shortly and we expect to begin offering x-ray irradiation opportunities to the RARAF users. ■

# Neutron Microbeam

*Yanping Xu, Gerhard Randers-Pehrson, Stephen A. Marino and David J. Brenner*

**Introduction**

There are many compelling reasons to study slow neutrons, because most neuron dose is deposited at neutron energies below 50KeV in a commercial nuclear reactor where personnel might be exposed. Also low-energy neutrons produce biological damage maybe in a fundamentally different way from most photon or high-energy charged particle irradiations. To study human exposure to low energy neutrons (especially those with energies 10 to 100 KeV), we started to develop a neutron microbeam system combined with existing RARAF microbeam techniques.

**The Principle of the Neutron Microbeam**

The $^{7}$Li(p,n)$^{7}$Be nuclear reaction, which has a threshold at 1.881MeV, is a well-known source for generating neutrons. The near-threshold reaction provides a relatively high neutron yield, as well as a very narrow forwardly-peaked angular distribution for the outgoing neutrons.[1] The narrow forward-peaked neutron microbeam results from the fact that the velocity of the center of mass is greater than the relative outgoing velocity of the neutrons. As we show, this "kinematic collimation" enables us to produce neutron microbeams of diameter 8 to 20 m (depending on the setup), starting with a proton microbeam containing a diameter of 5μm.

A schematic of the experiment setup is shown below (Fig. 1). The electrostatic double-triplet lens system is used to focus the incoming proton beam onto a lithium layer on a metal backing plate. The proton beam will be absorbed and stopped by the backing plate, but the forward neutron beam will pass through the backing plate and irradiate the cells. The backing plate will also serve as the system vacuum window.

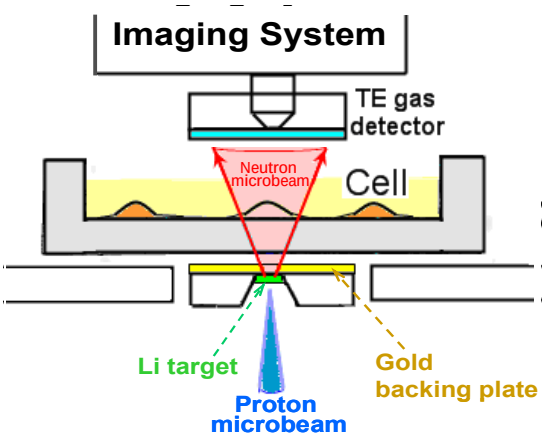


**Fig. 1.** Schematic layout of the neutron microbeam (not to scale). The proton microbeam is incident on a lithium target, and neutrons are produced with an angular distribution that is highly forward-peaked.

The geometry of the microbeam system requires the source-to-sample distance to be very small. Assuming a 1μm thick Li target layer with a 17μm thick backing plate and an additional 3μm for the thickness of the cell dish or cell channel, the total length from the target to the cells is about 20μm.

**Preliminary Design Studies of the Neutron Microbeam**

Figure 2 and Figure 3 show the calculated neutron angular distribution produced by protons of different energies near the neutron production threshold. Table 1 lists the calculated neutron yields and dose rates near the reaction threshold. The calculations are based on a 1nA proton beam,

**Table 1. Predicted neutron yields, microbeam diameters, neutron energies, and dose rates, for different proton energies**

| Proton Energy (MeV) | Neutron Yield (per nC) | Maximum neutron angle (degree) | Neutron beam diameter (μm) | Mean neutron energy (keV) | Dose Rate (cGy per min) |
|---|---|---|---|---|---|
| 1.882 | 270 | 9 | 8.1 | 30.0 | 8 |
| 1.883 | 800 | 13 | 10.5 | 30.2 | 14 |
| 1.884 | 1440 | 16 | 12.5 | 30.5 | 18 |
| 1.885 | 2230 | 19 | 14.7 | 30.7 | 20 |
| 1.886 | 3170 | 21 | 16.2 | 31.0 | 23 |

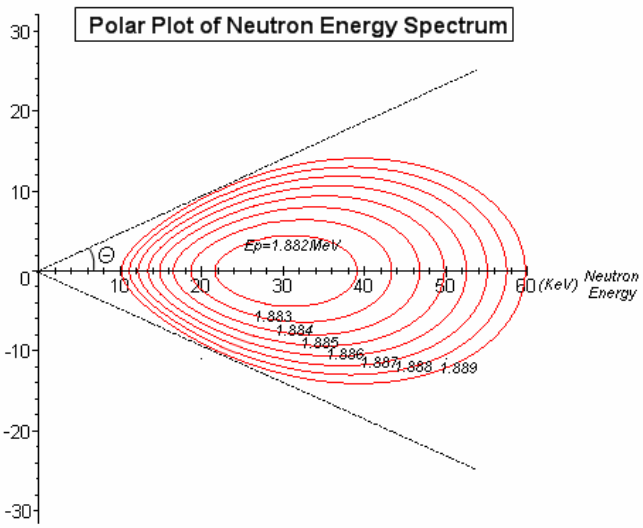


**Fig. 2.** Neutron energy-angular distribution for different proton energies.

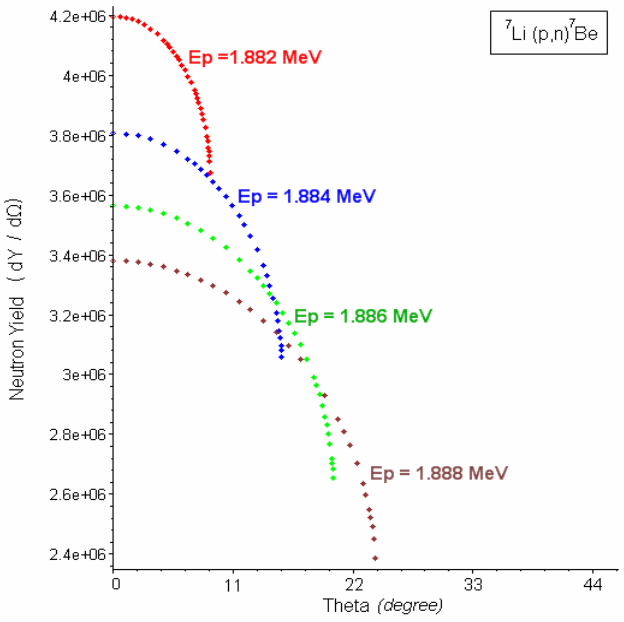


**Fig. 3.** Neutron yield vs. angle for different proton energies.

which we typically obtain. To keep the neutron microbeam spot generated from a 5μm diameter proton beam in the range from 8 to 15 μm, will require a proton beam energy between 1.882 MeV and 1.886 MeV. It is clear that central to the neutron microbeam design is the extremely high energy stability of our new Singletron accelerator.

Within a 20 degree forward angle, the generated neutrons have an energy range from 10keV to 50keV. The neutron yield is about 6,000 per nA of proton current for a lithium target and about one third of that yield for lithium fluoride. In these cases the flux is about 15 or 5 n/μm$^2$/second, respectively. Based on kerma factors from Bach and Caswell,[2] the predicted dose rates for the different diameter neutron microbeams are shown in Table 1.

The major background dose from a lithium target is due to a 478 keV gamma ray from the (p, p'γ) reaction. However, this contributes less than 1% of the total dose rate in our geometry and considerably less in terms of equivalent dose. The dose rate from other reactions, e.g. (p, γ), is negligible.

## Dosimetry and Spectroscopy

The neutron beam-spot size and position will be measured by the use of standard solid-state CR-39 track etch detectors. More than 95% of all recorded tracks will be due to proton recoils from the incident neutrons. The track length in this case will be roughly in a range 100nm to 600nm.

The neutron spectrum will be measured using a gas filled proportional counter which is currently mounted on the microbeam microscope objective, shown in schematic in Figure 4. For this purpose we will need to substitute propane TE gas for the P-10 gas that we presently use. This same detector will be used to measure the dose rate.

Because the electron and recoil proton have different rise

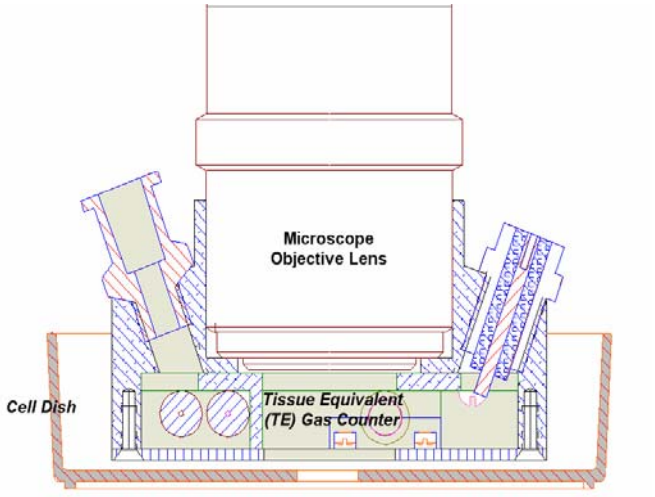


**Fig. 4.** Schematic of our gas filled counter, with high magnification lens.

times in the pulse from the proportional counter, the neutron energy can be extracted using a simple deconvolution of the measured spectrum, which for a monoenergetic beam would be a rectangle when plotted against energy. Knowing the TE gas pressure, we can calibrate the energy-weighted count rate detected by this counter and thus measure the total amount of energy deposition in a given sized biological target.

**References**


1. Lee CL and Zhou XL. Thick target neutron yields for the Li-7(p,n)Be-7 reaction near threshold. *Nucl Instr Meth B* **152**:1-11, 1999.
2. Bach RL and Caswell RS. Energy transfer to matter by neutrons. *Radiat Res* **35**:1-25, 1968. ■


# Microbeam Irradiation of Living Animals

*Antonella Bertucci, Roger D. J. Pocock,[a] Wendy Kuhne,[b] Gerhard Randers-Pehrson, William Dynan,[b] Oliver Hobert[a] and David J. Brenner*

Accumulated evidence shows that the biological effects of ionizing radiation can be expressed in unexposed neighboring cells near an irradiated cell or group of cells.[1-2] This so called "bystander effect" and has challenged the dogma that cellular damage is restricted to directly irradiated cells. Proposed mechanisms to explain this phenomenon are centered on the importance of intercellular communication. Therefore, the use of advanced tools to study inter- and intra-cellular mechanisms of damage signal transduction is of critical importance. Such inter-cellular studies have often been undertaken using microbeam irradiation of individual cells plated in 2-D monolayers[3-6] and more recently in a 3-D tissue-like construct with extensive and complex cell-to-cell communication and extra-cellular matrix interactions. Pioneering studies using 3-D models started at the Gray Laboratory in the UK, where an organotypic explant model technique was exploited.

Efforts to expand the use of more reproducible culture models were undertaken at the Columbia University Radiological Research Accelerator Facility (RARAF) microbeam.[7-8] While useful, single cell *in vitro* systems do not have a realistic multicellular morphology, and *in vitro* studies using 3-D tissues do not necessarily mimic inter-cellular communication which involves tissue-level stress responses, often among multiple cell types, and mediated by microenvironment signaling. Therefore, studies using whole organisms, targeting specific cells, cell groups or organs are needed to elucidate mechanisms of radiation-induced long-distance effects in a realistic model.

We have developed different techniques to expose at RARAF, for the first time, living organisms. The animal models used were the nematode *C. elegans* and the Japanese medaka, Oryzias latipes, fish embryos.


[a] *Department of Biochemistry and Molecular Biophysics, Howard Hughes Medical Institute, Columbia University Medical Center, New York, NY*

[b] *Medical College of Georgia, Institute of Molecular Medicine and Genetics, Augusta, GA*


**The *C. elegans* Nematode**

*C. elegans* has several advantages for *in vivo* microbeam studies such as: rapid life cycle, short life span, fully sequenced genome and transparent body. Moreover *C. elegans* shares cellular and molecular structures and control pathways with higher organisms, thus, biological information learned from *C. elegans* may be directly applicable to more complex organisms. From a practical perspective it is small enough to be compatible with microbeam irradiation since the diameter of its body is ~ 50μm and the full length is ~ 1mm. Based on these features we designed our animal model system for *in vivo* microbeam experiments. Specifically, we used the *C. elegans* strain SJ4005 *hsp-4::gfp(zcls4)V*, which has a GFP reporter for the *hsp-4* heat-shock gene. Heat shock proteins (HSPs) are a ubiquitous family of gene products present in cells under unstressed conditions. They are expressed in much higher concentration owing to the presence of stress, including heat, UV irradiation, γ-rays and chemicals.[9] *C. elegans* strain SJ4005 has been developed and used to study chemical-induced stress responses. Calfon *et al.* showed that transcription of the *hsp-4* gene is induced in the gut and in the hypodermis upon endoplasmic reticulum chemical stress

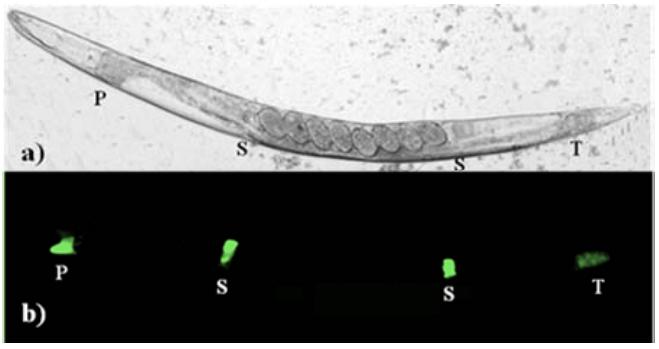


**Fig. 1. a)** Young gravid *C. elegans* SJ4005 strain imaged using Normarski optics. **b)** Fluorescent image of same worm. It is visible the basal GFP expression localized in the pharynx (P), spermathecae (S) and in the tail (T).

or heat shock,[10] leading to dramatically increased levels of the protein in a time dependent manner. Consequently, we used this well characterized system to develop a model for *in vivo* microbeam studies. In normal/nonstress conditions, GFP expression is most prominently localized in spermathecae and, to a lesser degree, in the tail (posterior intestine) and pharynx (anterior intestine) regions (Fig. 1).

**Results**

Young adult *C. elegans* hermaphrodites were exposed individually to 3MeV protons microbeams using the Columbia University RARAF charged-particle accelerator. The maximum penetration of the protons used was ~140µm with an entrance LET of 12.5 keV/µm and a beam diameter of 1µm. For microbeam irradiations, worms were anesthetized with 10mM sodium azide ($NaN_3$) in M9 buffer and placed in a customized microbeam dish with a micro cover-slip for individual exposure. Before exposure, worms were individually imaged using an epifluorescent microscope. Worms were exposed to 0, 25, 50 and 75 protons per target area. Animals were irradiated at the tail, in the center of the GFP expression region. Control worms were mock-irradiated, by targeting the microbeam just outside the worm (~ 200µm), keeping the same set-up time for anesthetic exposure and concentrations. After exposure, worms were washed in a buffer solution and cultured for further GFP expression evaluation.

Microbeam exposed worms showed a different GFP stress response in terms of intensity and localization, compared with the control group. Increase in expression was noted only after delivering 50 and 75 protons; these worms exhibited a strong stress response in the posterior intestine, between the spermatheca and the microbeam targeted area. Mock irradiated worms did not exhibit any GFP stress response after 24 hours (Fig. 2) and no apparent stress response was detected when 25 protons were delivered.

In conclusion, a one micrometer diameter proton beam was able to induce tail region *in situ* GFP over-expression as well as a distal stress response as far as >150µm away from the irradiated spot. No stress response was seen in other regions of the body of exposed worms and only basal levels of GFP expression were detected at the pharynx and spermathecae regions.

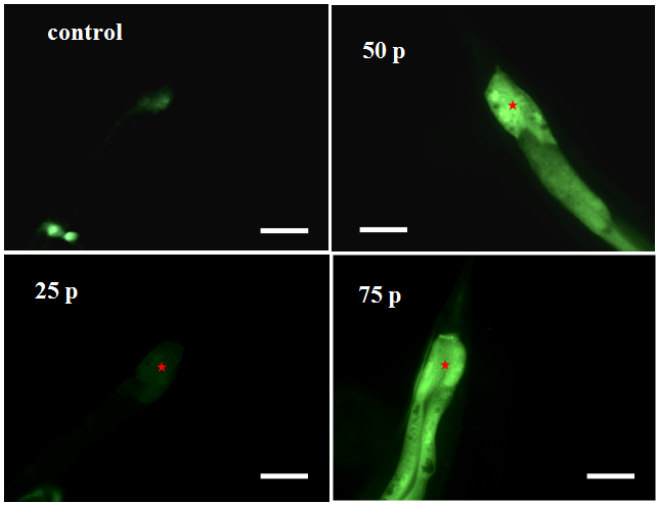


**Fig. 2.** *hsp-4::GFP* stress response in the *C. elegans* tail 24 hours after microbeam irradiation. **a)** Control. **b)** Worm tail irradiated with 25 particles. No stress response was detected. **c-d)** Stress response following microbeam irradiation with 50 and 75 protons. A strong stress response is visible in the posterior intestine up to 150µm from the irradiated area. Scale bar indicates 50µm. The red star indicates the irradiated area with 1µm proton beam.

**The Medaka Fish Embryo**

The Medaka Oryzias latipes is a small egg-laying freshwater fish, which is increasingly being used as a model system for developmental genetics and evolutionary biology. Of particular interest here is the Medaka embryo, because of its small size and optical clarity for imaging internal tissues and organs. A Medaka genome has recently been sequenced, and many transgenic and mutants are now available.

A fertilized Medaka egg has a diameter of 1.2mm; starting from stage 22 many anatomical structures are developed and clearly visible.[11] The embryo develops adjacent to the chorionic membrane, which is 10 µm thick. As illustrated in Figure 3, a 4.5MeV proton, having a total penetration of ~280µm, easily can penetrate the organs of the embryo.

The main issue we needed to overcome in adapting microbeam for irradiating the Medaka embryo is to orient it reliably with respect to the beam entrance / direction. To address this issue, we have adapted a modified version of the observation/orientation chamber used by Iwamatsu in his landmark observational studies of Medaka embryo stages.[11]

We exposed Medaka embryos, as a vertebrate model for microbeam irradiation studies. Medaka embryos at stage 28 were exposed to 4.5 MeV protons with a beam spot of ~25, 50 and 100 µm in diameter. At this stage, the ocular structures are clearly defined by the retinal pigmentary layer, the heart is functional and organogenesis is completed.[11] The targeted regions for this experiment were the left eye and the

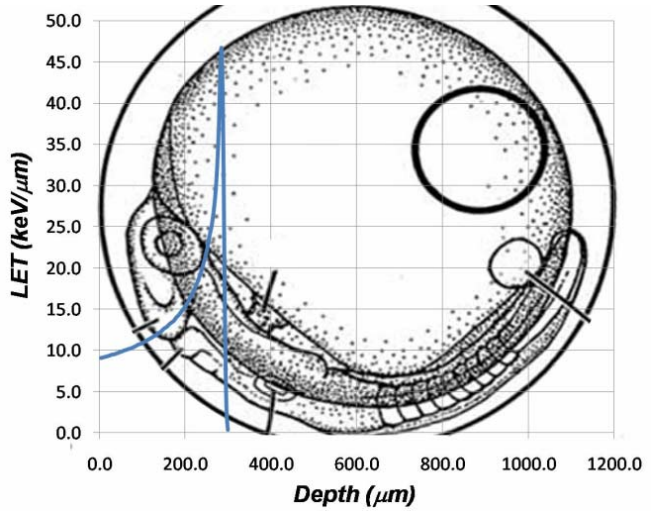


**Fig. 3.** Schematic illustration of a Medaka embryo, stage 22. The curve shows the energy loss for a 4.5MeV proton beam as it penetrates the embryo. The Bragg peak appears about at 275µm.

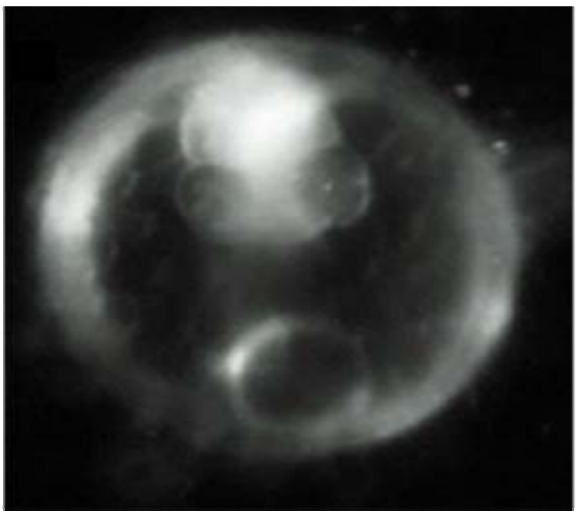

**Fig. 4.** Medaka embryo, stage 28, microbeam exposure set up. Embryo positioned in a microbeam dish for proton exposure.

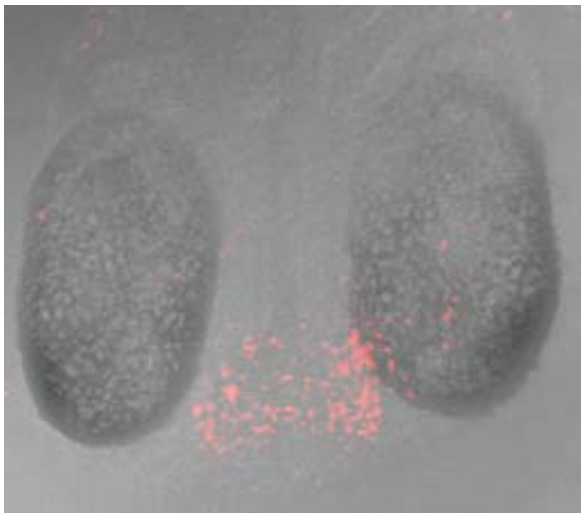

**Fig. 5.** Dorsal view of an exposed Medaka embryo. The beam direction was from top of head through bottom of jaw. The red spots indicate the apoptotic cells following microbeam irradiation.

forebrain. 10,000 and 20,000 protons were delivered in each target. Individual Medaka embryos were placed in a microbeam irradiation dish and aligned, so that the targeted region faces vertically down (Fig. 4). Embryos were then imaged and irradiated. After 24 hours the embryos were fixed with 4% paraformaldehyde and the number of apoptotic cells was measured using a whole-mount TUNEL-assay.

**Results**

Initial analysis of the results showed that mid-brain irradiation of embryos with 4.5MeV protons induced an increase of apoptotic nuclei at the target region as well as in adjacent areas far away from the exposed point (Fig. 5).

The average number of TUNEL-positive cells in the irradiated areas of the brain was determined for the 50μm microbeam exposed group. Some apoptotic cells are normally present in the developing brain; thus, the average number of TUNEL-positive cells measured was 57.8±12.5 in the sham irradiated group. The average number of TUNEL-positive cells was 62.6±16.2 for embryos irradiated with 10,000 protons, and 185.3±36.2 for embryos irradiated with 20,000 protons.

**References**


1. Morgan WF. Non-targeted and delayed effects of exposure to ionizing radiation: I. Radiation-induced genomic instability and bystander effects *in vitro*. *Radiat Res* **159**:567-80, 2003.
2. Morgan WF and Sowa MB. Non-targeted bystander effects induced by ionizing radiation. *Mutat Res* **616**:159-64, 2007.
3. Zhou H, Randers-Pehrson G, Waldren CA, Vannais D, Hall EJ and Hei TK. Induction of a bystander mutagenic effect of alpha particles in mammalian cells. *Proc Natl Acad Sci USA* **97**:2099-104, 2000.
4. Lorimore SA and Wright EG. Radiation-induced genomic instability and bystander effects: related inflammatory-type responses to radiation-induced stress and injury? A review. *Int J Radiat Biol* **79**:15-25, 2003.
5. Osterreicher J, Prise KM, Michael BD, Vogt J, Butz T and Tanner JM. Radiation-induced bystander effects. Mechanisms, biological implications, and current investigations at the Leipzig LIPSION facility. *Strahlenther Onkol* **179**:69-77, 2003.
6. Mitchell SA, Randers-Pehrson G, Brenner DJ and Hall EJ. The bystander response in C3H 10T1/2 cells: the influence of cell-to-cell contact. *Radiat Res* **161**:397-401, 2004.
7. Belyakov OV, Mitchell SA, Parikh D, Randers-Pehrson G, Marino SA, Amundson SA, Geard CR and Brenner DJ. Biological effects in unirradiated human tissue induced by radiation damage up to 1 mm away. *Proc Natl Acad Sci U S A* **102**:14203-8, 2005.
8. Sedelnikova OA, Nakamura A, Kovalchuk O, Koturbash I, Mitchell SA, Marino SA, Brenner DJ and Bonner WM. DNA double-strand breaks form in bystander cells after microbeam irradiation of three-dimensional human tissue models. *Cancer Res* **67**:4295-302, 2007.
9. Santoro MG. Heat shock factors and the control of the stress response. *Biochem Pharmacol* **59**:55-63, 2000.
10. Calfon M, Zeng H, Urano F, Till JH, Hubbard SR, Harding HP, Clark SG and Ron D. IRE1 couples endoplasmic reticulum load to secretory capacity by processing the XBP-1 mRNA. *Nature* **415**:92-6, 2002.
11. Iwamatsu T. Stages of normal development in the medaka Oryzias latipes. *Mech Dev* **121**:605-18, 2004. ■

Center for Radiological Research 2008 Departmental Picnic. (L-r): Mr. Ahmad Hatami, Dr. David Brenner and Dr. Eric Hall.

Center for Radiological Research 2008 Departmental Picnic. (L-r): Dr. Antonella Bertucci, Dr. Tom Hei and Dr. Gloria Calaf.


Center for Radiological Research 2008 Departmental Picnic. (L-r): Dr. Charles Geard and Dr. Eric Hall.


Center for Radiological Research 2008 Departmental Picnic. (L-r): Dr. Hongning Zhou and Dr. Yanping Xu.

Center for Radiological Research 2008 Departmental Picnic. (L-r): Dr. Lubomir Smilenov, Ms. Oleksandra Lyulko and Dr. Corinne Leloup.

Center for Radiological Research 2008 Departmental Picnic. (L-r): Our member's guest, Dr. Yanping Xu, Ms. Jing Nie and her friend.

# Mitochondrial Function Modulates Cytoplasmic Irradiation Induced Bystander Effect

*Hongning Zhou, Masao Suzuki,[a] Mei Hong, Vladimir Ivanov, Michael Partridge, Alan Bigelow, Gerhard Randers-Pehrson and Tom K. Hei*

Radiation-induced bystander effect is defined as the induction of biological effects in cells that are not directly traversed by a charged particle, but are receiving signals from the irradiated cells that are in close proximity to them. Although bystander effects have been well described over the past decade,[1, 2] the precise mechanisms of the process remain unclear. It is likely that a combination of pathways involving both primary and secondary signaling processes is involved in producing a bystander effect. Previously, research indicated that cytoplasmic irradiation would induce DNA damage in both directly- and non-irradiated rodent or human cells, and reactive oxygen/nitrogen species play an essential role in the process.[3, 4] More recently, we found that mitochondrial DNA-depleted human skin fibroblasts showed a higher bystander mutagenic response compared with their parental, mitochondria functional cells, and the signals from one cell type can modulate expression of the bystander response in another cell type.[5] These results indicated that mitochondria might play an important role in the regulation of radiation-induced bystander effects.

Approximately 2500 exponentially growing normal human lung fibroblast (NHLF) /small airway epithelial (SAE) cells in 1.5µl volume were inoculated into each of a series of microbeam dishes coated with Cel-Tak to enhance cell attachment as described.[6] The next day after plating, after staining with 100µM H33342 for 30 minutes, the image analysis system located the centroid of cells and irradiated 10% of them randomly, one at a time through the nucleus or the cytoplasm, with an exact number of alpha particles accelerated with a 5MV Singletron accelerator at the Radiological Research Accelerator Facilities of Columbia University. After irradiation, cells were maintained in the dishes for different time points before being removed or fixed for further assay. All controls were similarly stained and sham-irradiated as well.

When 10% of the NHLF cells were irradiated with 8 alpha particles through the cytoplasm, the induced G2 premature chromosome condensation (G2 PCC) levels in the population were significantly higher than expected assuming there was no crosstalk between the irradiated and non-irradiated cells. Furthermore, the profile of chromatid breaks was very similar to that in which 100% of the cells in the population were hit (Fig. 1). In addition, the preliminary data indicated that mitochondrial morphology changed in both cytoplasmic directly irradiated cells and non-irradiated bystander cells; and the alteration of mitochondrial contents was also detected by using real-time PCR. These data implied that cytoplasmic irradiation could induce mitochondrial morphology and quantity alteration that might affect mitochondrial function, which might be essential in cytoplasmic irradiation induced bystander effect. Further experiments are ongoing to define the pathways involved in mitochondrial alteration. Results from this study would have high impact on our understanding of the mechanisms of the cytoplasmic irradiation-induced bystander response.

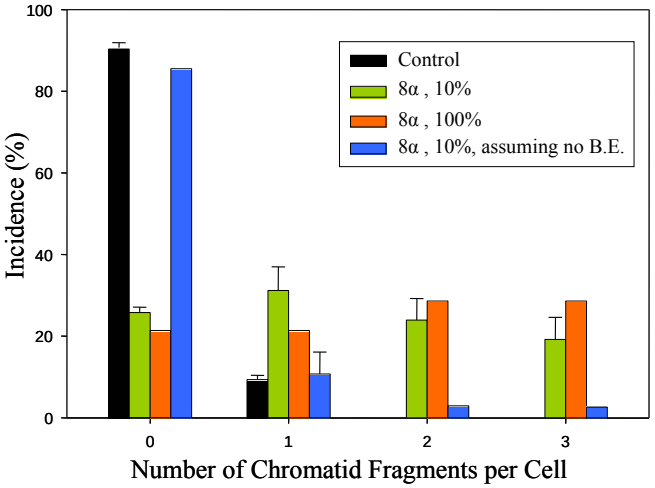


**Fig. 1.** Distribution of Chromatid-Type Breaks in Cytoplasmic Irradiated Cells. **Black**: control cells without radiation. **Green**: 10% of cells got 8α particles traversal through cytoplasm. **Orange**: Every cell got 8α particles traversal through cytoplasm. **Blue**: Assuming no bystander effect, only cells got α particle traversed showed chromosome damage.

**Acknowledgments**

This research was supported by funding from the National Institutes of Health Grants CA 49062, ES 12888. The Radiological Research Accelerator Facility (RARAF) is an NIH supported Resource Center through grants EB-002033 (NIBIB) and CA-37967 (NCI).

**References**

1. Morgan WF. Non-targeted and delayed effects of exposure to ionizing radiation: I. Radiation-induced genomic instability and bystander effects *in vitro*. *Radiat Res* **159**:567-80, 2003.
2. Hei TK, Persaud R, Zhou H and Suzuki M. Genotoxicity in the eyes of bystander cells. *Mutat Res* **568**:111-20, 2004.
3. Wu LJ, Randers-Pehrson G, Xu A, Waldren CA, Geard CR, Yu Z and Hei TK. Targeted cytoplasmic irradiation

[a] *National Institute of Radiological Sciences, Chiba, Japan.*

with alpha particles induces mutations in mammalian cells. *Proc Natl Acad Sci USA* **96**:4959-64, 1999.
4. Shao C, Folkard M, Michael BD and Prise KM. Targeted cytoplasmic irradiation induces bystander responses. *Proc Natl Acad Sci USA* **101**:13495-500, 2004.
5. Zhou H, Ivanov VN, Lien YC, Davidson M and Hei TK. Mitochondrial function and nuclear factor-kappaB-mediated signaling in radiation-induced bystander effects. *Cancer Res* **68**:2233-40, 2008.
6. Zhou H, Randers-Pehrson G, Waldren CA, Vannais D, Hall EJ and Hei TK. Induction of a bystander mutagenic effect of alpha particles in mammalian cells. *Proc Natl Acad Sci USA* **97**:2099-104, 2000. ■

# Role of Succinate Dehydrogenase C in Radiation Induced Bystander Effect

*Hongning Zhou, Vladimir N. Ivanov and Tom K. Hei*

Radiation induced bystander effects have been well documented in both rodent and human cells,[1, 2] and gap junction cell-cell communication, free radicals, and soluble factors released from irradiated cells are involved in the process. However, the precise mechanism(s) of this phenomenon is still not clear. It is likely that a combination of pathways involving both primary and secondary signaling processes is involved in producing a bystander effect. Our previous studies indicated that mitochondria might play an important role in the regulation of radiation-induced bystander effects.[3] Mitochondria are the main source of energy production as well as generators of free radicals in cells. Recently researchers found that mutation of succinate dehydrogenese subunit C (*SDHC*), an integral membrane protein in complex II of the electron transport chain, resulted in increased superoxide, oxidative stress, apoptosis, tumorigenesis, and genomic instability,[4, 5] indicating that SDHC plays a critical role in maintaining mitochondrial function.

In the present study, to determine the role of *SDHC* in the radiation induced bystander effect, the newly designed strip mylar dishes were used as described before.[6] Briefly, two concentric stainless steel rings were fitted with mylar bottoms with the outer and inner rings covered by a 6 μm- and 38 μm-thick mylar sheet, respectively. The thicker mylar sheet of the inner ring was sliced into strips. Exponentially growing B1 and B9 (*SDHC* mutated) Chinese hamster lung fibroblast cells were plated in the concentric strip dishes the day before irradiation to ensure a confluent state.

**Table 1.** Assessment of mitochondrial membrane potential (ΔΨm) and superoxide production in B1 and B9 cellsusing flow cytometry.

| | intracellular superoxide content (mean intensity, A.U.) | mitochondrial membrane potential (mean intensity, A.U.) |
|---|---|---|
| B1 | 18.64 | 169.95 |
| B9 | 98.76 | 490.72 |

Since the cells seeded on the 38μm thick mylar strips would not be irradiated due to the short penetrating distance of the alpha particles, these cells would effectively become the bystander cells, being seeded right next to cells plated on the 6 μm mylar dishes that were directly irradiated. A 50cGy dose of $^4$He ions (120keV/μm) was delivered to the B1 and B9 cells at the Radiological Research Accelerator Facilities of Columbia University. After irradiation, at selected time points, the inner and outer mylar dishes were separated and the cells from each growth surface were trypsinized, then individually pooled for endpoint analysis.

When the cells were stained with the mitochondrial membrane potential probe, DiOC6, B9 cells showed an increase in fluorescence intensity relative to B1 cells (Table 1). Likewise, B9 cells showed an increase in intracellular superoxide content when compared with B1 cells. Exposure of B1 cells to a dose of 0.5Gy alpha particles increased the bystander *HPRT*$^-$ mutant yield to a level 1.4 times higher than the background incidence. However, under similar irradiation conditions, B9 cells had a bystander mutant fraction that was 5.5 fold higher than non-irradiated B9 cells (Fig. 1). The

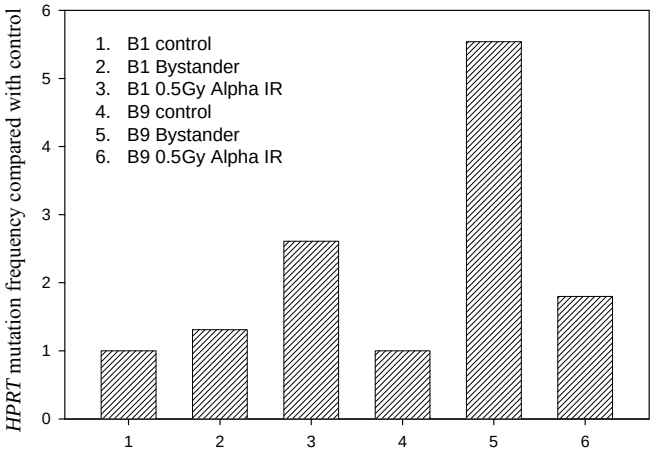


**Fig. 1.** *HPRT*$^-$ mutation of bystander and directly irradiated B1 and B9 cells exposed to a 0.5Gy dose of alpha particles using the specially designed strip dishes.

preliminary data also showed that pretreatment with DMSO or L-NMMA can significantly decrease bystander mutagenesis in B9 cells. Further experiments are ongoing to investigate how SDHC mutation can alter bystander mutagenesis.

**Acknowledgments**

This research was supported by funding from the National Institutes of Health Grants CA 49062, ES 12888. The Radiological Research Accelerator Facility (RARAF) is an NIH supported Resource Center through grants EB-002033 (NIBIB) and CA-37967 (NCI).

**References**

1. Morgan WF. Non-targeted and delayed effects of exposure to ionizing radiation: I. Radiation-induced genomic instability and bystander effects *in vitro*. *Radiat Res* **159**:567-80, 2003.
2. Hei TK, Persaud R, Zhou H and Suzuki M. Genotoxicity in the eyes of bystander cells. *Mutat Res* **568**:111-20, 2004.
3. Zhou H, Ivanov VN, Lien YC, Davidson M and Hei TK. Mitochondrial function and nuclear factor-kappaB-mediated signaling in radiation-induced bystander effects. *Cancer Res* **68**:2233-40, 2008.
4. Slane BG, Aykin-Burns N, Smith BJ, Kalen AL, Goswami PC, Domann FE and Spitz DR. Mutation of succinate dehydrogenase subunit C results in increased $O_2^{\cdot-}$, oxidative stress, and genomic instability. *Cancer Res* **66**:7615-20, 2006.
5. Ishii T, Yasuda K, Akatsuka A, Hino O, Hartman PS and Ishii N. A mutation in the SDHC gene of complex II increases oxidative stress, resulting in apoptosis and tumorigenesis. *Cancer Res* **65**:203-9, 2005.
6. Zhou H, Ivanov VN, Gillespie J, Geard CR, Amundson SA, Brenner DJ, Yu Z, Lieberman HB and Hei TK. Mechanism of radiation-induced bystander effect: role of the cyclooxygenase-2 signaling pathway. *Proc Natl Acad Sci USA* **102**:14641-6, 2005. ■

# A Role of IGFBP3 in Modulation of α-Radiation-Induced Bystander Signaling Pathways Followed by TRAIL-Mediated Apoptosis in Human Skin Fibroblasts

*Vladimir N. Ivanov, Hongning Zhou and Tom K. Hei*

Our previous investigations demonstrated an important role of mitochondria in radiation-induced bystander effects, partially through mitochondria-dependent regulation of NF-κB--COX2 and NF-κB--iNOS pathways in normal human fibroblasts.[1] Our next task was to determine effects of the primary α-irradiation-induced signaling pathways and the secondary bystander signaling pathways on general cell survival and an induction of programmed cell death via apoptosis in human fibroblasts. We used in this study mitochondrial DNA-depleted skin fibroblasts ($\rho^0$) and their parental human skin fibroblasts (HSF) with functional mitochondria ($\rho^+$). Figure 1A and B demonstrate the absence of mitochondrial DNA and a strong downregulation of oxygen consumption in $\rho^0$ cells. Alpha-irradiation of $\rho^0$ cells induced more pronounced G2/M arrest of the cell cycle compared to $\rho^+$ cells (Fig. 1C). As expected, induction of apoptosis via the intrinsic mitochondrial pathway using treatment with PI3-K--AKT inhibitor LY294002 (50μM) and sodium arsenite (5μM) alone in combination with α-radiation was substantially suppressed in $\rho^0$ cells (Fig. 1D). On the other hand, levels of TRAIL-R2/DR5 were similar in both HSF $\rho^0$ and $\rho^+$ cells. For a different cell system, small aeroepithelial cells (SAEC), ρ0 cells demonstrated even a small additional increase in DR5 surface expression (Fig. 2A). (TRAIL+CHX)-mediated apoptosis was substantially higher for $\rho^0$ cells, compared to the parent cell lines (Fig. 2B and data not shown) indicating, probably, a decreased efficacy of protein against TRAIL-mediated apoptosis in mitochondria-deficient cells. The nature of this attenuated protection against receptor-mediated apoptosis in $\rho^0$ cells is well correlated with decreased basal and induced NF-κB activity in these cells, compared to parental fibroblasts.[1]

Since activation of the ATM-p53 and ATM-NF-κB pathways with the subsequent upregulation of expression of the p53- and NF-κB-regulated genes is a hallmark of the cell radiation response,[2] we determined expression levels and activation of proteins involved in these cascades in directly α-irradiated and bystander human skin fibroblasts 24 h after irradiation when bystander effects were completely exhibited (Fig. 3). At this time point, cell bystander response included activation of ATM-p53-BAX, activation of AKT with a partial suppression of FOXO3A phosphorylation, while for directly irradiated cells these activities, especially p53 phosphorylation, were already declined (Fig. 3). Surprisingly, there were no well pronounced differences between $\rho^0$ and $\rho^+$ cells in the bystander response for the investigated protein levels, besides the previously observed partial downregulation of NF-κB--COX2 in mitochondria-deficient

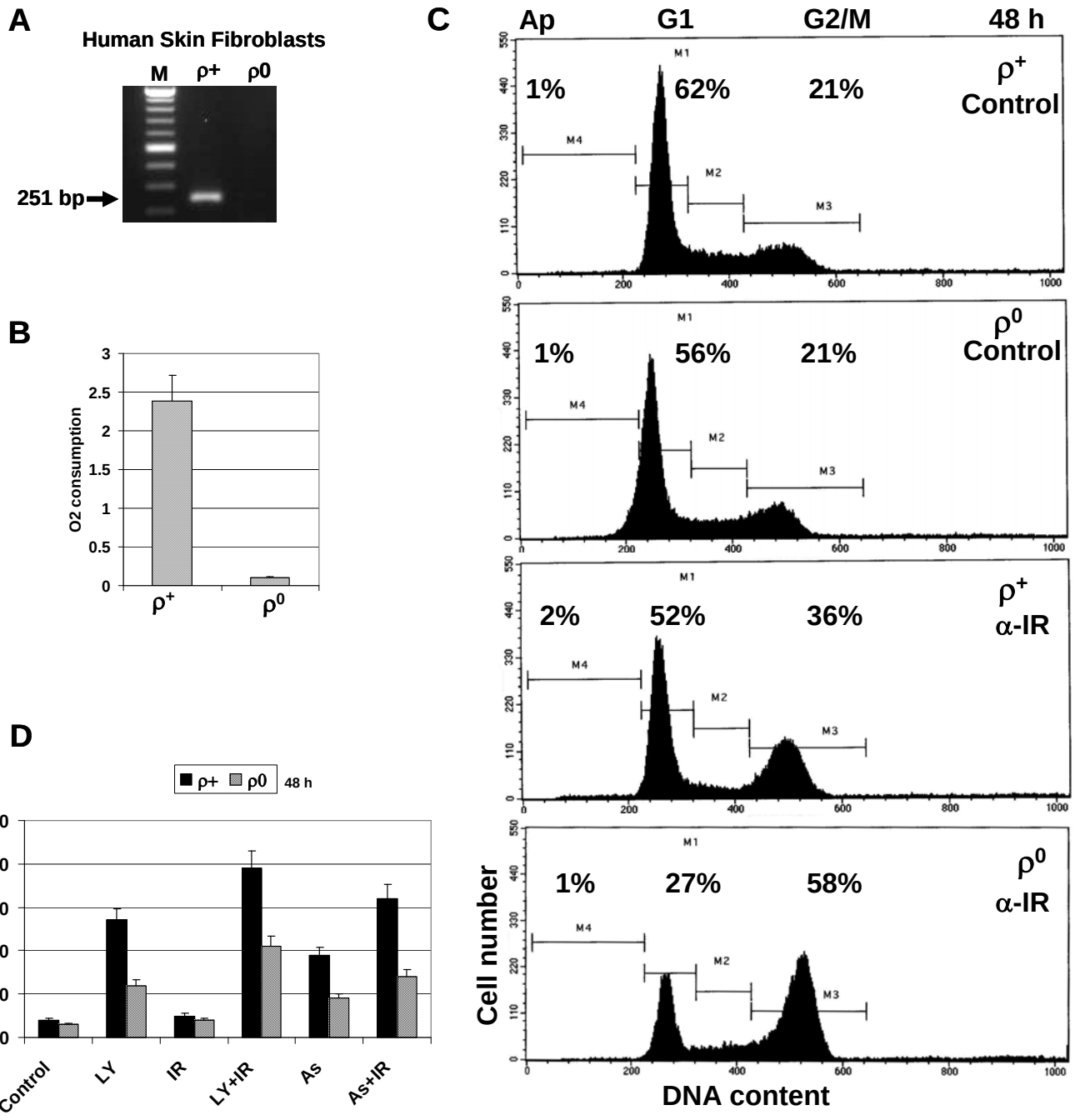


**Fig. 1.** Cell cycle and apoptotic analysis of mitochondrial DNA-depleted human skin fibroblasts ($\rho^0$) and their parental cells ($\rho^+$). **A.** PCR amplification of genomic DNA from $\rho^0$ and $\rho^+$ cells: a 251bp DNA fragment is characteristic for mitochondrial DNA. **B.** Rates of oxygen consumption for $\rho^0$ and $\rho^+$ cells. **C**. Cell cycle analysis of $\rho^0$ and $\rho^+$ cells 48 h after α-irradiation (0.5Gy). **D**. Apoptosis analysis of $\rho^0$ and $\rho^+$ cells treated with LY294002 (50μM), sodium arsenite (5μM), α-irradiation (0.5Gy) alone or in combinations. 48h after treatment, cells were stained with PI and apoptotic levels were determined by FACS analysis.

cells.[1] An additional exemption was IGFBP3 endogenous expression that was permanently downregulated in $\rho^0$ cells, while it was quite high in both control and irradiated parental fibroblasts, but strongly decreased in parental bystander cells. On the other hand, at least one remarkable change was observed for directly irradiated $\rho^0$ cells compared to the parental cells, a strong downregulation of XIAP levels (Fig. 3), which is a critical regulator of antiapoptotic activity in the cell.

Since endogenous IGFBP3 levels were decreased in bystander fibroblasts, we elucidated effects of exogenous IGFBP3, which was added to the culture medium, on cell signaling and apoptosis. IGFBP3 is the major member of the insulin-like growth factor binding protein (IGFBP) family. The protein forms a ternary complex with insulin-like growth factor acid-labile subunit (IGFALS) and either

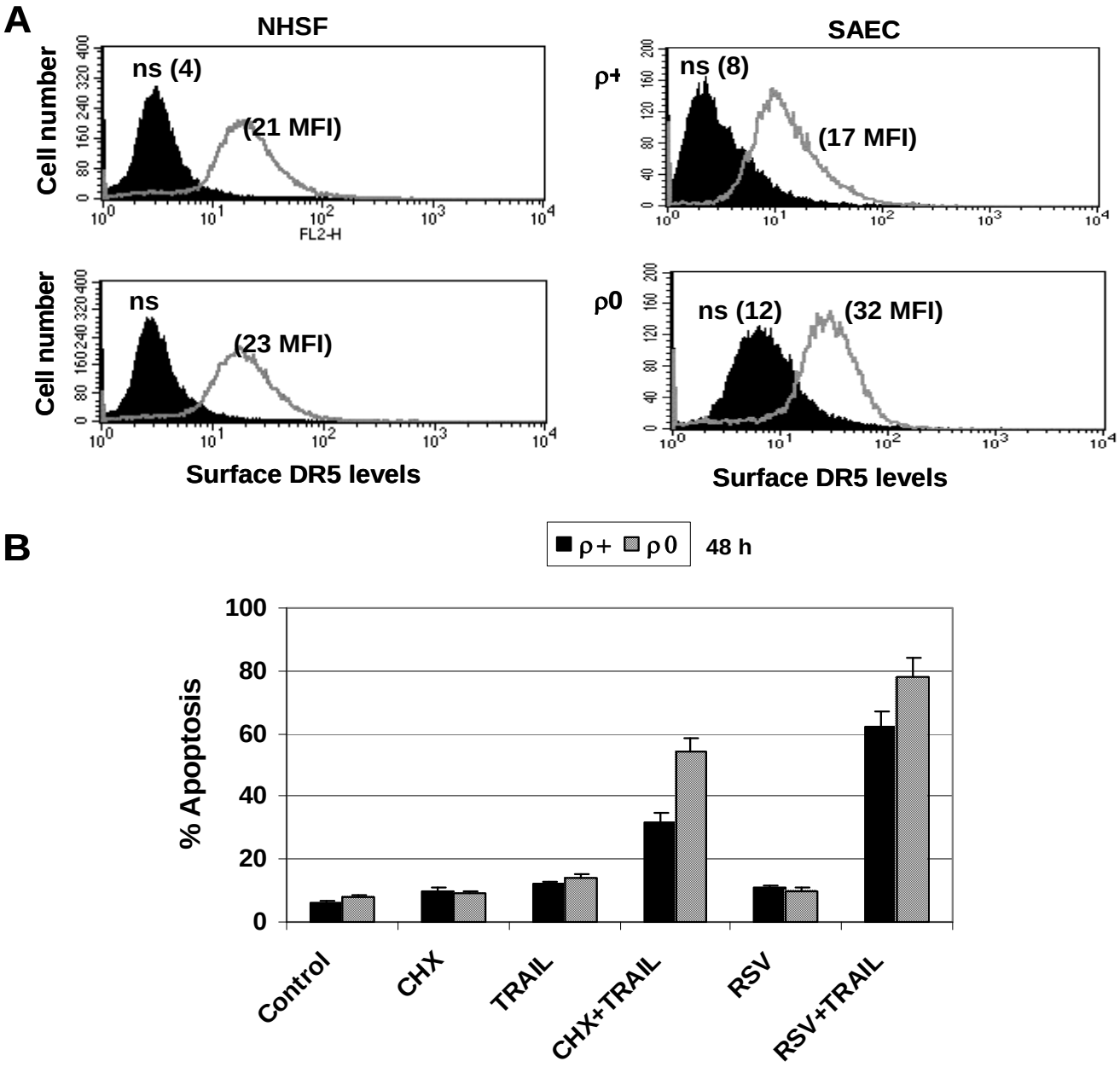


**Fig. 2. A**. Surface expression of TRAIL-R2/DR5 was determined using immunostaining and FACS analysis of ($\rho^0$) and their parental cells ($\rho^+$) for two cell systems, HSF and SAEC. Medium fluorescent intensity (MFI) is indicated. **B.** Apoptosis levels induced by TRAIL (50 ng/ml) and cycloheximide (CHX, 2 μg/ml) or TRAIL and resveratrol (RSV, 50μM) in mitochondrial DNA-depleted human skin fibroblasts ($\rho^0$) and their parental cells ($\rho^+$).

insulin-like growth factor (IGF) I or II. Such relations, prolonging the half-life of IGFs and altering their interaction with cell surface receptors may have very different effects on acute and continuous responses induced by IGF in target cells.[3] IGFBP3 was also described as an accelerator of TRAIL-mediated apoptosis in some human cancer cell lines.[4] In skin fibroblasts, exogenous IGFBP3 (100 ng/ml) upregulated the AKT-GSK-β-catenin pathway in control and irradiated cells, but moderately decreased activation of NF-κB in both irradiated and bystander cells. COX-2 expression levels (a target of the NF-κB and β-catenin pathways) and p21 expression levels (a target of ATM-p53) were substantially declined (Fig. 4). For $\rho^0$ cells, such changes were even more pronounced (data not shown). Quite surprisingly, IGFBP3 upregulated TRAIL-mediated apoptosis only in control non-irradiated cells, but decreased apoptosis levels in both irradiated and bystander cells 24 h after treatment. Such effects were observed for both $\rho^+$ and $\rho^0$ cells (Fig. 5). 48 h after treatment this effect was well pronounced only for parental cells. The data obtained have established new interesting correlations in the regulation of cell signaling and apoptotic pathways by IGFBP3 via regulation of COX-2 expression in normal skin fibroblasts. This hypothesis is under active investigation in our laboratory. The most important task is to find differences in the IGFBP3-induced signaling pathways in normal and cancer cells.

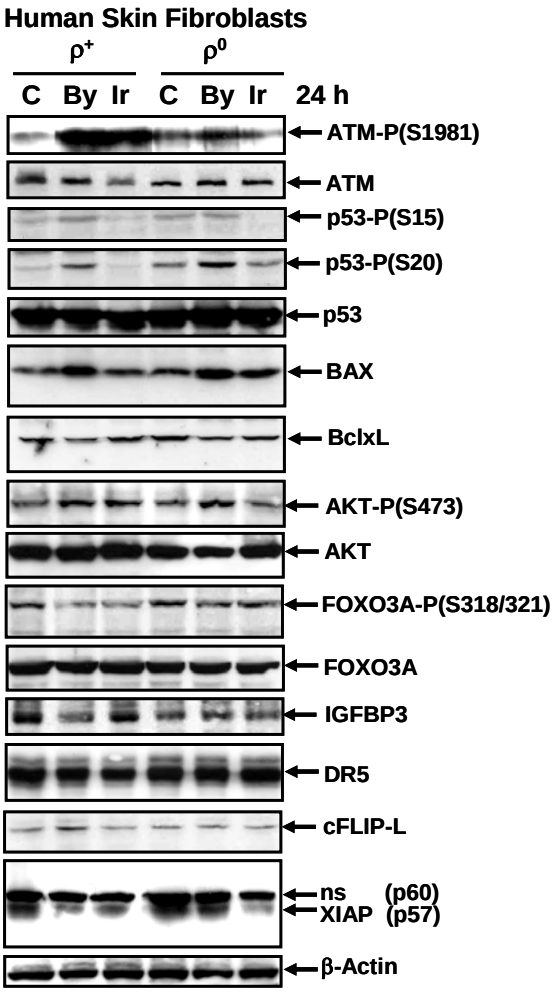


**Fig. 3.** Western blot analysis of indicated proteins in $\rho^0$ and $\rho^+$ cells (HSF) 24 after treatment. Non-treated control, bystander and α-irradiated cells were isolated, as previously described.[1]

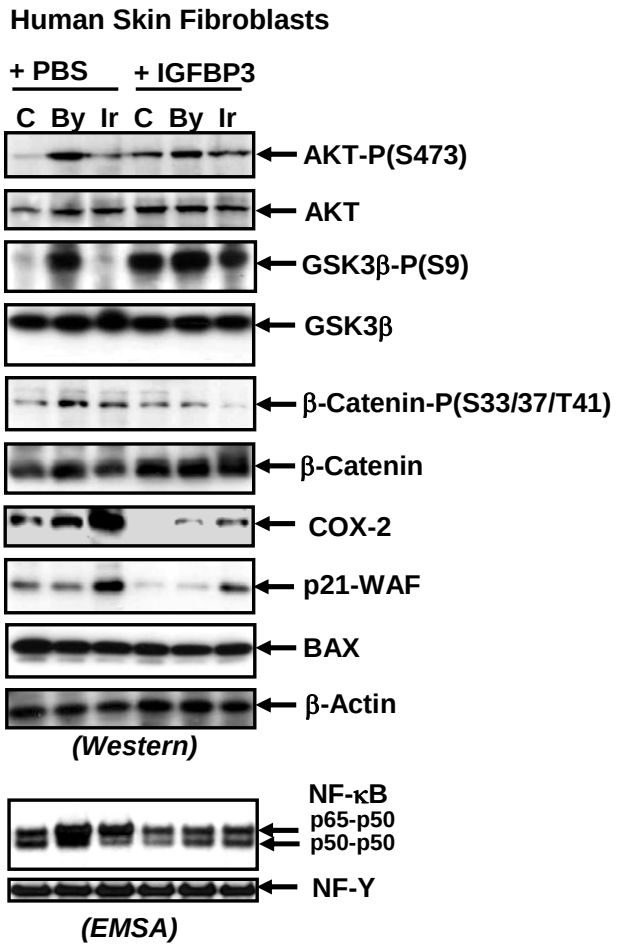


**Fig. 4.** Effects of IGFBP3 (100 ng/ml) on expression levels of indicated proteins from the control, bystander and α-irradiated HSF were determined 24 h after treatment by Western blot analysis or by EMSA, only for NF-κB and NF-Y transcription factors.

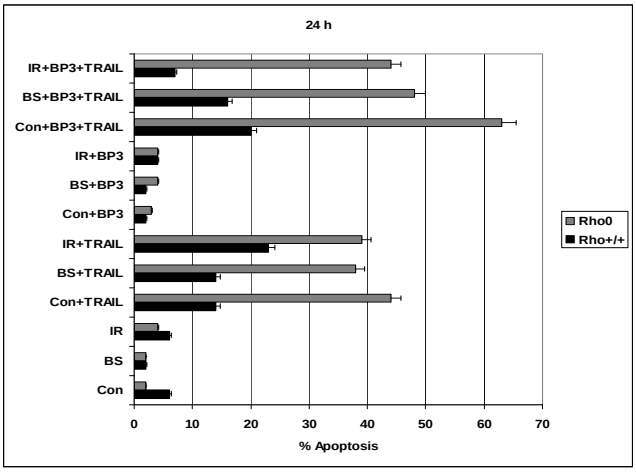


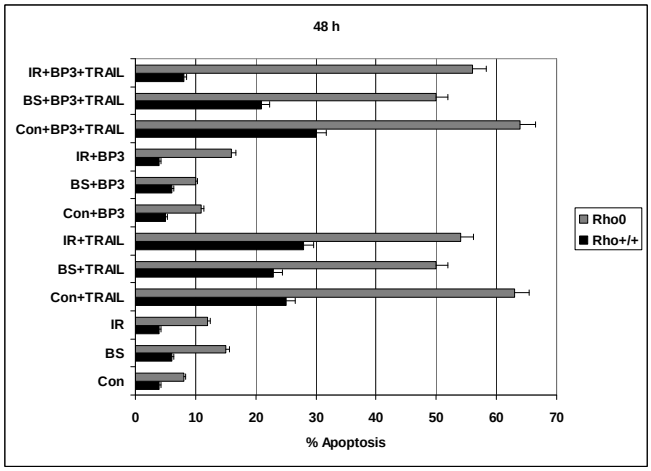


**Fig. 5. A**. Effects of IGFBP3 on TRAIL-mediated apoptosis proteins in $\rho^+$ and $\rho^0$ cells (HSF) 24 and 48 after treatment with indicated combinations. Non-irradiated control, bystander and α-irradiated cells (0.5Gy) were isolated, as previously described. TRAIL (50 ng/ml) was used in combination with CHX (2 μg/ml). After treatment (24 h and 48 h), cells were stained with PI and apoptotic levels were determined by FACS analysis.

**References**

1. Zhou H, Ivanov VN, Lien YC, Davidson M and Hei TK. Mitochondrial function and nuclear factor-kappaB-mediated signaling in radiation-induced bystander effects. *Cancer Res* **68**:2233-40, 2008.
2. Shiloh Y. The ATM-mediated DNA-damage response: taking shape. *Trends Biochem Sci* **31**:402-10, 2006.
3. Pollak M. Insulin and insulin-like growth factor signalling in neoplasia. *Nat Rev Cancer* **8**:915-28, 2008.
4. Williams AC, Smartt H, AM HZ, Macfarlane M, Paraskeva C and Collard TJ. Insulin-like growth factor binding protein 3 (IGFBP-3) potentiates TRAIL-induced apoptosis of human colorectal carcinoma cells through inhibition of NF-kappaB. *Cell Death Differ* **14**:137-45, 2007. ■

# Differential Expression of p53 Related Genes In Irradiated and Bystander Cell Populations

*Shanaz A. Ghandhi and Sally A. Amundson*

We are studying the gene expression response of human lung diploid fibroblasts IMR-90 to alpha particle irradiation. In our studies, we employed a global genomic approach to identify genetic changes at the level of mRNA in irradiated and bystander cells that were exposed to 0.5 Gy alpha particles. In a recently published study,[1] we have discussed the gene response in human cells to irradiation and more significantly the responses of bystander cells that were in shared medium and in contact with directly irradiated cells. Changes in mRNA expression levels were measured at 4 hours after irradiation and differentially expressed genes were analyzed using gene annotation ontology tools and pathway analysis for significant networks. These approaches allowed us to draw out significant functional groups of genes that were related by strict rules of annotation from the lists of changed genes.[2] In order to do this we imported lists of differentially expressed genes into the PANTHER online tool (www.pantherdb.org/). Requiring a false discovery rate of less than 10%, we queried lists of 197 genes and 137 responding genes in irradiated and bystander cells respectively, against the number of genes from the NCBI human genome in each functional category. This test measures the over-representation of pathways or biological processes among the genes responding to direct or bystander irradiation, and uses Bonferroni corrected p-values to assess the significance of that category. This analysis revealed that the most significant categories of genes affected in irradiated cells at 4hr after treatment were the p53 pathway (p-value $3.9 \times 10^{-3}$) and apoptosis signaling (p-value $3.5 \times 10^{-4}$). In contrast, gene expression changes in bystander cells at 4hrs were most significant in the inflammation pathway (p-value $6.4 \times 10^{-4}$) and p53 pathway genes were not scored as significant by this analysis.

Further analysis was done using the Ingenuity Pathway analysis (IPA) tool.[3] The gene lists and fold change in expression level were imported into IPA for analysis. A dataset containing gene (and/or chemical) identifiers such as platform specific probe identifiers and corresponding expression values was uploaded into the application. Each identifier in the gene lists was mapped to its corresponding gene or protein in the Ingenuity knowledge base. A 2-fold cutoff was set to identify genes whose expression was significantly differentially regulated. These genes, called focus genes, were overlaid onto a global molecular network developed from information contained in the Ingenuity knowledge base. Networks of these focus genes were then algorithmically generated based on their connectivity. The genes were analyzed as networks and pathways and scored using the Fisher exact test to calculate p-values for likelihood of belonging to a particular network and not being due to chance alone. In our analyses we found that the top scoring pathways in the irradiated cells belonged to p53 signaling (p-value $7X10^{-8}$) and NFκB signaling (p-value $4.4X10^{-3}$). In bystander cells the NFκB signaling pathway (p-value $4X10^{-8}$) was the most significant group of genes that showed changes in gene expression. The NFκB pathway was represented in the network analysis for both irradiated and bystander cells at 4hr after treatment, in the inflammation and cell-to-cell signaling and function network. This was the top scoring network in both conditions (p-values of $10^{-45}$ in irradiated and $10^{-48}$ in bystanders).

**Pathway analysis of cell-to-cell signaling between irradiated and bystander cells**

In order to understand the nature of signaling between irradiated and bystander cells at the early, 4hr time point after irradiation, we used another tool of the pathway analysis program to grow out a network of genes that were directly and indirectly, upstream and downstream of the transcriptional regulator molecule TP53 (Fig. 1) We selected genes from the irradiated group that were identified by the ingenuity pathway knowledge base (IPKB), the curated scientific findings which form the basis of IPA, as connected with TP53 and built a network (Fig. 1). The genes that encode extracellular compartment proteins are listed in Table 1 with corresponding gene expression changes. These genes are of

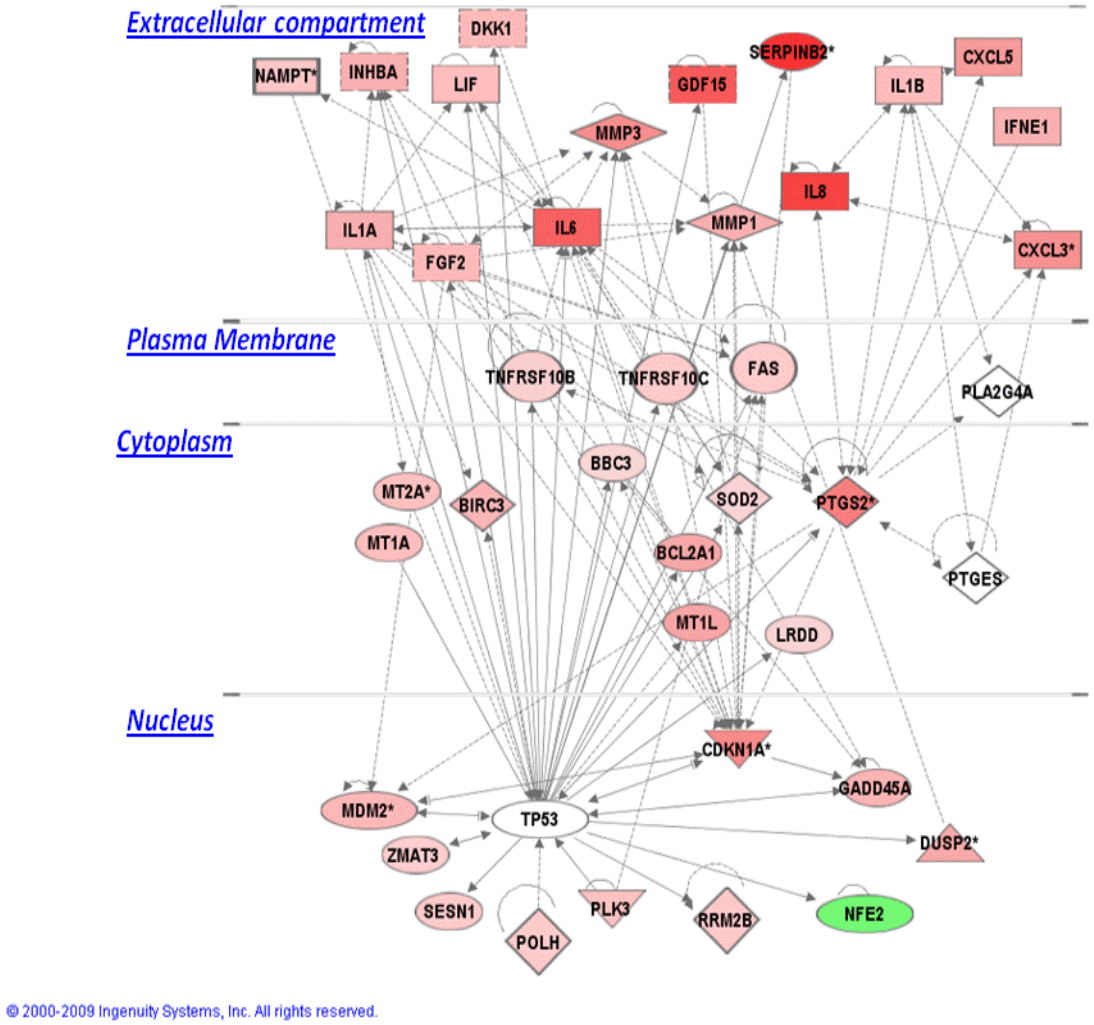




**Fig. 1. Network of p53 related genes grown from differentially expressed genes overlaid with expression levels in irradiated cells.** The diagram shows different compartments of the cell in which nodes represent proteins (in corresponding cellular compartments). Nodes are colored as red for up-regulated, green for down-regulated and white for unchanged mRNA levels. Solid lines represent a direct binding between the entities: DNA binding, protein-protein binding. Dashed lines represent indirect effects between genes and proteins, where physical contact between molecules is not a criterion. Arrow heads show direction of the effect.

**Table 1.** p53 related genes encoding proteins of the extracellular compartment of irradiated cells

| SYMBOL | NAME | FOLD CHANGE |
|---|---|---|
| **SERPINB2** | serpin peptidase inhibitor (ovalbumin), member 2 | 9.1 |
| **GDF15** | growth differentiation factor 15 | 7.3 |
| **IL6** | interleukin 6 (interferon, beta 2) | 7.0 |
| **MMP3** | matrix metallopeptidase 3 (stromelysin 1, progelatinase) | 5.0 |
| **IL1A** | interleukin 1, alpha | 3.5 |
| **MMP1** | matrix metallopeptidase 1 (interstitial collagenase) | 3.5 |
| **INHBA** | inhibin, beta A | 3.4 |
| **FGF2** | fibroblast growth factor 2 (basic) | 3.0 |
| **DKK1** | dickkopf homolog 1 | 3.0 |
| **LIF** | leukemia inhibitory factor | 2.9 |
| **NAMPT** | nicotinamide phosphoribosyltransferase | 2.5 |

**Note**: Genes are listed in order of gene expression change from highest to lowest; all genes are up-regulated.

particular interest because a major component of irradiated to bystander cell-to-cell signaling occurs in the inter-cellular medium and matrix compartment.

As seen in Figure 1, in the nuclear compartment, there were a number of genes encoding nuclear proteins that are known targets of p53 transcriptional regulation, which were selected by our network growing approach. In our previous analyses of networks[1], we showed that although there was differential regulation of some p53 related genes in bystander cells, there was a dampening of the p53 response in bystander cells. Further categorization of the genes by sub-cellular localization shows that this effect is primarily in the nuclear compartment of bystander cells and in targets of p53 involved in DNA damage and cell cycle response (compare nuclear compartments of Figure 1 and 2). This suggests that p53 does not have the same role in regulating the response of bystander cells as it does in the response to direct irradiation. This analysis also shows that the extra-cellular compartments of both cell populations are enriched for cell-to-cell signaling genes whose expression pattern may be the result of both p53-dependent and independent pathways.

In our study, we have used a whole genome expression approach to analyze the mRNA interactome of bystanders in the context of irradiated cells. The main goal of this approach was to understand the possible pathways that lead to gene expression changes in bystanders that are critical for the response. In a previous study, the cyclooxygenase-2 enzyme (PTGS2) was identified as having a crucial role in the bystander effect.[4] This gene (and its encoded protein) was a good candidate for pathway analysis in which we looked for extracellular signals generated by irradiated cells that could lead to the up-regulation of a central player in the bystander response. Enzymatic activity of PTGS2 results in the over-production of prostaglandin E2 and stimulation of surrounding cells. Additionally, specific drugs against PTGS2, such as NS-398 reduce the bystander response.[4] We have also found this gene to respond dramatically in both irradiated and bystander cells at the mRNA level.[1]

Using the network approach, as seen in Figure 1, to grow relationships (edges) between entities (nodes), and focusing on p53 as the major pathway induced in irradiated cells, there are multiple candidate inducers of *PTGS2* expression

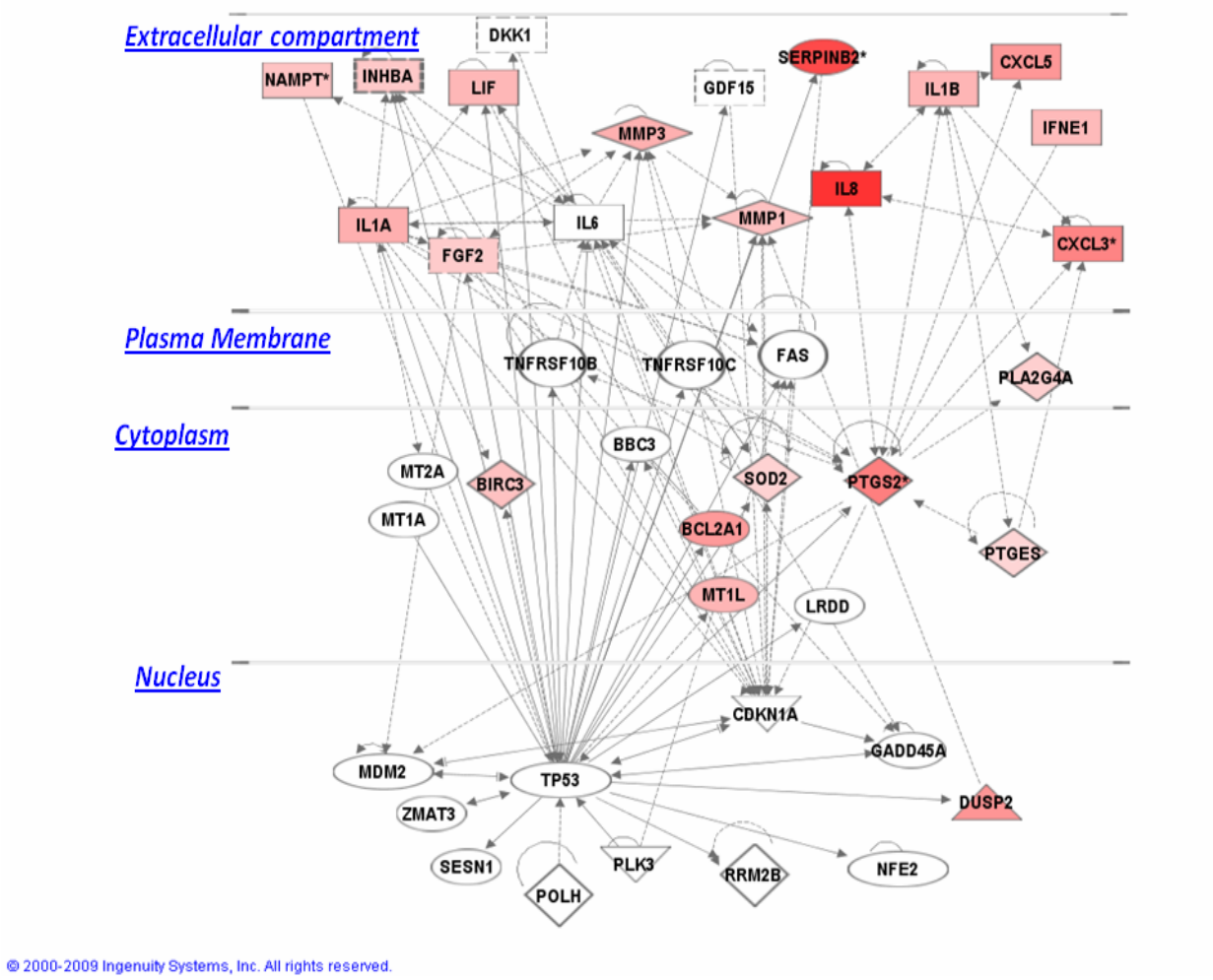


**Fig. 2. Network of p53 related genes grown from differentially expressed genes overlaid with expression levels in bystander cells.** The diagram shows different compartments of the cell in which nodes represent proteins (in corresponding cellular compartments). Nodes are colored as red for up-regulated, green for down-regulated and white for unchanged mRNA levels. Solid lines represent a direct binding between the entities: DNA binding, protein-protein binding. Dashed lines represent indirect effects between genes and proteins, where physical contact between molecules is not a criterion. Arrow heads show direction of the effect.

**Table 2.** Genes encoding extracellular proteins that are differentially expressed in bystander cells

| SYMBOL | NAME | FOLD CHANGE |
|---|---|---|
| **IL8** | interleukin 8 | 10.4 |
| **SERPINB2** | serpin peptidase inhibitor (ovalbumin) | 9.2 |
| **CXCL3** | chemokine (C-X-C motif) ligand 3 | 6.2 |
| **CXCL5** | chemokine (C-X-C motif) ligand 5 | 5.3 |
| **IL1A** | interleukin 1, alpha | 4.0 |
| **MMP3** | matrix metallopeptidase 3 (stromelysin 1, progelatinase) | 4.0 |
| **IL1B** | interleukin 1, beta | 3.7 |
| **LIF** | leukemia inhibitory factor | 3.6 |
| **IFNE1** | interferon, epsilon | 3.5 |
| **MMP1** | matrix metallopeptidase 1 (interstitial collagenase) | 3.2 |
| **NAMPT** | nicotinamide phosphoribosyltransferase | 3.1 |
| **INHBA** | inhibin, beta A | 2.8 |
| **FGF2** | fibroblast growth factor 2 (basic) | 2.6 |

**Note**: Genes are listed in decreasing order of gene expression change from highest to lowest, all genes are up-regulated. Underlined genes are unrelated to the p53 network.

in both irradiated and bystander cells. There are many signals released from irradiated cells, such as *IL6*, *IL1A* and *FGF2* that appear to feed into *PTGS2* expression. We then queried whether there were signals feeding into *PTGS2* induction, within bystander cells. In order to do this we grew out the network from *PTGS2*, selecting for directly and indirectly related genes in bystander cells. The subset of genes encoding extracellular proteins with corresponding changes in gene expression are listed in Table 2. Some of these genes, such as *IL8*, *CXCL3*, *CXCL5*, *IFNE1* and *IL1B*, were unrelated to p53, but were selected by the grow tool as possible regulators of *PTGS2*. This suggests that the extracellular messages from irradiated and un-irradiated bystander cells are the result of complex intra-cellular signals and contributions of two or more signaling networks. Although the genes included in these pathway analyses are not inclusive, by focusing on the role of p53 in irradiated and bystander cells, we can see there are major differences in the two cell populations. This could also be the outcome of studying only one time point after treatment. Extending our analyses to other time points for a limited set of genes[1] has shown that that there may be a close interaction between the networks of genes regulated both by NFκB and p53. Genes that respond to ionizing radiation in a p53-dependent fashion, such as *CDKN1A, GADD45A, MDM2, SESN1* or *PLK3*, show a larger response in irradiated cells, but genes that may be downstream of both transcription factors respond similarly in both irradiated and bystander cells.

In conclusion, using pathway tools such as IPA results in better visualization of possible interactions among responding genes and a clearer categorization of possible signaling mechanisms by analyzing top networks and pathways. However, the role of individual pathways, genes and encoded proteins must be tested to ascertain how critical they are to the bystander response.

## References


1. Ghandhi SA, Yaghoubian B and Amundson SA. Global gene expression analyses of bystander and alpha particle irradiated normal human lung fibroblasts: Synchronous and differential responses. *BMC Med Genomics* **1**:63, 2008.
2. Thomas PD, Campbell MJ, Kejariwal A, Mi H, Karlak B, Daverman R, Diemer K, Muruganujan A and Narechania A. PANTHER: a library of protein families and subfamilies indexed by function. *Genome Res* **13**:2129-41, 2003.
3. Ingenuity Pathways Analysis (Ingenuity Systems®, www.ingenuity.com).
4. Zhou H, Ivanov VN, Gillespie J, Geard CR, Amundson SA, Brenner DJ, Yu Z, Lieberman HB and Hei TK. Mechanism of radiation-induced bystander effect: role of the cyclooxygenase-2 signaling pathway. *Proc Natl Acad Sci USA* **102**:14641-6, 2005. ■

# TGFBI Deficiency Predisposes Mice to Spontaneous Tumor Development

*Ye Zhang, Gengyun Wen, Genze Shao, Chyuansheng Lin,[a] Adayabalam S. Balajee Govind Bhagat,[b] Tom K. Hei and Yongliang Zhao*

Tumor growth and metastasis is a multistep process involving cell adhesion, proteolytic enzyme degradation of the extracellular matrix (ECM) and motility factors that influence cell migration.[1, 2] Integrins are cell surface adhesive receptors composed of α- and β-chain heterocomplexes. Both subunits transverse the membrane and mediate the physical and functional interactions between cell and its surrounding ECM, thus serving as bidirectional transducers of extra- and intracellular signals which ultimately lead to regulation of adhesion, proliferation, differentiation, antiapoptosis and tumor progression.[3, 4]

*TGFBI* was first identified in a human lung adenocarcinoma cell line (A549) treated with TGF-β.[5] This gene encodes a highly conserved 683 amino-acid protein that contains a secretary signal sequence and four internal homologous domains, the last of which contains a RGD (Arg-Gly-Asp) motif which can serve as a ligand recognition site for integrins.[5] TGFBI product has been shown to be a component of ECM in lung and mediate cell adhesion and migration through interacting with integrin via integrin receptors: α3β1, αvβ3, and αvβ5.[6-10] It is ubiquitously expressed in human normal tissues; however, downregulation or lost expression of this gene has been found in a list of human tumor cell lines including lung, breast, colon, prostate, and leukemia as well as in human primary lung and breast tumor specimens.[11-14] CpG island hypermethylation in the promoter region, one of the mechanisms by which tumor suppressor genes are inactivated in human cancers, correlates with the silencing of *TGFBI* promoter and its subsequent down-expression.[15] *In vitro* studies have implicated its role in maintaining microtubule stability, and inhibiting tumorigenicity and tumor angiogenesis,[12, 13, 16-19] suggesting a tu-

[a] *Herbert Irving Comprehensive Cancer Center, Columbia University, NY*

[b] *Department of Clinical Pathology, Columbia University, NY*

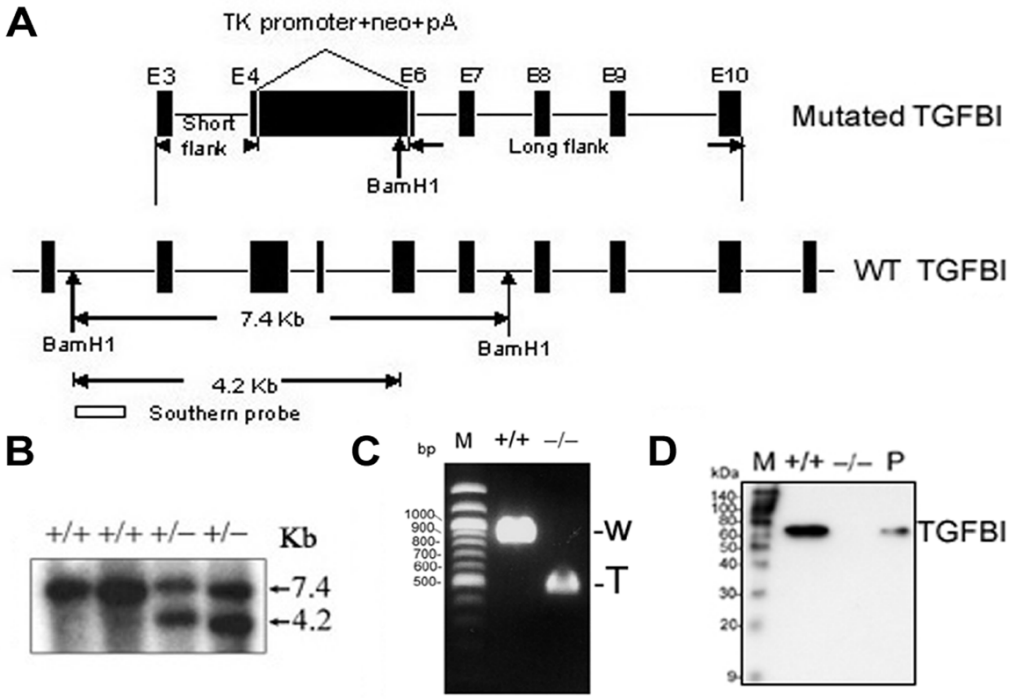


**Fig. 1.** Targeted disruption of *TGFBI* in mice. **A**.Strategy for generating the targeted *TGFBI* allele. Exons 4-6 were replaced by neomycin-resistance cassette (neo) with introduction of one BamH1 restriction site at 3' terminal. Targeting construct and wild type allele are shown. Successful targeting will yield a 4.2 kb BamH1-restricted fragment in the neo allele. **B.** Germinal transmission of the targeted *TGFBI* allele was identified by Southern blot. **C.** Identification of deletion of exons 4-6 in KO MEFs by RT-PCR using a pair of primers specific for the upstream and downstream regions of exons 4-6. W: wild type; T: truncated. **D.** Western blot of conditioned medium prepared from MEFs with indicated genotypic backgrounds. Mouse *TGFBI* recombinant protein was used as positive control (P).

mor suppressor function *in vivo*. To test this hypothesis, we have generated a *TGFBI*-null mouse model. The results demonstrated, for the first time, that *TGFBI* loss promotes cell proliferation and predisposes mice to spontaneous tumor development.

**Tumor development in mice lacking the *TGFBI* gene**

To explore the physiological function of *TGFBI* and its role in tumorigenesis, *TGFBI*-deficient mice were generated by targeted homologous recombination. The correct targeting resulted in replacement of exons 4-6 of the *TGFBI* gene in mice with a neomycin-resistance gene (Fig. 1A) and was identified by Southern analysis (Fig. 1B). $TGFBI^{-/-}$ MEFs still expressed *TGFBI* mRNA but the level was about six-fold lower than in wild type MEFs (data not shown). Moreover, deletion of exons 4-6 in $TGFBI^{-/-}$ MEFs was demonstrated by RT-PCR (Fig. 1C), and absence of TGFBI protein was revealed by Western blot (Fig. 1D). $TGFBI^{-/-}$ mice arose from crosses of $TGFBI^{+/-}$ mice at expected Mendelian frequency and showed a slower postnatal development with a 13.5 ± 3% lower body weight than that of sex-matched $TGFBI^{+/+}$ littermates from 2- to 6-months of age (n=10) (Fig. 2). Histological surveys of liver, lung, kidney, stomach, intestine and testis (n=10 per genotype, age 26 weeks) did not reveal morphological abnormalities. However, 2/10 $TGFBI^{-/-}$ mice showed splenomegaly that was identified as B cell hyperplasia (Data not shown).

To assess the tumor-suppressor activity of *TGFBI in vivo*, a large cohort of $TGFBI^{-/-}$ (n=54), $TGFBI^{+/-}$ (n=75) and $TGFBI^{+/+}$ (n=48) animals generated from crosses of $TGFBI^{+/-}$ mice were observed for the development of spontaneous malignancies for up to 20 months. Mice were sacrificed for complete necropsies either at earlier times due to clinical features of systemic illness (weight loss, inactivity, ruffling of fur, and hunched posture) or when reaching the end of the observation period. From ages of 9 to16 months,

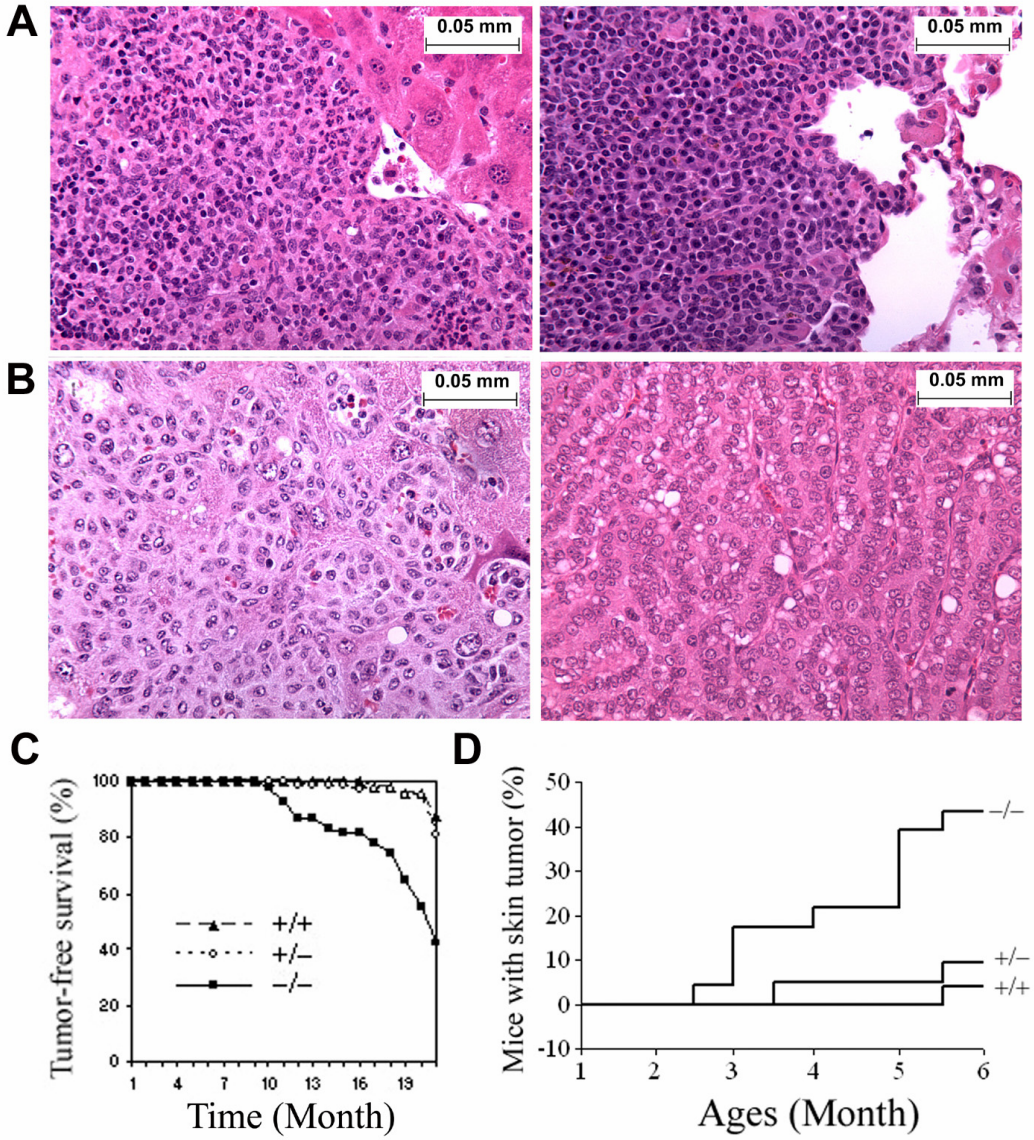


**Fig. 2.** $TGFBI^{-/-}$ mice showed an increased tumor incidence. **A.** Images of Low grade lymphoma in Liver (left panel) and Lung (right panel). **B.** Image of metastasized tumor in liver (left panel) and lung adenocarcinoma (right panel). Magnification of images (A-B): ×400. **C.** Tumor-free survival of $TGFBI^{-/-}$ mice compared with wild type and heterozygotes. **D.** Incidence of DMBA-induced skin tumors in wild type and $TGFBI^{-/-}$ mice.

over 20% of *TGFBI*$^{-/-}$ mice died of systemic illness, whereas all *TGFBI*$^{+/+}$ mice were still alive. To determine the cause of death, the moribund *TGFBI*$^{-/-}$ mice between ages 9 and 16 months were sacrificed and subjected to detailed histopathological analysis. Four out of 12 mice developed malignancies including one invasive lung adenocarcinoma and three lymphomas, one of which was a highly-disseminated lymphoma infiltrating liver and lung tissues (Fig. 3A). Others died of unidentified causes with no detectable tumors. Survival of heterozygotes was similar as *TGFBI*$^{+/+}$ mice, and only one died at the end of 16 months without detectable tumor burden. By the end of 20 months, 8.3% (4/48, lung adenocarcinoma and lymphoma) of *TGFBI*$^{+/+}$ mice, 13.3% (10/75, uterus histiocytic sarcoma, hepatocellular carcinoma, lymphoma and lung adenocarcinoma) of heterozygotes, and 37.04% (20/54) of *TGFBI*$^{-/-}$ mice had developed tumors (Fig. 3B, Table 1, $p<0.01$ for *TGFBI*$^{-/-}$ versus heterozygotes and *TGFBI*$^{+/+}$ mice, $\chi^2$ test). The tumor incidence in heterozygotes is higher than in wild type mice, but didn't reach statistical significance ($p>0.05$, $\chi^2$ test). Southern blot-based genotyping analysis showed that the second wild type allele of *TGFBI* gene was retained in all the ten tumors derived from heterozygous mice. However, 3/10 tumors displayed a dense methylation pattern in the *TGFBI* promoter identified by bisulfite sequencing (Data not shown). Tumor-free survival in *TGFBI*$^{-/-}$ mice was significantly lower than in heterozygote and *TGFBI*$^{+/+}$ mice ($p<0.01$, log-rank test, Fig. 3C).

**An increased skin tumor induction in mice with *TGFBI* deficiency**

In skin carcinogenesis assays, we treated *TGFBI*$^{+/+}$, *TGFBI*$^{+/-}$ and *TGFBI*$^{-/-}$ mice with a single dose of DMBA, a chemical carcinogen, on the dorsal skin 3-5 d after birth. The treated mice were checked weekly and monitored for up to six months. Ten of 23 *TGFBI*$^{-/-}$ mice developed skin tumors by 2.5- to 6-months of age, and two formed skin tumors at multiple sites. In contrast, only 2 out of 21 *TGFBI*$^{+/-}$ mice and 1 out of 25 *TGFBI*$^{+/+}$ mice developed tumors during 6 months of observation. Skin tumor incidence in *TGFBI*$^{-/-}$ mice was significantly higher ($p<0.01$, $\chi^2$ test) than in *TGFBI*$^{+/+}$ and heterozygous mice (Fig. 3D). Therefore, mice with *TGFBI* deficiency are prone to the development of both spontaneous malignancies and DMBA-induced skin tumors.

**Early passage (P2) *TGFBI*$^{-/-}$ MEFs exhibit increased frequency of chromosomal aberrations**

To clarify whether disruption of *TGFBI* resulted in an increased frequency of chromosomal aberrations, *TGFBI*$^{-/-}$ and wild type MEFs at passage 2 were treated with 0.05μg/ml colcemid for 3-6 h. Chromosomal metaphases were prepared from the treated cells, hybridized with cy3-conjugated (C3TA2)3 peptide nucleic acid (PNA) probe (Applied Biosystems) and counterstained with DAPI solution following the previously reported procedures (22). Digital images were recorded using a Zeiss Axioplan 2 microscope with a multicolor image analysis system (Fig. 4A). Various types of chromosomal aberrations in *TGFBI*$^{-/-}$ MEFs are shown in Fig. 4B (Arrows).

Overall, 43.75% (7/17) of metaphases prepared from *TGFBI*$^{-/-}$ MEFs contained chromatid breaks, centric fragments or chromosomal breaks, whereas only 13.3% (2/15) of metaphases from wild type MEFs contained only centric fragments (Fig. 4B).

In addition, the frequency of micronuclei was also examined in early passage of MEFs (P2). Twenty four hours post plating, cells were fixed with Acetone/ Methanol (1:1) for 10 mins and stained with 0.03mg/ml acridine orange in the dark for 10 mins. A total of 3,000 cells were counted for each experiment and three independent assays were performed. Numbers of micronuclei were recorded in each cell type using a Nikon Fluorescence microscope. Figure 4C shows multiple micronuclei found in *TGFBI*$^{-/-}$ MEFs (Arrows). Micronuclei frequency in *TGFBI*$^{-/-}$ MEFs was 4.7 fold higher than that in wild type MEFs, with 0.128 and 0.027 micronuclei per cell, respectively (Fig. 4D).

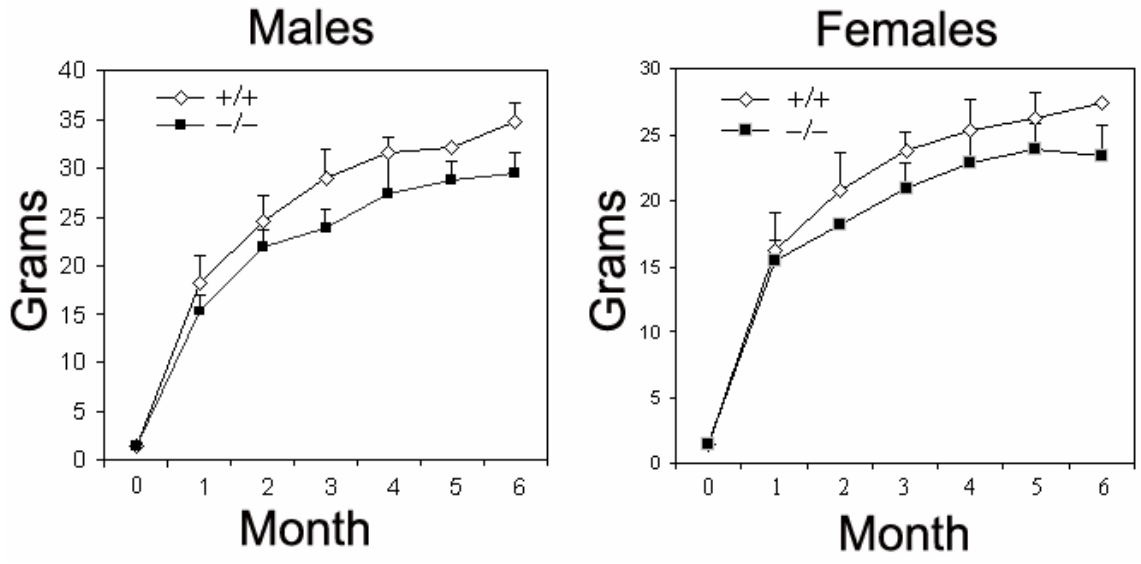


**Fig. 3.** Growth curve of male and female TGFBI-/- and wild type mice during 1-6 months of age. TGFBI-null mice showed retarded growth.

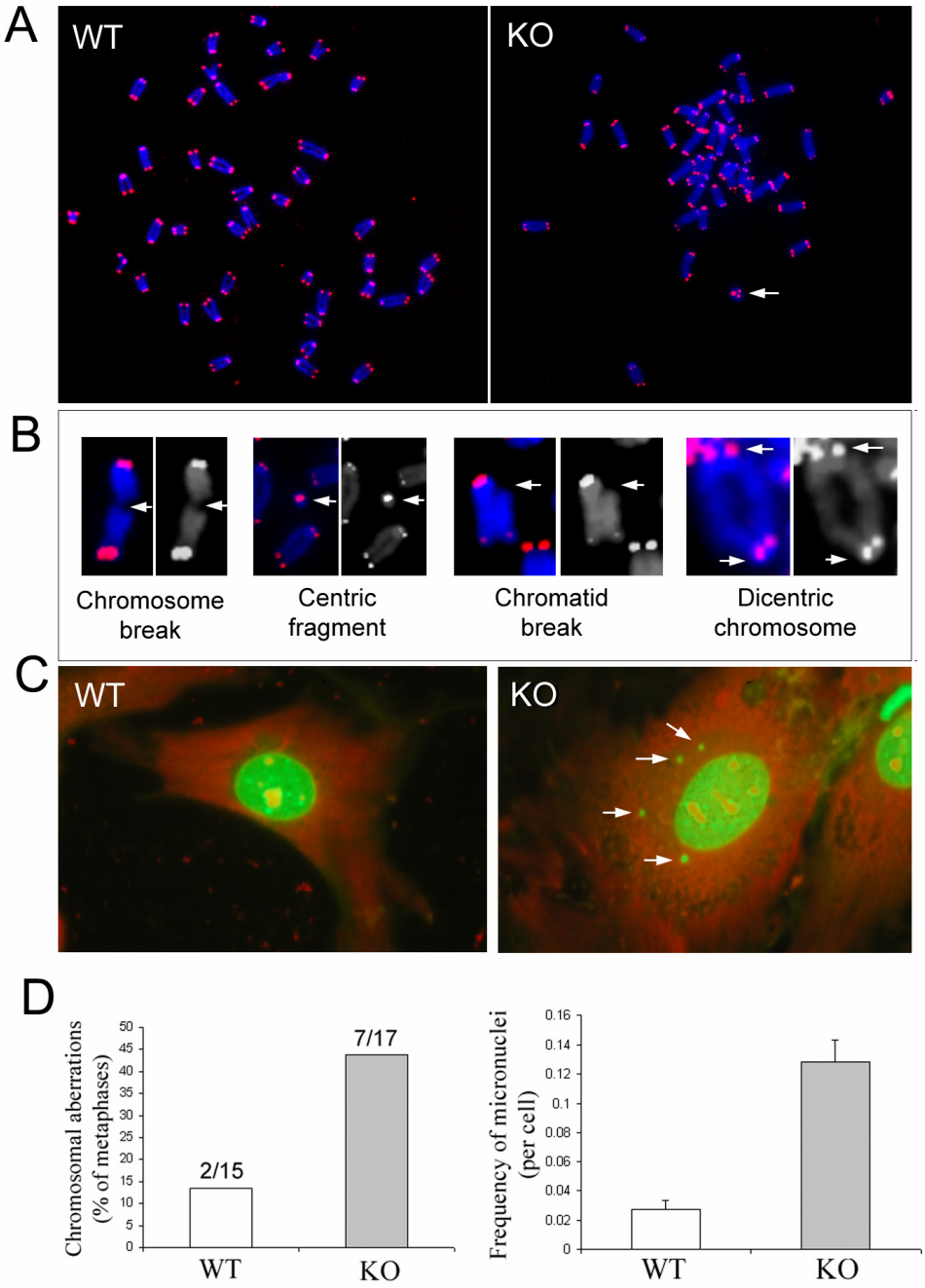


**Fig. 4.** Increased frequency of chromosomal aberrations and micronuclei in early passage (P2) of *TGFBI*$^{-/-}$ MEFs. **A.** Digital images of Cy-3 (identify telomeres) and DAPI (identify chromosomes)-stained chromosomal metaphases in wild type and *TGFBI* KO MEFs. Arrow: centric ring. **B.** Various types of chromosomal aberrations (Arrows) found in KO MEFs. **C.** Multiple micronuclei (Arrows) identified in KO MEFs. **D.** Frequency of chromosomal aberrations and micronuclei in wild type and *TGFBI*$^{-/-}$ MEFs.

**An accelerated G1-S progression in *TGFBI*$^{-/-}$ MEFs (passage 18)**

To investigate molecular mechanism(s) of tumorigenesis, we characterized mouse embryonic fibroblasts (MEFs) derived from *TGFBI*$^{-/-}$ and *TGFBI*$^{+/+}$ littermates. Long term *in vitro* growth of MEFs was assayed by a 3T3 protocol. *TGFBI*$^{-/-}$ MEFs showed a higher growth rate at early passage (P2), but grew significantly faster than *TGFBI*$^{+/+}$ MEFs after overcoming senescence (Fig. 5A). This prompted a comparison of the kinetics of S-phase entry in serum-stimulated quiescent cells. Using the BrdU incorporation assay, quiescent *TGFBI*$^{-/-}$ MEFs were consistently found to enter into S phase in advance of *TGFBI*$^{+/+}$ MEFs upon serum stimulation (Fig. 5B).

In summary, mice with a *TGFBI* disruption are prone to spontaneous tumors as well as DMBA-induced skin tumors. The most common tumors arising spontaneously in *TGFBI*$^{-/-}$ mice were lymphomas (65.0%, 13/20). Other tumor types were lung papillary adenocarcinoma, skin invasive adenocarcinoma, liver histiocytic sarcoma and testis hemangioendothelioma, which are less common in aged 129Sv/Ev, C56BL/6J mice. Compared with the tumors oc-

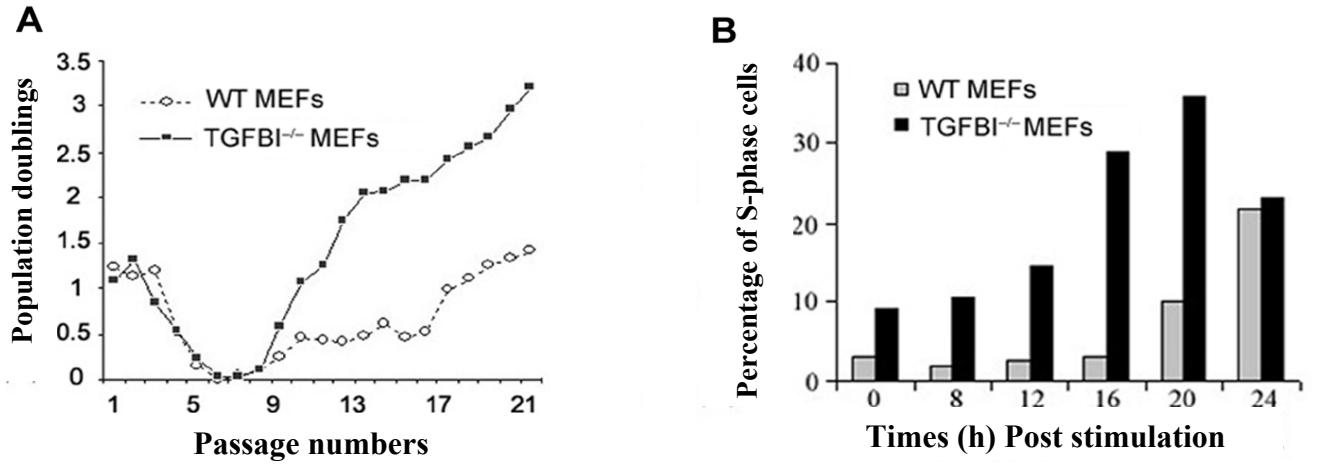


**Fig. 5.** Characterization of growth property of *TGFBI*-null MEFs. Cell proliferation using a 3T3 protocol. MEFs were isolated from 13.5-d embryos, and grown at 5% $CO_2$ in DMEM (Invitrogen) supplemented with 10% FCS. For the 3T3 protocol, $9 \times 10^5$ cells were plated into a 10cm-dish and cell numbers were counted at 3 day-intervals. At least three independent lines per genotype with two independent cultures per line were examined.

curring in *TGFBI*$^{+/+}$ and heterozygous mice, spontaneous tumors from *TGFBI*$^{-/-}$ mice demonstrated metastatic potential: (i) seven out of 13 lymphomas were classified as low grade types with infiltration to other non-lymphoid organs including liver, lung, kidney and pancreas; (ii) four out of 6 other types of tumors were either invasive or metastatic malignancies; (iii) one *TGFBI*$^{-/-}$ mouse developed both invasive lung adenocarcinoma and lymphoproliferative disorder. Hence, *TGFBI* disruption resulted in a dramatic predisposition to lymphomas and other cancers.

It is commonly accepted that malignant transformation is a lengthy multi-step process and arises through an accumulation of mutations at various genetic loci.[20] Genomic instability has been demonstrated to not only initiate tumorigenesis, but is at least a factor in tumor progression.[20, 21] In the present study, early passage of *TGFBI*$^{-/-}$ MEFs showed significantly increased chromosomal aberration and micronuclei frequency compared to wild type MEFs, suggesting that *TGFBI* deficiency induces genetic instability. This is supported by other study showing that TGFBI protein is involved in microtubule stability and silencing of its expression contributes to centrosome amplification and enhanced mitotic abnormalities.[17] The present studies provide the evidence, for the first time, that loss of *TGFBI* functions as a tumor suppressor *in vivo*. Because of frequent loss of TGFBI protein in human cancer cells,[11-14] *TGFBI* and its associated signaling represent promising targets for anticancer drug discovery.

**Acknowledgements**

Grant support: NASA NAG2-1637 (Y. Zhao), CA127120 (Y. Zhao) and NIH ES-11804 (T.K. Hei).

## References

1. Tlsty TD. Cell-adhesion-dependent influences on genomic instability and carcinogenesis. *Curr Opin Cell Biol* **10**:647-53, 1998.
2. Giancotti FG and Ruoslahti E. Integrin signaling. *Science* **285**:1028-32, 1999.
3. Danen EH. Integrins: regulators of tissue function and cancer progression. *Curr Pharm Des* **11**:881-91, 2005.
4. Ramsay AG, Marshall JF and Hart IR. Integrin trafficking and its role in cancer metastasis. *Cancer Metastasis Rev* **26**:567-78, 2007.
5. Skonier J, Neubauer M, Madisen L, Bennett K, Plowman GD and Purchio AF. cDNA cloning and sequence analysis of beta ig-h3, a novel gene induced in a human adenocarcinoma cell line after treatment with transforming growth factor-beta. *DNA Cell Biol* **11**:511-22, 1992.
6. LeBaron RG, Bezverkov KI, Zimber MP, Pavelec R, Skonier J and Purchio AF. Beta IG-H3, a novel secretory protein inducible by transforming growth factor-beta, is present in normal skin and promotes the adhesion and spreading of dermal fibroblasts in vitro. *J Invest Dermatol* **104**:844-9, 1995.
7. Billings PC, Herrick DJ, Kucich U, Engelsberg BN, Abrams WR, Macarak EJ, Rosenbloom J and Howard PS. Extracellular matrix and nuclear localization of beta ig-h3 in human bladder smooth muscle and fibroblast cells. *J Cell Biochem* **79**:261-73, 2000.
8. Kim JE, Jeong HW, Nam JO, Lee BH, Choi JY, Park RW, Park JY and Kim IS. Identification of motifs in the fasciclin domains of the transforming growth factor-beta-induced matrix protein betaig-h3 that interact with the alphavbeta5 integrin. *J Biol Chem* **277**:46159-65, 2002.
9. Nam JO, Kim JE, Jeong HW, Lee SJ, Lee BH, Choi JY, Park RW, Park JY and Kim IS. Identification of the alphavbeta3 integrin-interacting motif of betaig-h3 and its anti-angiogenic effect. *J Biol Chem* **278**:25902-9, 2003.
10. Jeong HW and Kim IS. TGF-beta1 enhances betaig-h3-mediated keratinocyte cell migration through the alpha3beta1 integrin and PI3K. *J Cell Biochem* **92**:770-80, 2004.
11. Genini M, Schwalbe P, Scholl FA and Schafer BW. Isolation of genes differentially expressed in human primary myoblasts and embryonal rhabdomyosarcoma.

*Int J Cancer* **66**:571-7, 1996.
12. Zhao YL, Piao CQ and Hei TK. Downregulation of Betaig-h3 gene is causally linked to tumorigenic phenotype in asbestos treated immortalized human bronchial epithelial cells. *Oncogene* **21**:7471-7, 2002.
13. Zhao Y, El-Gabry M and Hei TK. Loss of Betaig-h3 protein is frequent in primary lung carcinoma and related to tumorigenic phenotype in lung cancer cells. *Mol Carcinog* **45**:84-92, 2006.
14. Calaf GM, Echiburu-Chau C, Zhao YL and Hei TK. BigH3 protein expression as a marker for breast cancer. *Int J Mol Med* **21**:561-8, 2008.
15. Shao G, Berenguer J, Borczuk AC, Powell CA, Hei TK and Zhao Y. Epigenetic inactivation of Betaig-h3 gene in human cancer cells. *Cancer Res* **66**:4566-73, 2006.
16. Thapa N, Lee BH and Kim IS. TGFBIp/betaig-h3 protein: a versatile matrix molecule induced by TGF-beta. *Int J Biochem Cell Biol* **39**:2183-94, 2007.
17. Ahmed AA, Mills AD, Ibrahim AE, Temple J, Blenkiron C, Vias M, Massie CE, Iyer NG, McGeoch A, Crawford R, *et al.* The extracellular matrix protein TGFBI induces microtubule stabilization and sensitizes ovarian cancers to paclitaxel. *Cancer Cell* **12**:514-27, 2007.
18. Nam JO, Jeong HW, Lee BH, Park RW and Kim IS. Regulation of tumor angiogenesis by fastatin, the fourth FAS1 domain of betaig-h3, via alphavbeta3 integrin. *Cancer Res* **65**:4153-61, 2005.
19. Becker J, Volland S, Noskova I, Schramm A, Schweigerer LL and Wilting J. Keratoepithelin reverts the suppression of tissue factor pathway inhibitor 2 by MYCN in human neuroblastoma: a mechanism to inhibit invasion. *Int J Oncol* **32**:235-40, 2008.
20. Jefford CE and Irminger-Finger I. Mechanisms of chromosome instability in cancers. *Crit Rev Oncol Hematol* **59**:1-14, 2006.
21. Nowak MA, Komarova NL, Sengupta A, Jallepalli PV, Shih Ie M, Vogelstein B and Lengauer C. The role of chromosomal instability in tumor initiation. *Proc Natl Acad Sci USA* **99**:16226-31, 2002. ■

# Betaig-h3 Expression Reduces *In Vitro* and *In Vivo* Metastatic Ability in Lung and Breast Tumor Cells

*Gengyun Wen, Michael A. Partridge, Mei Hong, Bingyan Li,[a] Gloria M. Calaf, Yongliang Zhao, Tian Liu,[b] Jun Zhou,[b] Zengli Zhang[a] and Tom K. Hei*

Tumor metastasis, a complex, multistage process by which primary tumor cells migrate to and colonize distant tissues, is a critical factor in the progression of cancer to lethality.[1] Understanding the mechanisms underlying this process is crucial to improve anti-metastatic therapies.

Transformed cells must first escape the confines of the primary tumor by breaking down the basement membrane allowing the cancer cells to intravasate into blood vessels. Tumor cells can then be transported to distant tissues, extravasate out of the circulatory system and subsequently colonize remote sites. The capacity of malignant cells to undertake these two stages of metastasis, intravasation and extravasation, is thought to explain the substantial up-regulation of matrix metalloproteinase (MMPs) activity in cancer cells, enzymes that can degrade extracellular matrix (ECM) proteins and permit invasion through the basement membrane.[1]

An additional obstacle for metastatic cells is the requirement for adhesion signaling to promote survival. In fully spread cells, adhesion plaques called focal adhesions (FAs) create a link between the ECM outside the cell and the actin cytoskeleton inside the cell. FAs contain a variety of molecules that physically link the cytoskeleton and the ECM, as well as adaptor proteins and kinases that propagate signaling cascades in adherent cells.[2] In normal cells, adhesion molecules on the cell surface must be bound to their ligand to activate intracellular downstream signals, without which cells will cease proliferating and undergo apoptosis.[2] However, metastatic cells must, by definition, break away from their progenitor tissue/organ and migrate to distant sites, a process that presumably requires the cell to circumvent normal adhesion-mediated survival signaling. Consequently, down-regulation of adhesion signaling although,[3] crucially, not the elimination of adhesion ability is thought to be important for metastatic tumor cells to move through the lymphatic system or blood vessels.[4]

Betaig-h3 protein, also referred to as transforming growth factor-β–induced (TGFBI), is detected in most normal human tissues in the body although mRNA was not detected in the brain.[5, 6] Betaig-h3 has been implicated in a number of cellular disease process including tumorigenesis, angiogenesis, wound healing and inflammation.[7] However, the most extensive studies on Betaig-h3 have been directed toward understanding the role played by the protein in corneal dystrophies, and a number of mutations in the gene

[a] *School of Radiation Medicine and Public Health, Soochow University ,Soochow, China*
[b] *Department of Radiation Oncology, Columbia University Medical Center , NY*

have been shown to have a pathological manifestation.[7]

In our previous reports, we have focused on the role of Betaig-h3 in tumorigenesis. We have demonstrated that the absence of the protein was associated with increased tumorigenesis *in vivo* and *in vitro*,[6] and that this down-regulation was associated with hypermethylation of Betaig-h3 gene promoter regions.[8] However, since Betaig-h3 is a secreted protein and has been shown as a "linker" participating in the interaction between ECM and integrins,[9] we were curious to know whether the absence of the protein affects one of the most important traits of malignant tumors-metastasis. To do this we assessed some of the most prominent *in vitro* characteristics associated with metastatic tumors by expressing Betaig-h3 in two types of cancer cell lines, H522, a lung cancer cell line, MCF-7, a breast cancer cell line, that had little or no endogenous expression of the protein and measuring invasion ability, matrix metalloproteinase activity and dependence on adhesion for survival signaling. We found that expression of Betaig-h3 in these cells increased their ability to adhere to ECM proteins, form cytoskeleton structures and activate adhesion-mediated downstream signaling molecules, whereas, it significantly reduced the ability of these cells to grow in soft agar, to penetrate a matrix gel and activities of matrix metalloproteinases 2 and 9. Injection of Betaig-h3 expressing cells through the tail vein of immunodeficient mice resulted in a significant decrease in tumor cell metastasis compared to controls (Fig. 1). Taken together, these data suggest that Betaig-h3 expression moderates the metastatic potential of cancer cells, which is in agreement with our previous findings that Betaig-h3 is reduced in many types of cancer cells.

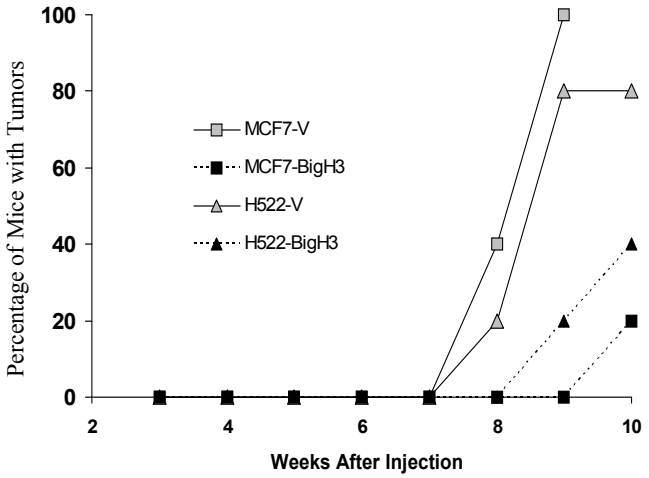


**Fig. 1. *In vivo* tumor cell metastasis of Betaig-h3 expressing cancer cells**. Time of tumor formation was measured in immuno-deficient nude mice injected with $1x10^5$ cancer cells expressing Betaig-h3 compared to controls. Cells were injected into nude mice via the tail vein, five mice for each group and animals with a tumor burden detected with ultrasound imaging were sacrificed and dissected. *In vivo*, tumor cell metastasis was reduced in Betaig-h3 expressing cancer cells.

## References

1. Gupta GP and Massague J. Cancer metastasis: building a framework. *Cell* **127**:679-95, 2006.
2. Hynes RO. Integrins: bidirectional, allosteric signaling machines. *Cell* **110**:673-87, 2002.
3. Lu Z, Jiang G, Blume-Jensen P and Hunter T. Epidermal growth factor-induced tumor cell invasion and metastasis initiated by dephosphorylation and downregulation of focal adhesion kinase. *Mol Cell Biol* **21**:4016-31, 2001.
4. Humphries MJ, Olden K and Yamada KM. A synthetic peptide from fibronectin inhibits experimental metastasis of murine melanoma cells. *Science* **233**:467-70, 1986.
5. Skonier J, Neubauer M, Madisen L, Bennett K, Plowman GD and Purchio AF. cDNA cloning and sequence analysis of beta ig-h3, a novel gene induced in a human adenocarcinoma cell line after treatment with transforming growth factor-beta. *DNA Cell Biol* **11**:511-22, 1992.
6. Zhao Y, El-Gabry M and Hei TK. Loss of Betaig-h3 protein is frequent in primary lung carcinoma and related to tumorigenic phenotype in lung cancer cells. *Mol Carcinog* **45**:84-92, 2006.
7. Thapa N, Lee BH and Kim IS. TGFBIp/betaig-h3 protein: a versatile matrix molecule induced by TGF-beta. *Int J Biochem Cell Biol* **39**:2183-94, 2007.
8. Shao G, Berenguer J, Borczuk AC, Powell CA, Hei TK and Zhao Y. Epigenetic inactivation of Betaig-h3 gene in human cancer cells. *Cancer Res* **66**:4566-73, 2006.
9. Billings PC, Whitbeck JC, Adams CS, Abrams WR, Cohen AJ, Engelsberg BN, Howard PS and Rosenbloom J. The transforming growth factor-beta-inducible matrix protein (beta)ig-h3 interacts with fibronectin. *J Biol Chem* **277**:28003-9, 2002. ■

# DNA Demethylating Agent Zebularine Preferentially Sensitizes Human Glioblastoma Cells Deficient in DNA-Dependent Protein Kinase (DNA-PK)

*Jarah A. Meador, Yanrong Su, Jean-Luc Ravanat,[a] Charles R. Geard and Adayabalam S. Balajee*

Glioblastoma multiforme (GBM) is one of the most lethal forms of brain cancer with a median survival rate of less than 12 months and a high rate of recurrence. Treatment of GBM poses a great challenge owing to a combination of efficient anti-apoptotic and DNA repair mechanisms that render gliomas resistant to chemo- and radiotherapies.[1] Further, recent studies have shown that glioma cancer stem cells possess an enhanced DNA repair capacity which increases their survival after treatment with either alkylating agents or ionizing radiation.[2, 3] Therefore, development of new strategies is certainly required for brain cancer therapy. As cancer cells often display abnormal DNA methylation patterns, an epigenome targeting strategy was attempted in this study to sensitize the brain tumor cells. Zebularine is a proven DNA methyltransferase inhibitor effective at reactivating the silenced genes *in vitro* and *in vivo* with a much higher specificity for cancer cells than normal cells.[4, 5] The stability and low cytotoxicity of Zebularine make it an attractive epigenetic agent. Owing to the high specificity for cancer cells, Zebularine was chosen in this study for epigenome targeting in the two human glioblastoma cell lines that are proficient (MO59K) and deficient (MO59J) in DNA-dependent protein kinase (DNA-PKcs).

As DNA-PK is an important kinase for the activation of diverse signal transduction pathways, use of glioblastoma cell lines differing in the functional status of DNA-PK may yield valuable information on the mode of action of Zebularine. To determine whether Zebularine sensitizes human

[a] *Laboratoire des lésions des Acides Nucléiques, LCIB (UMR-E 3 CEA-UJF), DRFMC CEA/Grenoble, 17 Avenue des martyrs 38054 Grenoble Cedex 9, France*

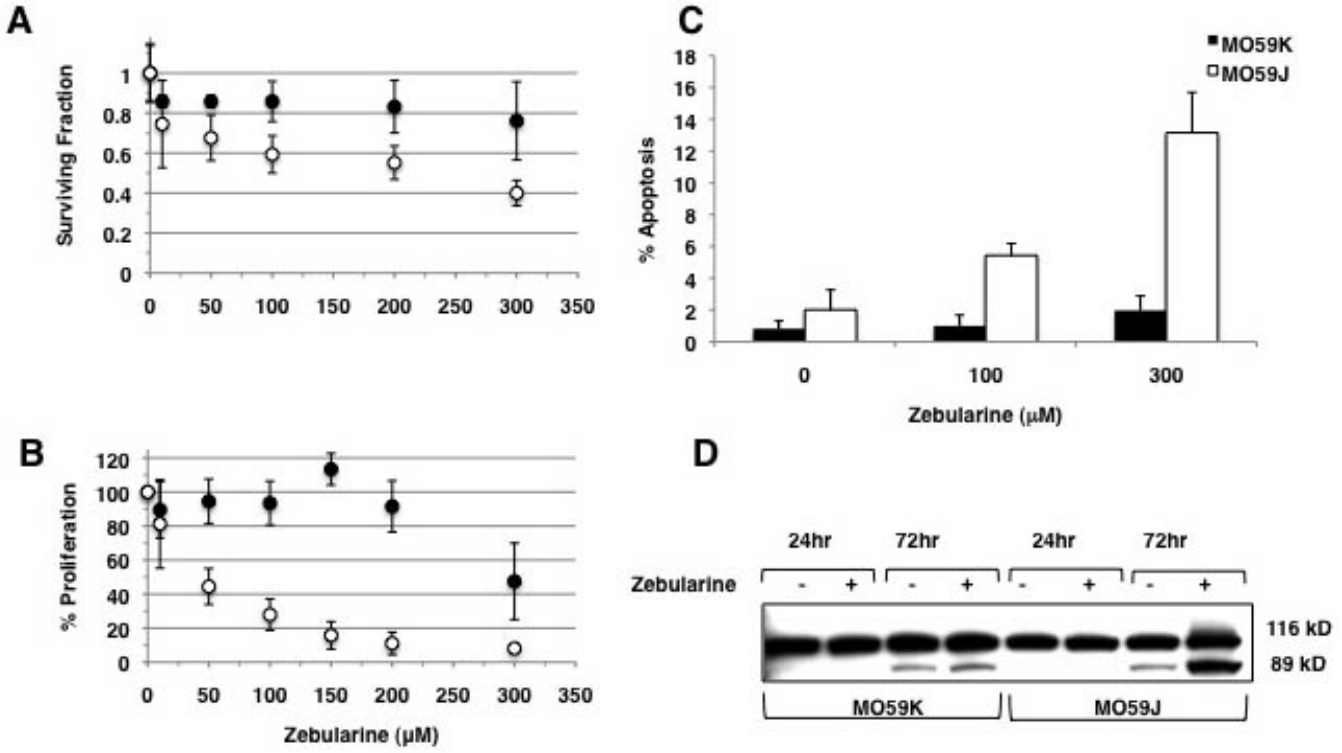


**Fig. 1.** Zebularine preferentially sensitizes DNA-PK deficient MO59J cells. MO59K and MO59J cells were incubated with increasing concentrations of Zebularine (10-300 μM) for 72h. **A.** Clonogenic survival of MO59J (open circles) and MO59K (closed circles) cells after treatment with different concentrations of Zebularine. **B.** Measurement of cellular proliferation in MO59J and MO59K cells after Zebularine treatment. MO59J cells showed a highly retarded proliferation upon 72h exposure to Zebularine. **C.** Determination of apoptotic cell death after Zebularine exposure in MO59J and MO59K cells. Apoptosis was determined by flow cytometry based Apo-BrdU TUNEL assay. **D.** Western blot analysis of PARP-1 cleavage in MO59J and MO59K cells following exposure to 200 μM Zebularine for 72 h. Note the increased abundance of cleaved 89kDa fragment of PARP-1 in MO59J cells.

gliomas, DNA-PK proficient (MO59K) and deficient (MO59J) cells were exposed to different concentrations of Zebularine (10–300μM) for 72h and assayed for clonogenic survival and proliferation. The survival assay clearly showed the preferential sensitivity of DNA-PK deficient MO59J cells to Zebularine (Fig. 1A) as judged by the dose dependent reduction in survival. The LD50 (lethal dose that reduces the survival to 50%) value of Zebularine was found to be approximately 245μM for MO59J cells and at this concentration MO59K cells showed only 20% reduction in survival. Interestingly, MO59J cells showed a 20% reduction in survival even at the minimal concentration of Zebularine (10μM). To determine whether or not Zebularine affects the cell growth, cellular proliferation was measured using a fluorescence based CyQuant assay (Invitrogen, USA). The results demonstrated a dose dependent effect in MO59J cells with proliferation being inversely proportional to Zebularine concentration. LD50 value for proliferation was determined to be 50μM for MO59J and 300μM for MO59K cells. Both clonogenic survival and proliferation assays (Fig. 1A&B) clearly demonstrated the preferential sensitization of DNA-PK deficient gliomas to Zebularine. These data further suggest that DNA-PK is a critical determinant of cellular fate after Zebularine treatment. Consistent with reduced survival and proliferation, the apoptotic cells detected by Apo-BrdU TUNEL assay were much higher in DNA-PK deficient MO59J (14%) than in MO59K (2%) cells (Fig. 1C). To verify whether apoptosis occurs by poly (ADP) ribose polymerase I (PARP-1) dependent manner, PARP-1 cleavage was analyzed after incubation with 200μM Zebularine for 24h and 72h. Caspase-dependent apoptosis is often accompanied by the cleavage of PARP-1 protein (116kDa) into 85kDa and 29kDa fragments. PARP-1 cleavage after Zebularine treatment was readily detectable in MO59J after 72h of Zebularine exposure (Fig. 1D). The cleaved fragment of PARP-1 (89kDa) was slightly increased in MO59K at 72h compared to mock treated cells but was significantly less than that observed for MO59J cells (3.5 fold) suggestive of an enhanced sensitivity of MO59J cells to Zebularine.

We next verified whether or not the differential response of the two glioblastoma cell lines to Zebularine is attributable to variations in the extent of DNA methyl transferase (DNMT) inhibition. As DNMT associates with chromatin, DNMT1 level was measured in both soluble and chromatin bound insoluble fractions. In mock treated cells, DNMT1 was enriched only in the soluble protein fraction in both cell lines and Zebularine treatment completely depleted DNMT1 protein from both soluble and insoluble fractions in both cell lines (Fig. 2A). Interestingly, Zebularine also significantly depleted DNMT3b only in MO59K cells but not in MO59J. As DNMT1 mRNA level detected by quantitative real-time PCR appeared to be unaffected by Zebularine treatment, depletion of DNMT1 protein is presumably due to the trapping of the enzyme of Zebularine. The relative expression of

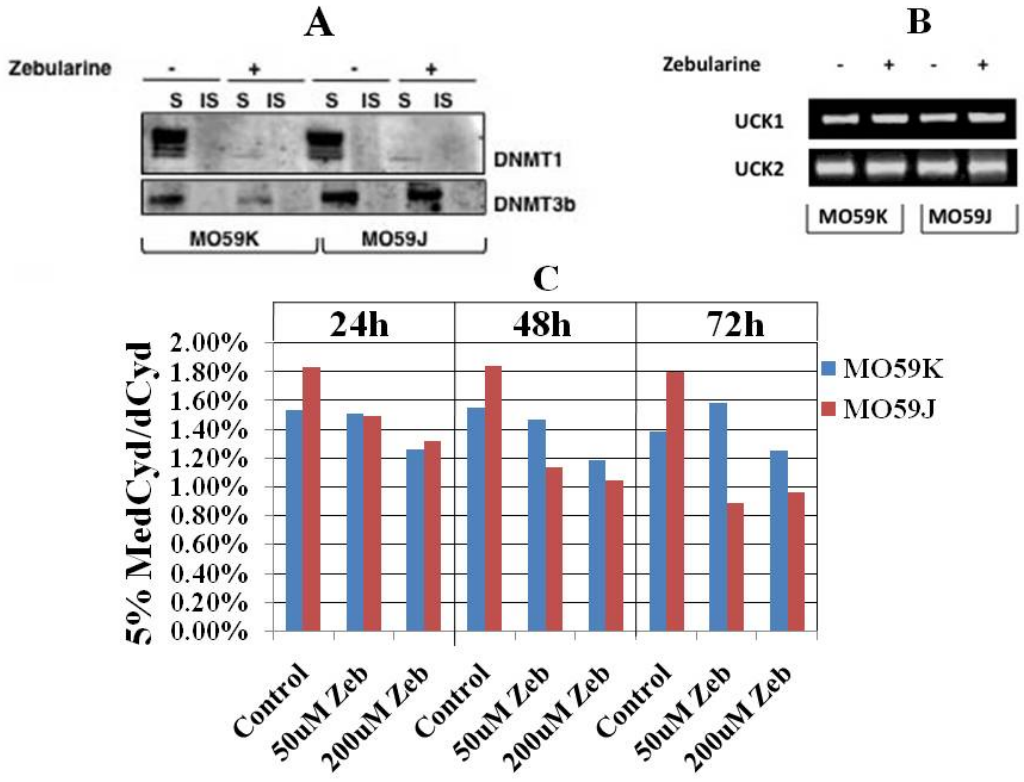


**Fig. 2. A.** Zebularine treatment increases DNA demethylation in MO59J and MO59K cell lines by inhibiting DNMT1 protein. Both cell lines were incubated with 200μM Zebularine for 72h. DNMT1 and DNMT3b protein levels were measured in total soluble (S) and insoluble (IS) (chromatin bound) fractions. **B.** RT-PCR analysis of UCK 1 and 2 mRNA expression levels in MO59J and MO59K cells. Total RNA was isolated from mock treated and Zebularine (200μM) treated MO59J and MO59K cells after 72h. **C.** Zebularine treatment caused a decrease in 5-methyl cytosine at the genome level in both MO59K and MO59J in a time and dose dependent manner. Zeb-Zebularine

DNMT3b at the mRNA level was increased in MO59J cells after Zebularine treatment, suggesting that DNMT3b may be up-regulated through a DNA damage response (Data not shown). Uridine cytidine kinases (UCK 1 and 2) phosphorylate Zebularine and the phosphorylation is a prerequisite for its incorporation into the genomic DNA. Also, the increased specificity of Zebularine for cancer cells is mainly due to the fact that cancer cells have much higher levels of UCK in comparison to normal human cells. Therefore, we wished to determine whether there are differences in the levels of UCK between MO59J and MO59K cells which might influence the uptake of Zebularine. Detection of UCK at the mRNA level by RT-PCR indicated similar levels of UCK 1 and UCK 2 in both cell lines (Fig. 2B).

Impact of DNMT1 protein depletion on DNA methylation was next evaluated both at the overall genome and gene specific levels. Zebularine induced global DNA demethylation in both cell lines in a time and dose dependent manner (Fig. 2C). HPLC-MS/MS was used to detect both 5-MedCyd and dCyd in hydrolyzed DNA samples as described previously for the detection of oxidative DNA lesions.[6, 7] In MO59J cells, Zebularine exposure at a low concentration (50μM) for 24 hours was sufficient to reduce the 5-methylcytosine content approximately by 40%. In contrast, a 200 μM dose of Zebularine was required to yield about a 30% reduction in global methylation in MO59K cells (Fig. 2C). It is worth noting that the basal level of DNA methylation in mock treated control cells was higher in MO59J compared to MO59K cells. This observation clearly suggests a critical role for DNA-PK in the maintenance of epigenome integrity.

Although our finding showed that Zebularine effectively depleted DNMT1 protein from the soluble protein fraction and resulted in DNA hypomethylation in both cell lines, it was important to determine the effects of DNMT1 depletion on promoter methylation of specific genes. To address this issue, a commercially available promoter methylation array was utilized (Panomics, USA). This array contains a total of 82 genes including some of the well-known tumor suppressor genes such as BRCA1, TP73, VHL and Maspin. The promoter regions were analyzed in mock treated control and Zebularine (200μM for 72h) treated MO59K and MO59J cells. The promoter methylation pattern was found to be grossly similar in both cell lines after mock and Zebularine treatments albeit a slightly increased level of demethylation in MO59J cells (Data not shown).

Comparable levels of DNMT inhibition in both MO59J and MO59K cells prompted us to verify whether the increased sensitivity of MO59J cells to Zebularine is due to inefficient DNA damage/repair response. To address this issue, features of genomic instability, indicative of impaired DNA repair activity, were assessed in both glioblastoma cell lines after Zebularine treatment. Increased frequencies of micronuclei as well as polyploid cells with multiple centrosomes were observed after Zebularine treatment in MO59J cells. In MO59J cells, Zebularine treatment increased polyploidy compared to sham treated control cells indicating that Zebularine induced cell death might be due to increased genomic instability. To determine if genomic instability features and cell death observed in MO59J were due to defective mitotic spindle checkpoint, we treated MO59K and MO59J with nocodazole and measured the DNA content using flow cytometry. In the presence of a functional mitotic spindle checkpoint, nocodazole treatment is expected to trigger an efficient mitotic arrest like that observed in MO59K cells. However, MO59J cells failed to show mitotic arrest and the cell cycle profile obtained after nocodazole treatment was very similar to that that observed after Zebularine treatment. These observations clearly indicate that MO59J cells are deficient in mitotic checkpoint imposed by Zebularine. Our study brings out two important novel findings regarding the mode of action of Zebularine induced killing of brain tumor cells: (I) the functional status of DNA-PK is the major determining factor for the cellular protection against Zebularine and (II) cancer cells deficient in mitotic checkpoint regulation are selectively sensitized by Zebularine.

## References


1. DeAngelis LM. Brain tumors. *N Engl J Med* **344**:114-23, 2001.
2. Bao S, Wu Q, McLendon RE, Hao Y, Shi Q, Hjelmeland AB, Dewhirst MW, Bigner DD and Rich JN. Glioma stem cells promote radioresistance by preferential activation of the DNA damage response. *Nature* **444**:756-60, 2006.
3. Johannessen TC, Bjerkvig R and Tysnes BB. DNA repair and cancer stem-like cells--potential partners in glioma drug resistance? *Cancer Treat Rev* **34**:558-67, 2008.
4. Cheng JC, Matsen CB, Gonzales FA, Ye W, Greer S, Marquez VE, Jones PA and Selker EU. Inhibition of DNA methylation and reactivation of silenced genes by zebularine. *J Natl Cancer Inst* **95**:399-409, 2003.
5. Cheng JC, Yoo CB, Weisenberger DJ, Chuang J, Wozniak C, Liang G, Marquez VE, Greer S, Orntoft TF, Thykjaer T*, et al.* Preferential response of cancer cells to zebularine. *Cancer Cell* **6**:151-8, 2004.
6. Frelon S, Douki T, Ravanat JL, Pouget JP, Tornabene C and Cadet J. High-performance liquid chromatography--tandem mass spectrometry measurement of radiation-induced base damage to isolated and cellular DNA. *Chem Res Toxicol* **13**:1002-10, 2000.
7. Ravanat JL, Duretz B, Guiller A, Douki T and Cadet J. Isotope dilution high-performance liquid chromatography-electrospray tandem mass spectrometry assay for the measurement of 8-oxo-7,8-dihydro-2'-deoxyguanosine in biological samples. *J Chromatogr B Biomed Sci Appl* **715**:349-56, 1998. ■

# DNA-PK Plays a Regulatory Role in Cisplatin Induced Toxicity in Human Brain Tumor Cells

*Patricia de Oliveira Carminati,[a] Jarah A. Meador, Charles R. Geard and Adayabalam S. Balajee*

Astrocytoma is the most common neoplasm of the central nervous system, and the average survival time of patients with the most malignant type, glioblastoma multiforme, is about 1 year from diagnosis, despite an aggressive combination of surgery, radiotherapy and chemotherapy. As the brain tumor cells are refractory to radio and chemotherapies, development of new strategies is required for brain cancer therapy. Cisplatin {cis-diamminedichloridoplatinum (CDDP)} is an anti-tumor agent employed for the treatment of testicular, bladder, lung, gullet (oesophagus), stomach and ovarian cancers. Cisplatin predominantly induces DNA inter- and intrastrand crosslinks which are efficiently removed by nucleotide excision repair. This study was aimed to evlauate the effects of cisplatin on human glioblastoma cell lines. As DNA dependent protein kinase (DNA-PK) plays critical roles in the activation of diverse signal transduction pathways, glioblastoma cell lines differing in the functional status of DNA-PK were chosen for our study. This approach may yield valuable mechanistic information on the role of DNA-PK and its associated signal transduction pathways in mediating cisplatin induced toxicity.

To determine whether cisplatin sensitizes human gliomas, DNA-PK proficient (MO59K) and deficient (MO59J) cells were exposed to different concentrations of cisplatin (5–75µM) for 72h and assayed for proliferation using a fluorescence based CyQuant assay (Invitrogen, USA). In contrast to DNA-PK proficient MO59K cells, MO59J cells showed a dose dependent decline in proliferation and the proliferation was reduced to 20% of the vehicle (DMSO) treated control cells at the highest concentration of cispaltin (75µM, Fig. 1). This observation clearly points out that DNA-PK is critical for cellular protection against cisplatin toxicity.

In addition to DNA-PK deficient MO59J cells, another human glioblastoma cell line (U343) was also found to be very sensitive to cisplatin exposure. Treatment of U343 cells with different concentrations of cisplatin (5, 10 and 25µM) resulted in a dose dependent increase in apoptotic cells (Fig. 2). Apoptosis was measured in U343 cells *in vivo* using multiple fluorescent dyes (Hoechst 33252, propidium iodide and fluorescein diacetate).

Cell cycle analysis was next performed to verify whether or not the enhanced cisplatin toxicity observed in MO59J cells is due to impaired cell cycle checkpoints. For this, cells in exponential growth phase were treated with different concentrations of cisplatin (5-25µM) for 90 min and the cells were subjected to flow cytometry 24hr, 48hr and 72hr after treatment. MO59J cells showed only a slight enrichment of S-phase cells (7% more than DMSO treated control) at the highest cisplatin concentration used (25µM) at 24hr of analysis which got obliterated at 48hr and 72hr of treatment (Fig. 3). In contrast to MO59J, MO59K cells showed an efficient S-phase arrest at all of the tested cisplatin concen-

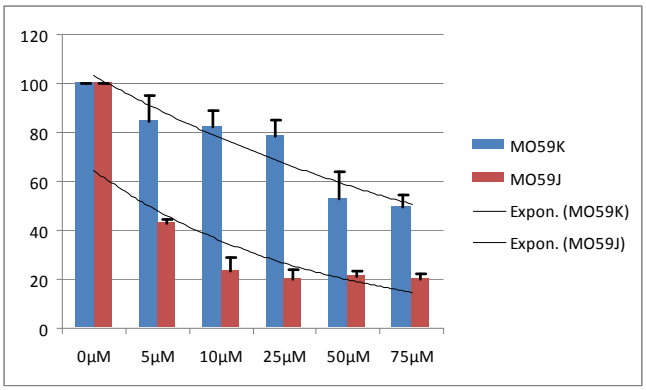


**Fig. 1.** Cisplatin drastically reduces the proliferation of DNA-PK deficient human glioblastoma cells. Cells (2.5-5X 103) in exponential growth were seeded in 96 well plates 24 hr prior to cisplatin treatment. Cells were treated for 90 min with different cisplatin concentrations and proliferation was assayed by CyQuant 72 hr after treatment. Cisplatin concentration is plotted in the X axis and percent survival is plotted in the Y axis.

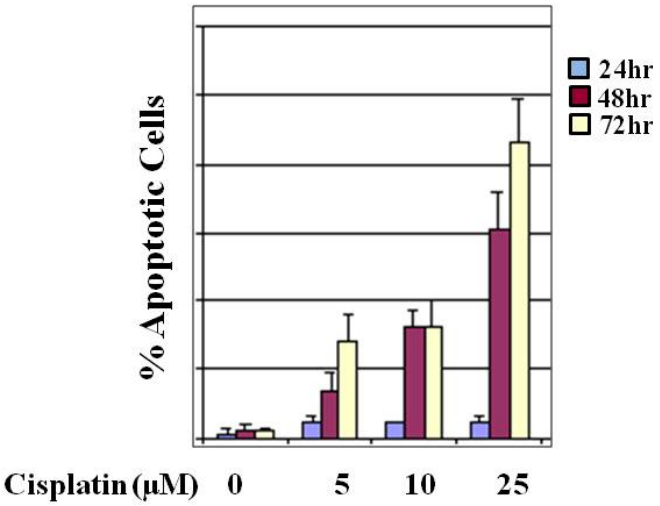


**Fig. 2.** Detection of cisplatin induced apoptosis in human glioblastoma cell line U343. Cells in exponential growth phase were treated with different concentrations of cisplatin for 90min. Apoptosis was detected 24hr, 48hr and 72 hr after treatment *in vivo* using multiple fluorescent dyes.

[a] *Laboratório de Citogenética e Mutagênese, Departamento de Genética, Faculdade de Medicina de Ribeirão Preto-USP, Brazil*

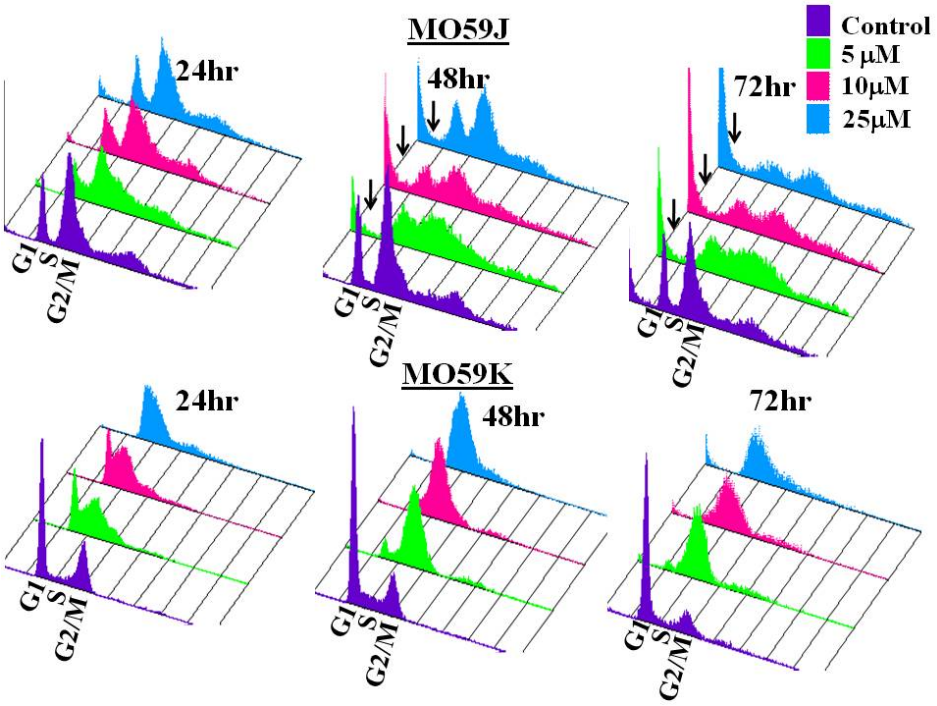


**Fig. 3.** DNA-PK is required for efficient S-phase arrest following cisplatin exposure. MO59J and MO59K cells in exponential growth phase were treated for 90min with different concentrations of cisplatin (5μM, 10μM and 25μM). Cells fixed at 24hr, 48hr and 72hr after treatment were subjected to flow cytometry. Arrows indicate the increased apoptotic sub-G1 fraction after 48hr and 72 hr of cisplatin treatment in MO59J cells.

trations (50-62%) compared to DMSO treated control cells and the S-phase arrest persisted up to 72hr of analysis (Fig. 3). A great majority of apoptotic sub-G1 cells were observed in 48hr and 72 hr samples of MO59J cell line. This observation clearly indicates that DNA-PK is critical for cisplatin induced S-phase arrest. We next analyzed the cell cycle progression at early and late time points (3hr, 6hr and 24hr) in MO59J and MO59K cells after relatively low concentrations of cisplatin (2.5-10μM) treatment to accurately determine the onset of S-phase checkpoint arrest. In MO59K cells, S-phase arrest was not detectable at relatively early time points (3hr and 6hr) but the dose dependent S-phase arrest was detectable in samples analyzed at 24hr time point. These data indicate that cisplatin induced S-phase arrest occurs later than 6hr in MO59K cells. In contrast, MO59J failed to show S-phase arrest (Data not shown).

Collectively, our study indicates that DNA-PK is a critical determinant of cell survival after cisplatin exposure and the lack of S-phase arrest in MO59J cells is presumably responsible for the increased cell death after cisplatin exposure. In support of our study, activities of DNA-PK and Ku86 have been demonstrated to predict the sensitivity to cisplatin in human gliomas.[1] Available data suggest that ATR kinase is responsible for the DNA damage induced S-phase arrest in mammalian cells.[2] In this study, we have shown that cisplatin induced S-phase arrest is dependent on the functional status of DNA-PK. An earlier study demonstrated that DNA-PK is critical for RPA2 hyperphosphorylation after cisplatin treatment, indicating the possibility that DNA-PK can regulate the S-phase checkpoint by controlling RPA activity.[3] This possibility is strongly supported by the observation that RPA2 is a downstream target for ATR to regulate the S-phase checkpoint.[4] It is likely that both DNA-PK and ATR are required for an efficient S-phase checkpoint after cisplatin exposure. We are verifying this possibility by using specific inhibitors for DNA-PK in MO59K cells. Our future experiments would determine the precise role of DNA-PK in cisplatin induced S-phase arrest. Additionally, experiments are also in progress to critically evaluate the role of DNA-PK in the repair of cisplatin induced DNA inter- and intrastrand crosslinks in these glioblastoma cell lines. The present study suggests the possibility that DNA-PK can be an effective therapeutic target for sensitizing the human gliomas to cisplatin.

## References

1. Shao CJ, Fu J, Shi HL, Mu YG and Chen ZP. Activities of DNA-PK and Ku86, but not Ku70, may predict sensitivity to cisplatin in human gliomas. *J Neurooncol* **89**:27-35, 2008.
2. Brown EJ and Baltimore D. Essential and dispensable roles of ATR in cell cycle arrest and genome maintenance. *Genes Dev* **17**:615-28, 2003.
3. Cruet-Hennequart S, Glynn MT, Murillo LS, Coyne S and Carty MP. Enhanced DNA-PK-mediated RPA2 hyperphosphorylation in DNA polymerase eta-deficient human cells treated with cisplatin and oxaliplatin. *DNA Repair (Amst)* **7**:582-96, 2008.
4. Olson E, Nievera CJ, Klimovich V, Fanning E and Wu X. RPA2 is a direct downstream target for ATR to regulate the S-phase checkpoint. *J Biol Chem* **281**:39517-33, 2006. ■

# Combined Heterozygosity for DNA Repair Genes Has Significant Effect on Radiation Response

*Lubomir B. Smilenov, Guangming Zhou, Howard B. Lieberman and Eric J. Hall*

In recent years data from both mouse models and human tumors suggest that heterozygosity for genes involved in DNA repair pathways may play a central role in genomic instability and carcinogenesis. Haploinsufficiency for APC, ARF, ATM, BRCA1, BRCA2, LKB1, p53, RB and other proteins has been shown to contribute to tumorigenesis.[1-6] Additionally several examples in mouse models confirmed that double heterozygosity for functionally related genes may have an additive effect on tumor development. Combined heterozygosity for *Xpc*, and *p53*, *ATM* and p53 and *Fen1* and *Apc* genes predisposed to UVB radiation-induced skin cancer, mammary carcinoma or adenocarcinomas respectively.[7, 8, 9] Importantly, heterozygosity of some of these genes does not contribute to tumor development alone, but if combined with heterozygosity for another gene its contribution is significant. Very recent and important work enhanced further this view. A whole genome sequencing of cytogenetically normal and acute myeloid leukemia genomes from the same individual show that the only difference between the normal and tumor cells are 9 heterozygous genes. Since heterozygosity frequently results in haploinsufficiency for the corresponding protein, all of this evidence suggests that tumorigenesis depends on the expression levels of single or a combination of proteins. An open question is how environmentally induced DNA damage may contribute to tumorigenesis. Will DNA damage induced by X-ray or CT scans for example result in early onset of tumors in heterozygous individuals? The societal importance of this question is high, specifically having in mind that the number of single heterozygous individuals in the general population was shown to be between 1 and 3% for some genes. We hypothesize that tumor related processes like apoptosis for example could be less efficient in double heterozygous cells. Respectively if DNA damage is induced, transformation frequencies in this genetic background could be higher than the one in wild type cells. Therefore environmentally induced DNA damage may be more critical for individuals heterozygous for DNA repair genes. To test this hypothesis we focused our attention to three genes linked to tumor formation and DNA repair – *Atm*, *Rad9* and *Brca1*. ATM is a Ser/Thr checkpoint protein kinase that is involved in the DNA-damage response[10] ATM has multiple substrates but most importantly associates with the MRE11–RAD50–NBS1 complex initiating massive downstream signaling. Individuals deficient in ATM survive but most of them develop progressive neurodegeneration and lymphoid tumors (30% incidence). Rad9 participates in promoting resistance to DNA damage, cell cycle checkpoint control, DNA repair, and apoptosis. Other functions include a role in embryogenesis, the transactivation of multiple target genes, co-repression of androgen-induced transcription activity of the androgen receptor, a 3'-5' exonuclease activity, and the regulation of ribonucleotide synthesis.[11]

BRCA1 plays multiple roles in DNA repair mechanisms. Phosphorylation of BRCA1 by ATM is an important event in the activation of the S/G2 and G2/M checkpoints. Both ATM and BRCA1 are part of a large supramolecular protein complex named BASC for BRCA1 associated genome surveillance complex, *BRCA1* mutation carriers have 50-85% life time risk of developing breast cancer.[12]

In this study we investigated the role of heterozygosity on apoptosis and transformation in mouse models for single and double heterozygosity for *Atm/Rad9* or/and *Atm*/*Brca1* genes (no expression from the mutant allele). Apoptosis was measured in mouse thymocytes where ATM deficiency is strongly related to tumor formation. Apoptosis was assessed either after irradiation *ex vivo* (Atm/*Rad9*) or *in vivo* (*Atm*/*Brca1*). Transformation was measured by an *in vitro* assay in MEF isolated from the hybrid mice.

## Results

### Apoptosis

#### *Atm/Rad9* genotypes:

We examined thymocytes from single and double heterozygous animals for radiation-induced apoptosis. The number of animals and the genotypes used were, respectively: *Atm*wt/*Rad9*wt (five), *Atm*hz/*Rad9*hz (seven), *Atm*wt/*Rad9*hz (five), *Atm*hz/*Rad9*wt (six), *Atm*ko/*Rad9*wt (three). The mice were from four different litters. The results show differences in apoptotic frequencies related to genotype (Fig.

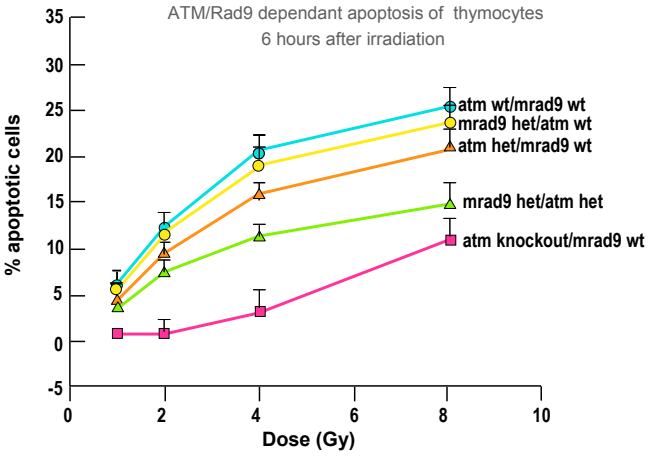


**Fig. 1.** Apoptosis of thymocytes having different genetic backgrounds. Thymocytes from mice were irradiated with different doses of γ-rays and apoptosis was measured 6 hours after irradiation. The percentage of apoptotic cells at 0 Gy were subtracted from the rest of the data points for each genotype.

1).[13] Wild-type cells display the highest apoptotic frequencies after irradiation, whereas *Atm*-deficient cells show the lowest. The differences between apoptotic frequencies in *Atm* wild-type and heterozygous cells were small but statistically significant and show that *Atm* heterozygosity could be a factor influencing programmed cell death. *Rad9* heterozygous cells show the same apoptotic rates as the wild-type control. Remarkably, the apoptotic frequencies were significantly reduced in the double heterozygous cells. The results for this genotype were closer to those obtained for the *Atm* null cells than for the wild-type, showing that haploinsufficiency for two functionally related proteins may have an additive negative effect on pathways where both proteins are normally involved.

***ATM/Brca1* genotypes:**

We examined apoptosis by measuring survival of the most numerous type of cells in the thymus (more than 80% of all cells), $CD4^+/CD8^+$ thymocytes, after *in vivo* irradiation of mice (fig. 2). As expected, 24 hrs after irradiation the numbers of $CD4^+/CD8^+$ cells were significantly reduced. The survival of $CD4^+/CD8^+$ cells from *Atm* heterozygous mice was 10% higher than the wild type ones. Interestingly, the survival of *Brca1* heterozygous thymocytes follow the same trend. However, compared with the other three genotypes, survival of the *Atm/Brca1* double heterozygous thymocytes was significantly higher. Almost 40% of these thymocytes survived, which shows that they are more resistant to radiation and less apoptotic than cells with the other genotypes. Since statistically, the number of damaged cells was the same for all genotypes, this result implies that more thymocytes with damage survived from the double heterozygous genotype and that cells from this genotype may accumulate mutations at a higher rate than those with the other genotypes.

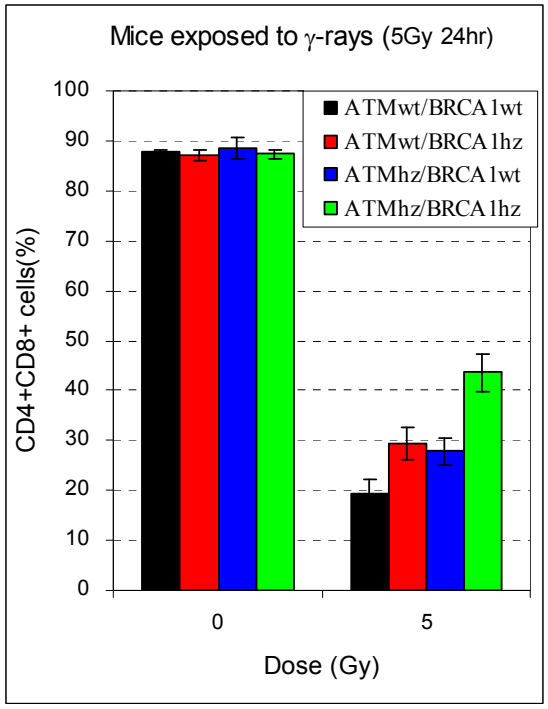


**Fig. 2.** Apoptosis $CD4^+$ $CD8^+$ cell survival after exposure to γ-ray irradiation. Cell survival was highest (apoptosis was lowest) in the double heterozygous background. In contrast the percent of $CD4^+$ $CD8^+$ cells does not depend of the genotype in nonirradiated cells. The numbers of mice used was three per genotype for the controls and five per genotype for the irradiated.

**Cell transformation**

***Atm*/*Rad9* genotype:**

Radiation-induced transformation of MEFs was examined to begin to access the impact of genotype on this end point. A total of 21 embryos from five litters were used and included five for genotypes *Atm*wt/M*Rad9*wt, *Atm*hz/M*Rad9*wt, and *Atm*wt/M*Rad9*hz and six for *Atm*hz/M*Rad9*hz. Yields of transformed clones were measured both for unexposed controls and after a dose of 2 Gy. The relative transformation, defined as the ratio of the number of transformed clones per surviving heterozygous cell relative to the number of transformed clones per surviving wild type cell was respectively: *Atm*hz/*Rad9*wt – 1.91 (p=0.03), *Atm*wt/*Rad9*hz – 1.45 (p=0.31), *Atm*hz/*Rad9*hz – 3.1 (p=0.001). These results indicate a statistically significant higher transformation frequency for the double heterozygous cells. Transformation frequencies for these cells are more than double that of the wild-type population. The M*rad9* heterozygous cells show a transformation frequency close to that of the wild-type cells, and the frequency for the *ATM* heterozygous cells is between the wild-type and double heterozygous cells. There were small differences in the clonogenic survival for all populations after irradiation.

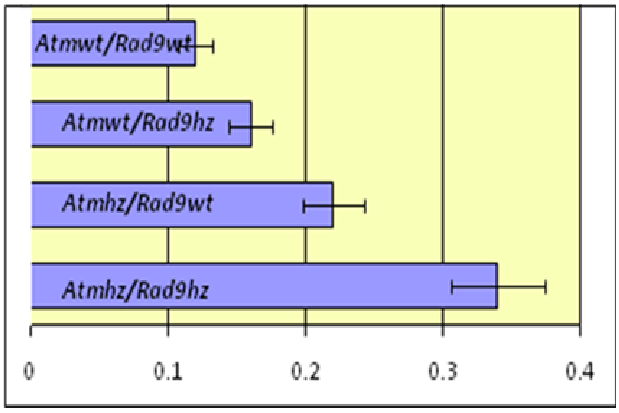


**Fig. 3.** Transformation frequency following a dose of 2 Gy γ-rays in mouse embryo fibroblasts as a function of the status of the *Atm* and *Rad9* genes.

***Atm/Brca1* genotype:**

Radiation-induced transformation of MEFs were examined as a surrogate for carcinogenesis *in vivo*. Embryos from five litters were used and included the following genotypes: *Atm*wt/*Brca1*wt, *Atm*hz/*Brca1*wt, *Atm*wt/*Brca1*hz, and *Atm*hz/*Brca1*hz. Yields of transformed clones were measured both for unexposed controls and after a dose of 2 Gy. (Fig. 4). The relative transformation, defined as the ratio of the number of transformed clones per surviving heterozygous cell relative to the number of transformed clones per surviving wild type cells was respectively: *Atm*hz/*Brca1*wt -

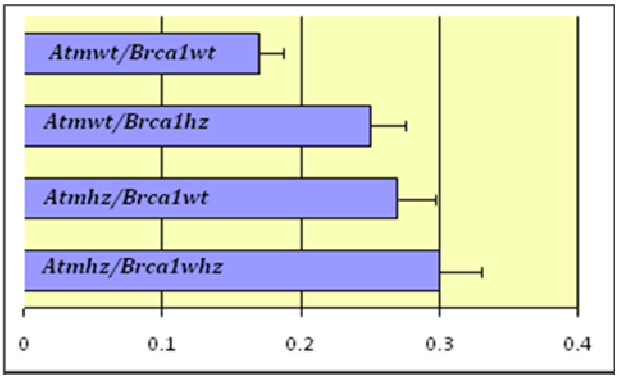


**Fig. 4.** Transformation frequency following a dose of 2 Gy γ-rays in mouse embryo fibroblasts as a function of the status of the Atm and BRCA1 genes.

2.28 (p=0.04), *Atm*wt/*Brca1*hz - 2.54 (p=0.03), *Atm*hz/*Brca1*hz - 2.7 (p=0.03). *Atm* heterozygotes show twice the transformation frequency of the wild-type cells following a dose of 2 Gy. *Brca1* heterozygotes show a similar transformation frequency as the *Atm* hz, however, the interesting point to note is that the double heterozygote *Atm/Brca1* shows little or no increase over *Brca1*hz or *Atm* hz alone.

**Discussion**

The main goal of this study is to investigate to what degree hz for DNA repair genes affects key processes involved in tumor formation. In recent years epidemiological data as well as studies in mouse models confirmed that heterozygosity may play a significant role in tumor initiation and development. The most striking conclusion from these experiments is that heterozygosity for a single gene may contribute to tumor formation. There are indications that in the general population the number of heterozygous individuals for some genes could be quite substantial. *ATM* heterozygotes for example could be as high as 1-3% of the US population.[14] To what degree these or other heterozygous carriers may have increased cancer risk is very important issue which can be resolved only after revealing the mechanisms underlying the role of heterozygosity in tumor formation. The role of heterozygosity is usually well defined in cases where the product of the mutant allele is a truncated protein having a dominant negative effect. Truncated versions of p53, Rb, Ras, NF1, ATM, BRCA1 and 2, INK4 family of proteins, CREB binding protein (CBP) and others have been identified in different tumors.[15] Much more difficult to explain are the cases where the mutant allele does not produce any protein since usually the carriers of these mutations are asymptomatic. We hypothesize that haploinsufficiency is a factor mostly in acute cell conditions, where different factors trigger stress response pathways. Due to the network mode of this response, the insufficient expression level(s) of some proteins may lead to a reduced overall network response. As a consequence, stress related processes like apoptosis for example may be less effective. Our results confirmed this hypothesis. Combined haploinsufficiency for *Atm* and *Rad9* and *Atm* and *Brca1* genes show an additive negative effect on apoptosis induction after irradiation. Cell transformation in similar conditions shows an additive effect for *Atm*/*Rad9* genes. Heterozygosity for *Atm* and *Brca1* alone led to higher transformation frequency while heterozygosity for *Rad9* was the same as in the wt cells. The degree of cell transformation and induced genomic instability depends on the efficiency of apoptosis in the affected cells. In our models, apoptosis depended largely on the genetic background. The lowest level of apoptosis was registered in double heterozygous cells, where the frequency was two times lower than those in wild type cells and 1.5 times lower than in the single heterozygous cells. Since statistically the number of damaged cells was the same for all genotypes, the differences in cell survival suggests that damage detection was less efficient in the double heterozygous cells and that initially more cells with DNA damage will accumulate in the thymuses of double heterozygous animals. Many of those cells will undergo apoptosis in subsequent division attempts but a very small fraction may survive increasing the probability of cells transformation in later stages. How reduced levels of expression of a single protein may have such a big overall role in cell events may be understood in the context of network interactions active in cells. Biological networks are self assembly/disassembly networks. For example, many local networks may be assembled only when they are needed – for instance after DNA double-strand breaks are induced. The requirement for assembly in response to an event at an unknown point in a relatively large (on molecular scale) area, introduces spatial and quantitative limitations on the process. DNA double-strand breaks for example are a local event that may appear at any place in the nucleus. A local network has to be assembled at the points of DNA double-strand breaks in order to signal and initiate the repair. The proteins, potential members of the local networks, have to be in close proximity to the break or to be able to translocate quickly to the site. Several experiments confirmed that scenario. Immunofluorescence analysis of cells after radiation induced DNA double-strand breaks show that many DNA repair proteins, like ATM, p53, MRE11, Rad50 and NBS1, ATR, colocalize and form discrete foci on the sites of DNA damage.[16, 17] In addition, migration of DNA repair proteins toward the site of DNA damage has been analyzed by FRAP. By measuring the diffusion coefficient of various repair proteins it has been shown that translocation and transient immobilization of RAD51, RAD52, RAD54 as well as the NER repair complex ERCC1-XPF[18, 19] occurs on DNA repair sites in mammalian cells. In the case of multiple DNA dsb, haploinsufficiency for Atm/Rad9 or Atm/Brca1 may lead to incomplete DNA damage detection and reduced apoptosis. All this could likely lead to mutation accumulation.

In summary, we have shown that haploinsufficiency and combined haploinsufficiency for Atm/Rad9 and ATM/Brca1 is a factor in cell transformation and apoptosis. While it has long been hypothesized that radiosensitivity in some individuals may well be the result of SNP in a multitude of genes of low penetrance, little progress has been made in elucidating specific examples. On the other hand, we have now identified three low frequency, high penetrance genes that are all very likely candidates to confer sensitivity to

radiation induced effects, such as cancer. While the frequency of any one is relatively low in the general population, though not so low in certain ethnic groups, added together individuals heterozygous for one or more of these genes constitute a sub-population that are relatively radiosensitive, and there are special circumstances in which this needs to be taken into account.

### References


1. Santarosa M and Ashworth A. Haploinsufficiency for tumour suppressor genes: when you don't need to go all the way. *Biochim Biophys Acta* **1654**:105-22, 2004.
2. Kastan MB and Bartek J. Cell-cycle checkpoints and cancer. *Nature* **432**:316-23, 2004.
3. Vladutiu GD. Heterozygosity: an expanding role in proteomics. *Mol Genet Metab* **74**:51-63, 2001.
4. Yan H, Dobbie Z, Gruber SB, Markowitz S, Romans K, Giardiello FM, Kinzler KW and Vogelstein B. Small changes in expression affect predisposition to tumorigenesis. *Nat Genet* **30**:25-6, 2002.
5. Le Toriellec E, Despouy G, Pierron G, Gaye N, Joiner M, Bellanger D, Vincent-Salomon A and Stern MH. Haploinsufficiency of CDKN1B contributes to leukemogenesis in T-cell prolymphocytic leukemia. *Blood* **111**:2321-8, 2008.
6. Bartek J, Lukas J and Bartkova J. DNA damage response as an anti-cancer barrier: damage threshold and the concept of 'conditional haploinsufficiency'. *Cell Cycle* **6**:2344-7, 2007.
7. Cheo DL, Meira LB, Burns DK, Reis AM, Issac T and Friedberg EC. Ultraviolet B radiation-induced skin cancer in mice defective in the Xpc, Trp53, and Apex (HAP1) genes: genotype-specific effects on cancer predisposition and pathology of tumors. *Cancer Res* **60**:1580-4, 2000.
8. Umesako S, Fujisawa K, Iiga S, Mori N, Takahashi M, Hong DP, Song CW, Haga S, Imai S, Niwa O*, et al.* Atm heterozygous deficiency enhances development of mammary carcinomas in p53 heterozygous knockout mice. *Breast Cancer Res* **7**:R164-70, 2005.
9. Kucherlapati M, Yang K, Kuraguchi M, Zhao J, Lia M, Heyer J, Kane MF, Fan K, Russell R, Brown AM*, et al.* Haploinsufficiency of Flap endonuclease (Fen1) leads to rapid tumor progression. *Proc Natl Acad Sci USA* **99**:9924-9, 2002.
10. Lavin MF. Ataxia-telangiectasia: from a rare disorder to a paradigm for cell signalling and cancer. *Nat Rev Mol Cell Biol* **9**:759-69, 2008.
11. Lieberman HB. Rad9, an evolutionarily conserved gene with multiple functions for preserving genomic integrity. *J Cell Biochem* **97**:690-7, 2006.
12. Gudmundsdottir K and Ashworth A. The roles of BRCA1 and BRCA2 and associated proteins in the maintenance of genomic stability. *Oncogene* **25**:5864-74, 2006.
13. Smilenov LB, Lieberman HB, Mitchell SA, Baker RA, Hopkins KM and Hall EJ. Combined haploinsufficiency for ATM and RAD9 as a factor in cell transformation, apoptosis, and DNA lesion repair dynamics. *Cancer Res* **65**:933-8, 2005.
14. Khanna KK. Cancer risk and the ATM gene: a continuing debate. *J Natl Cancer Inst* **92**:795-802, 2000.
15. Payne SR and Kemp CJ. Tumor suppressor genetics. *Carcinogenesis* **26**:2031-45, 2005.
16. Rouse J and Jackson SP. Interfaces between the detection, signaling, and repair of DNA damage. *Science* **297**:547-51, 2002.
17. Falck J, Coates J and Jackson SP. Conserved modes of recruitment of ATM, ATR and DNA-PKcs to sites of DNA damage. *Nature* **434**:605-11, 2005.
18. Essers J, Houtsmuller AB, van Veelen L, Paulusma C, Nigg AL, Pastink A, Vermeulen W, Hoeijmakers JH and Kanaar R. Nuclear dynamics of RAD52 group homologous recombination proteins in response to DNA damage. *Embo J* **21**:2030-7, 2002.
19. Houtsmuller AB, Rademakers S, Nigg AL, Hoogstraten D, Hoeijmakers JH and Vermeulen W. Action of DNA repair endonuclease ERCC1/XPF in living cells. *Science* **284**:958-61, 1999.


■

# Alteration of p53-Binding Protein 1 Kinetics in Hypoxic Cells

*Alexander V. Kofman, Burong Hu and Charles R. Geard*

Hypoxia can influence radio resistance of tumors directly through the deprivation of oxygen, and indirectly through different mechanisms, such as promoting genomic instability, selecting for radiation resistant cells, and regulating gene expression. The tumor suppressor p53 binding protein 1 (53BP1) enhances p53-mediated transcriptional activation. 53BP1 exhibits a more homogeneous nuclear distribution in the absence of exogenous DNA damage but forms discrete nuclear foci in response to ionizing radiation (IR) induced DNA double strand breaks (DSB). The focal sites of 53BP1 are believed to represent the sites of DSB, and 53BP1 foci co-localize with one of the well known surrogate DSB

marker, phosphorylated histone H2AX (γ-H2AX).[1, 2]

The aim of this study was to compare the kinetics of 53BP1 in irradiated normoxic vs. hypoxic mammalian cells. NIH/3T3 mouse cells and normal human lung fibroblasts (NHLF) were cultured under normoxic and hypoxic conditions and subjected to gamma-irradiation at the dose of 2Gy. The custom-made hypoxic chambers allowed us to avoid re-oxygenation of cells before irradiation. Cells were cultured with and without 2-nitroimidazole (pimonidazole hydrochloride, PMDZ), a radiosensitizer, which is also used to detect hypoxic cells *in vivo*. The 53BP1 foci formation was analyzed at 30 min and 120 min after IR by immunological staining using a polyclonal rabbit antibody (Novus Biologicals, USA). The relative size and number of 53BP1 foci were analyzed both manually and by using NIH software (Image J). The intensity of 53BP1 nuclear staining in non-irradiated normoxic vs. hypoxic cells was evaluated with the software Image J by measuring the Mean Grey Value, the average grey value within the selection, which represents the mean optical density of the selected area.

**Results**

We established a model for the growth of cells under chronic hypoxic conditions where the concentration of dissolved oxygen gradually decreases over time (Fig. 1). The cells were positively stained for 2-nitroimidazole adducts formed with thiol groups exclusively in the hypoxic environment (Fig. 2). Hypoxia resulted in significantly lower micronuclei incidence after IR (Fig. 3). The hypoxic non-irradiated cells showed an elevated 53BP1 expression as compared to the normoxic cells (Fig. 4A, 4B). In the preliminary experiments performed with NIH/3T3 cells, a positive correlation was observed between the number of 53BP1 foci per nucleus and the total area occupied by foci as a function of radiation dose (0.5-2Gy of γ-rays; data not shown). Since a dose of 2Gy of γ-rays produced significant differences in micronuclei frequency between normoxic and hypoxic cells, we have chosen this radiation dose for analyzing the kinetics of 53BP1 foci formation. For the kinetic analysis of 53BP1, we have preferred to count the area of foci size instead of the foci number[3] for the following reasons: (I) 53BP1 foci number greatly increased after 2Gy of γ-rays making it very difficult to accurately determine the number and (II) most of the foci merge together which cannot be clearly distinguished by the Imaje J software pro-

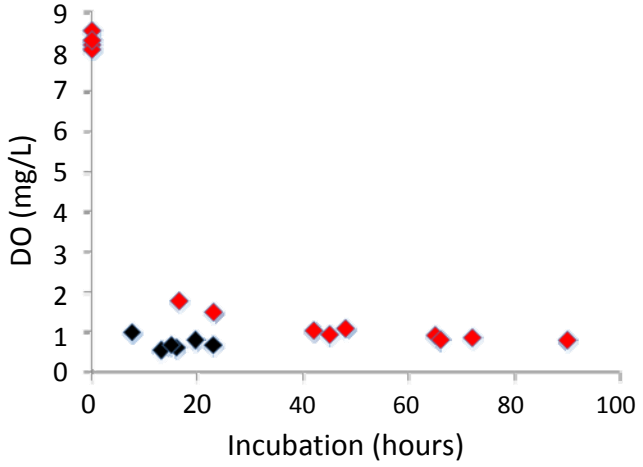


**Fig. 1.** Changes of the concentration of dissolved oxygen (DO) in the culturing medium. Red and black dots represent two different sets of experiments where cell culture vessels were kept with (red) and without (black) lids.

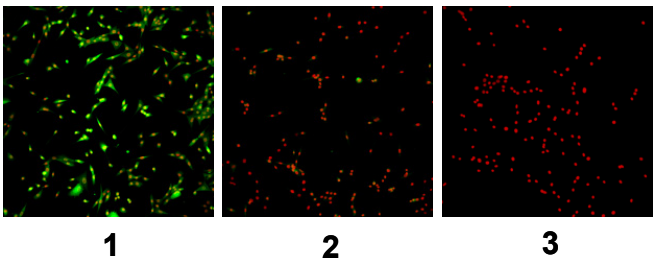


**Fig. 2.** Detection of 2-nitroimidazole adducts in hypoxic cells after 14 hours of incubation. **1.** DO concentration = 0.5 mg/L; **2.** DO concentration = 7 mg/L; **3.** DO concentration = 0.5 mg/L without 2-nitroimidazole.

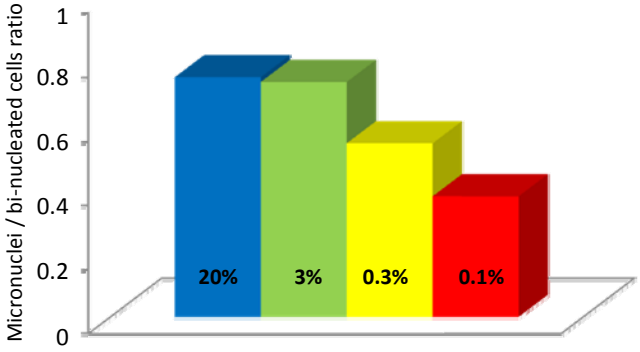


**Fig. 3.** Micronuclei incidence in NIH/3T3 cells cultured for 16 hours in the atmosphere with 20%, 3%, 0.3% and 0.1% oxygen.

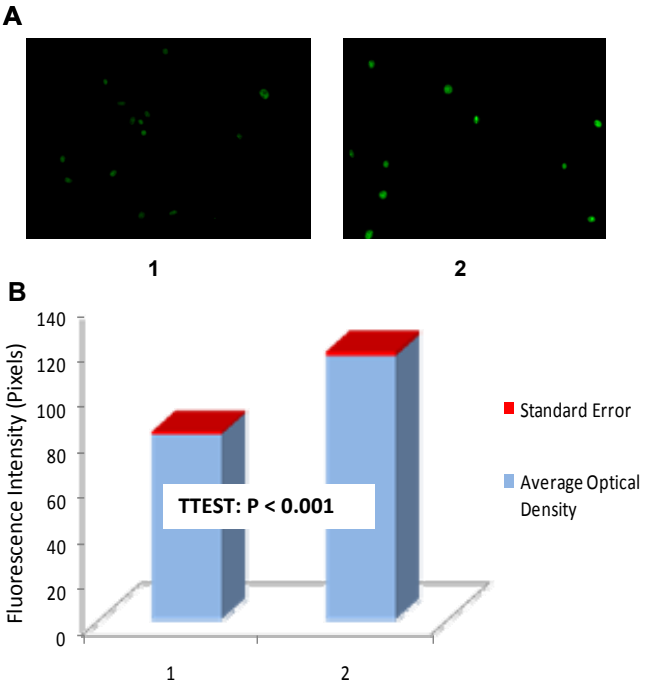


**Fig. 4. A.** 53BP1 expression in non-irradiated cells. **B.** 53BP1 optical density 1– normoxic, and 2- hypoxic conditions.

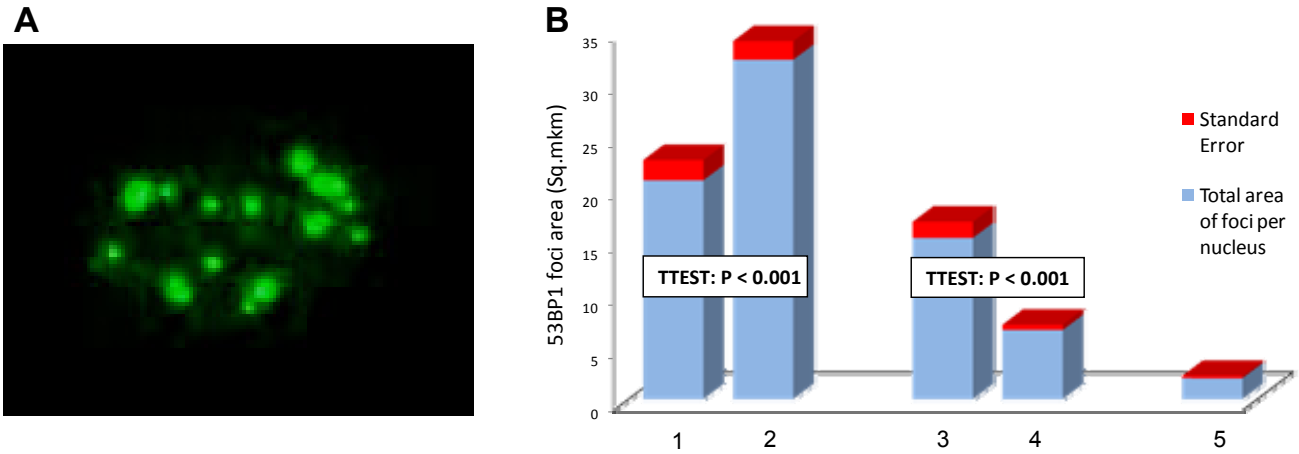


**Fig. 5. A.** 53BP1 foci **B.** 53BP1 foci as the total area per nucleus. 1- and 2- correspondingly normoxic and hypoxic cells at 30 min after IR; 3- and 4- normoxic and hypoxic cells at 2 hours after IR; 5 – non-irradiated cells (control).

gramme. At 30 min after IR, hypoxic cells showed significantly more 53BP1 foci than normoxic cells. However, by 2 hours after IR the total foci positive area in the nuclei of both hypoxic cells and normoxic cells decreased and the decrease was found to be rapid for hypoxic cells as compared to normoxic cells (Fig. 5). The presence of radiosensitizer PMDZ in the growth medium abrogated the disappearance of 53BP1 foci in the nuclei of hypoxic cells at the two-hour time point after IR (data not shown). Similar results were obtained with NHLF cells. However, due to an apparently higher sensitivity of NHLF to IR as compared to NIH/3T3 cells, IR dose as well as the parameters for foci analysis, need more optimization for NHLF cells.

The elevated expression and turnover of 53BP1 in hypoxic cells apparently results in the higher efficiency of DNA DSBs repair processes, which is confirmed by the lower incidence of micronuclei in irradiated hypoxic cells. The obtained data support the hypothesis that hypoxic conditions may cause the shift toward the error-prone DNA repair, rather than toward apoptosis of irradiated tumor cells.

### References

1. Santarosa M and Ashworth A. Haploinsufficiency for tumour suppressor genes: when you don't need to go all the way. *Biochim Biophys Acta* **1654**:105-22, 2004.
2. Kastan MB and Bartek J. Cell-cycle checkpoints and cancer. *Nature* **432**:316-23, 2004. ■

# Use of geNorm to Identify Appropriate Endogenous Controls for Normalization of Gene Expression in a Macro Array

*Shanaz A. Ghandhi and Sally A. Amundson*

Gene expression analysis involves many different methodological approaches such as microarray analysis and real-time PCR. These two methods are the preferred approaches for a lot of work that is published today, but researchers also use serial analysis of gene expression, RNase protection assays and northern blotting methods to analyse RNA. Microarray and real-time quantitative PCR approaches employ different chemistries for identifying target gene expression levels and facilitate the measurement of the full spectrum from whole genomic analyses to individual gene analyses. Real-time PCR in particular may be used to measure the steady state mRNA level of a target gene in a RNA pool and this can be extended to the simultaneous measurement of a few (less than 10 genes) in multiplexed reactions. A specific type of real-time PCR method is the Taqman assay, which utilizes a sequence specific probe (onto which a fluorophore and quencher are attached) in addition to sequence specific primers. Binding of the primers and probe to the cDNA target initiates the polymerase and releases the fluorophore into the solution. The quencher molecule can no longer block light emission from the fluorophore, and the fluorescent reporter signal is recorded in real time. The advantages of this system are many, including miniaturization into very small volumes of <10 µL. Therefore, we can select multiple genes

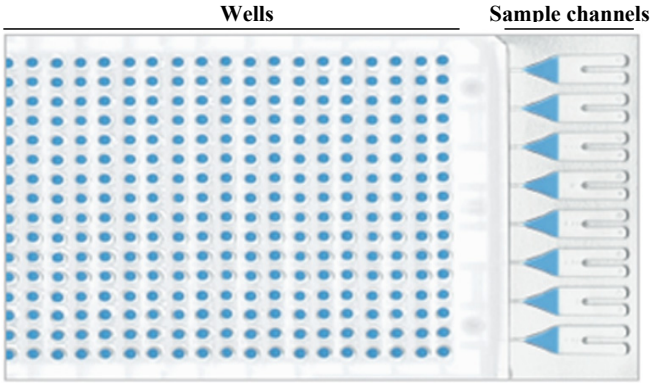


**Fig. 1.** Low-density array card showing 384 reaction wells which are <1.8 µL in volume and sample injection channels to the right. cDNA pools are pipetted into these channels and the card is carefully centrifuged to distribute the liquid equally into the reaction wells. The card is sealed and gene specific primers and reagents previously loaded into the wells go into solution. The cards are then run on the ABI 7900 FAST cycler. Readouts are generated using SDS software (ABI).

of interest and process them simultaneously in a microfluidic-based platform such as the low-density array available from Applied Biosystems (ABI).

This platform allows for the quick processing of multiple target genes from a single cDNA pool reducing the need for replication and numerous negative controls (such as no DNA control and primer controls) for the reaction itself. The inclusion of multiple housekeeping genes on the low density PCR array is crucial for the simultaneous analysis of multiple (>10 genes) targets from the same cDNA pool. The ABI low-density array platform has many configurations of 384 individual reactions on a micro-fluidic card. The choices range from 4 replicates of 11 assays plus 1 control in 8 separate sample channels to 380 assays plus 4 controls for 1 sample in 8 channels. For our study we chose the 48 gene format made up of 41 assays plus 7 housekeeping genes per sample channel for a total of 8 samples per card, as seen in Figure 1. The choice of housekeeping genes is a subject of debate and constant review in research and the use of more than one housekeeping gene for the analysis of greater than 10 target genes as in this platform is reasonable. We will discuss one method of normalizing real time PCR results, geNorm in detail.[1]

## Description of the experiment

We are using IMR-90 primary human diploid lung fibroblast cells in studies of the radiation bystander effect. The cells are plated in special Mylar dishes[2] with thicker strips of Mylar to shield the bystander cells during irradiation and separate them from the directly irradiated cells. After irradiating the cells with 0.5Gy alpha particles at the RARAF accelerator we isolated total RNA from the two treated cell populations and corresponding untreated controls at various times after exposure. These samples are processed to obtain RNA, which is then quantified and assessed for quality of RNA using the Nanodrop spectrophotometer to measure A260/A280 and A260/A230 ratios. Acceptable ratios are >1.8 for good quality RNA preparations. We then reverse transcribed 100ng of total RNA to complementary cDNA using the High capacity RT kit (Applied Biosystems). The entire cDNA reaction was mixed with 2X universal PCR mix (Applied Biosystems) and loaded into sample channels (Fig. 1). Using the 48-gene Low Density array format we simultaneously analyzed the gene expression levels of 41 target genes identified as of interest in our bystander studies[3] and 7 housekeeping genes.

## Description of the problem

In real-time PCR analysis of mRNA levels, the crossover threshold cycle number (Ct) is used for calculating the relative level of gene expression by the $2^{-\Delta\Delta Ct}$ method.[4] This method is extremely sensitive to the initial logarithmic phase of the amplification curve where the Ct values of each gene and sample are detected. This point is inversely related to the starting amount of the specific target mRNA in a specific sample. In the $2^{-\Delta\Delta Ct}$ method there are two choices to be made, first, the choice of calibrator sample. In studies of stress response this is usually the untreated control sample. Second, an endogenous control gene, often referred to as a housekeeping gene, must be selected to normalize between samples. This is done primarily as a loading control to calculate internal variations between samples with the assumption that the housekeeping gene expression level should not vary across samples. Therefore when choosing a housekeeping gene for normalizing the data it is preferred that Ct values of this gene remain as constant as possible across all samples and conditions (Fig. 2), and to be as close as possible to the Ct range of the target samples. As seen in Figure 2, there is a difference in the range of Ct values for each potential housekeeping gene across all samples and application of a normalizing method is required to identify the most suitable normalizing genes. Another problem when measuring 41 genes simultaneously as in our study is that there will be high abundance mRNA genes (overall low Ct values) and low abundance mRNA genes (overall high Ct values) and since they are selected as differentially expressed genes from microarray studies, they are also expected to show a range of Ct values across the samples. The use of a single endogenous control gene would then exclude genes with a range of Cts that differed from that of the chosen housekeeping gene. For this reason we included seven housekeeping genes (Table 1) in our LDA design and applied geNorm to find those

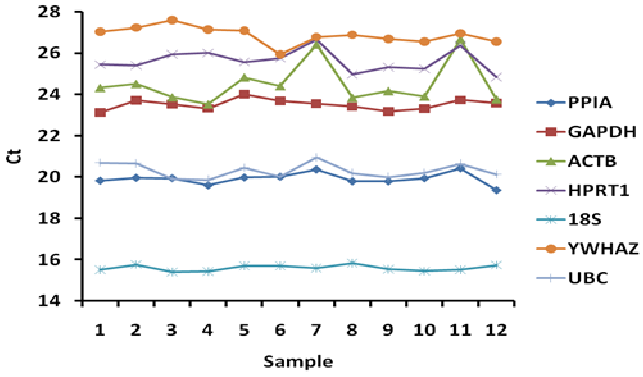


**Fig. 2.** Real time PCR analysis results, showing Ct values of 12 samples included in this study.

**Table 1.** Candidate housekeeping genes that were analyzed by geNorm on low-density arrays

| Number | Assay ID | Gene Symbol | Name |
|---|---|---|---|
| 1 | Hs99999904_m1 | *PPIA* | peptidylprolyl isomerase A (cyclophilin A) |
| 2 | Hs99999905_m1 | *GAPDH* | glyceraldehyde-3-phosphate dehydrogenase |
| 3 | Hs99999903_m1 | *ACTB* | actin, beta |
| 4 | Hs00824723_m1 | *UBC* | ubiquitin C |
| 5 | Hs99999909_m1 | HPRT1 | hypoxanthine phosphoribosyltransferase 1 (Lesch-Nyhan syndrome) |
| 6 | Hs00237047_m1 | YWHAZ | tyrosine 3-monooxygenase/tryptophan 5-monooxygenase activation protein, zeta polypeptide |
| 7 | Hs99999901_s1 | 18S | Ribosomal subunit 18s coding gene |

that were most stable in our experiments and most appropriate for use as normalizers.

The geNorm algorithm is a two step method based on two assumptions, first, the expression ratio between two ideal internal control genes should be identical in all samples and second, that these genes are not co-regulated. All seven housekeeping genes in our study were assessed for pair wise variation, which reflects the systematic variation between replicates of the same sample (Fig. 3). The algorithm calculates a measure M, which estimates the effect on stability of adding one more housekeeping gene to the normalization factor. The algorithm started by calculating the most stable gene pair, then added one more gene and measured the stability again. It continued to add one gene at a time and assess stability after each addition. The algorithm repeated the calculation until all housekeeping genes were included in the iterative analysis. This analysis provided the number of genes that can be used to normalize the data set and a ranking of the most stable genes. In our study we found that two genes, *UBC* and *PPIA*, were most stable (Fig. 4) and sufficient for normalization (Fig. 3). Adding a third gene to the normalization factor not only did not result in any gain of stability, but actually increased the variation (Fig. 3).

**Verification of housekeeping genes for IMR90 fibroblast study**

In our studies we were interested in identifying the minimum number and the specific housekeeping genes that would help optimize our real-time PCR results. We measured Cts of all 48 genes on the low-density array of four biological replicates of control, irradiated and bystander cells assayed 4 hours after exposure. To decide how many housekeeping genes would be most appropriate for our study we applied geNorm, and used the selected genes *PPIA* and *UBC* to normalize the rest of the data set using the $2^{-\Delta\Delta Ct}$ method. As a result we could assess the stability of all other housekeeping genes included on the low density array. As mentioned earlier, theoretically the relative expression of all housekeeping genes is expected to be constant across all conditions and replicates, and should not be affected by irradiation, but that is not the case (Fig. 5). In human tissue culture systems, *ACTB* is often used as a normalizing gene in

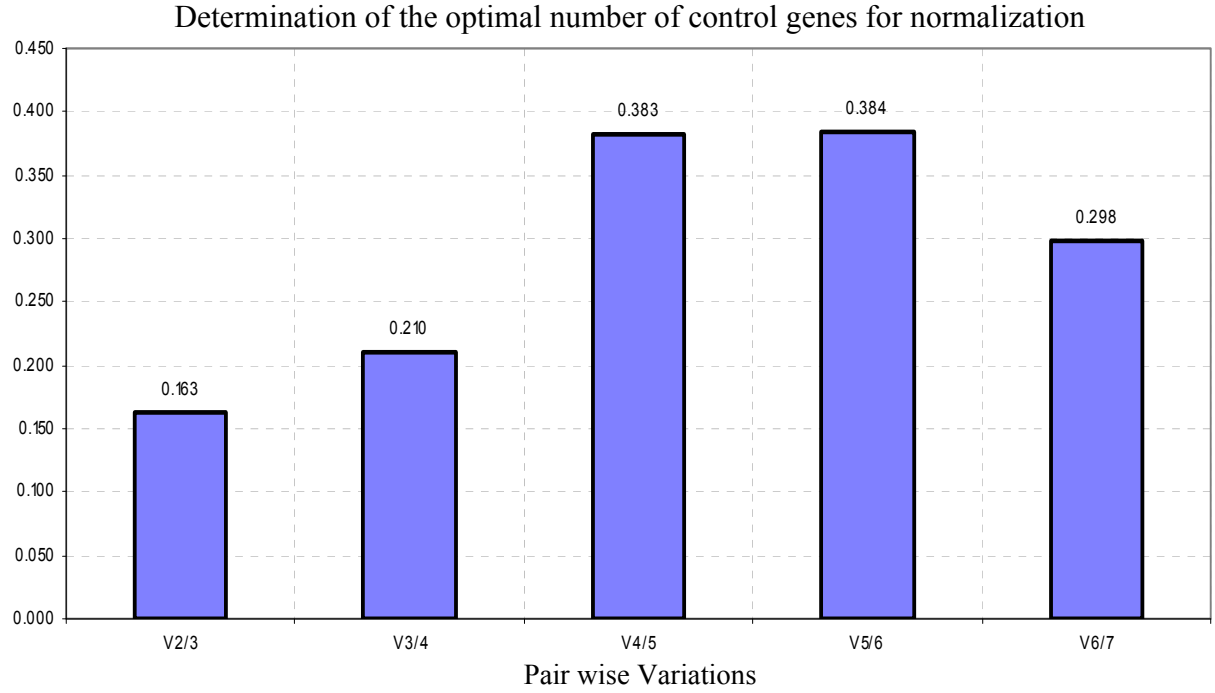


**Fig. 3.** Pair wise analysis of housekeeping genes in geNorm.

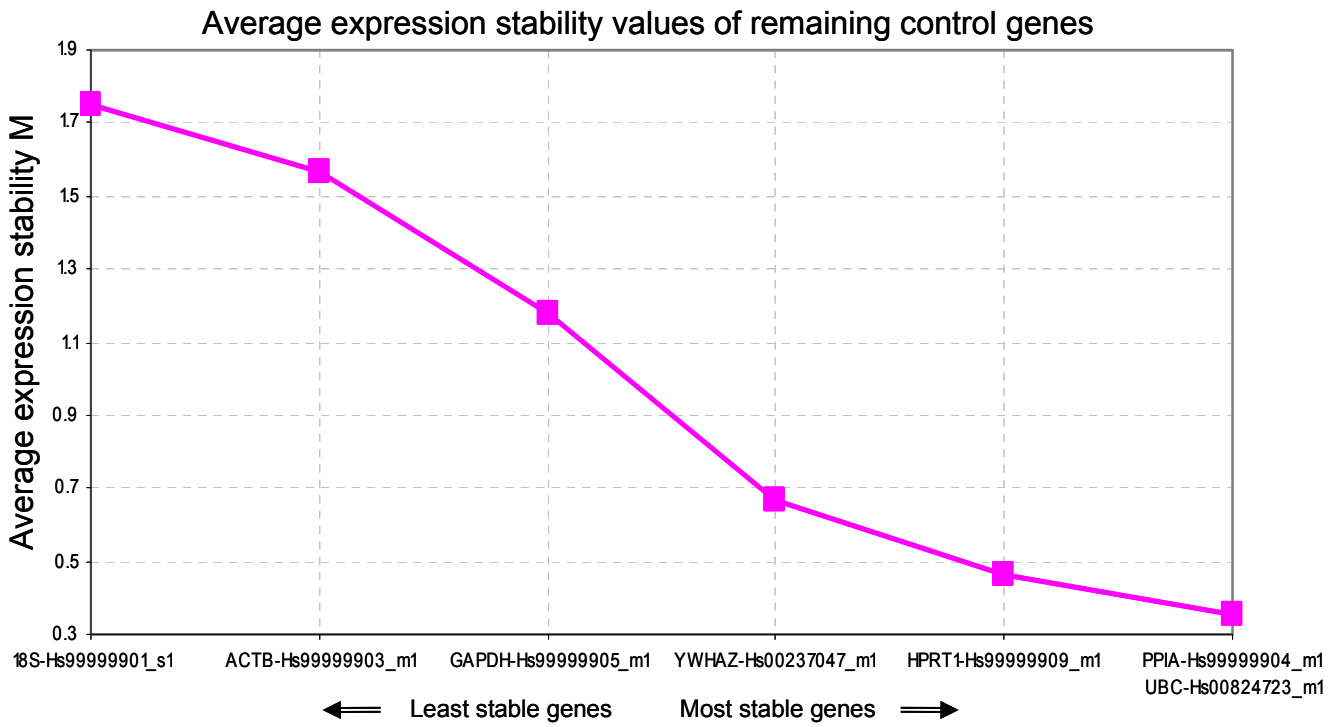


**Fig. 4.** geNorm ranking of genes by stability metric M.

real-time PCR. However, in our study the expression of *ACTB* is decreased relative to controls in irradiated and bystander IMR90 fibroblasts. If *ACTB* were used as a housekeeping gene, it would over-estimate relative mRNA abundance of target genes. Other genes such as *YWHAZ* and *HPRT1* are induced by irradiation in the same study, which would have the opposite effect on target gene quantitation. Use of multiple housekeeping genes and application of geNorm to gene expression data improve quantitation of gene expression by increasing the sensitivity of detection of both subtle and more dramatic differences in gene expression. The geNorm methodology does have several drawbacks, however. It requires the assumption that the endogenous control genes used are not co-regulated, which is not known. It is also only appropriate for use when studying a small number of genes and is difficult to extend to a genome-wide analysis because assessing the housekeeping genes across an entire genome would be computationally intensive. Other methods attempt a more meta-analytical approach which can lead to discovery of more appropriate normalizing genes and on a more global scale.[5] Overall, when using relative quantitative methods such as real time PCR to estimate mRNA

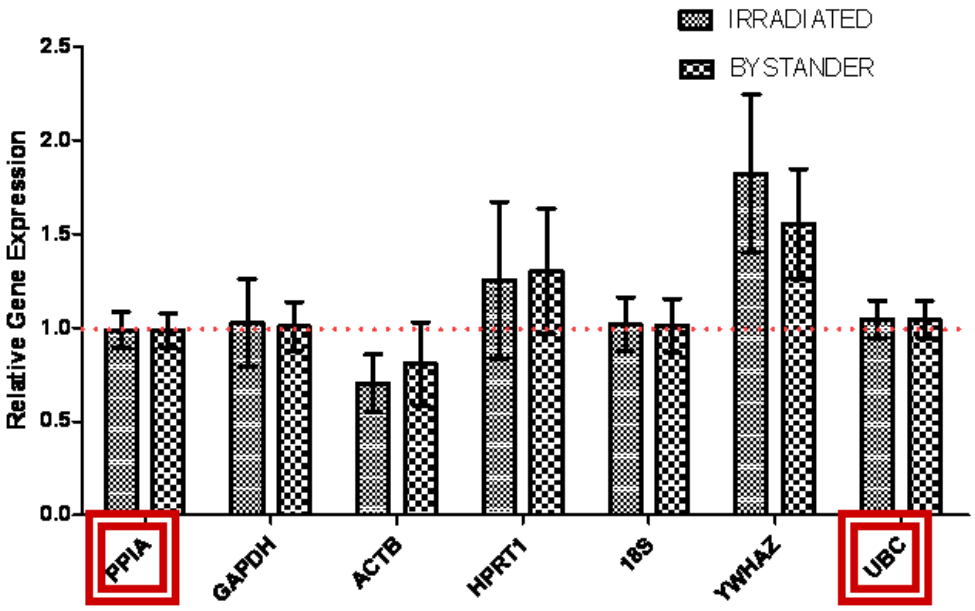


**Fig. 5.** Graph of relative expression of 7 housekeeping genes in treated IMR90 cells relative to controls as measured using geNorm. Red boxes indicate the genes selected using Genorm as most stable genes and suitable as housekeeping genes.

abundance in a model system, it is important to use an approach such as geNorm to identify a suitable set of housekeeping genes instead of using conventionally accepted housekeeping genes whose inherent instability would give misleading results.

### References


1. Vandesompele J, De Preter K, Pattyn F, Poppe B, Van Roy N, De Paepe A and Speleman F. Accurate normalization of real-time quantitative RT-PCR data by geometric averaging of multiple internal control genes. *Genome Biol* **3**:RESEARCH0034, 2002.
2. Zhou H, Ivanov VN, Gillespie J, Geard CR, Amundson SA, Brenner DJ, Yu Z, Lieberman HB and Hei TK. Mechanism of radiation-induced bystander effect: role of the cyclooxygenase-2 signaling pathway. *Proc Natl Acad Sci USA* **102**:14641-6, 2005.
3. Ghandhi SA, Yaghoubian B and Amundson SA. Global gene expression analyses of bystander and alpha particle irradiated normal human lung fibroblasts: Synchronous and differential responses. *BMC Med Genomics* **1**:63, 2008.
4. Livak KJ and Schmittgen TD. Analysis of relative gene expression data using real-time quantitative PCR and the 2(-Delta Delta C(T)) Method. *Methods* **25**:402-8, 2001.
5. Popovici V, Goldstein DR, Antonov J, Jaggi R, Delorenzi M and Wirapati P. Selecting control genes for RT-QPCR using public microarray data. *BMC Bioinformatics* **10**:42, 2009. ■


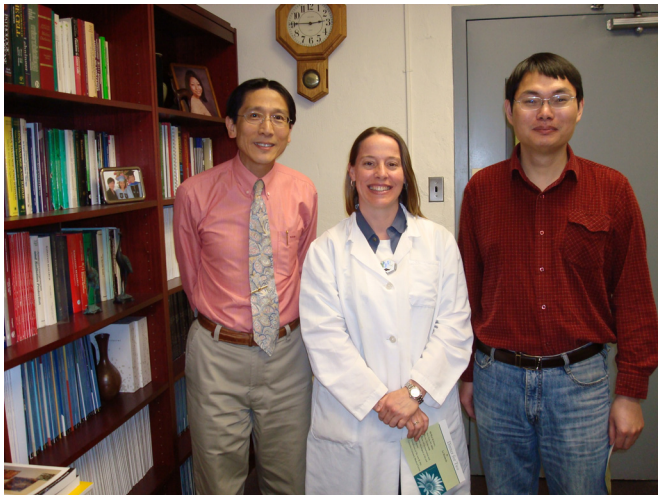

The winners of 2007-2008 Journal Club. (L-r): Dr. Tom Hei, host of Journal Club, Dr. Jarah Meador, the best moderator, Dr. Chuanxin Huang, the best presenter.

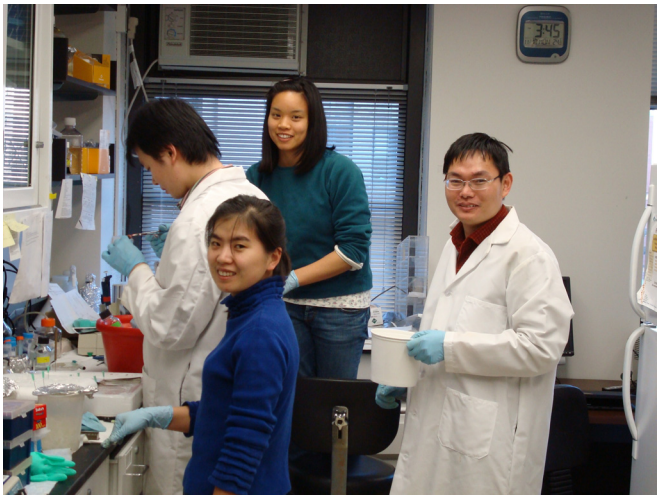

Team work of Dr. Yuxin Yin's Lab. (L-r): Mr. Ying Kong, Ms. Tingting Gu, Ms. Annie Chow and Dr. Chuanxin Huang.

Dr. Shanaz Ghandhi (left) is discussing science with Dr. Eleanor Blakely (right), the external advisory committee member of the Center for Radiological Research program project grant on mechanism of radiation-induced bystander effect.

Dr. Tom Hei's Ph.D. student, Sarah Huang (right) won the Best Poster Award at the International Mineral Fiber meeting in Cape Town in September, 2008. Professor Sam Kacew presented the award to Sarah.

# Agilent One Color Low RNA Input Linear Amplification Microarrays: Modified Protocol and Evaluation of Expression Profiling Quality Control Measurements

*Sunirmal Paul and Sally A. Amundson*

Microarray technology has dramatically advanced in the past few years and the demand for low RNA input amplification kits to generate biologically meaningful and reproducible microarray data from limited biological samples is increasing. Although use of microarray technology has exploded in recent years in all areas of biological and clinical research, the widespread use of this technology can be hindered by the high cost associated with the technology itself. Due to extensive usage, a large number of biotech companies presently manufacture and supply direct labeling DNA microarray products, hence the prices are getting cheaper. On the other hand, the price of low input RNA amplification kits, produced by only a few manufacturers, is still increasing, in spite of increasing demand in research and in clinical practice. For limited samples, Agilent Technologies has developed T7-based one- or two- color linear amplification kits that produce high quality, labeled cRNA targets for oligonucleotide microarrays. Each kit costs nearly $2,200, and is designed to provide 20 amplification reactions using 50 – 1,000 ng total RNA sample input per reaction. In the current work, we assess the effect of reduction of transcription master mix volume to nearly half of the recommended volume and compare the results with those of standard labeling reactions. We also include an adapted protocol to reduce the cost per reaction.

## METHODOLOGY

### RNA extraction, quantitation and purity assessment

Human peripheral blood RNA was isolated using the PerfectPure RNA blood kit (5-PRIME Inc., Gaithersburg, MD), according to the manufacturer's recommendation. The extracted RNA was further purified with the removal of globin transcripts using Ambion's GLOBINclear™ Kit (Applied Biosystems/Ambion, Austin, TX). Concentration and purity (A260/280 or A260/230 ≥2) of extracted RNA were determined by NanoDrop spectrophotometer (Thermo Sci., Wilmington, DE). RNA integrity (RIN) and purity were further evaluated using an Agilent 2100 Bioanalyzer (Santa Clara, CA). rRNA ratio [28S/18S] ≥1.5 and RIN values ≥8 are considered acceptable for expression profiling.

### Linear amplification of fluorescent cRNA

One-color Quick Amp Labeling Kit, Agilent p/n 5190-0442 (Santa Clara CA) was used for RNA amplification and labeling. The reagents of the kit are listed in Table 1. Hybridization probe synthesis is carried out in 2 steps: a) cDNA synthesis from total RNA and b) one round of cRNA amplification from cDNA. For cDNA synthesis, 1.2μL T7 promoter primer and 2μL diluted one-color spike-in mix (as recommended in protocol) were added to 500 ng total RNA input and the final volume was brought to 11.8μL. The primer-RNA mixture was denatured at 65 ºC for 10 min and immediately snap-cooled on ice for at least 5 min. 8.2μL of a master cDNA mix containing 4μL First strand synthesis buffer, 2μL DTT, 0.8μL dNTP, 1μL MMLV-RT and 0.4μL RNase inhibitor per reaction was added to each reaction tube. Samples were incubated at 40ºC for 2hr, heated at 65ºC for 15 min and cooled on ice. It is worth mentioning that, with the exception of dNTP and RNase inhibitor, the kit reagents for cDNA preparation were sufficient to perform more than 30 reactions (Table 1). In all our experiments, we used highly pure RNA so the lessening of RNase inhibitor from 0.5μL to 0.4μL should not have an effect in cDNA yield. Similarly, a slight decrease in the available dNTP pool (use of 0.8μL vs. 1.0μL recommended) for 500ng input RNA should not compromise cDNA yield as the standard protocol[1] was optimized for up to 1μg input RNA.

**Table 1.** Quick amplification kit contents

| |
|---|
| MMLV-RT, 45 μL (2 vials) |
| T7 Promotor Primer, 110 μL |
| *RNase Inhibitor, 25 μL |
| Inorganic Pyrophosphatase, 15 μL |
| 5x First Strand Reaction buffer, 195 μL |
| *4x Transcription buffer, 430 μL |
| *10 mM dNTP mix, 25 μL |
| *NTP mix, 175 μL |
| 0.1M DTT, 230 μL |
| *T7 RNA Polymerase, 20 μL |
| 50% PEG (Polyethylene glycol, 140 μL |
| *Cyanine 3-CTP |

**Note:** Limiting reagents are marked with asterisks.

For the standard cRNA amplification and labeling reaction, a transcription mix was prepared following the manufacturer's protocol,[1] resulting in a total volume of 60μL (Table 2, standard volume). In the cRNA master mix, some reagents like transcription buffer, DTT and PEG maintained the reaction buffering condition so their proportions in a reaction needed to be kept constant relative to the total volume. Other reagents like NTP, inorganic pyrophosphatase and T7 RNA polymerase could compromise amplification of transcribed products if any of the components became limit-

**Table 2.** Fluorescent cRNA transcription master mix preparation following standard or modified protocol

| Components | Standard volume (µL) | Modified volume (µL) |
|---|---|---|
| Nuclease-free water | 15.3 | 3.4 |
| *4x Transcription buffer, 430µL | 20 | 14 |
| *0.1 M DTT, 230 µL | 6 | 4 |
| *NTP mix, 175 µL | 8 | 5.5 |
| *50% PEG, 140 µL | 6.4 | 4.5 |
| RNaseOUT, 25 µL | 0.5 | 0.4 |
| Inorganic pyrophos, 15 µL | 0.6 | 0.5 |
| *T7 RNA Polymerase, 20 µL | 0.8 | 0.7 |
| Cyanine 3-CTP, 50 µL | 2.4 | 2 |
| **Total volume** | **60** | **35** |

**Note:** * The proportion of each of these components was kept constant in the final reaction (once the 20µl cDNA reaction was added).

ing for the reaction. Inadequate quantity of Cyanine 3-CTP in a reaction might have an adverse effect on specific activity of cRNA. However, Schothorst *et al*.,[2] have demonstrated that using half of Agilent's recommended Cy3 amount yielded cRNA specific activity within the expected range (9.5 to 13.2). This indicated that the standard reaction contained Cy3 dye well in excess of actual requirements. Here, we formulated kit reagents in different proportions that allowed us to set up 30 reactions from a single kit rather than the 20 reactions recommended by the manufacturer. To compare the effects of a reduced volume reaction, a modified amount of different transcription master mix components was used, in a total volume of 35µL (Table 2, modified volume). In the modified transcription mix, the amount of some reagents (marked with asterisks in Table 2) was adjusted in comparison to standard volume so their concentration was kept constant in the final reaction once the 20µL cDNA reaction mix was added.

Either 60 µL (standard volume) or 35µL (modified volume) of transcription master mix was added to the standard 20µL cDNA reaction and the labeling was carried out for 2h at 40ºC. Then nuclease-free water was added to each tube to bring the volume to 100µL, which subsequently was purified using Qiagen RNeasy mini-spin columns (Valencia, CA). Total yield, dye incorporation and purity (A260/280 ≥2.2) of fluorescent cRNA products were determined by NanoDrop spectrophotometer (Thermo Sci., Wilmington, DE). Specific activity is calculated as pmol of dye/µg cRNA. Specific ac-

**Table 3.** cRNA synthesis following Agilent's Quick Amp labeling kit[1]

| Sample | Dose (Gy) | Yield (µg) | SD | Mean Yield | SpActivity | SD | Mean SpAc |
|---|---|---|---|---|---|---|---|
| P | 0 | 14.39672 | 2.404285 | 12.433926 | 11.19699 | 0.952787 | 11.1683614 |
| " | 0.5 | 13.4472 | | | 11.71694 | | |
| " | 2 | 13.70356 | | | 11.61158 | | |
| " | 5 | 12.54552 | | | 11.2327 | | |
| O | 0 | 7.9742 | | | 9.846756 | | |
| " | 0.5 | 9.1936 | | | 9.106335 | | |
| " | 2 | 12.8284 | | | 10.09323 | | |
| " | 5 | 11.36252 | | | 9.335957 | | |
| Q | 0 | 15.52668 | | | 11.42034 | | |
| " | 0.5 | 12.98128 | | | 11.21615 | | |
| " | 2 | 13.91052 | | | 11.32668 | | |
| " | 5 | 13.45292 | | | 11.86657 | | |
| R | 0 | 17.29676 | | | 11.4241 | | |
| " | 0.5 | 13.28548 | | | 10.76363 | | |
| " | 2 | 11.90072 | | | 11.36066 | | |
| " | 5 | 15.05244 | | | 12.26379 | | |
| S | 0 | 8.84785 | | | 11.127 | | |
| " | 0.5 | 10.6007 | | | 11.31057 | | |
| " | 2 | 9.59035 | | | 12.9036 | | |
| " | 5 | 10.7811 | | | 12.24365 | | |

**Table 4.** Fluorescent cRNA was synthesized using modified amount of transcription mater mix (as described in Methodology)

| Sample | Dose (Gy) | Yield (µg) | SD | Mean Yield | SpActivity | SD | Mean SpAc |
|---|---|---|---|---|---|---|---|
| C | 0 | 10.5952 | 2.491056 | 12.58838 | 12.42072 | 0.93404 | 12.43350979 |
| " | 0.1 | 13.9308 | | | 13.66756 | | |
| " | 0.5 | 9.7572 | | | 13.93842 | | |
| " | 2 | 12.5912 | | | 13.43796 | | |
| G | 0 | 16.1728 | | | 13.40522 | | |
| " | 0.1 | 12.468 | | | 13.57074 | | |
| " | 0.5 | 11.9248 | | | 11.90796 | | |
| " | 2 | 11.764 | | | 12.37674 | | |
| H | 0 | 15.7108 | | | 12.52641 | | |
| " | 0.1 | 12.1944 | | | 11.93991 | | |
| " | 0.5 | 14.2024 | | | 12.64575 | | |
| " | 2 | 14.2696 | | | 12.24982 | | |
| V | 0 | 12.2032 | | | 11.30851 | | |
| " | 0.1 | 13.0568 | | | 11.54954 | | |
| " | 0.5 | 14.2372 | | | 12.89579 | | |
| " | 2 | 18.1976 | | | 13.34242 | | |
| Z | 0 | 10.2004 | | | 11.01918 | | |
| " | 0.1 | 8.2668 | | | 10.79015 | | |
| " | 0.5 | 8.874 | | | 12.30561 | | |
| " | 2 | 11.1504 | | | 11.37179 | | |

tivity of 9 or greater was considered optimal for hybridization.

**Hybridization**

Hybridization was performed by the standard protocol following Agilent's microarray hybridization user's manual[1] indicated for 4x44k microarray format. 1.65µg labeled cRNA was mixed with 11µL of 10x blocking reagent (Agilent p/n 5188-5281) and the final volume was brought to 52.8µL with nuclease-free water. 2.2µL of 25x fragmentation buffer (Agilent p/n 5185-5974) was added to each sample and the reactions were incubated in the dark at 60ºC for 30 min. 55µL of 2x Hi-RPM hybridization buffer (Agilent p/n 5188-6420) was added to terminate the reaction. 100µL of hybridization mix was immediately applied to each array (Agilent p/n G4112-60520 and G2534-60012) and hybridized with rotation in a hybridization oven at 65ºC for 17h. The slides were dismantled in Wash buffer 1 (Agilent p/n 5188-5325), washed 1 min in Wash buffer 1 at RT followed by another min in pre-warmed (37ºC) Wash buffer 2 (Agilent p/n 5188-5326). The array slides were immediately scanned on the Agilent microarray scanner using the one-color scanning protocol, extracted by Agilent's Feature Extraction software 9.1 and analyzed by BRB ArrayTools.[3]

## RESULTS AND DISCUSSION

The linear amplification showed no significant difference in yield whether the cRNA was synthesized following standard (Table 3) or modified (Table 4) protocol. Comparing specific activities, cRNA prepared by our adapted protocol actually showed slightly higher specific activities than that of the standard protocol (mean specific activity 12.43 vs. 11.17, respectively). In microarray studies, specific activity of fluorescent cRNA probes is an important determinant for overall array performance. Next, we examined the perform-

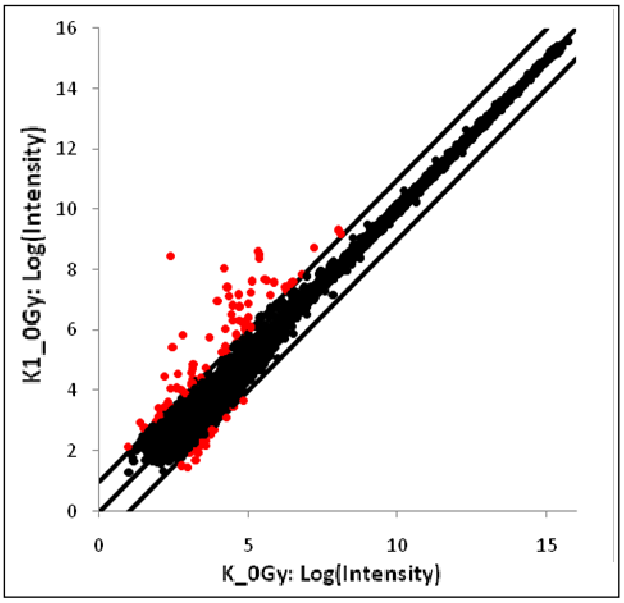


**Fig. 1.** BRB scatterplot compares log-ratios of samples prepared by standard (K_0Gy) versus modified (K1_0Gy) protocol. A total of 23,207 spots (which represent genes) that passed the selected filtering criteria are used in this scatter plot.[4, 5] Most of the plotted points (23,105 genes) remain unchanged in both experiments and are tightly lined up along a 45-degree diagonal line within cutoff outlier lines. Genes that are differentially expressed (red spots) between the two protocols fall outside the outlier lines.

ance of these cRNA targets on arrays by analyzing the number of genes (features) differentially expressed between samples. Microarray plots (BRB Scatter plot between samples) showed no systemic differences between samples prepared by standard or adapted protocols (Fig. 1). When the same RNA was labeled with the two protocols, the majority of genes (23,105) showed the same abundance in both samples, with 77 and 25 genes showing significantly higher or lower abundance respectively in the sample prepared with the adapted protocol, indicating probe synthesis by the adapted protocol did not introduce systemic bias (Fig. 1). The slightly higher number of up-regulated genes in the adapted protocol sample might result from the higher specific activities obtained compared to those obtained by the standard protocol, although these numbers are not significant.

Taken together with linear amplification, Cy3 dye incorporation (specific activity) and microarray performance we recommend the use of the adapted protocol that ensures consistent, reproducible and robust performance of labeled cRNA targets on the oligonucleotide arrays. The reaction procedure is simple, easy to follow and does not require any longer timing or additional treatment. Most importantly, our proposed protocol is a cost-efficient procedure with regard to kit reagents, performing 30 reactions vs. only 20 reactions by the standard method, without compromising data quality.

### References


1. One-color microarray-based gene expression analysis (Quick Amp Labeling) protocol for use with Agilent gene expression oligo microarrays Version 5.7, March 2008. Agilent Technologies Inc.
2. van Schothorst EM, Pagmantidis V, de Boer VC, Hesketh J and Keijer J. Assessment of reducing RNA input for Agilent oligo microarrays. *Anal Biochem* **363**:315-7, 2007.
3. Simon R, Lam A, Li MC, Ngan M, Menenzes S and Zhao Y. Analysis of gene expression data using BRB-Array Tools. *Cancer Informatics* **3**: 11–7, 2007.
4. Amundson SA and Paul S. Triage of medically significant radiation exposures using gene expression signatures in human PBL. *CRR Annual Report* 86-7, 2008.
5. Paul S and Amundson SA. Development of gene expression signatures for practical radiation biodosimetry. *Int J Radiat Oncol Biol Phys* **71**:1236-44, 2008. ■


# *HRAD9* Overexpression in Prostate Cancer Cell Line DU145 is Caused by Aberrant DNA Methylation

*Aiping Zhu, Kevin M. Hopkins, Xiaojian Wang and Howard B. Lieberman*

*HRAD9*, an evolutionarily conserved human gene, has multiple functions. It regulates cell cycle checkpoints, maintains genomic stability, induces apoptosis, binds p53 consensus DNA-binding sequences, and up-regulates transcription of *p21* and other downstream genes,[1, 2] and has other functions as well. *HRAD9* over-expression in small lung cancer,[3] breast cancer[4] and prostate cancer[5] was reported recently. What is the mechanism of HRAD9 overespression in cancers? We found that the DNA in the *HRAD9* 3' intron 2 region is highly methylated in CpG islands in DU145 prostate cancer cells and some primary human prostate cancer cells. In order to further analyze the DNA methylation process and its role in causing aberrantly high levels of HRAD9 in DU145 cells, we used in vivo complex of methylation assay (ICM) and a CHIP assay to find out whether DNA methyltransferases (DNMTs) can physically interact with HRAD9 very actively in the specific DNA region that demonstrates the aberrant hypermethylation.

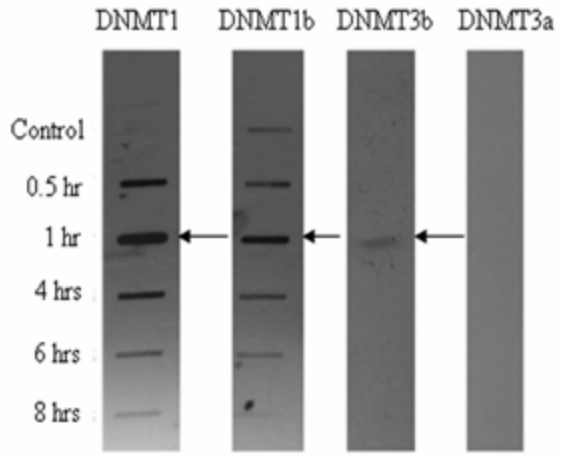


**Fig. 1.** Slot-blots indicating that antibodies against DNMT1, DNMT1b and DNMT3b detected DNMTs/*Hrad9*DNA complexes in DU145 prostate cancer Cells. Peak complex formation was detected after 1 hour aza-dC treatment.

**In vivo complex of methylation assay (ICM)**

ICM was performed according to the assay kit manufacturer's protocol (Methylation, Ltd.). Prostate cancer cells were cultured in 100 mm culture dishes with 10% FBS in RPM-1640 medium. When cells were 80 to 90% confluent, they were treated with 10 um 5'- aza-2'deoxycyticine (aza-dC). A negative control (no drug, DMSO only) was also

used. The cells were collected and lysed with 2% Sarkosyl in 1XTE buffer after treating with drug for 30 min, 2 hrs, 4 hrs, 6 hrs or 8 hrs. The lysates, which contained free DNA plus DNMT/DNA complexes, were purified by using CsCl step Gradient ultracentrifugation. Detection of DNMT/DNA complexes was carried out by slot blot analysis using antibody against DNMT1, DNMT1b, DNMT3b and DNMT3a (Methylation, Ltd.), which are known to methylate CpG islands. The results showed that endogenous DNMT isoform DNMT1, DNMT1b and DNMT3b as chromosomal DNA complexes were detected in DU145 prostate cancer cells. A DNMT3a/DNA complex was not detected by slot blotting. The peak complex formation was detected after 1 hr of azadC treatment (Fig. 1).

**Chromatin Immunoprecipitation (CHIP)**

CHIP was carried out following the manufacturer's (Millipore) protocol with some modification. Noncancer prostate cells PrEC and RWPE-1, and prostate cancer cell lines DU145, PC-3, CWR22 and LNCaP were cultured in Lonza and ATCC company suggested medium. Protein and DNA from cells ($2x10^6$) representing each population were cross-linked by 0.5% formaldehyde for 10 min at $37^oC$, followed by washing twice with cold PBS. Cells were lyzed in SDS buffer and incubated 10 min on ice, followed by sonication 4X for 10 sec each round at a maximum setting to shear DNA to lengths between 200 and 1000 base pairs. Half the sheared DNA was used for reverse crosslinking as input control. The rest was used for immunoprecipitation with antibody against different DNMT isoforms. After immunoprecipitation, the binding beads were washed with low salt, high salt, LiCl immune complex wash buffer, then with TE buffer. The histone-DNA complexes were eluted with 1% SDS, 0.1M $NaHCO_3$ elution buffer. The eluted histone-DNA complex was treated to reverse crosslinks at $65^0C$ overnight and DNA was purified by GFX $^{TM}$ PCR DNA and Gel band purification kit (GE healthcare), then examined by PCR with primer pairs flanking the hypermethylated DNA sequence in the 3' region of *HRAD9* intron 2. The forward PCR primer is 5'-ACC GCT GGC AGA TTT GTC G-3', and backward primer is 5'-CTC CCG CTC CGC CAC CAC CTG-3'.The PCR conditions were 1 cycle of $95^0C$ for 2 min, and 33 cycles of $95^0C$ 30 sec, $62^0C$ for 30 sec, and $72^0C$ for 2 min. The results showed that the 3' region of *HRAD9* intron 2

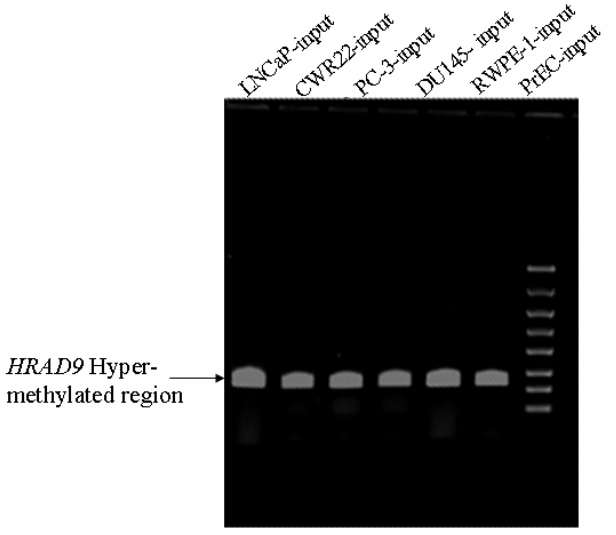


**Fig. 2.** Input-PCR products visualized by gel electrophoresis showed that the 3' region of *HRAD9* intron 2, which is hypermethylated, was amplified in all prostate cell lines. About the same amount of input DNA was detected in all samples.

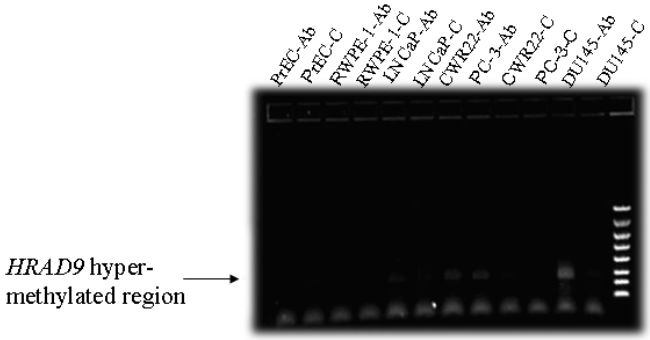


**Fig. 3A.** Chip-PCR-gel electrophoresis shows a band in DU145, PC-3 and CWR22 prostate cancer cell samples of the DNMT1antibody mediated immunoprecipitation. The band is much more intense in DU145 cells than in PC-3 and CWR22 cells. No band is detected in all cell lines without DNMT1 antibody in the reactions. Ab, DNMT1 antibody; C, control.

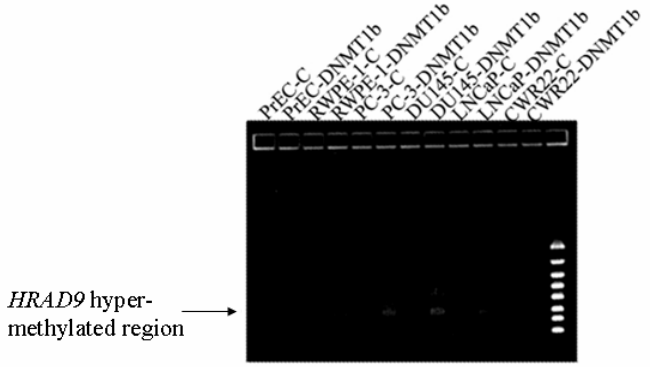


**Fig. 3B.** Chip-PCR-gel electrophoresis shows a band in DU145 and PC-3 prostate cancer cell samples of the DNMT1b antibody mediated immunoprecipitation. The band is much more intense in DU145 cells than in PC-3 cells. No band is detected in all cell lines without DNMT1b antibody in the reactions.

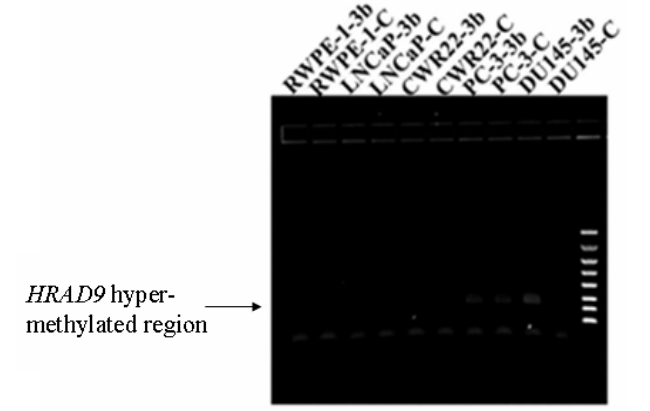


**Fig. 3C.** Chip-PCR-gel electrophoresis shows a band in DU145 and PC-3 prostate cancer cell samples of the DNMT3b antibody mediated immunoprecipitation. The band is much more intense in DU145 cells than in PC-3 cells. No band is detected in all cell lines without DNMT3b antibody in the reactions.

was amplified by PCR from input genomic DNA (Fig. 2). The DNMT1, DNMT1b and DNMT3b antibodies pulled down the 3' region of *HRAD9* intron 2 in DU145 cells, but not in prostate normal cells and LNCaP prostate cancer cells. There is a much weaker band with DNMT1 antibody pull down in PC-3 and CWR22 cells and also a very weak band in PC-3 cells by DNMT1b and DNMT3b antibody immunoprecipitation. There is no band in all controls of cell lines without DNMT antibodies or instead with mouse IgG (Fig. 3A, 3B, 3C). The CHIP experiment demonstrated that DNMT isoforms DNMT1, DNMT1b and DNMT3b specifically bind to the 3' hypermethylated region of *HRAD9* intron 2 in DU145 prostate cancer cells *in vivo*.

In summary, DNMT isoforms bind to DNA and form DNMT/DNA complexes in DU145 cells. CHIP is a powerful technique for studying specific protein-DNA interactions within cells. DNA and protein are reversibly cross-linked to maintain the association of proteins with their target DNA sequence. Our experiments demonstrated that DNMT isoforms specifically interact with the 3' region of the *HRAD9* intron 2 in DU145 cells. The biological and translational significance of these studies are being pursued.

**References**


1. Lieberman HB. Rad9, an evolutionarily conserved gene with multiple functions for preserving genomic integrity. *J Cell Biochem* **97**:690-7, 2006.
2. Yin Y, Zhu A, Jin YJ, Liu YX, Zhang X, Hopkins KM and Lieberman HB. Human RAD9 checkpoint control/proapoptotic protein can activate transcription of p21. *Proc Natl Acad Sci USA* **101**:8864-9, 2004.
3. Maniwa Y, Yoshimura M, Bermudez VP, Yuki T, Okada K, Kanomata N, Ohbayashi C, Hayashi Y, Hurwitz J and Okita Y. Accumulation of hRad9 protein in the nuclei of nonsmall cell lung carcinoma cells. *Cancer* **103**:126-32, 2005.
4. Cheng CK, Chow LW, Loo WT, Chan TK and Chan V. The cell cycle checkpoint gene Rad9 is a novel oncogene activated by 11q13 amplification and DNA methylation in breast cancer. *Cancer Res* **65**:8646-54, 2005.
5. Zhu A, Zhang CX and Lieberman HB. Rad9 has a functional role in human prostate carcinogenesis. *Cancer Res* **68**:1267-74, 2008. ■


# *Mrad9B* is Expressed in the Brain of Mouse Embryos

*Corinne Leloup, Xiang Yuan Wang,[a] Kevin M. Hopkins, Aiping Zhu, Debra J. Wolgemuth[a] and Howard B. Lieberman*

## Introduction

*HRAD9B* and *Mrad9B* were identified as paralogs of *HRAD9* and *HRAD9B*, respectively.[1] *Rad9* is involved in DNA repair, cell cycle checkpoints, apoptosis, breast and prostate cancers and embryonic development.[2, 3, 4, 5] In the adult, both human and mouse *Rad9B* are expressed specifically in the testis.[1] In order to characterize *Mrad9B*, we have generated knock out embryonic stem (ES) cells and mice. *Mrad9B* is essential for early embryonic development since homozygous *Mrad9B* knock out mice are embryonic lethal. After E8.5, all $Mrad9B^{-/-}$ embryos are resorbed. Moreover, some of the heterozygous embryos display retarded growth and some display an abnormal brain.[6]

## Results

### $Mrad9B^{-/-}$ embryos display less cell proliferation than $Mrad9B^{+/+}$ or $Mrad9B^{+/-}$ littermates.

Mouse embryo thin sections were stained with BrdU to monitor cell proliferation. As seen in 40x magnification of the forebrain (Fig. 1A, a-c) and dorsal ganglia (Fig. 1A, d-f), $Mrad9B^{+/+}$ and $Mrad9B^{+/-}$ embryos display much more dividing cells than $Mrad9B^{-/-}$ embryos as shown by the higher density of brown stained cells. E9.5 embryos were also examined for apoptotic death by Tunnel staining of the forebrain (Fig. 1B, a-c) and dorsal ganglia (Fig. 1B, d-f). There is no difference in frequency of apoptotic cells found in $Mrad9B^{-/-}$, $Mrad9B^{+/-}$ and $Mrad9B^{-/-}$ embryos, as there is a similar amount of brown stained cells in these sections.

### *Mrad9B* is expressed specifically in the brain of mouse embryos.

Expression of *Mrad9B* in wild type mouse embryos was examined by in situ hybridization of whole mount embryos, and is illustrated in Fig. 2. *Mrad9B* mRNA was hybridized in situ with digoxigenin-11-UTP labeled full-length antisense probe. We found that *Mrad9B* is expressed in the neural ectoderm, the headfolds and the amnion of E7.5 embryos and in the brain of E8.5 and E9.5 mouse embryos. The sense control probe was negative for signal, as predicted.

## Conclusions

*Mrad9B* is expressed in embryos, between days E7.5 and E9.5, in neural tissues or regions that will ultimately form neural structures. The lack of *Mrad9B* leads to embryonic lethality, probably due to impaired cell division rather than extensive apoptosis.

[a] *Department of Genetics & Development, and Obstetrics & Gynecology and The Institute for Human Nutrition, Columbia Universitv. New York. NY*

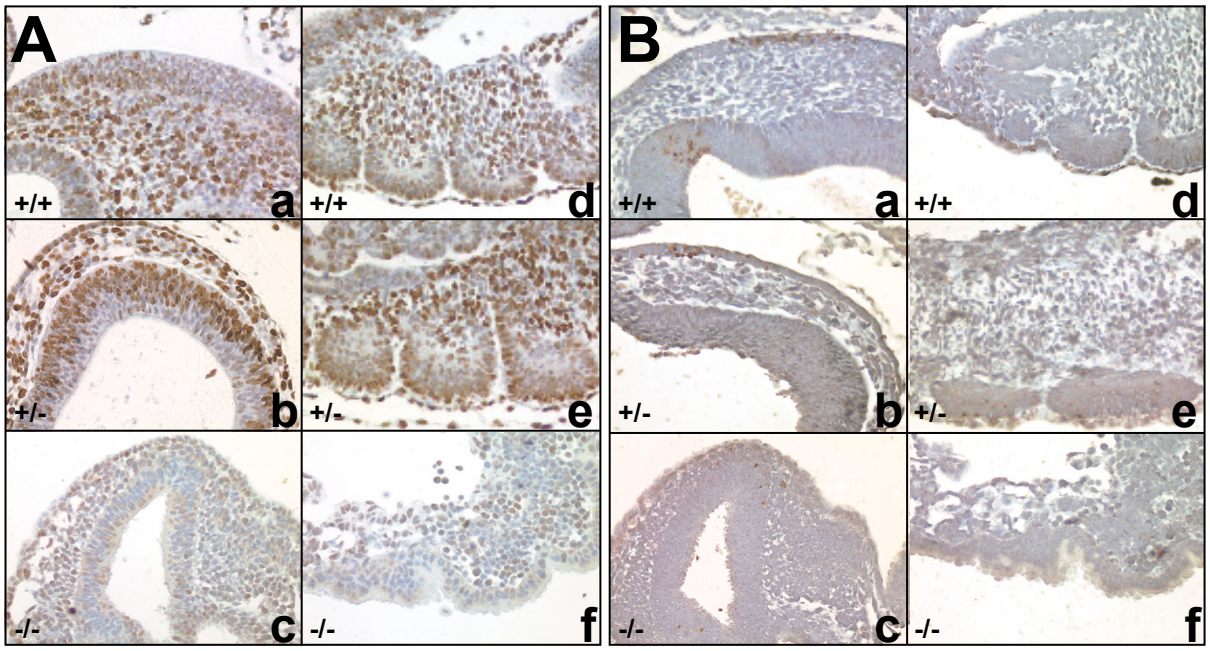


**Fig. 1.** Mid-sagittal sections of E9.5 embryos derived from *Mrad9B*$^{+/-}$ x *Mrad9B*$^{+/-}$ crosses. **(A)** BrdU uptake in E9.5 embryos from the same litter. (a,b,c) forebrain. (d,e,f) dorsal ganglia. Proliferating cells incorporate BrdU and stain brown. Non-replicating cells are stained blue. *Mrad9B*$^{-/-}$ embryos have less replicating cells than *Mrad9B*$^{+/+}$ and *Mrad9B*$^{+/-}$ embryos. **(B)** Tunnel staining in E9.5 embryos from the same litter. (a,b,c) forebrain. (d,e,f) dorsal ganglia. Apoptotic cells are stained brown, live cells blue. There is no striking difference in the frequency of apoptotic cells in embryos representing each of the three genotypes. In this figure, +/+ indicates *Mrad9B*$^{+/+}$, +/- indicates *Mrad9B*$^{+/-}$ and -/- indicates *Mrad9B*$^{-/-}$.

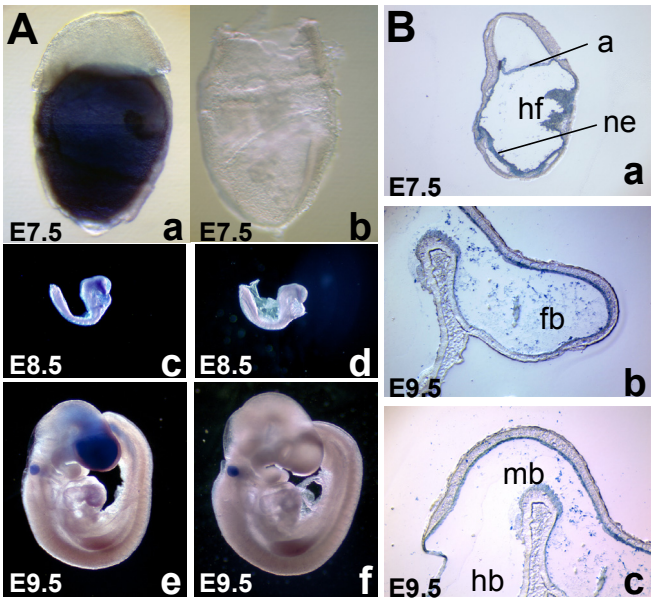


**Fig. 2.** Whole mount in-situ hybridization of *Mrad9B*$^{+/+}$ mouse embryos. (**A**) Whole embryos. (a,b) E7.5 embryos (x10), (c,d) E8.5 embryos (x3.3), (e,f) E9.5 embryos (x3.3). (a,c,e) *Mrad9B* antisense probe was used to hybridize with *Mrad9B* mRNA, (b,d,f) sense probe was used as a negative control probe. *Mrad9B* is localized in the neural ectoderm, the headfolds and the amnion at E7.5 and in the brain at E8.5 and E9.5. (**B**) Thin sections of the mouse embryos from figure **2A** (x10). (a) E7.5 embryos. (b,c) E9.5 embryos. a: amnion, hf: headfolds, ne: neural ectoderm, fb: forebrain, mb: midbrain, hb: hindbrain. Numbers in parentheses indicate magnification.

## References


1. Hopkins KM, Wang X, Berlin A, Hang H, Thaker HM and Lieberman HB. Expression of mammalian paralogues of HRAD9 and Mrad9 checkpoint control genes in normal and cancerous testicular tissue. *Cancer Res* **63**:5291-8, 2003.
2. Hopkins KM, Auerbach W, Wang XY, Hande MP, Hang H, Wolgemuth DJ, Joyner AL and Lieberman HB. Deletion of mouse rad9 causes abnormal cellular responses to DNA damage, genomic instability, and embryonic lethality. *Mol Cell Biol* **24**:7235-48, 2004.
3. Cheng CK, Chow LW, Loo WT, Chan TK and Chan V. The cell cycle checkpoint gene Rad9 is a novel oncogene activated by 11q13 amplification and DNA methylation in breast cancer. *Cancer Res* **65**:8646-54, 2005.
4. Lieberman HB. Rad9, an evolutionarily conserved gene with multiple functions for preserving genomic integrity. *J Cell Biochem* **97**:690-7, 2006.
5. Zhu A, Zhang CX and Lieberman HB. Rad9 has a functional role in human prostate carcinogenesis. *Cancer Res* **68**:1267-74, 2008.
6. Leloup C, Hopkins KM, Wang XY, Zhu A, Wolgemuth DJ and Lieberman HB. Mouse *Rad9B* is essential for embryonic development. Manuscript in preparation. ■

# Human RAD9 Can Activate Transcription of the *Cox-2* Promoter after Ionizing Radiation Exposure

*Xiaojian Wang, Chuanxin Huang, Wenhong Shen, Yuxin Yin and Howard B. Lieberman*

## Introduction

Human RAD9 can bind to a palindrome motif in the *Cox-2* promoter both *in vitro* and *in vivo*.[1] Nevertheless, unlike our observation that HRAD9 binds to the p53 consensus DNA-binding sequence in the *p21* promoter and acts as a positive transcription activator of that gene,[2] we previously failed to detect transcriptional upregulation of *Cox-2* by HRAD9 in luciferase reporter assays conducted in unirradiated H1299 cells (data not shown). In this report, we describe experiments that address whether HRAD9 can transactivate the *Cox-2* promoter after cells are exposed to ionizing radiation.

## Materials and methods

### Cell Culture

H1299 cells (p53 null) were cultured in MEM (Invitrogen), with 10% FBS at 37°C, in a 5% $CO_2$ atmosphere.

### Plasmids Constructions

The *Cox-2* promoter region, a 356bp fragment containing the palindrome motif was amplified by PCR using the following primers:
Forward, 5'-GAGGAGAAAGGCTTCCTAGATGAG-3';
Reverse, 5'-ATCTATCATGGGTAGTGCTCAGG-3'.

The PCR product was TA cloned into pCR2.1 (Invitrogen). Sequencing of the insert confirmed that there were no mutations generated during PCR amplification. The insert was cut from the construct by partially digesting with *KpnI* and completely with *XhoI*, followed by ligation into the same sites of pGL3 basic vector (Promega). This construct was named pfr.1-luc and functioned as the reporter vector in luciferase assays. The vector that expresses human *RAD9*, pZeoSV2(+)-RAD9, was described previously.[2]

### Luciferase Assays

Luciferase assays were performed using the Promega dual luciferase reporter assay system, according to the manufacturer's instructions but with some modifications. In brief, $2x10^5$ H1299 cells were seeded per well in 6-well plates. The next day, cells were transiently transfected with 1μg of pZeoSV2(+)-RAD9 or 1.35μg of pZeoSV2(+) and 0.33ng of one of the reporter vectors per well. pRL-TK (0.33ng) was cotransfected as the internal control to normalize for transfection efficiency. All transfections were done in triplicate. Cells were exposed to 4Gy of γ rays 24 hours after transfection. Luciferase activity was measured 2 hours after ionizing radiation exposure with a TD 20/20 luminometer (Turner Designs). The final luciferase values were normalized against *Renilla reniformis* luciferase activity.

## Results

### Transactivation of the promoter region of *Cox-2* by RAD9 after ionizing radiation exposure

To determine whether the *Cox-2* promoter fragment containing the palindromic sequence is regulated by RAD9 after cells are exposed to γ rays, this fragment was ligated into pGL3-basic to generate luciferase reporter plasmid pfr.1-luc. To detect luciferase activity, the luciferase reporter, together with pZeoSV2(+) vector (control) or with *RAD9* expression vector pZeoSV2(+)-RAD9 were transfected into H1299 cells. After 24hrs, cells were irradiated, then luciferase activity was measured 2hrs later. As shown in Fig. 1, pGL3 transfected into H1299 cells resulted in very low luciferase activity irregardless of whether cells were cotransfected with pZeo or pZeo-Rad9 (column 1 and 2). There was a basal luciferase activity produced by the *Cox-2* promoter in the absence of RAD9, mediated by pZeo+pfr.1-luc. Nevertheless, the luciferase activity was three and half fold induced by RAD9 (column 4 versus column 3). These results provided strong evidence that the *Cox-2* promoter can be up regulated by RAD9 after H1299 cells are irradiated.

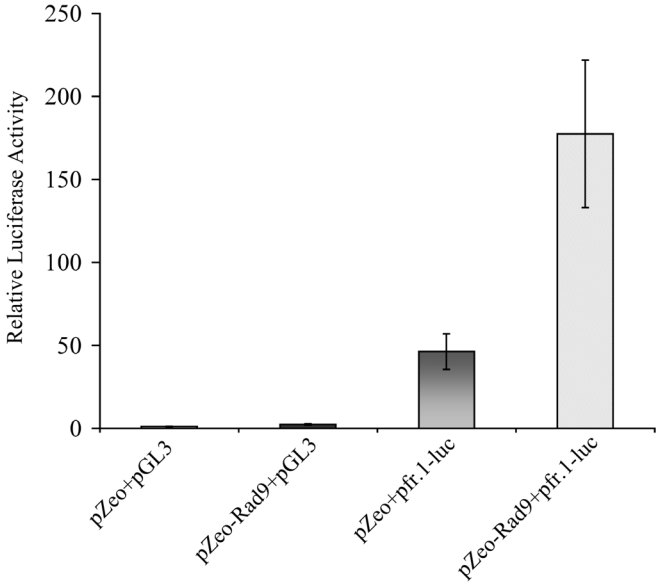


**Fig. 1.** Transactivation of the *Cox-2* promoter byRAD9. H1299 cells were transiently transfected with plasmids listed in the X-axis. Twenty-four hrs after transfection, cells were exposed to 4Gy of γ rays. Two hrs later, cell lysates were assayed for luciferase activity. The readout is indicated as average±SD of triplicate transfections. The transfection groups are: (1) empty pZeo plus pGL3-basic; (2) pZeo-Rad9 plus pGL3-basic; (3) empty pZeo plus pfr.1-luc; (4) pZeo-Rad9 plus pfr.1-luc.

## Discussion

The interesting finding here that Rad9 can activate transcription of *Cox-2* promoter only when H1299 cells are treated with radiation indicates that Rad9 may bind to some unknown protein(s) after cells are exposed to γ rays. The transactivity function very likely impacts on how cells respond to irradiation. The cellular response to ionizing radiation exposure leads to the induction of sets of genes that participate in DNA repair, cell cycle checkpoints, apoptosis etc.[3] In addition, bystander effects are observed after irradiation and Cox-2 is essential for these effects.[4] We also demonstrate that Rad9 is crucial for *p21* and *Cox-2* expression induction by γ rays. Our findings will help to better understand Rad9 function in cellular radioresponse mechanisms.[3]

## Acknowledgments

We thank Mr. Kevin M. Hopkins for technical guidance.

## References

1. Wang X, Hopkins KM, Yin Y and Lieberman HB. Human RAD9 binds *in vitro* and *in vivo* to a palindrome motif in the *Cox-2* promoter. *CRR Annual Report* 45-7, 2007.
2. Yin Y, Zhu A, Jin YJ, Liu YX, Zhang X, Hopkins KM and Lieberman HB. Human RAD9 checkpoint control/proapoptotic protein can activate transcription of p21. *Proc Natl Acad Sci USA* **101**:8864-9, 2004.
3. Zhu A, Wang X, Shen WH, Yin Y, Hei TK and Lieberman HB. Rad9 is essential for the ionizing radiation induction of *p21* and *Cox-2* expression. In preparation.
4. Zhou H, Ivanov VN, Gillespie J, Geard CR, Amundson SA, Brenner DJ, Yu Z, Lieberman HB and Hei TK. Mechanism of radiation-induced bystander effect: role of the cyclooxygenase-2 signaling pathway. *Proc Natl Acad Sci USA* **102**:14641-6, 2005. ■

# Characterization of *Mrad1* Deficient Mouse Embryos

*Kevin M. Hopkins, Xiangyuan Wang,[a] Haiying Hang[b] and Howard B. Lieberman*

*Rad9*, *Rad1* and *Hus1* are genes conserved from yeast to human and are important for controlling cell cycle checkpoints. The protein products of the three genes form a heterotrimer ring shaped structure.[1] It is believed that this heterotrimer is important for the function of the proteins in DNA repair as well as activation of cell cycle checkpoints.

We have cloned mouse genomic and cDNA orthologues of the fission yeast *S. pombe* cell cycle checkpoint control gene *rad1*. The *rad1* gene of *S. pombe* is involved in repair of damaged DNA caused by exposure to ionizing radiation, ultraviolet light, and hydroxyurea.[2] To determine the role of a mammalian version of this gene in radioresistance and cell cycle checkpoint control, we used the cloned *Mrad1* gene to generate *Mrad1* deficient mouse embryonic stem (ES) cells and adult heterozygous mice. To accomplish this goal a promoterless neomycin gene was inserted in frame after the third exon of the *Mrad1* gene in mouse ES cells. These cells were then used to make heterozygous *Mrad1* null mice.

**Table 1.** Genotypes of embryos from timed *Mrad1*+/- X *Mrad1*+/- crosses

| Day | *Mrad1*+/+ embryos | *Mrad1*+/- embryos | *Mrad1*-/- embryos |
|---|---|---|---|
| 11.5 | 5 | 1 | 0 |
| 10.5 | 2 | 5 | 6 resorbed |
| 8.5 | 6 | 17 | 5 |
| 7.5 | 5 | 12 | 4 |
| 6.5 | 8 | 10 | 9 |

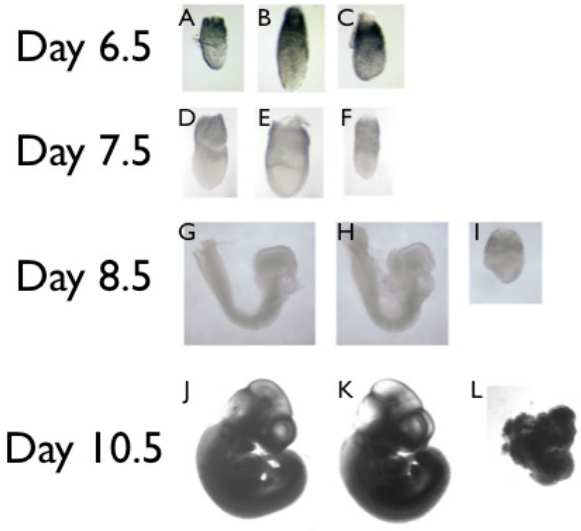


**Fig. 1.** Gross morphology of mouse embryos derived from *Mrad1*+/- X *Mrad1*+/- crosses. Photographs of intact embryos from day 6.5 (A, *Mrad1*+/+) (B, *Mrad1*+/-) (C, *Mrad1*-/-), day 7.5 (D, *Mrad1*+/+) (E, *Mrad1*+/-) (F, *Mrad1*-/-), day 8.5 (G, *Mrad1*+/+) (H, *Mrad1*+/-) (I, *Mrad1*-/-) and day 10.5 (J, *Mrad1*+/+) (K, *Mrad1*+/-) (L, *Mrad1*-/-) are presented.

[a] *Department of Genetics & Development, and Obstetrics & Gynecology and The Institute for Human Nutrition, Columbia University, New York, NY*
[b] *National Laboratory of Biomacromolecules, Institute of Biophysics, Chinese Academy of Sciences, Beijing, China*

Although heterozygous *Mrad1* mice were generated, paired heterozygous *Mrad1* crosses produced no mutant *Mrad1* offspring, thus indicating that loss of *Mrad1* leads to embryonic lethality. To determine the time of the embryonic lethality we analyzed the morphology of embryos from timed crosses between heterozygous *Mrad1* mice at different stages of embryonic development (Table 1). Between d7.5 and d8.5 mutant *Mrad1* embryos start to appear smaller than heterozygous or wild type *Mrad1* embryos (Fig.1 D, E, F, G, H, and I).

**References**


1. Hang H and Lieberman HB. Physical interactions among human checkpoint control proteins HUS1p, RAD1p, and RAD9p, and implications for the regulation of cell cycle progression. *Genomics* **65**:24-33, 2000.
2. Rowley R, Subramani S and Young PG. Checkpoint controls in Schizosaccharomyces pombe: rad1. *Embo J* **11**:1335-42, 1992. ■


# A Signaling Pathway Involving 4-HNE and COX-2 in Cytoplasmic Irradiation-induced Genotoxic Effect

*Mei Hong, Hongning Zhou, Gerhard Randers-Pehrson, and Tom K. Hei*

**Introduction:**

Direct damage to DNA has been considered the main reason leading to the deleterious effects such as mutation and cancer induction caused by environmental carcinogens and ionizing radiation. However, evidence has been accumulating in recent years suggesting that extracellular/extranuclear targets may play a role in mediating the genotoxic effects of radiation.[1, 2] In our previous studies, we showed that irradiation of cytoplasm produces gene mutations in the nucleus and that this process is mediated by free radicals.[3] The presence of oxidants as well as free radicals in cellular systems can also adversely alter lipids, proteins and DNA.[4] Decomposition of the lipid peroxyl radicals or the primary free radical intermediate of lipid peroxidation lead to the generation of reactive aldehydes such as 4-hydroxynonenal (4-HNE). 4-HNE has been implicated in a number of oxidative stress-related diseases, including atherosclerosis,[5] neurodegenerative diseases,[6] and fibrosis.[7] Moreover, there have been numerous studies indicating that 4-HNE can stimulate cellular proliferation,[8-10] differentiation,[11, 12] and cytoprotective response,[13-18] through its effect on multiple signaling pathways. In the present study, we detected a significant enhancement of lipid peroxidation in cytoplasmic irradiated $A_L$ cells, which was evident by increased level of 4-hydroxynonenal (4-HNE). Moreover, $A_L$ cells that were irradiated with α particles at the cytoplasm showed increased expression of COX-2. The extracellular signal-related kinase (ERK) was also found to be involved in cytoplasmic irradiation-induced responses.

**Results**

**Cytoplasmic irradiation induces lipid peroxidation**

As the major α, ß-unsaturated aldehyde derived from lipid peroxidation, 4-HNE is considered as a biomarker of oxidative stress[19, 20] and has been shown to stimulate cellular proliferation,[8-10] differentiation [11, 12] and cytoprotective responses[13-18] through various signaling pathways. Previously we have detected the induction of oxidative stress in cytoplasmic irradiation $A_L$ cells, so we next analyzed the lipid peroxidation level in irradiated cells. As indicated in Figure 1A, cells irradiated at cytoplasm with eight α-particles showed a significant higher level ($p<0.05$) of 4-HNE compared with that in control, non-irradiated cells. Moreover, pre-treated cells with butylated hydroxyl toluene (BHT), a well known lipid peroxidation chain blocker, suppressed the induction of lipid peroxidation.

To further evaluate the involvement of lipid peroxidation in cytoplasmic irradiation, we compared the $CD59^-$ mutant yield at $A_L$ cells pre-treated with BHT and the untreated cells. In Figure 1B, $A_L$ cells irradiated by eight alpha parti-

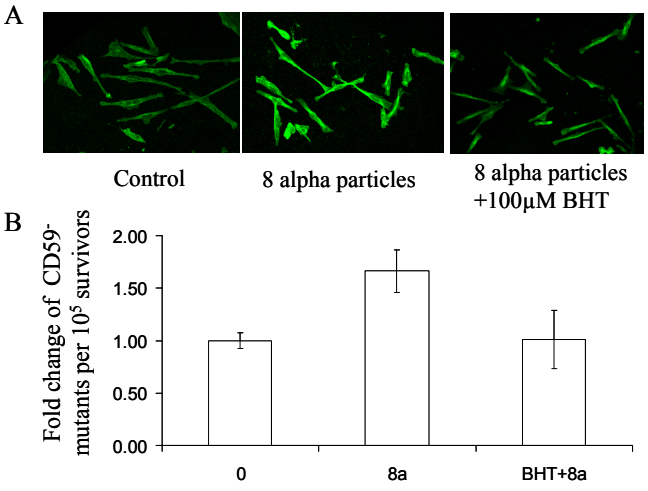


**Fig. 1. 4-HNE expression in cytoplasmic irradiated $A_L$ cells. A.** Representative image of 4-HNE fluorescent signal of AL cells after irradiated with 0 (control) or 8 alpha particles through cytoplasm with or without 100μM BHT treatment. **B.** Effect of BHT on the mutagenic potential of cytoplasmic irradiation at the *CD59* locus of AL cells.

cles at cytoplasm showed around 1.8 fold mutant yield as compared with the control, non-irradiated cells, which is consistent with our previous report. However, when $A_L$ cells were pre-treated with 100μM of BHT overnight before irradiation, the $CD59^-$ mutation fraction was reduced back to a level that is comparable with the non-irradiated control, suggesting a link between lipid peroxidation and the mutagenic effect of cytoplasmic irradiation.

**COX-2 is induced in cytoplasmic irradiated cells**

Cyclooxygenases (COXs) are a group of enzymes that catalyze the conversion of arachidonic acid into eicosanoids. COX-2 is an inducible isoform of the COXs and is responsible for production of high levels of prostaglandin in inflammation and immune responses. It has been demonstrated that in foamy macrophages within human atheromatous lesions, COX-2 expression was associated with accumulation of lipid peroxidation product 4-HNE, which suggested an inducer role of 4-HNE on COX-2 in this system.[21-23] To evaluate whether there is a similar relationship between lipid peroxidation and COX-2 in our cytoplasmic irradiation system, we measured COX-2 expression in $A_L$ cells by immunostaining. It was found that COX-2 was up-regulated significantly after cells were irradiated at cytoplasm. In addition, cells pre-treated with BHT could suppress COX-2 expression partially but significantly (Fig. 2A). Experiments using COX-2 inhibitor NS-398 further supported its involvement in cytoplasmic irradiation-induced mutagenesis. Because overnight treatment with 50μM of NS-398 before irradiation significantly reduced $CD59^-$ mutant yield back to basal level (Fig. 2B).

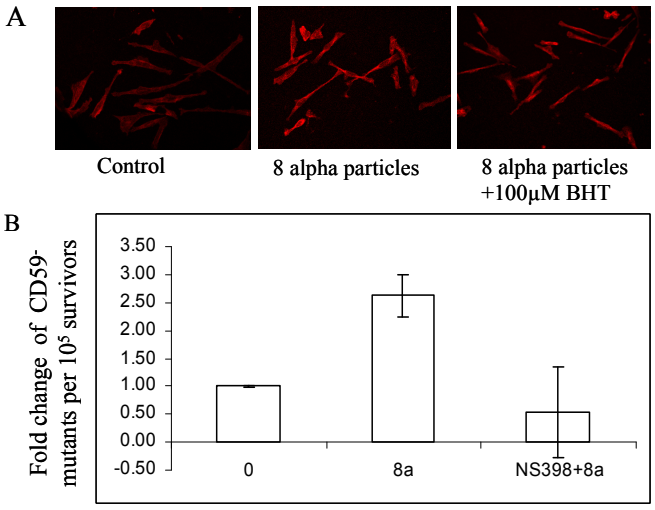


**Fig. 2. COX-2 expression in cytoplasmic irradiated $A_L$ cells. A.** Representative image of COX-2 fluorescent signal of AL cells after irradiation with 0 (control) or 8 alpha particles through cytoplasm with or without 100μM BHT treatment. **B.** Effect of NS-398 on the mutagenic potential of cytoplasmic irradiation at the *CD59* locus of AL cells.

**The involvement of MAPK pathway in cytoplasmic irradiation**

MAPK pathways are responsible for various growth factor-mediated cellular events such as proliferation, senescence, differentiation and apoptosis. It has been demonstrated that in normal human lung fibroblasts (NHLF), both α-irradiated and bystander cells exhibited increased expression of COX-2, and that as an upstream event, up-regulation of phosphor-ERK levels was observed.[24] In our cytoplasmic irradiation $A_L$ cell system, we also detected induction of COX-2. To investigate whether MAPK pathway is also involved in the cytoplasmic irradiation event, we analyzed the phosphorylation level of ERK after treatment. As shown in Figure 3, cells irradiated with 8 alpha particles had a higher level of phosphor-ERK when compared with that of the control, non-irradiated cells, suggesting activation of ERK after cytoplasmic irradiation. Treatment of BHT before irradiation reduced phosphor-ERK back to the control, non-irradiated level, indicating that lipid peroxidation may act as an upstream factor to activate the MAPK pathway.

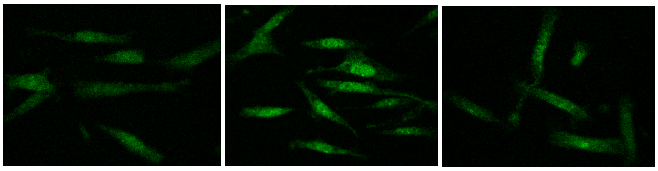


**Fig. 3. Erk Activity in Cytoplasmic Irradiated $A_L$ Cells.** Representative image of p-Erk fluorescent signal of AL cells after irradiation.

**Conclusions**

Consistent with the increment of oxidative stress, lipid peroxidation increased significantly after transversal of alpha particles through the cytoplasm of $A_L$ cells, which was evident by higher level of 4-HNE. The enhanced production of 4-HNE in cytoplasmic irradiated cells is likely to induce downstream responses that lead to its mutagenic effect. Indeed, in addition to the induction of 4-HNE, we also detected increased COX-2 expression in the irradiated cells. Cytoplasmic irradiated $A_L$ cells exhibited an activation of ERK and pre-treatment with lipid peroxidation blocker BHT resulted in reduced ERK phosphorylation, implicating an upstream regulatory role of lipid peroxidation on ERK activation.

**References**

1. Little JB. Radiation carcinogenesis. *Carcinogenesis* **21**:397-404, 2000.
2. Morgan WF. Is there a common mechanism underlying genomic instability, bystander effects and other nontargeted effects of exposure to ionizing radiation? *Oncogene* **22**:7094-9, 2003.
3. Wu LJ, Randers-Pehrson G, Xu A, Waldren CA, Geard CR, Yu Z and Hei TK. Targeted cytoplasmic irradiation with alpha particles induces mutations in mammalian cells. *Proc Natl Acad Sci U S A* **96**:4959-64, 1999.
4. Burney S, Tamir S, Gal A and Tannenbaum SR. A mechanistic analysis of nitric oxide-induced cellular toxicity. *Nitric Oxide* **1**:130-44, 1997.
5. Requena JR, Fu MX, Ahmed MU, Jenkins AJ, Lyons TJ

and Thorpe SR. Lipoxidation products as biomarkers of oxidative damage to proteins during lipid peroxidation reactions. *Nephrol Dial Transplant* **11 Suppl 5**:48-53, 1996.

6. Floyd RA and Hensley K. Oxidative stress in brain aging. Implications for therapeutics of neurodegenerative diseases. *Neurobiol Aging* **23**:795-807, 2002.
7. Leonarduzzi G, Scavazza A, Biasi F, Chiarpotto E, Camandola S, Vogel S, Dargel R and Poli G. The lipid peroxidation end product 4-hydroxy-2,3-nonenal up-regulates transforming growth factor beta1 expression in the macrophage lineage: a link between oxidative injury and fibrosclerosis. *Faseb J* **11**:851-7, 1997.
8. Dianzani MU, Barrera G and Parola M. 4-Hydroxy-2,3-nonenal as a signal for cell function and differentiation. *Acta Biochim Pol* **46**:61-75, 1999.
9. Cambiaggi C, Dominici S, Comporti M and Pompella A. Modulation of human T lymphocyte proliferation by 4-hydroxynonenal, the bioactive product of neutrophil-dependent lipid peroxidation. *Life Sci* **61**:777-85, 1997.
10. Semlitsch T, Tillian HM, Zarkovic N, Borovic S, Purtscher M, Hohenwarter O and Schaur RJ. Differential influence of the lipid peroxidation product 4-hydroxynonenal on the growth of human lymphatic leukaemia cells and human periopherial blood lymphocytes. *Anticancer Res* **22**:1689-97, 2002.
11. Yang Y, Sharma R, Sharma A, Awasthi S and Awasthi YC. Lipid peroxidation and cell cycle signaling: 4-hydroxynonenal, a key molecule in stress mediated signaling. *Acta Biochim Pol* **50**:319-36, 2003.
12. Rinaldi M, Barrera G, Spinsanti P, Pizzimenti S, Ciafre SA, Parella P, Farace MG, Signori E, Dianzani MU and Fazio VM. Growth inhibition and differentiation induction in murine erythroleukemia cells by 4-hydroxynonenal. *Free Radic Res* **34**:629-37, 2001.
13. Fukuda A, Nakamura Y, Ohigashi H, Osawa T and Uchida K. Cellular response to the redox active lipid peroxidation products: induction of glutathione S-transferase P by 4-hydroxy-2-nonenal. *Biochem Biophys Res Commun* **236**:505-9, 1997.
14. Singhal SS, Godley BF, Chandra A, Pandya U, Jin GF, Saini MK, Awasthi S and Awasthi YC. Induction of glutathione S-transferase hGST 5.8 is an early response to oxidative stress in RPE cells. *Invest Ophthalmol Vis Sci* **40**:2652-9, 1999.
15. Raza H, Robin MA, Fang JK and Avadhani NG. Multiple isoforms of mitochondrial glutathione S-transferases and their differential induction under oxidative stress. *Biochem J* **366**:45-55, 2002.
16. Ishii I, Akahoshi N, Yu XN, Kobayashi Y, Namekata K, Komaki G and Kimura H. Murine cystathionine gamma-lyase: complete cDNA and genomic sequences, promoter activity, tissue distribution and developmental expression. *Biochem J* **381**:113-23, 2004.
17. Zhang H, Dickinson DA, Liu RM and Forman HJ. 4-Hydroxynonenal increases gamma-glutamyl transpeptidase gene expression through mitogen-activated protein kinase pathways. *Free Radic Biol Med* **38**:463-71, 2005.
18. Dickinson DA, Iles KE, Watanabe N, Iwamoto T, Zhang H, Krzywanski DM and Forman HJ. 4-hydroxynonenal induces glutamate cysteine ligase through JNK in HBE1 cells. *Free Radic Biol Med* **33**:974, 2002.
19. Poli G, Albano E and Dianzani MU. The role of lipid peroxidation in liver damage. *Chem Phys Lipids* **45**:117-42, 1987.
20. Esterbauer H, Schaur RJ and Zollner H. Chemistry and biochemistry of 4-hydroxynonenal, malonaldehyde and related aldehydes. *Free Radic Biol Med* **11**:81-128, 1991.
21. Uchida K. 4-Hydroxy-2-nonenal: a product and mediator of oxidative stress. *Prog Lipid Res* **42**:318-43, 2003.
22. Zarkovic N. 4-hydroxynonenal as a bioactive marker of pathophysiological processes. *Mol Aspects Med* **24**:281-91, 2003.
23. Kumagai T, Matsukawa N, Kaneko Y, Kusumi Y, Mitsumata M and Uchida K. A lipid peroxidation-derived inflammatory mediator: identification of 4-hydroxy-2-nonenal as a potential inducer of cyclooxygenase-2 in macrophages. *J Biol Chem* **279**:48389-96, 2004.
24. Hei TK. Cyclooxygenase-2 as a signaling molecule in radiation-induced bystander effect. *Mol Carcinog* **45**:455-60, 2006. ■

# Identification of DUSP1 as a p53 Target during the Cellular Response to Oxidative Stress

*Yu-Xin Liu, Jianli Wang, Jianfen Guo, Jingjing Wu, Howard B. Lieberman and Yuxin Yin*

p53 is a tumor suppressor that regulates cell cycle progression and the programmed cell death response to DNA damage.[1, 2] Genes controlled by p53 contain DNA consensus recognition sites primarily in their promoters. These sites are bound with specificity by the p53 protein, leading to the transcriptional control of these target genes.[3] DUSP1 has a p53 binding site within an intron and an exon that can regulate transcription of the gene.[4, 5] DUSP1 is a phosphatase, which was originally cloned as CL100 by subtraction hybridization using cells treated with hydrogen peroxide.[6, 7] DUSP1 encodes a dual threonine/tyrosine phosphatase that specifically dephosphorylates and inactivates MAPKs.[8] There is evidence that DUSP1 is controlled at the transcriptional level by p53 during cell cycle progression.[4] However, conditions relevant for the induction of one DUSP1-mediated function in vivo versus another are not yet well defined. In this report, we show that DUSP1 is a transcriptional target of p53 in signaling apoptosis after oxidative stress.

**Selective regulation of DUSP1 by p53 under stress conditions**

A wide variety of mutagenic agents are toxic to cells, but the mechanisms of toxicity can vary. Some agents irreversibly induce growth arrest, whereas others induce cell death by apoptosis or necrosis. For example, radiation causes cell cycle arrest in mouse embryo fibroblasts (MEF) in a p53-dependent manner,[9] whereas oxidative stress induces cell death by apoptosis in the same type of mouse cells and that also depends on p53.[10] The molecular basis for differential regulation of cell cycle arrest versus cell death by p53 is not known. Using gene expression microarray screening, we previously identified >60 p53-regulated genes, including *DUSP1*.[11] We used the EB-1 system to confirm the data from the microarray. The EB cell line was derived from a human colon cancer with mutant p53. EB-1 is a stable clone containing a wild-type (wt) p53 transgene under control of the metallothionein promoter and expressing wt p53 upon administration of zinc chloride ($ZnCl_2$). These cells undergo

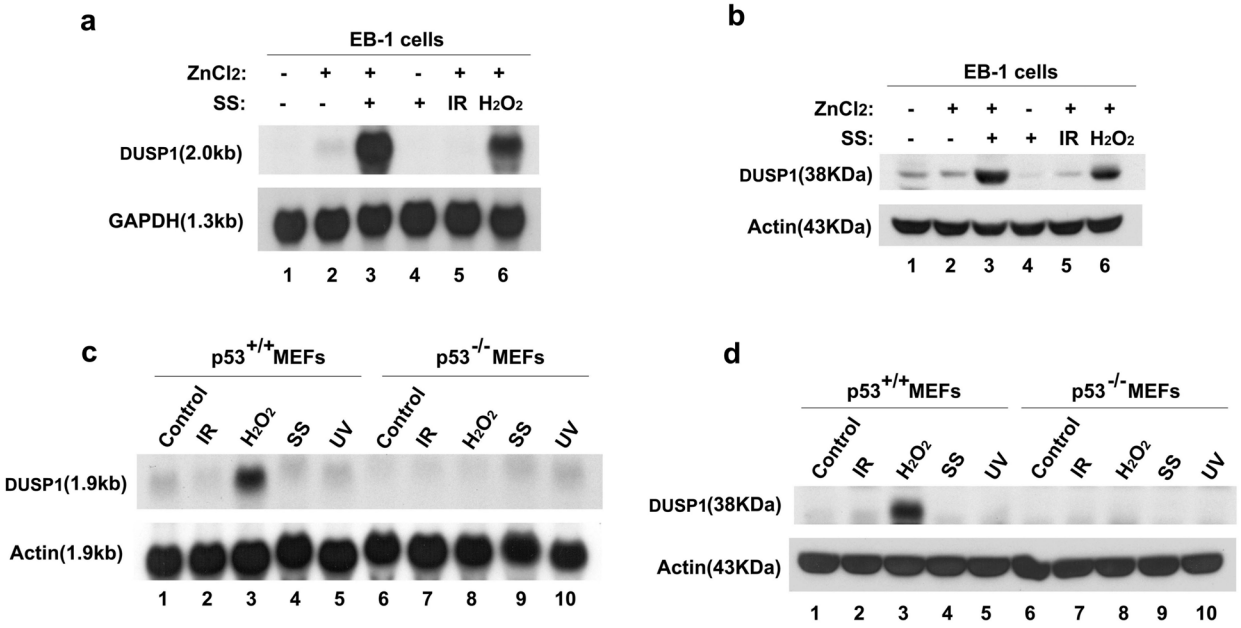


**Fig. 1. Transcriptional regulation of DUSP1 by p53. a.** Induction of DUSP1 transcription during p53-mediated apoptosis by serum deprivation. EB-1 cells were cultured under the following conditions: EB-1 with 10% FBS (*lane 1*), EB-1 with10% FBS plus 100 μmol/L $ZnCl_2$ (*lane 2*), EB-1 with 0.1% FBS (SS, serum starvation) plus 100 μmol/L $ZnCl_2$ (*lane 3*), EB-1 with 0.1% FBS without $ZnCl_2$ (*lane 4*), EB-1 with 100 μmol/L $ZnCl_2$ and □-irradiation (6 Gy, 6 h postirradiation; *lane 5*), EB-1 with $ZnCl_2$ and $H_2O_2$ (100 μmol/L, 6 h; *lane 6*). **b.** Induction of DUSP1 protein by p53 under serum starvation. Exponentially growing EB-1 cells were treated as indicated. Cell extracts were resolved by 10% SDS-PAGE and transferred for Western blotting. **c.** Expression of DUSP1 transcription in MEFs under various conditions. Exponentially growing MEF cells were exposed to □-irradiation (6 Gy), $H_2O_2$ (100 μmol/L), serum starvation (0.1%FBS), or UV irradiation (10 J/m$^2$), respectively, as indicated. The cells were harvested after 6 h, and mRNA from each group was fractionated on 1.2% formaldehyde agarose gel and transferred for Northern blotting. **D.** Western analysis of DUSP1 in $p53^{+/+}$ and $p53^{-/-}$ MEFs treated as indicated.

apoptosis after serum deprivation in the presence of p53.[12] As shown in Figure 1a, the DUSP1 transcript is undetectable in EB-1 without p53 (top, lane 1). Interestingly, DUSP1 is not increased in EB-1 cells with $ZnCl_2$ (lane 1 versus lane 2), which causes cell cycle arrest.[13] However, DUSP1 expression is greatly increased in the EB-1 cells treated with $ZnCl_2$ and starved for serum (Fig. 1a, top, lane 3), which activates p53 and induces apoptosis.[12, 13] As expected, DUSP1 is not induced by serum starvation in the absence of p53 (lane 4). Also, in the presence of p53, irradiation does not induce DUSP1 (lane 5), whereas $H_2O_2$ increases DUSP1 transcript levels (lane 6) and also causes apoptosis.[13] Correspondingly, the abundance of DUSP1 protein is increased by p53 upon serum starvation (Fig. 1b, lane 3) or under oxidative stress (lane 6). These results suggest that *DUSP1* transcription can be regulated by p53, and induction of DUSP1 is dependent on p53 status and influenced by stress conditions. To determine whether DUSP1 expression is responsive to stress conditions in a different cell system, normal and p53 null MEFs ($p53^{+/+}$ and $p53^{-/-}$ MEFs) were treated with γ-rays, which causes cell cycle arrest at G1,[14] or $H_2O_2$, which induces cell death by apoptosis.[15] As shown in Figure 1c, DUSP1 is low in $p53^{+/+}$ MEFs and is not induced by γ-irradiation (top, lanes 1 and 2). However, DUSP1 is markedly increased after oxidative damage by $H_2O_2$ (Fig. 1c, top, lane 1 versus lane 3). Furthermore, the transcriptional response of DUSP1 to oxidative damage is completely eliminated in $p53^{-/-}$ MEFs (lane 3 versus lane 8). Interestingly, DUSP1 is not induced by either serum starvation or a moderate dose of UVC exposure (Fig. 1c, lanes 4 and 5), which causes cell cycle arrest.[16] Western blot analysis indicates that DUSP1 protein abundance coincides with RNA levels detected (compare Fig. 1c and d). These observations suggest that DUSP1 is inducible by oxidative stress in a p53-dependent manner, when apoptosis is triggered, and that p53 can selectively regulate DUSP1 in response to oxidative damage.

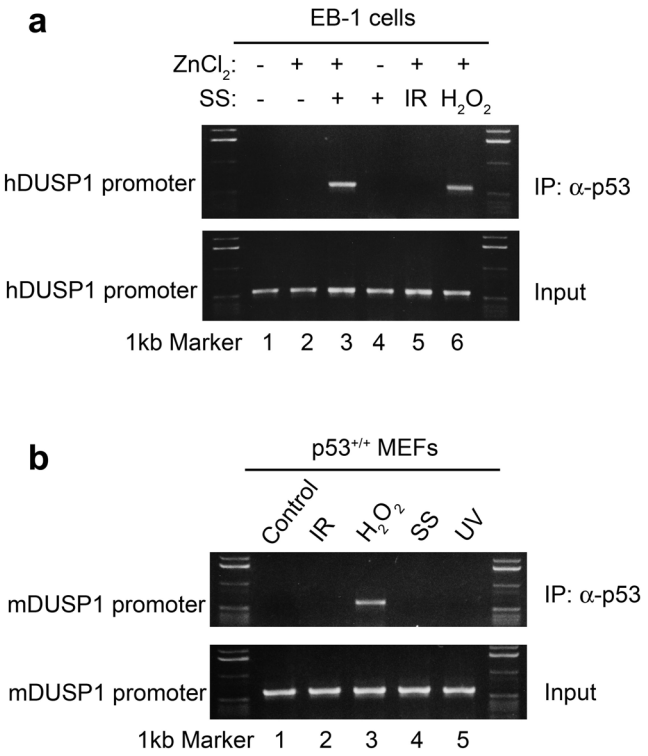


**Fig. 2. ChIP analysis of the physical association of p53 with chromatin containing the regulatory regions of DUSP1. a.** EB-1 cells were treated as Fig. 1A for 2h and processed for ChIP using an anti-p53 antibody (PAb1801) and a ChIP assay kit (UBI) according to the manufacturer's protocol. The DUSP1 promoter fragment from p53 immunoprecipitates was amplified by PCR. The regulatory fragment was directly amplified by PCR of genomic DNA from each group as input. **b.** Exponentially growing MEF cells were exposed to γ-irradiation (6 Gy), $H_2O_2$ (100 μmol/L), serum starvation (0.1% FBS), or UV irradiation (10 J/m$^2$), respectively, as indicated for 2h. Cells were processed for ChIP with an anti-p53 antibody (Systems Biomed) plus an anti-phosphorylated p53 (Ser$^{15}$). The p53 bound mouse DUSP1 promoter fragment was amplified by PCR. The same regulatory fragment directly amplified from genomic DNA was used as input.

**Physical Interaction between p53 and the DUSP1 Promoter In vivo**

To test whether p53 can interact with the regulatory region of *DUSP1* in vivo, we did a chromatin immunoprecipitation (ChIP) assay using an anti-p53 antibody to detect the physical interaction between p53 and the *DUSP1* regulatory region. We first chose the p53 inducible system, EB-1, for induction of p53. As shown in Figure 2a, the *DUSP1* regulatory region was PCR amplified from the ChIP products pulled out by the p53 antibody in group 3 where EB-1 cells were treated by 100 μmol/L ZnCl2 plus serum deprivation (lane 3) or in group 6 where EB-1 was treated with hydrogen peroxide ($H_2O_2$) in the presence of 100 μmol/L ZnCl2 (lane 6). However, there is no evidence for p53 binding to the same region when cells were irradiated (lane 5). Next, we examined the possible association of endogenous p53 with the regulatory fragment of mouse *DUSP1*. As shown in Figure 2b, p53 is associated with the mouse *DUSP1* regulatory fragment when MEFs were under oxidative stress but not after incurring damage or exposed to stress by treatment with irradiation, serum starvation, or UV irradiation. These results indicate that oxidative signals may result in p53 modification that influences p53 binding to chromatin containing the regulatory region of *DUSP1*.

**The Role of DUSP1 in Signaling Apoptosis after Oxidative Stress**

To determine more directly the role of DUSP1 in the apoptotic process, we constructed a human DUSP1 expression vector and transfected DLD-1, a colon cancer cell line containing mutant p53 and a low level of DUSP1. We chose DLD-1/pcDNA3 cells and DLD-1/DUSP1 cells containing a high level of ectopic DUSP1 expression (Fig. 3a) for functional studies. To determine whether DUSP1 can mediate cell death, we examined the efficiency of cell killing in both DLD-1/pcDNA3 cells and the DLD-1/DUSP1 cells under oxidative stress. Indeed, whereas DLD-1/pcDNA3 cells are resistant to oxidative stress, the DLD-1/DUSP1 population is highly susceptible to cell killing by $H_2O_2$ treatment, as re-

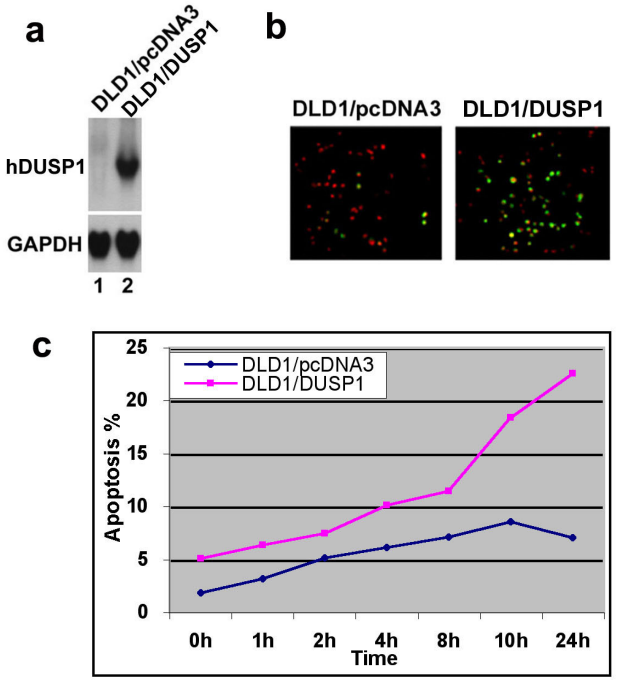


**Fig. 3. DUSP1 inhibits MAPK activity and mediates apoptosis. a.** Ectopic expression of DUSP1 in DLD-1 cells. DLD-1 cells were transfected with either pcDNA3 or pcDNA3/DUSP1. Equal amounts of total RNA were resolved on 1.2% formaldehyde gels and transferred for Northern blotting using the corresponding [□-$^{32}$P]dCTP-labeled cDNA probes. **b.** TUNEL analysis of DUSP1-mediated apoptosis. The indicated cells (1 x $10^6$) were treated with $H_2O_2$ (200 µmol/L) for 12 h. The cells were harvested together with supernatant for TUNEL staining using an *in situ* apoptosis detection kit (Intergen). Double-colored cells were counted as apoptotic cells. c. Mediation of cell killing by DUSP1 after indomethacin treatment. DLD1/pcDNA3 and DLD1/DUSP1 cells were treated with indomethacin (200 mmol/L) for various times as indicated. The rate of cell death was determined by TUNEL. The values are the means ± SD of three independent experiments.

flected by the increased frequency of apoptotic cells (Fig. 3b). Because DUSP1 is involved in the cellular response to oxidative stress and it mediates cell death after oxidative damage, it is possible that DUSP1 mediates cell killing by chemotherapeutic treatment through oxidative signaling. Indomethacin is a nonsteroidal antiinflammatory drug that has been shown to cause cancer cell death by apoptosis.[17] Therefore, we determined whether the cells with ectopically expressing DUSP1 are more sensitive to treatment with indomethacin. As shown in Figure 3c, the DLD-1/DUSP1 cell population has a higher percentage demonstrating apoptosis when compared with the cells not expressing DUSP1 (DLD-1/pcDNA3) and similarly treated with indomethacin. These results suggest that DUSP1 mediates cell killing of DLD-1 cells by indomethacin.

These new findings indicate that p53 is a transcriptional regulator of DUSP1 in stress responses. Our results reveal a mechanism whereby p53 selectively regulates target genes and suggest a way in which subgroups of those target genes might be controlled independently.

## References


1. Levine AJ. p53, the cellular gatekeeper for growth and division. *Cell* **88**:323-31, 1997.
2. Vogelstein B, Lane D and Levine AJ. Surfing the p53 network. *Nature* **408**:307-10, 2000.
3. el-Deiry WS, Kern SE, Pietenpol JA, Kinzler KW and Vogelstein B. Definition of a consensus binding site for p53. *Nat Genet* **1**:45-9, 1992.
4. Li M, Zhou JY, Ge Y, Matherly LH and Wu GS. The phosphatase MKP1 is a transcriptional target of p53 involved in cell cycle regulation. *J Biol Chem* **278**:41059-68, 2003.
5. Yang H and Wu GS. p53 Transactivates the phosphatase MKP1 through both intronic and exonic p53 responsive elements. *Cancer Biol Ther* **3**:1277-82, 2004.
6. Keyse SM and Emslie EA. Oxidative stress and heat shock induce a human gene encoding a protein-tyrosine phosphatase. *Nature* **359**:644-7, 1992.
7. Noguchi K, Nakajima M, Naito M and Tsuruo T. Inhibition by differentiation-inducing agents of wild-type p53-dependent apoptosis in HL-60 cells. *Jpn J Cancer Res* **86**:217-23, 1995.
8. Sun H, Charles CH, Lau LF and Tonks NK. MKP-1 (3CH134), an immediate early gene product, is a dual specificity phosphatase that dephosphorylates MAP kinase in vivo. *Cell* **75**:487-93, 1993.
9. Kastan MB. P53: a determinant of the cell cycle response to DNA damage. *Adv Exp Med Biol* **339**:291-3; discussion 5-6, 1993.
10. Yin Y, Terauchi Y, Solomon GG, Aizawa S, Rangarajan PN, Yazaki Y, Kadowaki T and Barrett JC. Involvement of p85 in p53-dependent apoptotic response to oxidative stress. *Nature* **391**:707-10, 1998.
11. Zhao R, Gish K, Murphy M, Yin Y, Notterman D, Hoffman WH, Tom E, Mack DH and Levine AJ. Analysis of p53-regulated gene expression patterns using oligonucleotide arrays. *Genes Dev* **14**:981-93, 2000.
12. Shaw P, Bovey R, Tardy S, Sahli R, Sordat B and Costa J. Induction of apoptosis by wild-type p53 in a human colon tumor-derived cell line. *Proc Natl Acad Sci USA* **89**:4495-9, 1992.
13. Yin Y, Liu YX, Jin YJ, Hall EJ and Barrett JC. PAC1 phosphatase is a transcription target of p53 in signalling apoptosis and growth suppression. *Nature* **422**:527-31, 2003.
14. Kastan MB and Kuerbitz SJ. Control of G1 arrest after DNA damage. *Environ Health Perspect* **101 Suppl 5**:55-8, 1993.
15. Yin Y, Solomon G, Deng C and Barrett JC. Differential regulation of p21 by p53 and Rb in cellular response to oxidative stress. *Mol Carcinog* **24**:15-24, 1999.
16. Huang RP, Wu JX, Fan Y and Adamson ED. UV activates growth factor receptors via reactive oxygen intermediates. *J Cell Biol* **133**:211-20, 1996.
17. Husain SS, Szabo IL, Pai R, Soreghan B, Jones MK and Tarnawski AS. MAPK (ERK2) kinase--a key target for NSAIDs-induced inhibition of gastric cancer cell proliferation and growth. *Life Sci* **69**:3045-54, 2001. ■

Center for Radiological Research 2008 Christmas Party. (L-r): Ms. Yvette Acevedo, Ms. Lilian Oling and Dr. Alan Bigelow.

Center for Radiological Research 2008 Christmas Party. (L-r): Dr. Gloria Calaf, Dr. Adayabalam Balajee and Dr. Vladimir Ivanov.

Center for Radiological Research 2008 Christmas Party. (L-r): Mr. Carl Elliston, Dr. David Brenner and Mr. Gary Johnson.

Center for Radiological Research 2008 Christmas Party. (L-r): Dr. Jarah Meador and Mr. Kevin Hopkins.


Christmas Lunch. (L-r): Ms. Lilian Oling, Ms. Angela Lugo, Dr. David Brenner, Dr. Tom Hei, Ms. Margaret Zhu, Ms. Annerys Rodriguez and Ms. Yvette Acevedo.

Center for Radiological Research 2008 Christmas Party. (L-r): Dr. Shanaz Ghandhi, Dr. Gerhard Randers-Pehrson and Dr. Gloria Calaf.

# Human Endothelial Cells in 3D Model Vessel Systems; Differential Effects of High and Low LET Space Radiations

*Peter Grabham, Burong Hu, Alan Bigelow and Charles R. Geard*

Travel into space will result in exposure to both low LET (proton) ionizing irradiation and high LET (eg. iron ion [Fe]) ionizing irradiation. Very little is known about the effects of these types of radiation on the human body. In addition to the primary concern of the carcinogenic potential, there is more recent concern of non-carcinogenic effects, which can be comparable to those seen for cancer. Among these risks are diseases of the vasculature such as heart disease and stroke. The human vasculature represents a prime target for ionizing radiation. There is an estimated 60,000 miles of vessels that network the entire body. The present study is aimed at understanding the non-cancer effects of space ionizing radiation on the formation and maintenance of blood vessels. To date, studies on the effects of irradiation on endothelial cells *in vitro* have been in 2-dimensional monolayers, although data on space radiations are scarce.

Studies we carried out on proliferating monolayers showed that human umbilical cord endothelial cells (HUVEC) respond to protons and Fe ions much the same as fibroblasts. Low and high LET irradiation induced chromosome damage, repair, and long-term chromosome aberrations such as reciprocal translocations suggesting that *in vivo* endothelial stem cells could be transformed into cancer cells.

Proliferating endothelial stem cells are a relatively minor population in the body and endothelial cancers are not common. For non-cancerous effects of space radiation we wanted to assess the effects on more typical endothelial cells in the body, that is, post mitotic endothelial cells arranged in vessel like tubes. When the cells are exposed to growth factors such as VEGF and FGF and embedded in collagen gels, they become post-mitotic and fully differentiate and assemble into capillary tubes. The cytoskeleton changes dramatically, cell to cell contacts are more developed and the cells express a different profile of genes.

**Structure and function of vessel models**

To examine the effect of space radiations on mature vessels, fully formed vessels were exposed to doses of protons (1GeV) and Fe ions (1GeV) up to 3.2Gy. Twenty-four and forty-eight hours after irradiation the vessel cultures were fixed and cells visualized by a total protein stain (DTAF) and propidium iodide. Three-dimensional images were collected using a confocal microscope. This allowed us to assay for the structural integrity of the vessels. Vessel structure is an arrangement of endothelial cells formed in a tube that surrounds a central lumen. For an accurate measure of structure we determined the length of lumen per cell.

Mature vessels were found to be sensitive to high LET Fe ions. At least 50% of tubular structures became narrow and spindly without a discernable lumen when exposed to 3.2Gy (Fig. 1 and 2). Low LET protons up to the same dose appeared to have no effect on the vessel structure. Control vessel cultures were indistinguishable from vessels exposed to 3.2Gy (Fig. 1 and 2). Vessel structure was also found to be highly resistant to doses of gamma rays up to 6Gy. Although Fe ions are more effective at breaking down the structure of vessels, the doses of HZE particles on a mars trip would be as low as 3 mGy per day per person, well below that which breaks down structure in our assay. Furthermore, vessel tissue in vivo is likely to be more resilient than the 3D model tissue. We have also observed vessel repair after a further 10-12 days culture following irradiation. The physical structure of human vessels is, therefore, unlikely to be affected by high or low LET space radiation.

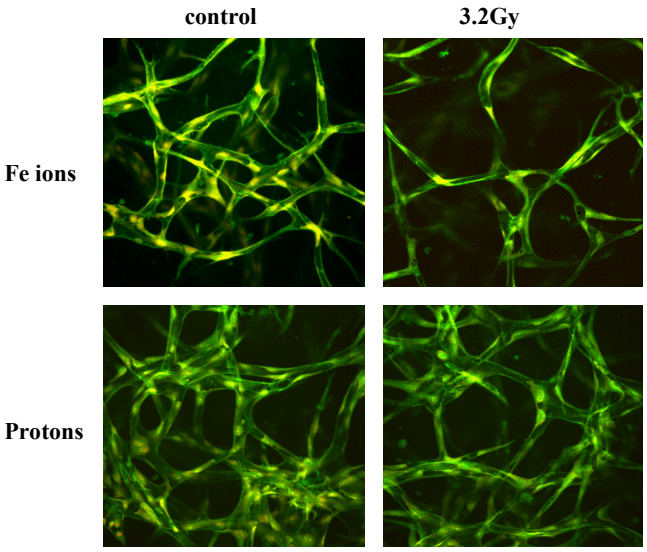


**Fig. 1. Morphology of vessel models exposed to space radiation**. Tissue models were exposed to doses of 3.2Gy (1GeV) Fe ions and protons. Each panel contains 10 slices 2 microns apart projected onto a single frame. Fe ion irradiated cultures contain less length of vessels with a discernable lumen.

In addition we have observed the effects of space radiation on the development of vessels. Vessel cultures at day one, 4 days before maturation, were exposed to Fe ions and protons and structure assayed at 5 days in the same way. Vessels were sensitive to Fe ions in much the same way as mature vessels. However, protons affected vessel formation at a similar dose effect to Fe ions (Fig. 2). This result indicates that sensitivity to protons is dependant on the cell behavior. Cells in developing vessels have biological pathways activated that may make them more sensitive to ionizing radiation. The protons may be activating cell signaling pathways rather than physically destroying cell structure.

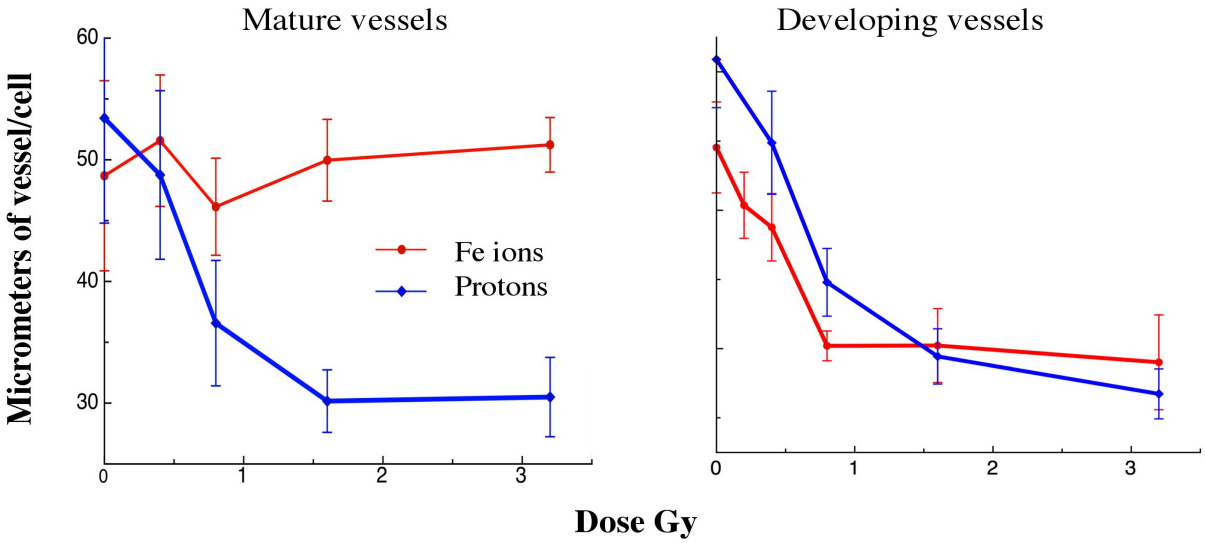


**Fig. 2. Effects of Fe ions and protons on mature and developing human 3-D vessel models.** Tissue models were exposed to doses (1 GeV) Fe ions and protons, fixed and imaged as in Figure 1 24 hours after irradiation for mature vessels and 5 days after irradiation for developing vessels, and then each analyzed for micrometers of vessel per cell.

Even so, at a daily dose of 250 mGy per day in space, protons would not be expected to affect vessel formation. This does not rule out other effects on vessels that may be cumulative or involve other cell types.

**Examination of DNA repair mechanisms by visualization of p53 binding protein**

We have also assessed the dynamics of DNA repair in these post-mitotic endothelial cells that make up the 3-D tissue vessels. Using 53 BP-1 localization as a marker for DNA repair, we have examined the appearance and decline of 53 BP-1 nuclear foci following irradiation by Fe ions (1Gy), protons (1Gy) and gamma rays at a dose of 80cGy each. Each ionizing radiation produced a comparable number of foci per nucleus in this assay at the time point of 1h 30min (Fig. 3). Cells exposed to the high LET (LET = 150) Fe ions are expected to receive 6.9 particle hits per nucleus and the count of foci was an average of 7.1 indicating that Fe ions are efficient at inducing repair and that secondary effects might be present. Cells exposed to the low LET protons (LET = 0.2225) are expected to receive 4269 particle hits per nucleus and the count of foci was an average of 9.0. Thus, particle for particle protons are less efficient at inducing DNA repair foci.

Following the reduction of foci with time, we observed that Fe ions, protons and gamma rays have different rates of decline (successful repair), with high LET exhibiting slowest repair and gamma rays the fastest repair (Fig. 3). High LET, as in dividing cells, probably produces more complex damage that is difficult to repair. Comparisons of DNA damage and repair between 2D differentiated cells and 3D tissue culture models show no difference in the case of protons or gamma rays. Fe ions however, show more damage (foci) in 2D cultures than 3D models. One explanation is that 2D cell nuclei present a larger flatter thinner target than rounder 3D nuclei. After 48 hours of repair the remaining foci in each case is the same. If Fe ions produce ionizing tracks then analysis by projecting depth slices on to one frame will render multiple damage sites onto one foci. After repair however, the remaining foci, which are now only less than 20% of the original, are represented more accurately by this kind of analysis.

We have attempted to visualize Fe ion tracks by higher power 3D confocal microscopy. Figure 4 shows Fe ion tracks visualized in this way. Foci are made up of a mixture of tracks and individual foci. Tracks represent the paths of Fe ions and the foci are probably sites where Fe ions only hit chromatin at one site along a pathway due to varying densities of chromatin, or represent damage by secondary radiation such as delta rays. Protons and gamma rays only induced individual foci of varying sizes. Ongoing studies are aimed at resolving DNA damage and repair using 2-photon microscopy at RARAF.

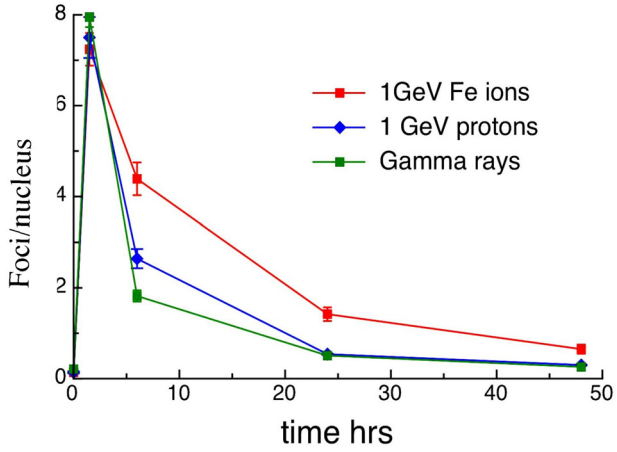


**Fig. 3. DNA repair dynamics after exposure to space radiations and gamma rays**. Tissue models were exposed to an 80cGy dose of (1 GeV) Fe ions, (1GV) protons, and gamma rays. Fixed at appropriate times and immunostained for 53BP-1. Confocal slices of tissue were taken and analyzed for foci number per nucleus.

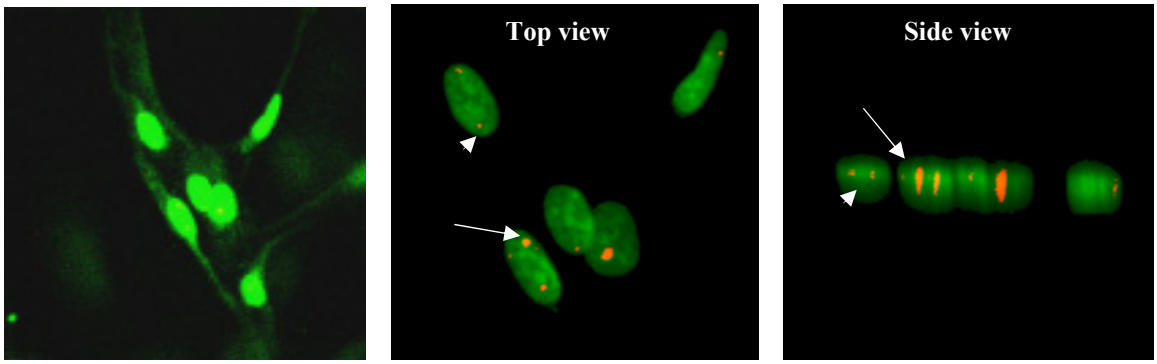


**Fig. 4. DNA damage 1h 30 mins after exposure to Fe ions. Left**: Vessel model 1h 30 min after exposure to 80cGy 1GeV Fe ions. **Middle and right**: The same cells stained for nuclei (YOYO green and 53BP-1 (red). Tissue models were exposed to an 80cGy dose of (1 GeV) Fe ions, fixed and immunostained for 53BP-1. Confocal slices of tissue were taken and rendered in 3D using NIH image software. Arrowhead shows a small focus that is revealed to be an individual focus. Arrow shows a large focus that is revealed to be made up of multiple damage sites along the path of the ion.

This work was supported by NASA grant NNJ05H137G.

**Publications**

1. Grabham PW, Burong Hu and Charles R. Geard. Effects of space radiation and gamma rays on the structure of 3-D human vessel tissue culture models (Manuscript submitted).
2. Grabham PW, Burong Hu, Alan Bigelow and Charles R. Geard. DNA damage and repair in human vessel tissue culture models (Manuscript submitted). ■

# Effect of Organophosphorus Pesticides and Estrogen on Mammary Carcinogenesis

*Gloria M. Calaf and Carlos Echiburú-Chau*[a]

Studies on mammary tumorigenesis suggest that cancer cells acquire malignancy through the activation and inactivation of genes over a long period of time.[1] For breast cancer development, this multistep process may manifest itself as a sequence of pathologically defined stages. An important but unclarified question is the effect that environmental carcinogens may play in the neoplastic process.[2] Malathion is an organophosphorous pesticide, widely used in agriculture, with a high risk for human exposures.[3] Many of the risk factors for breast carcinogenesis are associated with prolonged high levels of estrogen exposure.[4] It is expected that estrogen would couple with genetic predisposition and other factors in determining individual risk.[5] The recognition of early parallel phenotypical changes may be a critical step to the prognosis of the disease.[6-8]

An *in vivo* rat mammary gland model was developed and there were four experimental groups: (i) control (physiological saline), (ii) malathion (M) (22mg/100gr body weight), (iii) 17β-estradiol (E2) (30 ug/100gr body weight) and (iv) combination of both (M+E2). Animals were treated for 5

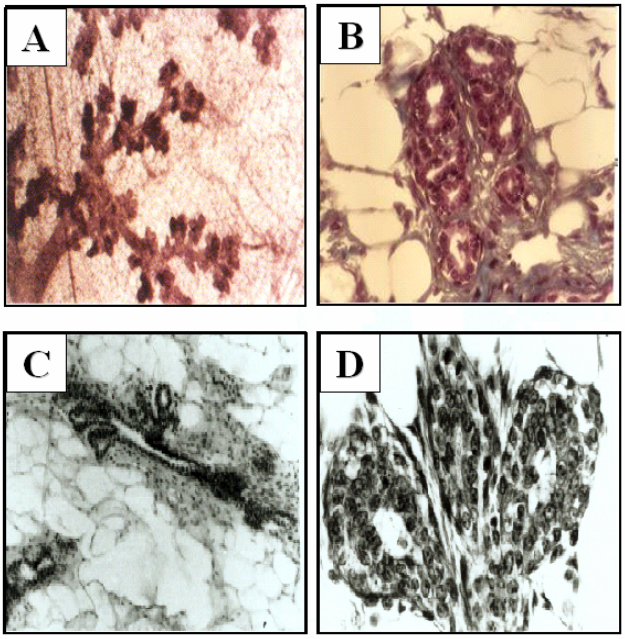


**Fig. 1.** Rat mammary gland development of alveolar buds (Abs) (**A**-**B**) and terminal end buds (TEBs) (**C**-**D**).

[a] *Institute for Advanced Research, Tarapaca University, Arica, Chile*

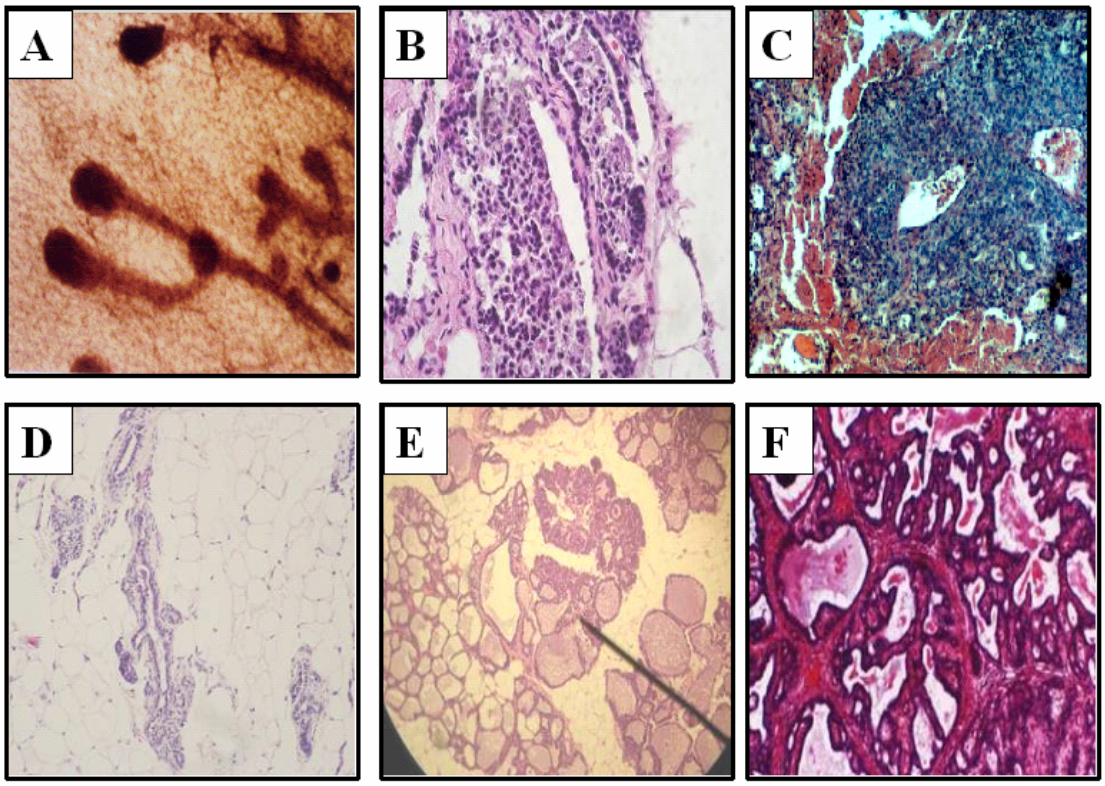


**Fig. 2.** Cancer progression of rat mammary gland induced by malathion (**A-B**) that became transformed in tumor (**C**) and estrogen (**D-E**) that also became transformed in tumor with different morphology (**F**).

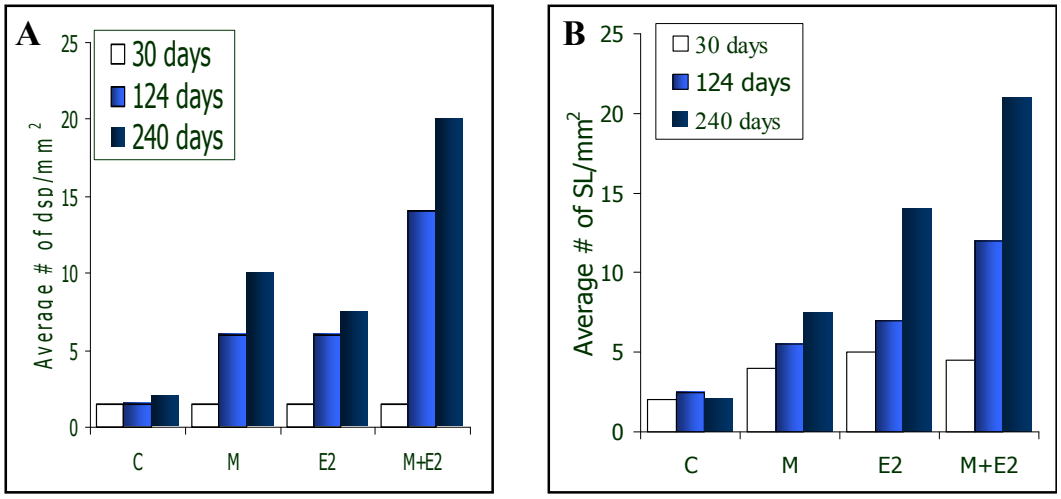


**Fig. 3.** Effect of malathion, estrogen and combination of both on the ducts, referred as ducts in stage of proliferation (dsp) (cells in ducts/mm$^2$) and the number of secretory lobules (SL) (number of SL/mm$^2$) (**A-B**).

days and then killed after 30, 124 and 240 days after treatment. Figure 1 shows normal rat mammary gland development of Alveoli (Abs) (Fig. 1A-B) and terminal end buds (TEBs) (Fig. 1C-D). The rat mammary gland showed progressive alterations in TEBs in the presence of malathion (Fig. 2A-C), as wells as in ABs in the presence of estrogen (Fig. 2D-F) after 30, 124 and 240 days in comparison to controls. There was a significant ($p<0.05$) increase in the number of cells in the in ducts, referred as to ducts in stage of proliferation (dsp), (cells in ducts/mm$^2$) (Fig. 3A) and in the number of secretory lobules (SL) (number of SL/mm$^2$) (Fig. 3B) observed after 240 days. The M+E2 treatment showed a significantly ($p<0.05$) higher number of dsp and SL after 240 days in comparison with M, E2 and control (Fig. 3A-B). The M+E2 showed a significantly ($p<0.05$) higher number of dsp and SL after 240 days in comparison with M, E2 and control (Fig. 3A-B). The M+E2 treatment showed significantly ($p<0.05$) higher expression of mp53, CYPA2, c-myc and c-fos proteins after 120 and 240 days of treatment in comparison to control as seen in Figure 4.

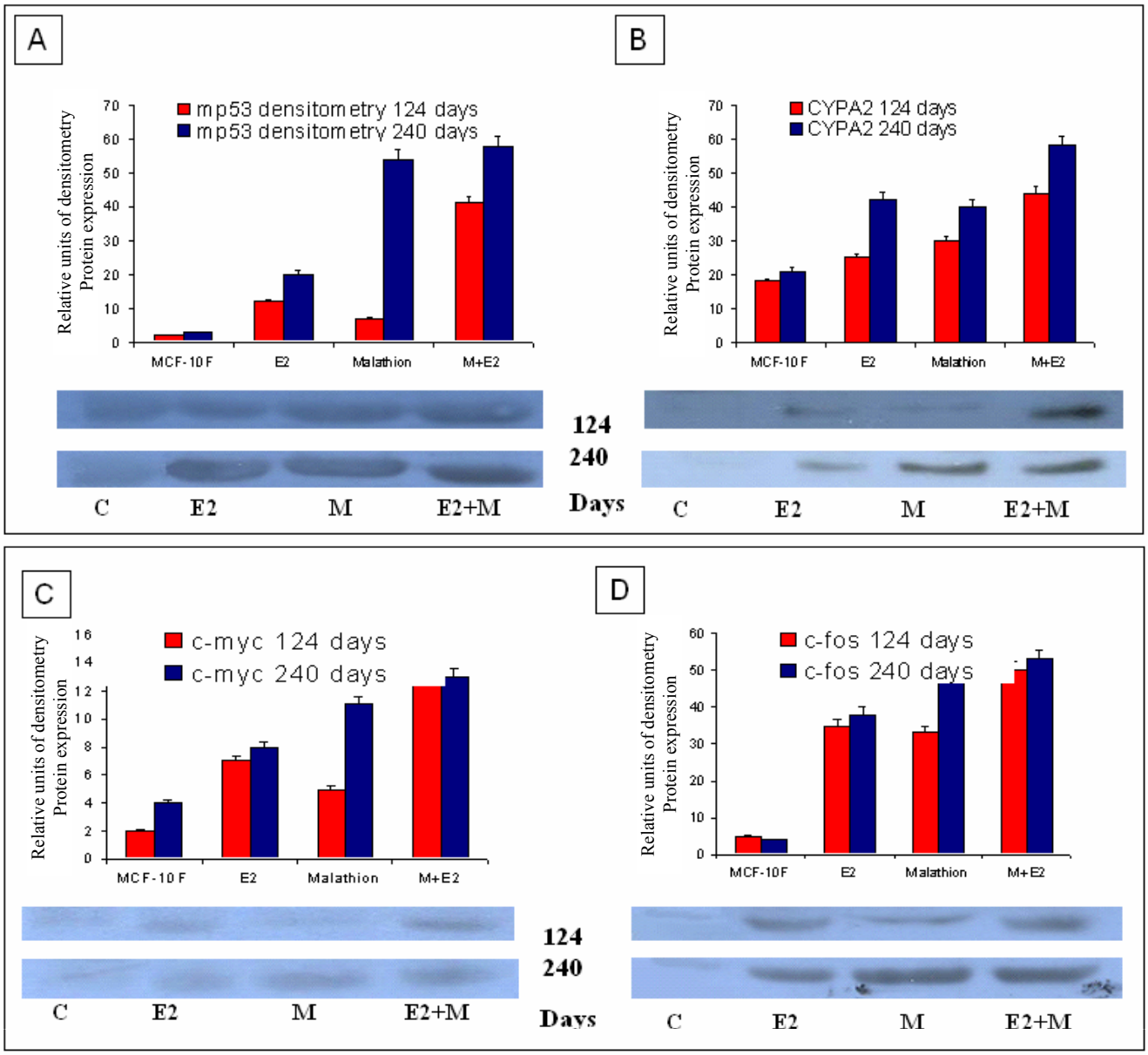


**Fig. 4.** Effect of malathion, estrogen and combination of both on mp53 (**A**), CYPA2 (**B**), c-myc (**C**) and c-fos (**D**) protein expression after 120 and 240 days of treatment.

## References


1. Loeb LA. Mutator phenotype may be required for multistage carcinogenesis. *Cancer Res* **51**:3075-9, 1991.
2. Falck F, Jr., Ricci A, Jr., Wolff MS, Godbold J and Deckers P. Pesticides and polychlorinated biphenyl residues in human breast lipids and their relation to breast cancer. *Arch Environ Health* **47**:143-6, 1992.
3. National Cancer Institute. Bioassay of Malathion for Possible Carcinogenicity. Technical Report Series No. 24. DHEW Publication No. (NIH) 78-824, 1978.
4. Kelsey JL and Bernstein L. Epidemiology and prevention of breast cancer. *Annu Rev Public Health* **17**:47-67, 1996.
5. Kelloff GJ, Crowell JA, Steele VE, Lubet RA, Boone CW, Malone WA, Hawk ET, Lieberman R, Lawrence JA, Kopelovich L, *et al.* Progress in cancer chemoprevention. *Ann N Y Acad Sci* **889**:1-13, 1999.
6. Wistuba, II and Gazdar AF. Lung cancer preneoplasia. *Annu Rev Pathol* **1**:331-48, 2006.
7. Calaf GM. A critical approach to the malignant transformation of human breast epithelial cells with physical and chemical carcinogens. 10th World Congress on Advances in Oncology and 8th International Symposium on Molecular Medicine. Hersonissos. Greece, 2005.
8. Calaf GM. Critical steps in breast carcinogenesis induced by estrogen. 11th World Congress on Advances in Oncology and 9th International Symposium on Molecular Medicine. Hersonissos. Greece, 2006. ■

At the Reception and Banquet of the Symposium in Honor of Professor Eric J. Hall, Columbia University, New York, October 14, 2008. (L-r): Dr. and Mrs Chao and Mrs and Dr. Hall.

At the Reception and Banquet of the Symposium in Honor of Professor Eric J. Hall, Columbia University, New York, October 14, 2008. (L-r): Dr. Tom Hei, Dr. Mary Helen Barcellos-Hoff's husband, Dr. Barcellos-Hoff and Dr. Diane Waldren.

At the Reception and Banquet of the Symposium in Honor of Professor Eric J. Hall, Columbia University, New York, October 14, 2008. (L-r): Dr. David Brenner, Dr. Robert Ullrich and Dr. Sally Amundson.

At the Reception and Banquet of the Symposium in Honor of Professor Eric J. Hall, Columbia University, New York, October 14, 2008. (L-r): Ms. Monique Rey, Dr. Antonella Bertucci, Ms. Yvette Acevedo and Ms. Lilian Oling.

At the Reception and Banquet of the Symposium in Honor of Professor Eric J. Hall, Columbia University, New York, October 14, 2008. (L-r): Dr. Hongning Zhou, Dr. Yanping Xu and Mr. Yunfei Chai.

At the Reception and Banquet of the Symposium in Honor of Professor Eric J. Hall, Columbia University, New York, October 14, 2008. (L-r): Dr. Charles Geard and Mrs. Monica Hei.

# Protons for Radiotherapy: A 1946 Proposal

*Eric J. Hall*

The medical application of charged particles has peaked at a time when nuclear physics research has lost some of its glamour, but nevertheless particles for radiotherapy are a spin-off from the halcyon days of nuclear physics. In the early years of the 20th century, beams of charged particles were used in nuclear disintegration experiments to produce artificial radioactive materials. This was the precursor of the nuclear age. As President of the Royal Society in 1927, Rutherford called for a supply of "atoms and electrons which have an energy far transcending that of α and β particles from radioactive bodies". At Cambridge, Cockroft and Walton used a voltage multiplier and were first to demonstrate transmutation using an accelerated particle. Higher and higher energies were called for and made possible, largely, by the invention of the cyclotron by Lawrence in 1931 at the University of California, Berkeley.

Robert Wilson was born in Wyoming and went to graduate school at Berkeley with Ernest Lawrence, so not surprisingly he was an expert on cyclotrons. He was recruited as the youngest group leader at Los Alamos, working on the Manhattan project in WW11. They needed a cyclotron, so the United States government bought the Harvard cyclotron (built in 1937) for $1 with the promise to replace it after the war.

Wilson wrote his seminal paper proposing protons for radiotherapy in 1946, after leaving Los Alamos and moving to Harvard to design and build their new cyclotron.[1] He came from a strong Quaker background, and it is said that he wanted to use nuclear physics to benefit mankind, as an atonement for his part in developing the A-bomb.[2]

Wilson pointed out that protons have advantages over x-rays for the treatment of cancer because of their physical dose distribution. The dose deposited by a beam of monoenergetic protons increases slowly with depth, but reaches a sharp maximum near the end of the particles range, in the so-called Bragg Peak. The beam has sharp edges, with little side-scatter, and the dose falls to zero at the end of the particle's range. The possibility of precisely confining the high-dose region to the tumor volume, while minimizing the dose to the surrounding normal tissue is the attractive feature of charged particle beams.

Patients were first treated at accelerators built initially for physics research, but which had become obsolete as bigger and better accelerators were built elsewhere. The earliest efforts were at the Lawrence-Berkeley National Laboratory (CA. USA) in 1954 and in Uppsala, Sweden in 1962.[3, 4] In the 1960's, a collaboration was formed between the Harvard Cyclotron and physicians from the Massachusetts General Hospital, led by Herman Suit, with the first patient treated in 1973. It was this effort that was inspired by the paper of Robert Wilson. By the time that the cyclotron was closed in 2002, over 9000 patients had received proton treatment.

At the present time, several dozen purpose- built hospital- based facilities are in operation, or under construction, in the United States, Europe and Japan. Most involve protons, but some employ heavier ions such as Carbon. Proton facilities typically cost about $125 million, with heavier ions involving much higher costs. Such facilities may well revolutionize Radiation Oncology principally because of the decrease in normal tissue morbidity associated with the improved dose distribution.

## References

1. Wilson RR. Radiological Use of Fast protons. *Radiology* **47**:487, 1946.
2. Wilson R. A Brief History of the Harvard University Cyclotrons. *Harvard University press*, 2004.
3. Lawrence JH, Tobias CA, Born JL, Mc CR, Roberts JE, Anger HO, Low-Beer BV and Huggins CB. Pituitary irradiation with high-energy proton beams: a preliminary report. *Cancer Res* **18**:121-34, 1958.
4. Falkmer S, Fors B, Larsson B, Lindell A, Naeslund J and Stenson S. Pilot study on proton irradiation of human carcinoma. *Acta radiol* **58**:33-51, 1962.

## Key findings of the 1946 paper by Wilson

- Proton energies needed to treat human cancer, namely about125 to 200MeV, were readily available with the technology of the day.
- The beam currents needed to result in treatments lasting no more than a few minutes were readily attainable.
- The proton depth dose curve is characterized by a sharp Bragg Peak near the end of the particles range, where most energy is deposited, with no dose beyond.
- A rotating wheel of variable thickness was proposed to spread out the Bragg peak over a large tumour volume, which is the commonly used technique to this day.
- Wilson calculated that the number of ionizations per cm of track, and therefore the biological effectiveness, would be considerably greater at the end of the particle range compared to the incident particle.
- It was predicted that heavier nuclei, including energetic carbon ions, may eventually become therapeutically practical. ■

# Integrating Short- and Long-Term Mechanistic Models of Radiation-Induced Carcinogenesis. I: Rationale and Methods

*Igor Shuryak, Philip Hahnfeldt,[a] Lynn Hlatky,[a] Rainer K. Sachs[b] and David J. Brenner*

Mathematical models of radiation carcinogenesis are important for understanding mechanisms and for interpreting or extrapolating risk. There are two classes of such models: 1) Long-term formalisms, which track pre-malignant cell numbers throughout an entire lifetime but treat radiation dose-response simplistically. 2) Short-term formalisms, which provide a detailed dose-response, but address its modulation, during the subsequent latency period leading to cancer, only indirectly. We argue that models integrating short- and long-term mechanisms are needed. As an example of a unified approach, we discuss and implement the following assumptions. Radiation initiates, promotes, or kills pre-malignant cells. Any pre-malignant cell can generate a clone, which quickly reaches a size limitation (e.g. by filling up a niche), subsequently grows more slowly, and can generate a malignant cell by transformation. The carcinogenic potential of pre-malignant cells decreases with age. Applications of the formalism for estimating radiotherapy-induced second cancer risks are given in a companion paper.

This formalism is the first comprehensive attempt to unify short- and long-term modeling approaches. The short-term part of the model tracks the numbers of pre-malignant cells throughout irradiation stochastically. The long-term part of the model builds on the concepts developed in previous two-stage formalisms by adding an analysis of some aspects of tissue architecture (i.e. stem cell niches/compartments) and aging of pre-malignant stem cells.

The unified approach has a number of advantages. The short-term part can generate reasonable predictions even at high doses, such as those in cancer radiotherapy. The long-term part analyzes the entire lifetime of the individual, putting the short-term predictions in an appropriate context by estimating the effects of age at exposure and time since exposure. The combined approach therefore allows the dose response for the number of pre-malignant cells to be examined at any time point, from the start of irradiation until development of cancer years to decades later, which is not possible using either short- or long-term models alone.

A schematic representation of model assumptions is shown in Figure 1 below.

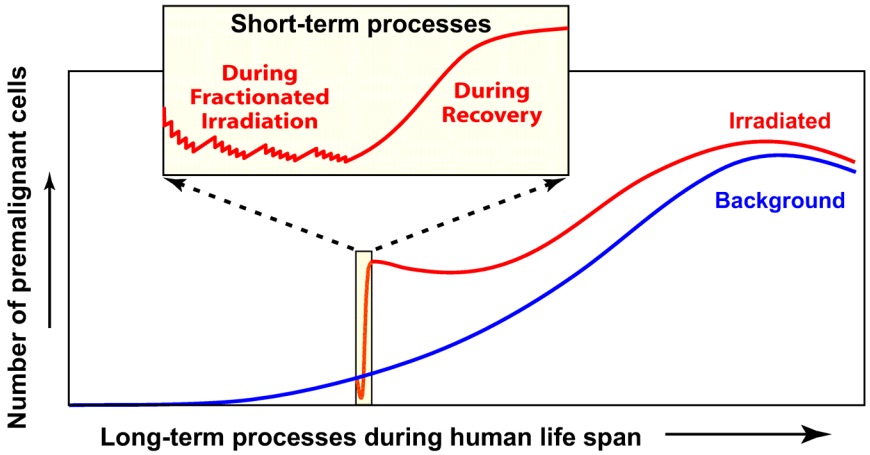


**Fig. 1.** A general scheme of short- and long-term processes governing the total number of pre-malignant cells. As the individual ages, the number of viable pre-malignant cells grows, but may turn over and decrease at very old age (blue line in the main graph). This pattern parallels background cancer incidence, since cancer risk is assumed to be proportional to the number of pre-malignant cells. Radiation exposure (e.g. radiotherapy for an existing cancer) initially causes the number of pre-malignant cells to decrease due to cell killing (red line). After exposure stops, the irradiated tissues recover, allowing pre-malignant cells to repopulate and reach a number somewhat higher, than was present before irradiation, i.e. a net excess radiogenic cancer risk is produced. Fluctuations in the number of pre-malignant cells throughout the irradiation and recovery periods (i.e. the short-term processes) are shown in the inset graph.

[a] *Caritas St. Elizabeth's Medical Center, Tufts University School of Medicine, Boston, MA*

[b] *Department of Mathematics and Physics, University of California, Berkeley, CA*

## References

1. Shuryak I, Hahnfeldt P, Hlatky L, Sachs RK and Brenner DJ. Integrating short- and long-term mechanistic models of radiation carcinogenesis. I: Rationale and methods. *Rad Evriron Biophys*, submitted. ■

# Integrating Short- and Long-Term Mechanistic Models of Radiation-Induced Carcinogenesis. II: Second Cancer Risk Estimation

*Igor Shuryak, Philip Hahnfeldt,[a] Lynn Hlatky,[a] Rainer K. Sachs[b] and David J. Brenner*

As the number of cancer survivors grows, prediction of radiotherapy-induced second cancer risks becomes increasingly important. Because the latency period for solid tumors is long, the risks of recently introduced radiotherapy protocols are not yet directly measurable. In the previous article, we presented a new biologically-based mathematical model, which, in principle, can estimate second cancer risks for any protocol. The novelty of the model is that it integrates, into a single formalism, mechanistic analyses of pre-malignant cell dynamics on two different time scales: short-term during radiotherapy; long-term during the entire human life span.

[a] *Caritas St. Elizabeth's Medical Center, Tufts University School of Medicine, Boston, MA*

[b] *Department of Mathematics and Physics, University of California, Berkeley, CA*

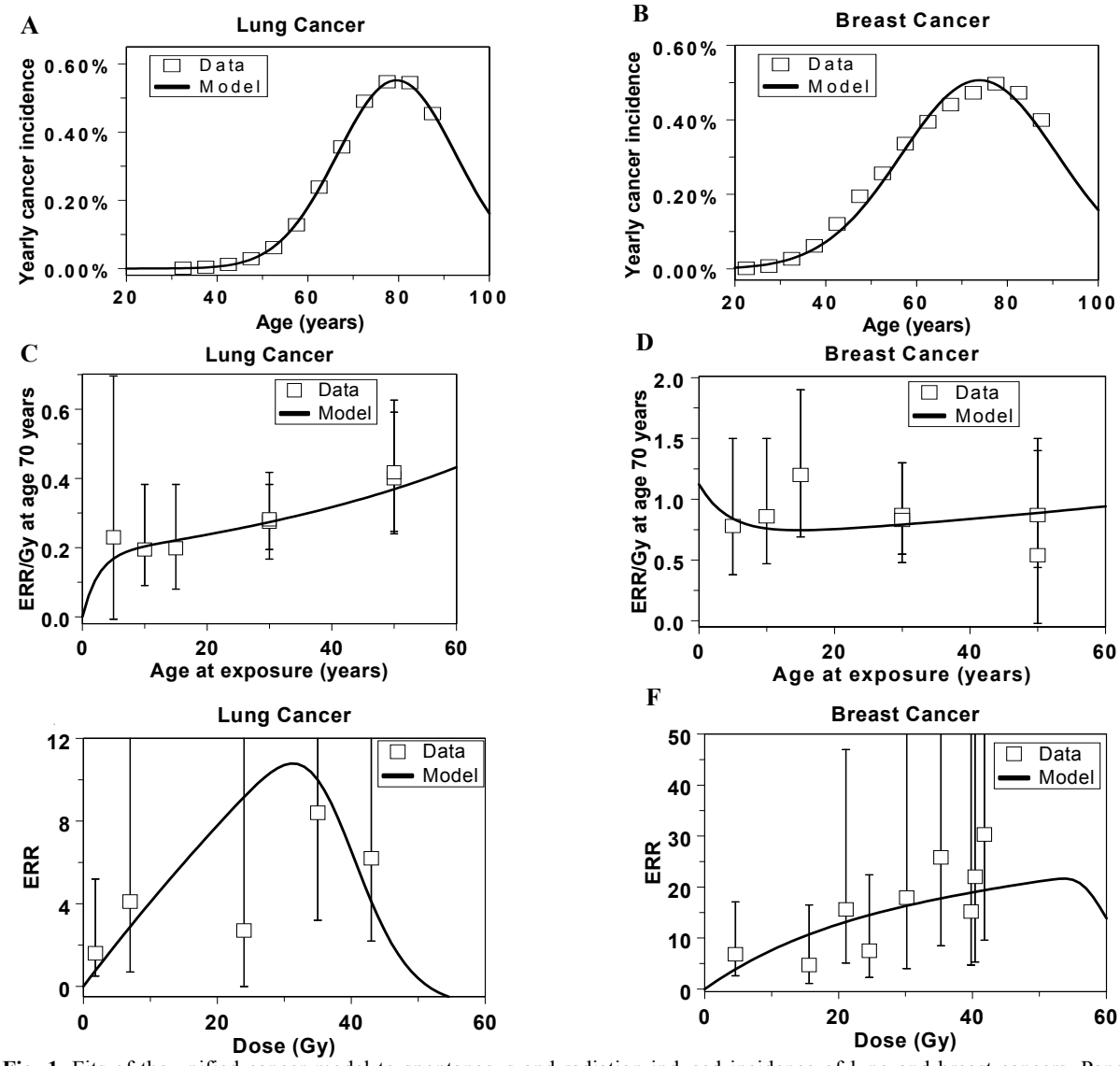


**Fig. 1.** Fits of the unified cancer model to spontaneous and radiation-induced incidence of lung and breast cancers. Panels A-B show spontaneous cancer incidence from SEER. Panels C-D show radiation-induced cancer ERRs for atomic bomb survivors from reference.[1] Panels E-F show ERRs for high-dose radiotherapy-induced second cancers, from references.[2-5]

Here we apply the model to 9 solid cancer types (stomach, lung, colon, rectal, pancreatic, bladder, breast, CNS, and thyroid) using data on radiotherapy-induced second malignancies, on Japanese atomic bomb survivors, and on background US cancer incidence. Potentially, the model can be incorporated into radiotherapy treatment planning algorithms, adding second cancer risk as an additional optimization criterion.

The model presented here was able to describe the observed patterns of background and radiation-induced cancer risk for the 9 selected cancer types, both at relatively low and high fractionated radiation doses. Examples for breast and lung cancers are shown in Figure 1. It can potentially be used to predict cancer risks from current or prospective radiotherapy protocols, provided a dose-volume histogram (DVH) is available.

## References


1. Preston DL, Ron E, Tokuoka S, Funamoto S, Nishi N, Soda M, Mabuchi K and Kodama K. Solid cancer incidence in atomic bomb survivors: 1958-1998. *Radiat Res* **168**:1-64, 2007.
2. Travis LB, Gospodarowicz M, Curtis RE, Clarke EA, Andersson M, Glimelius B, Joensuu T, Lynch CF, van Leeuwen FE, Holowaty E*, et al.* Lung cancer following chemotherapy and radiotherapy for Hodgkin's disease. *J Natl Cancer Inst* **94**:182-92, 2002.
3. Travis LB, Hill DA, Dores GM, Gospodarowicz M, van Leeuwen FE, Holowaty E, Glimelius B, Andersson M, Wiklund T, Lynch CF*, et al.* Breast cancer following radiotherapy and chemotherapy among young women with Hodgkin disease. *Jama* **290**:465-75, 2003.
4. van Leeuwen FE, Klokman WJ, Stovall M, Dahler EC, van't Veer MB, Noordijk EM, Crommelin MA, Aleman BM, Broeks A, Gospodarowicz M*, et al.* Roles of radiation dose, chemotherapy, and hormonal factors in breast cancer following Hodgkin's disease. *J Natl Cancer Inst* **95**:971-80, 2003.
5. Gilbert ES, Stovall M, Gospodarowicz M, Van Leeuwen FE, Andersson M, Glimelius B, Joensuu T, Lynch CF, Curtis RE, Holowaty E*, et al.* Lung cancer after treatment for Hodgkin's disease: focus on radiation effects. *Radiat Res* **159**:161-73, 2003.
6. Shuryak I, Hahnfeldt P, Hlatky L, Sachs RK and Brenner DJ. Integrating short- and long-term mechanistic models of radiation carcinogenesis. II: Second cancer risk estimation. *Rad Evriron Biophys*, submitted. ■


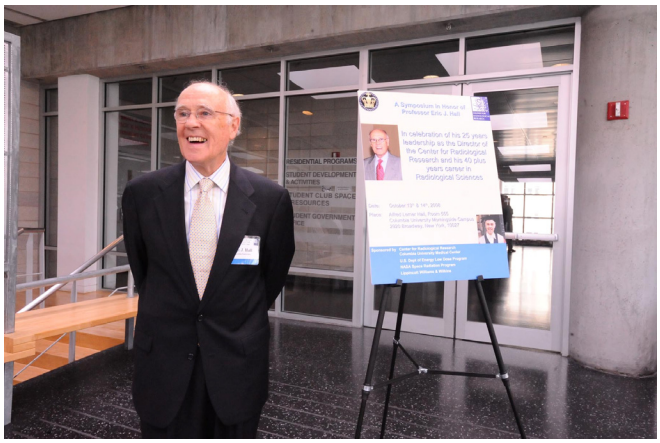

A Symposium in Honor of Professor Eric J. Hall entitled "From Beans to Genes: A Forty Year Odyssey in Radiation Biology" was held at Columbia University, New York, October 13-14, 2008.

Science Sessions of the Symposium in Honor of Professor Eric J. Hall, Columbia University, New York, October 13-14, 2008.

# Triage of Medically Significant Radiation Exposures Using Gene Expression Signatures in Human PBL

*Sally A. Amundson and Sunirmal Paul*

As part of our efforts toward developing radiation biodosimetry using gene expression signatures measured in self-contained biochips, we have investigated the ability of gene expression profiles to predict the radiation dose to which a blood sample has been exposed. We have used ex vivo irradiation of human peripheral blood lymphocytes (PBL) drawn with informed consent from healthy donors as an initial model for these studies. The irradiation and culture protocols, as well as the microaray protocols used, have been described in the 2007 annual report and have been published.[1] We here discuss some of the different approaches for using this microarray data to build algorithms for dose prediction of unknown samples.

Whole genome measurements of gene expression were made using Agilent microarrays at 6 and 24 hours after exposure of blood to doses of 0, 0.5, 2, 5 or 8 Gy gamma-rays. BRB-ArrayTools, Version 3.5[2] was used to log2-transform and median normalize the data from 5 donors at each dose and time point. Non-uniform outliers or features not significantly above background intensity in 25% or more of the hybridizations were filtered out. A further filter requiring a minimum 1.5-fold change in at least 10% of the hybridizations was also applied yielding a final set of 17313 features that were used in subsequent analyses. BRB-ArrayTools was used to build gene expression classifiers using several different algorithms and to test the ability of these classifiers to predict the dose to which an individual sample had been exposed.

All experiments involving human subjects were approved by the Columbia University Medical Center Institutional Review Board IRB #3, and were conducted according to the principles expressed in the Declaration of Helsinki.

**Prediction of medically significant exposures**

Since the main goal of this biodosimetry project is to provide radiological triage to identify those individuals who will benefit from medical intervention, and those who will not, we first looked at the ability of gene expression measurements to predict exposures of 2Gy and above, as doses below this level would not require any immediate medical treatment. In this analysis, we combined all data from both the 6 and 24 hour time points, in the hopes of identifying genes that can predict radiation exposure status across a window of time.

For this two-group classification problem, we used BRB-ArrayTools to construct seven different prediction algorithms using the filtered set of 17313 genes. The classifiers were tested using leave-one-out cross validation to assess the sensitivity and specificity of individual sample prediction. Three hundred and twenty-two genes were used by the various classifiers. Surprisingly, all methods tested, compound covariate (CCV), Bayesian compound covariate (BCC), linear discriminant analysis (LDA), 1- and 3-nearest neighbors (1NN, 3NN), nearest centroid and support vector machines (SVM), predicted the irradiation status (≤0.5Gy or ≥2Gy) of 100% of the samples correctly.

In an attempt to reduce the number of genes required to correctly predict exposure status of the samples, we investigated the effect of using a core set of radiation response genes that we had identified as responding in a dose-dependent fashion at both 6 and 24 hours after exposure.[1] This gene set performed nearly as well as that selected *de novo* by the classification algorithms. BCC, 1NN, 3NN and SVM again predicted the exposure status of 100% of the samples correctly. The CCV, LDA and nearest centroid classifiers also performed well with the reduced gene set, predicting the status of 98% of the samples correctly with one false positive identification of a 0.5Gy sample as significantly exposed. A low rate of false positives is acceptable for a radiological triage application such as this, where additional testing can be applied to further screen those who appear to be exposed. Eliminating exposed individuals from further testing is considered a more serious failing in this situation. Thus it appears that a smaller number of genes may be required for accurate prediction that the number used by traditional classification techniques.

**Prediction between times**

We were interested to see how well the data collected at one time point could predict the exposure status of samples collected at a different time point. We addressed this by separating the data from the two time points into a training set, which was used to build the classifiers, and an independent set of samples that were used to test the performance of the classifiers. First we assigned all the 6-hour samples to the training set and used the same seven algorithms to build classifiers. This process selected 506 genes for use by the classifiers. When we challenged these classifiers to predict the exposure status of the 24-hour samples, correct prediction ranged between 48% and 80%, all due to false negatives (Table 1). The nearest centroid classifier performed the best in this case, missing all the 2Gy samples, but calling all others correctly. None of the 2Gy samples were correctly identified as exposed by any of the methods.

In contrast, using the 24-hour data as the training set and challenging the classifiers to predict the status of the 6-hour samples produced much more robust classification, and a smaller gene set (174 genes). The LDA classifier yielded two false positives (0.5Gy samples), and all other algorithms correctly predicted the exposure status of 100% of the 6-

**Table 1.** Performance of classifiers built using 6-hour data in predicting status of 24-hour samples

| | CCV | BCC | LDA | 1NN | 3NN | Centroid | SVM |
|---|---|---|---|---|---|---|---|
| False Negative | 9 | 9 | 13 | 10 | 7 | 5 | 7 |
| False Positive | 0 | 0 | 0 | 0 | 0 | 0 | 0 |

hour samples. Taken together, these results seem to indicate that many of the genes with the strongest classification power at 6 hours are returning to baseline levels by 24 hours. While genes that are informative at 24 hours are not late responders, but rather persistent responders that were differentially expressed at 6 hours. The complete failure of classification of the 2Gy dose point also suggests that the fading of the 6-hour responses occurs more rapidly at the lower doses.

In summary, these analyses demonstrate that gene expression can predict medically relevant radiation exposures with a high degree of accuracy across a window of time, and that this prediction is most accurate when data from across the window of time of interest are used to train the classifiers. Because of the dynamics of gene expression responses following radiation exposure, prediction of earlier samples based on classifiers trained using data from later times post-exposure appears to be much more accurate than the reverse.

### References

1. Paul S and Amundson SA. Development of gene expression signatures for practical radiation biodosimetry. *Int J Radiat Oncol Biol Phys* **71**:1236-44, 2008.
2. Simon R, Lam A, Li M-C, Ngan M, Menenzes S and Zhao Y Analysis of gene expression data using BRB-Array Tools. *Cancer Informatics* **2**:11-7, 2007. ■

# The RABIT: A Rapid Automated Biodosimetry Tool for Radiological Triage

*Guy Garty and David J. Brenner*

### Introduction

The development of improved methods for radiation biodosimetry has been identified as a high priority need[1] in an environment of heightened concern over possible nuclear or radiological terrorist attacks. In such situations, in that the general population would not be carrying physical dosimeters, a very high throughput means of assessing the radiation exposure based on biological endpoints will be needed. This will serve both to reduce panic by reassuring those who were not significantly exposed, as well as triaging those in need of medical attention.

The **R**apid **A**utomated **BI**odosimetry **T**ool (RABIT) is designed to be a completely automated, ultra-high throughput robotically-based biodosimetry workstation.[2] It analyzes fingerstick-derived blood samples (30µl, essentially a single drop of blood), either to estimate past radiation dose, or to identify individuals exposed above or below a cutoff dose.

Although individual stages of cytogenetically-based bioassays have previously been automated,[3-5] most systems have focused on scoring and there are no other systems designed for **complete automation**, from lymphocyte harvesting to scoring. This aspect, together with the use of fingerstick samples and high speed imaging innovations, are the basis for the high throughput of the RABIT.

The RABIT automates two mature, but currently manual, biodosimetry assays (micronucleus[6, 7] and γ-H2AX[8]).

Based on measurements with these biomarkers, the RABIT is designed to estimate whole-body doses of 0.75 to 8Gy, with a 95% confidence interval of ±20% at 1Gy. A higher-throughput option for identifying individuals below or above a cutoff dose can potentially be applied. The RABIT is designed initially to have a throughput of ~6,000 samples per day, with parallelizing various steps potentially increasing this to 30,000 samples per day. Improved precision, if required, can be balanced against reduced throughput. There are a number of potential obstacles to achieving these target throughputs, and the RABIT addresses these by incorporating the following key technological innovations:

- Use of small volumes of blood (~30µl) from a lancet fingerstick; this is a minimally invasive, and thus high throughput, approach to sample acquisition–conventional venipuncture-based blood collection is not compatible with ultra high throughput. The sample collection is described below in a paper by G. Garty.
- Complete robotically-based automation of the biology, with processing and imaging performed *in situ* in multi-well plates; this allows rapid processing of multiple simultaneous samples. The use of filter-bottomed multi-well plates allows faster reagent changes and prevents loss of cells during processing. Adaptation of the assays

for robotic processing is described in a paper by H. Turner, below.

- Innovations in high-speed imaging allow rapid analysis following biological processing. The imaging and image analysis are described below in a paper by O. Lyulko.

### References


1. Pellmar TC and Rockwell S. Priority list of research areas for radiological nuclear threat countermeasures. *Radiat Res* **163**:115-23, 2005.
2. Salerno A, Zhang J, Bhatla A, Lyulko OV, Nie J, Dutta A, Garty G, Simaan N, Randers-Pehrson G, Yao YL and Brenner DJ. Design Considerations for a Minimally Invasive High-Throughput Automation System for Radiation Biodosimetry. In Proceedings of the Third Annual IEEE Conference on Automation Science and Engineering (CASE), Scottsdale, AZ, September 2007, pp. 846-852.
3. Hayata I, Tabuchi H, Furukawa A, Okabe N, Yamamoto M and Sato K. Robot system for preparing lymphocyte chromosome. *J Radiat Res (Tokyo)* **33 Suppl**: 231-41, 1992.
4. Schunck C, Johannes T, Varga D, Lorch T and Plesch A. New developments in automated cytogenetic imaging: unattended scoring of dicentric chromosomes, micronuclei, single cell gel electrophoresis, and fluorescence signals. *Cytogenet Genome Res* **104**:383-9, 2004.
5. Martin PR, Berdychevski RE, Subramanian U, Blakely WF and Prasanna PG. Sample Tracking in an Automated Cytogenetic Biodosimetry Laboratory for Radiation Mass Casualties. *Radiat Meas* **42**:1119-24, 2007.
6. Fenech M, Chang WP, Kirsch-Volders M, Holland N, Bonassi S and Zeiger E. HUMN project: detailed description of the scoring criteria for the cytokinesis-block micronucleus assay using isolated human lymphocyte cultures. *Mutat Res* **534**:65-75, 2003.
7. IAEA, *Cytogenetic analysis for radiation dose assessment: A manual.* Technical reports series No. 405. International Atomic Energy Agency, Vienna, 2001.
8. Nakamura A, Sedelnikova OA, Redon C, Pilch DR, Sinogeeva NI, Shroff R, Lichten M and Bonner WM. Techniques for gamma-H2AX detection. *Methods Enzymol* **409**:236-50, 2006. ■


# Sample Collection for High Throughput Radiation Biodosimetry

*Guy Garty, Helen C. Turner, Gerhard Randers-Pehrson and David J. Brenner*

The **R**apid **A**utomated **BI**odosimetry **T**ool (RABIT) is a fully automated, ultra-high throughput robotically-based biodosimetry workstation. It screens fingerstick-derived blood samples, either to estimate past radiation dose, or to sort individuals exposed above or below a cutoff dose. One of the major challenges of high throughput screening is that of sample collection. Due to the necessary interaction with people, this is the only part of the RABIT that cannot be automated.

We present here our operational concept for sample collection, as well as the first tests of its reliability.

### Requirements

- To achieve high throughput, sample collection must be **minimally invasive** and should not require highly trained personnel. Samples will be collected in the field and will need to be transported to the RABIT with **no spillage** and **no cross contamination**.
- Patient information needs to be **tracked** and **correlated** with the samples.
- To ensure separation of lymphocytes out of whole blood samples, the blood needs to be **layered** above separation medium with **no mixing**.
- Finally, the lymphocytes in the collected blood need to be kept **viable** as the CBMN assay requires them to be cultured to division.

### Collection sites

Following a radiological event, multiple collection sites (e.g., at doctor's offices, church halls, PODs, hospitals, etc.) as well as onsite RABIT location(s) will be set up by local authorities. A scheme of such a site is shown in Figure 1.

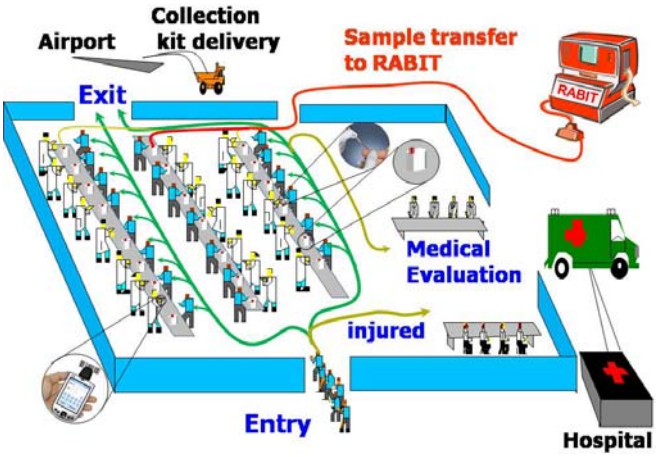


**Fig. 1.** Scheme of RABIT sample collection site.

Each site will have a number of individuals as sample collectors, who will draw the blood and verify the contact information. Individuals who are obviously injured will be taken to a hospital. Those who are not will be sent home after the sample collection. Samples will then be packed and transported to the RABIT (across the hall or to a different state).

**Sample collection**

In order to facilitate sample collection we have developed a sample collection kit (Fig. 2a), consisting of lancets, bar-coded, heparin coated, capillary tubes with matched personal data cards, alcohol wipes and sample holders for filled capillaries. The kit is designed to match a 2-3 hour collection period by one sampler.

Personal and contact information is first entered into the collection card. The card has a printed barcode which is matched to the barcode etched on a heparinized PVC capillary (Fig. 2b). The advantage of plastic capillary tubes is that they are safer to handle than glass and are easily laser etched, allowing bar-coding and rapid cutting, both of which are required for use in the RABiT.

A single drop of blood (~30µl) is drawn, using a disposable lancet, into the capillary. To refine the requirements for the collection kit a variety of lancets were tested, offering a wide range of blade depths and needle gauges to optimize blood flow with minimal pain. Microtainer® Contact-Activated Genie™ Lancets (BD Diagnostic Systems, Franklin Lakes, NJ) have proven to be the most reliable in providing on average a 50µl drop of blood and in all cases more than the required 30µl.

The blood-filled capillaries (Fig. 3a) are then loaded into centrifuge inserts (Fig. 3b) that are prefilled with sealing putty (Fisherbrand Hemato-Seal Capillary Tube Sealant, Fisher Scientific) and separation medium (Histopaque-1083, Sigma Aldrich). As the blood in the capillary does not reach its edge, an air bubble is trapped between the blood and separation medium, preventing their mixing during shipping (up to 24 hours) (Fig. 3c). In addition the sealing putty is compressed into and around the capillary ensuring a seal and requiring 0.2-0.8 N of force to extract the capillary from the holder.

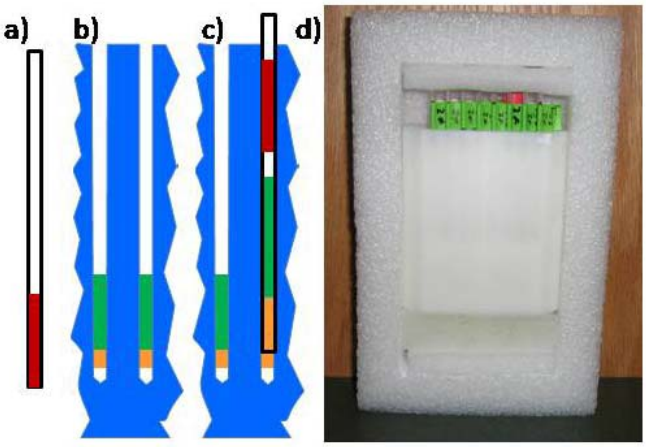


**Fig. 3.** Scheme of the sample collection. **a)** Blood in a capillary. **b)** sample holder with sealing putty (orange) and separation medium(green). **c)** capillary loaded into sample holder. **d)** samples packaged for shipping.

As the bottom of the capillary is sealed, the blood and separation medium cannot leak out of the capillary even if it is inverted and shaken.

The top of the capillaries is then sealed with a foam rubber mat, to prevent contamination of the samples, as shown in Figure 3d.

This allows the sample to be collected by an individual with minimal training, while maintaining the required layering of the blood and separation medium and preventing contaminations.

**Testing**

The In initial field tests, 40 blood samples were collected at Arizona State University, loaded into the capillary holders and shipped to Columbia University in the city of New York, using a commercial carrier. All capillaries arrived without spillage (Fig. 4a) and without disruption of the blood and lymphocyte separation medium layering (Fig. 4b). The lymphocytes were then separated by centrifugation and successfully cultured to division (Turner et al., below). ■


**Fig. 2.** (**a**) sample collection kit, (**b**) close-up of bar-coded capillary.

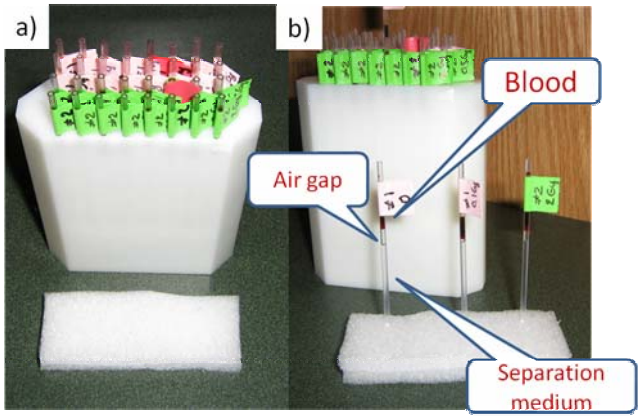


**Fig. 4.** (**a**) Samples from ASU. Note that there are no red stains on the foam rubber mat that sealed the top of the capillaries during shipping. (**b**) Individual capillaries showing the required layering of blood and separation medium.

# Adaptation of MN and γ-H2AX Assays For Automated Processing

*Helen C. Turner, Guy Garty, Oleksandra V. Lyulko, Antonella Bertucci, Julia Schäfer, Gerhard Randers-Pehrson and David J. Brenner*

As part of the development of our high-throughput, robotically-based biodosimetry workstation, RABIT (Rapid Automated Biodosimetry Tool),[1, 2] we have adapted established protocols for the cytokinesis-block micronucleus[3, 4] (CBMN) and γ-H2AX[5, 6] biological assay for use in 96 multi-well format. Both assays, as implemented manually, are in current use in radiation biodosimetry, and are highly radiation-specific.[7-9]

The γ-H2AX assay measures DNA damage directly by immune-staining the phosphorylated H2AX histone which localizes to DNA double strand breaks (DSBs). The yield of DSBs can be quantified either by counting foci or integrating the fluorescent intensity. The micronucleus assay quantifies long term chromosome damage expressed as post-mitotic micronuclei. Lymphocytes are cultured to division but cytokinesis is blocked, preventing separation of the two new cells. Healthy lymphocytes form binucleate cells, while those with chromosome damage form an additional micronucleus containing chromosomal fragments. The advantages and disadvantages of both assays as well as our concept of use are detailed in Figure 1. For the first 36 hours following the radiation event, all samples arriving at the RABIT will be analyzed using the γ-H2AX assay. At 36 h the RABIT is taken offline for up to 1 hour, in order to change reagents, so that all subsequent samples will be analyzed using the micronucleus assay, which takes approximately 70 hours. This concept provides for the maximal number of samples to be processed using the faster γ-H2AX assay.

**Blood sample collection and cell harvesting**

In response to a large scale radiological event, 30µl fingerstick of blood samples will be collected in heparin-coated capilliaries using contact-activated lancets at specific collection sites and transported to the RABIT for screening. In collaboration with Frederic Zenhausern's group at Arizona State University (ASU), we received 30 µl of irradiated blood samples that had been transported in heparin capillaries from ASU to our lab at Columbia University, NY. The presence of an air bubble incorporated between the lymphocyte separation media and blood sample served to prevent the blood from mixing with the separation medium during transport. Specific details regarding sample collection for high throughput radiation biodosimetry are described by Garty et al., 2008 annual report. In the present study, peripheral whole blood (2ml) was collected by venipuncture from healthy donors and irradiated ex vivo with γ-rays (0.5, 2 and 4 Gy). For lymphocyte isolation, 30µl blood samples were pipetted into heparin-coated PVC capilliaries (Safe-T-Fill capilliaries; RAM Scientific) containing 50µl lymphocyte separation media (Histopaque-1083; Invitrogen) and spun at 4000 rpm for ~ 5 minutes. The separated lymphocyte bands were released into filter-bottomed multi-well plates (HTS Solubility Filter Plates with polycarbonate membranes; pore size, 0.4µm; Millipore).

**γ-H2AX foci detection in isolated lymphocytes**

A crucial step for the development of both the γ-H2AX and MN assay for high throughput was to ensure that the centrifugation step and subsequent release of the lymphocyte band into the multi-well plate, showed the following: (i) adequate lymphocyte dispersal, (ii) sufficient lymphocyte number to perform the assay and, (iii) healthy looking lymphocytes. To do this, we collected blood samples of varying volumes (10 to 50 µl) from six different donors. The isolated lymphocytes were washed twice with Hanks Balanced Salt Solution (HBSS) to remove traces of separation media and blood plasma and fixed with ice-cold methanol for 10 min. The nuclei were stained with DAPI (DAPI dilactate, 4000ng/ml; Invitrogen) for 10 min followed by five washes with phosphate buffered saline (PBS). Next, the underdrain of the multi-well plate was removed and the membrane patted dry with a paper towel. To generate compact, sealed archival specimens, the filter bottoms are detached from the multi-well plate, transferred to an adhesive surface and sealed using a transparent adhesive film to keep them intact. We have tested several commercially available adhesive and lamination films for clarity and low autofluorescence. Clear View packing tape (Staples) or acetate plate sealing tape (Corning) were found to be optimal to detect fluorescent images. Once the filter bottoms are attached and sealed, the continuous film containing the filter bottoms is directed to the imaging system and, after imaging, collected on a roll for archiving. The fluorescence images presented here were

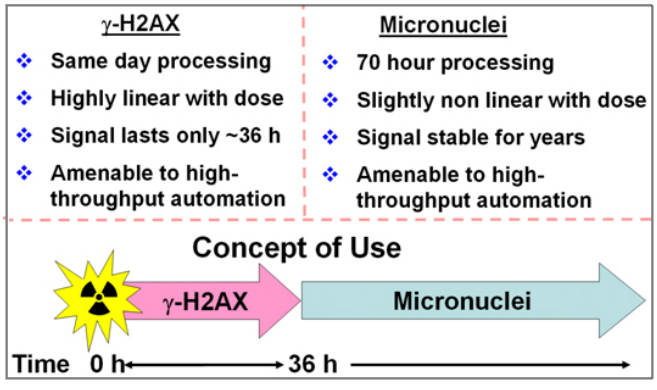


**Fig. 1.** RABIT concept of use.

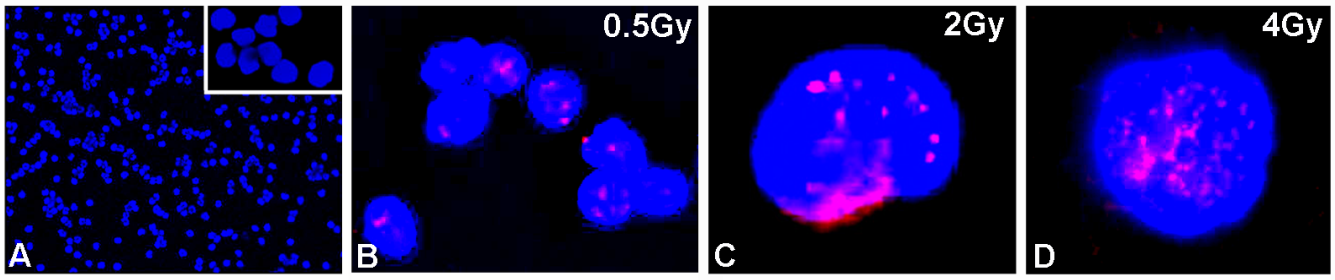


**Fig. 2. Formation of γ-H2AX foci in human lymphocytes.** Panel **A** shows the dispersal and integrity of the lymphocytes on the filter membrane. Panels **B**, **C** and **D** show the presence of γ-H2AX foci in lymphocytes irradiated with 0.5, 2 and 4 Gy, respectively; visualized with Alexa Fluor 555 and counterstained with DAPI.

captured using a Zeiss Axioplan-2 fluorescence microscope and stored using custom software.

Figure 1 demonstrates that the protocol and conditions that we have developed so far result in adequate dispersal of the lymphocyte pellet (Panel A) on the polycarbonate filter membrane. Magnification of the lymphocytes (Panel A, insert) confirmed that the lymphocytes appeared healthy. Although we found that the isolation of lymphocytes from ~30µl of whole blood yields a wide range of lymphocyte counts between blood donors, we found that this volume of blood produced a suitable spread on the filter membrane for all donors tested. For the immunodetection of γ-H2AX, fixed lymphocytes were blocked with 2% BSA for 30 min and incubated with an anti-human γ-H2AX monoclonal antibody (dilution 1:800; Abcam) for 30 min. After five, 2 min washes with PBS, the cells were labeled with an Alexa 555 secondary antibody (dilution 1:800; Invitrogen) for 30 min. The nuclei were counterstained with DAPI. Figure 2, Panels B-D show the effect of γ-rays (0.5, 2 and 4 Gy) on γ-H2AX foci formation in human peripheral lymphocytes. Lymphocytes were isolated and fixed 2 hours following irradiation. The results show that there is a good nuclei to foci contrast and resolution such that we are able to detect a dose-response in foci formation.

**Analysis of MN formation *in situ***

The irradiated blood samples received from ASU were procured for the MN assay. The capilliaries were spun at 4000 rpm for 5 min and released into the multi-wells. Following two washes with HBSS, the lymphocytes were cultured in 100µl RPMI1640 culture medium containing L-glutamine, 10% fetal calf serum, 1.5% Pen/Strep and phytohemagglutin (PHA; 20µg/ml) and incubated at 37ºC, 5% CO2. After 44 h, the culture medium was replaced with fresh complete medium containing cytochalasin B (6.0µg/ml) and incubated for a further 28 h. After two washes with PBS, the cells were fixed with ice cold methanol for 10 min and labeled with DAPI dilactate (4000 ng/ml). The results show that lymphocytes remained viable following their trip to New York as determined by their response to PHA stimulation (Fig. 3; Panel A) The presence of MN formation was detected in samples irradiated with 2Gy (Fig. 3; Panel B). The DAPI-labeled nuclei show good contrast on the polycarbonate filter membrane, such that we were able to manually score nearly 200 binucleated cells in one micro-well.[10] Statistically, our goal is to be able to reproducibly score 250 binucleates in each well since this will give us a 95 % confidence interval of ±20% at 1Gy.

The RABIT imaging system uses multiple CMOS cameras sensitive to the colors of different fluorophores. This allows for the simultaneous imaging of the nuclei using DAPI and γ-H2AX foci exploying Alexa Fluor 555. To optimize the staining protocol to detect binucleated cells and MN, we found that a combination of the nuclear stain DAPI and cytoplasmic stain, CellMaskTM Orange solution (5µg/ml; for 5 min) showed the most uniform staining across the cell and the sharpest image of nuclear and cell boundaries on the polycarbonate membrane (Fig. 3, Panels C-E). Down the line, the use of equivalent illumination and filters will allow us to switch the RABIT operating system from γ-H2AX to CBMN within an hour.

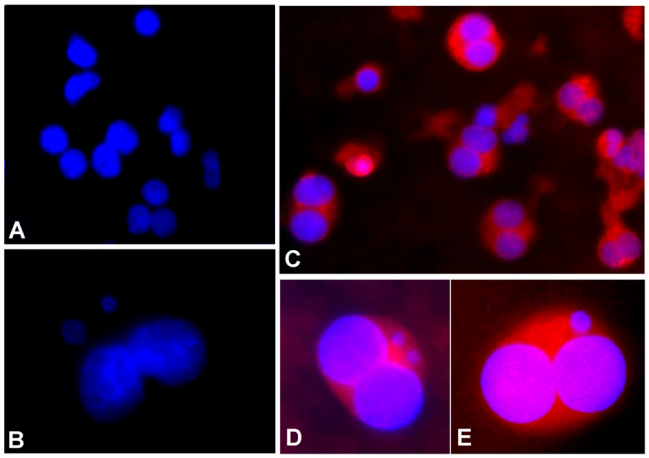


**Fig. 3. Detection of MN in human lymphocytes.** Example of DAPI stained binucleated cells formed following cytokinesis-block (Panel **A**) and the detection of MN following irradiation with 2Gy (Panel **B**). Detection of dual staining with DAPI and CellMask™ Orange; cells irradiated with 0Gy (Panel **C**) and 2Gy (Panels **D**, **E**), respectively.

**Summary**

The RABIT is a fully automated, ultra-high throughput biodosimetry system, based on robotic sample handling and high speed imaging systems, that will reliably screen blood samples (from a single drop of blood), to estimate individual past radiation exposures. In this report, we have progressed towards the optimization of two standard biodosimetric assays, γ-H2AX and micronucleus for *in situ* analysis in multi-well plates.

**References**

1. Garty G, Chen Y, Salerno A, Turner H, Zhang J, Lyulko OV, Xu Y, Wang H, Simaan N, Randers-Pehrson G, *et al*. The RABIT: A Rapid Automated Biodosimetry Tool for radiological triage. *Health Physics* (In Press 2009).
2. Salerno A, Zhang J, Bhatla A, Lyulko OV, Nie J, Dutta A, Garty G, Simaan N, Randers-Pehrson G, Yao YL and Brenner DJ. Design Considerations for a Minimally Invasive High-Throughput Automation System for Radiation Biodosimetry. In IEEE International Conference on Automation Science and Engineering, 2007. CASE 2007. 846-52.
3. Fenech M. Cytokinesis-block micronucleus cytome assay. *Nat Protoc* **2**:1084-104, 2007.
4. Fenech M, Chang WP, Kirsch-Volders M, Holland N, Bonassi S and Zeiger E. HUMN project: detailed description of the scoring criteria for the cytokinesis-block micronucleus assay using isolated human lymphocyte cultures. *Mutat Res* **534**:65-75, 2003.
5. Nakamura A, Sedelnikova OA, Redon C, Pilch DR, Sinogeeva NI, Shroff R, Lichten M and Bonner WM. Techniques for gamma-H2AX detection. *Methods Enzymol* **409**:236-50, 2006.
6. Bonner WM, Redon CE, Dickey JS, Nakamura AJ, Sedelnikova OA, Solier S and Pommier Y. GammaH2AX and cancer. *Nat Rev Cancer* **8**:957-67, 2008.
7. IAEA. Cytogenetic analysis for radiation dose assessment: A manual, (International Atomic Energy Agency, Vienna, 2001).
8. Fenech M, Perepetskaya G and Mikhalevich L. A more comprehensive application of the micronucleus technique for biomonitoring of genetic damage rates in human populations--experiences from the Chernobyl catastrophe. *Environ Mol Mutagen* **30**:112-8, 1997.
9. Rothkamm K, Balroop S, Shekhdar J, Fernie P and Goh V. Leukocyte DNA damage after multi-detector row CT: a quantitative biomarker of low-level radiation exposure. *Radiology* **242**:244-51, 2007.
10. Lyulko OV, Turner H, Garty G, Randers-Pehrson G and Brenner DJ. Optimization of Lymphocyte Imaging in Filter Bottomed Plates. *CRR Annual Report* 95-6, 2007. ■


# High-Throughput Image Acquisition and Analysis for Rapid Automated Biodosimetry Tool

*Oleksandra V. Lyulko, Guy Garty, Helen C. Turner, Gerhard Randers-Pehrson and David J. Brenner*

In the context of a large-scale radiological event, we are developing a high-throughput cell imaging system that is exclusively dedicated to quantifying the amount of DNA damage using a fingerstick of whole blood. The Rapid Automated Biodosimetry Tool (RABIT) utilizes two well-characterized biodosimetric assays: γ-H2AX and Micronucleus assay.[1-3] Adaptation of these assays to use in the RABIT is described in reference 4. The present report focuses on the micronucleus assay.

## Imaging Module

Despite much current focus on high-throughput, high-content imaging systems,[5] there is, in fact, no commercial system fast enough with adequate spatial resolution to allow the throughput necessary for the RABIT system. The RABIT imaging system (Fig. 1) incorporates three novel techniques for accelerating the imaging: (i) use of light steering rather than sample motion, (ii) single-step auto-focusing and, (iii) parallel use of multiple high-speed cameras. Using these techniques an imaging time of significantly less than 10 seconds per sample can be achieved.

**(i) Light Steering.** In order to obtain sufficient statistics, more than one hundred 200-μm frames (fields of view) need to be imaged for each sample. Typically, imaging different frames within the same sample is achieved by mechanically moving a stage carrying the samples. However, mechanical motion takes tens of milliseconds per motion, which is too slow. Instead of moving the sample, in the RABIT light is steered into the camera using fast galvanometric mirrors (HurryScan II, ScanLab America, IL). Typical transit times

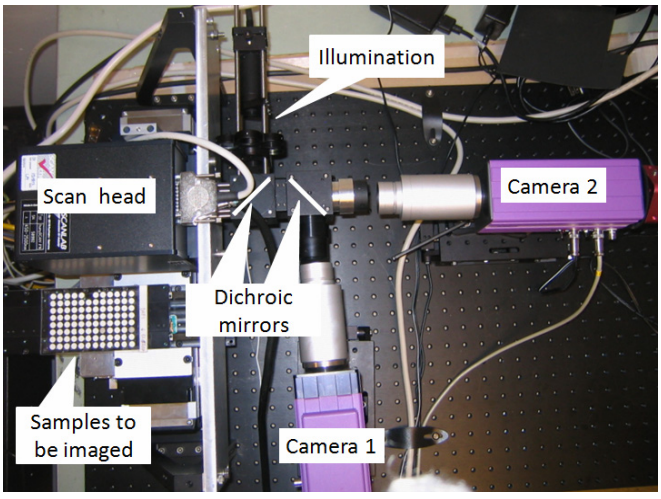


**Fig. 1.** Prototype RABIT imaging system.

between adjacent fields of view are less than 1 msec.

**(ii) One-step focusing** is performed by incorporating an astigmatic element (a cylindrical lens) into one component of the optics. This results in a known focus-dependent distortion. For example, a spherical bead is imaged as an ellipse, and the aspect ratio of the ellipse indicates exactly how far the sample is out of focus. Based on this information from a single image, the objective, mounted on a piezoelectric actuator (Mad City Labs, WI), can be moved, allowing one-step (rather than iterative) focusing.

**(iii) The simultaneous use of multiple CMOS cameras** allows for simultaneous acquisition of separate images of either cytoplasm (stained with Cell Mask Orange) and the nucleus (stained with DAPI) or the nucleus and γ-H2AX foci (stained with Alexa fluor 555), as well as focus information. The RABIT uses three CMOS Photonfocus MV-1024D-160E cameras (Upstate Technical, NY). These cameras allow a continuous frame rate of 150 frames per second. Each camera is mounted on a VS-1485 image intensifier (Videoscope International, VA).

The imaging module of RABIT grabs multiple pairs of images (nuclei/cytoplasm) and transfers them to the analysis software. Acquisition is stopped when sufficient statistics (nominally 250 cells) are collected.

**Image Analysis and Micronuclei Scoring**

The RABIT micronuclei-scoring software is implemented in C, using the Matrox Imaging Library.

The scoring algorithm is based on the protocol for the cytokinesis-block micronucleus (CBMN) assay developed by Michael Fenech.[1, 2] The frequency of micronuclei (MNi) occurrence in once-divided binucleated (BN) cells is scored as a biomarker of DNA damage events.

The two images, corresponding to nuclei and cytoplasm, are first subject to background correction, followed by noise removal and binarization (Fig. 2). The threshold for the binarization may be either determined automatically from the image histogram or set by a user. Touching nuclei are then separated. Cell areas are determined from the cytoplasm image and the objects that are too small to be counted as cells are eliminated from the analysis.

**Selecting viable cells**

The micronucleus assay requires that only viable BN cells are scored. Such cells should have intact cytoplasm and be approximately circular in shape. To select cells according to this criterion, we measure the compactness parameter. The compactness describes how close the shape of an object is to a circle and is higher for more convoluted shapes. It is

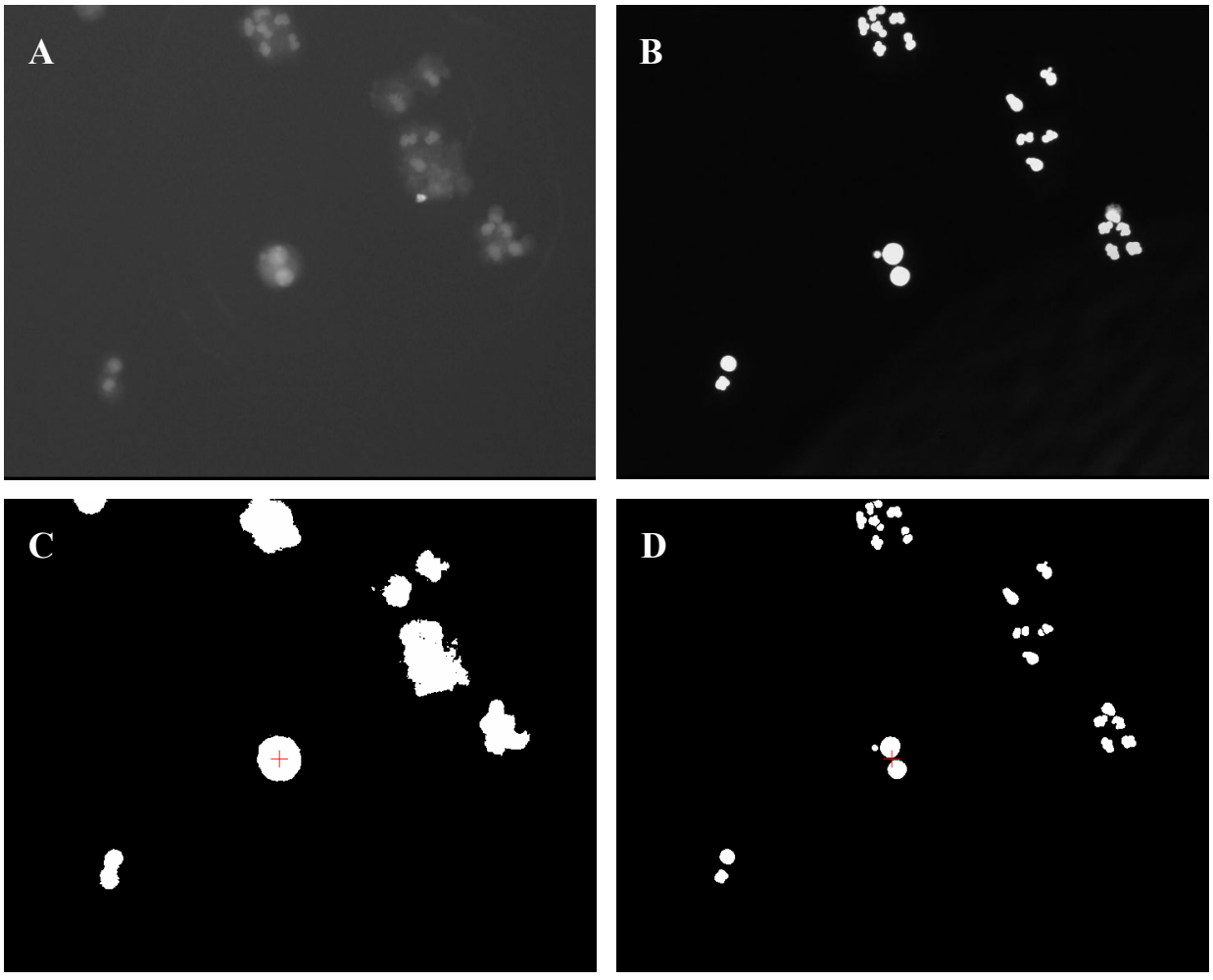


**Fig. 2.** Example of the image analysis: **A**. cytoplasm, **B**. nuclei of the same cells, **C**. binarized image of cytoplasm with an intact binucleated cell marked for analysis and **D**. the corresponding binarized image of the nuclei with the nuclei of the same cell marked.

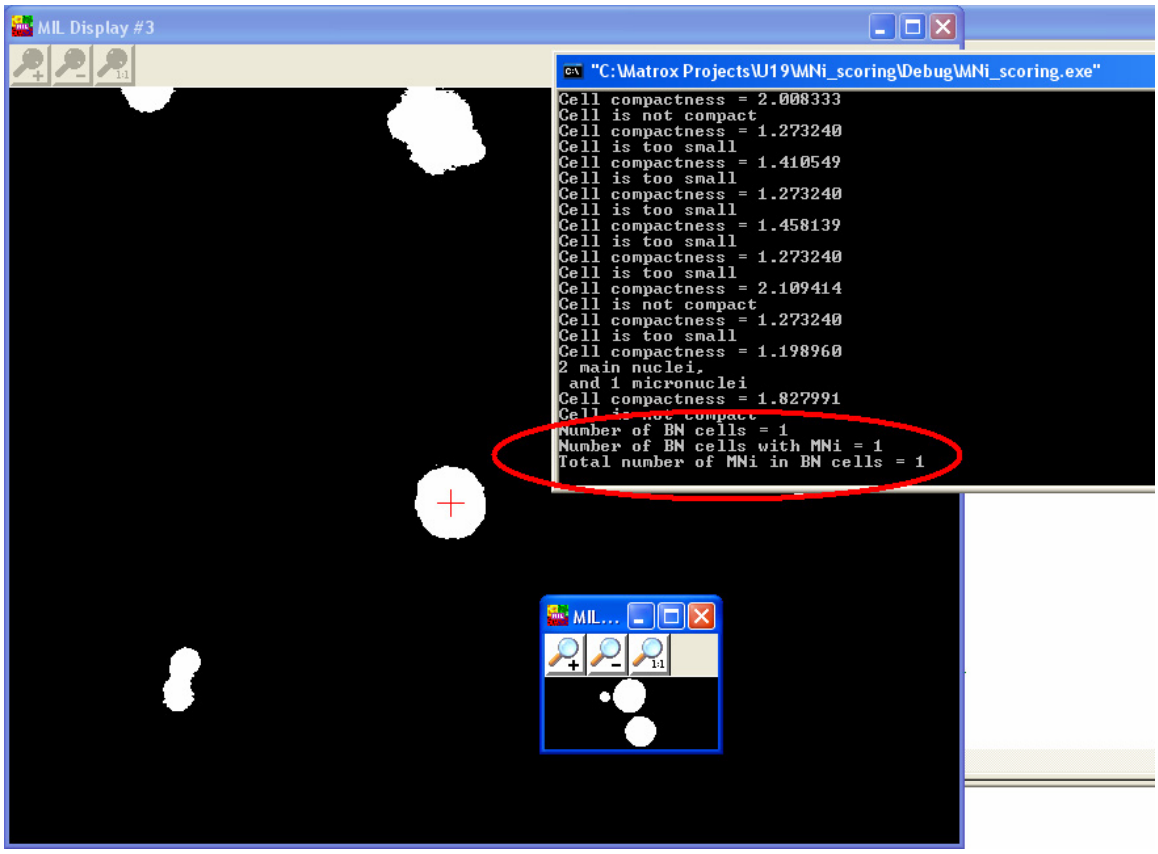


**Fig. 3.** Example of MNi scoring output: one binucleated cell found with one micronucleus. The nuclei of the binucleated cell are displayed in the separate window and the user's output is circled in red.

equal to $P^2/(4\pi A)$, where $p$ is the perimeter and $A$ is the area. The cells that are not circular enough (e.g. apoptotic cells) are eliminated. The acceptable compactness level can be set by the user.

This method for selecting viable cells proved to be reliable (Fig. 3).

**Identifying and scoring micronuclei**

The area of MNi in binucleated human lymphocytes varies between 1/256$^{th}$ and 1/9$^{th}$ of the area of the main nuclei.[2] The analysis of the binucleated cells either on glass slides or on polycarbonate membranes lining the multi-well plates showed that the cell and the nuclei sizes may differ not only between the samples (i.e. between different individuals), but also within a single frame. This variability is high enough so that the criterion described above could only be applied if each nucleus is compared to the nuclei of the same cell. This requires each cell to be analyzed individually and the analysis to be restricted only to the nuclei of this cell.

After identifying which nuclei in the DAPI image belong to a particular cell in the cytoplasm image, these nuclei are compared by size and divided into two categories: main nuclei and micronuclei. If the cell appears to be binucleated, the information about the presence and number of micronuclei is stored and the analysis continues on the next cell. The information about number of binucleated cells and frequency of MNi is then presented to the user.

Initial tests showed correlation between automatic and hand scoring. The samples featured on the images and used in the performance tests were prepared as described in reference 4.

**References**

1. Nakamura A, Sedelnikova OA, Redon C, Pilch DR, Sinogeeva NI, Shroff R, Lichten M and Bonner WM. Techniques for gamma-H2AX detection. *Methods Enzymol* **409**:236-50, 2006.
2. Fenech M. Cytokinesis-block micronucleus cytome assay. *Nat Protoc* **2**:1084-104, 2007.
3. Fenech M, Chang WP, Kirsch-Volders M, Holland N, Bonassi S and Zeiger E. HUMN project: detailed description of the scoring criteria for the cytokinesis-block micronucleus assay using isolated human lymphocyte cultures. *Mutat Res* **534**:65-75, 2003.
4. Turner H, Garty G, Lyulko OV, Bertucci A, Schäfer J, Randers-Pehrson G and Brenner DJ. Adaptation of MN and γ-H2AX Assays For Automated Processing. *CRR Annual Report* 90-2, 2008.
5. Gough AH and Johnston PA. Requirements, features, and performance of high content screening platforms. *Methods Mol Biol* **356**:41-61, 2007. ■

# Immunoassays to Detect Paracrine Signaling Molecules Induced by Radiation Exposure: Developing an *in vivo* Proof of Principle Animal Model

*Michael A. Partridge*

After a radiological "dirty bomb" incident in a major metropolitan center, substantial numbers of people may be exposed to radiation. However, only a fraction of those individuals will need urgent medical attention. Consequently, a rapid screening test is needed to identify those people who require immediate treatment. Antibody-based assays are well suited to high-throughput diagnostic applications because they are non-toxic, inexpensive and can be adapted to a rapid, automated 96- or 384-well plate format. There are a number of biological markers that are indicators of radiation exposure, one of which is the induction of a paracrine response categorized by expression of cytokines, their receptors and downstream cell adhesion molecules. Highly specific antibodies are commercially available for a number cytokines and we wanted to systematically screen a range of cytokines using a variety of cultured cells to identify potential biomarkers of radiation exposure that could then be applied to an in vivo animal model.

Although the published record regarding changes in cytokine levels after radiation exposure was substantial there were two major problems with these findings. First, data obtained from in vitro experiments and animal studies were hampered by inconsistency of dose, time and method of analysis, experimental format as well other important factors such as reproducibility. Second, the substantial body of literature on cytokine response to radiation obtained from studies of radiotherapy patients is not directly applicable. In the context of radiation biodosimetry this clinical data suffers from two systemic drawbacks: A) radiotherapy patients are almost always exposed to partial body doses; B) cytokine secretion in tumor tissues is known to be dramatically different from normal cells. A number of groups have investigated cytokine response to radiation in animal models. However, these observations were made with tissues that could only be acquired using an invasive biopsy which would not be suitable for a high-throughput screen in a human population. As a result, we wanted to determine whether ELISAs can detect radiation-induced changes in protein levels in samples from animals that can be obtained using minimally-invasive techniques.

In our initial screen we analyzed 10 normal human cell lines for hanges in the level of a dozen cytokine signaling molecules after irradiation. One molecule, interleukin 6 (IL6), was consistently increased in a dose dependent manner in numerous cell lines after radiation exposure, and hence we examined this candidate biomarker in an animal model after irradiation. We wanted to use samples obtained from mice that could, in humans, be obtained using minimally invasive techniques, such as a blood from finger prick.

To accomplish this, female mice were irradiated with 5Gy X-rays and, six hours later, blood was obtained and serum analyzed from these mice for an increase in IL6 levels. The results from these experiments clearly showed that IL6 levels in irradiated mice were all higher than the levels in the control animals. Collectively, the average IL6 levels were 16-fold greater in the serum of irradiated group of mice compared to controls.

This quite dramatic result prompted us to re-screen some of the antigens that showed modest (but not statistically significant) changes in level after irradiation of cultured cells, or that were prominent cytokines important in cell signaling or tumorigenesis. Using serum from irradiated mice we tested for changes in the levels of five other cytokines, IL1α, IL1β, TNFα, TGFβ and ICAM. Interestingly, after irradiation serum levels of three of these cytokines (IL1β, TNFα, TGFβ) showed substantial changes compared to controls (although IL1β just escaped statistical significance).

Having identified at least four cytokines that displayed a clear change in serum levels after irradiation with 5 Gy, we wanted to determine whether these changes could be observed at lower doses. Three groups, of mice, were γ-irradiated with 0, 2 and 5 Gy and serum was analyzed for changes in the level of IL6, IL1β, TGFβ and TNFα. Significant changes were observed in serum levels of IL6, and TGFβ even at doses as low as 2Gy. Average IL1β serum-levels were increased after 2Gy irradiation, but only at 5Gy was the increase over controls statistically significant. Importantly, average levels of IL6 in serum from irradiated mice increased in a dose responsive manner from 2 to 5 Gy.

There are a number of variables that may affect the level of discrimination in immunoassays. By changing the concentration of the secondary and tertiary reagents, we were able to improve the level of discrimination between irradiated and control cell cultures by much as 25% (not shown). This is important because there is a direct relationship between maximizing the performance of the assay and lowering the threshold for detection of exposure. Furthermore, it indicates that by incorporating straightforward optimization strategies we may be able to detect changes in cytokine levels at doses below 2Gy.

One complication with assaying protein markers indicative of a radiation-induced cytokine response is that other stimuli can induce a similar reaction, such as acute infection and physical or chemotoxic trauma. However, it is important to note that other potential markers of radiation exposure, such as induction of micronuclei and the phosphorylation of

H2AX, are also induced by environmental stressors other than radiation. This highlights an important aspect of developing markers of radiation exposure; multiple biomarkers will likely be needed to unambiguously identify any exposed individuals. Given that terrorists would likely target a busy metropolitan area, the vast majority of potential victims would be healthy individuals engaged in typical daily activities and hence would not otherwise exhibit upregulated cytokine levels. As a result, evidence of an elevated cytokine response would strongly suggest the individual had been irradiated, and this could provide an initial marker of exposure to identify individuals that require further testing.

As mentioned, there are a number of potential biomarkers of radiation exposure. In fact, excellent radiation-specific methodologies for accurate dose assessment, such as the measurement of dicentric chromosomes, have existed for decades. However, these techniques are not well suited for use in the event of radiological terrorist incident because they are neither rapid (>48 hours to begin analysis) nor high-throughput (scores of samples per experimenter/day), and the analysis requires well-trained personnel. In contrast, immunoassays take only a few hours from sampling to final results, can be fully automated to process tens of thousands of samples at a time and provides simple numerical readouts that require little technical analysis.

Another advantage of immunoassays is that they can be used in different formats. The immunochromatography format is widely used in situations where the user is untrained, such as the home pregnancy test. It may be possible to adapt reagents identified in this study that discriminate between samples in the ELISA for use in an immunochromatography format, which could be particularly valuable for first responders to quickly identify individuals who require immediate medical attention. Another alternative is to combine multiple probes (IL6 and TGFβ, for example) in the same ELISA assay. Potentially, a suite of antibodies labeled with different fluorophores could simultaneously detect different antigens in the same assay, likely improving the level of sensitivity. Both these potential outcomes are routinely used elsewhere and the technology to develop these tests is both highly advanced and accessible.

In this study we wanted to employ immunoassays to systematically investigate the change in cytokine levels in a range of normal cell lines after exposure to radiation and use the findings as a guide for detecting changes in cytokine levels from irradiated whole animals. Our findings underscore the potential for IL6 as marker for an immunoassay-based, rapid, high-throughput biodosimeter. The next stage of this work will be to assess the ability of IL6 (and other proteins) to serve as a radiation biomarker at different time points after exposure. It will then be critical to confirm efficacy of these assays in larger populations. ■

# Expression of Activated Checkpoint Kinase 2 And Histone 2AX in Exfoliative Oral Cells After Exposure to Ionizing Radiation

*Angela J. Yoon,[a] Jing Shen,[b] Hui-Chen Wu,[b] Christos Angelopoulos,[a] Steven R. Singer,[a] Rongzhen Chen[c] and Regina M. Santella[b]*

**Background**

An efficient screening modality is of critical importance during an accident involving radiation or in a nuclear bioterrorist event to identify those who are exposed to ionizing radiation. Such a modality should be easily applicable and also high-throughput so that a large segment of a population may be screened in the least amount of time. The aim of our study is to assess a potentially high-throughput modality that detects signature biomarkers for radiation exposure in oral cell samples. The exfoliated oral cell samples can be obtained non-invasively using a mouthwash technique and are representative of a whole body exposure to ionizing radiation. The biomarkers, γH2AX and pChk2, are DNA damage response molecules expressed in irradiated cells and can serve as signature molecules of exposure.

**Methods**

A total of 100 healthy individuals taking full mouth series (routine dental radiographic, exposure to approximately 23.4 mGy) were enrolled from the Columbia University College of Dental Medicine Oral Radiology clinic. We collected exfoliated oral epithelial cells using a mouthwash technique in which participants were asked to rigorously rinse with a commercially available mouthwash for 40 seconds and expectorate into a collecting cup. The oral cell samples were collected before and 20 minutes after the radiographs were taken. Collected oral cells were then cytospun onto glass

[a] *College of Dental Medicine, Division of Oral & Maxillofacial Pathology, Columbia University, NY*

[b] *Department of Environmental Heath Sciences, Mailman School of Public Health, Columbia University, NY*

[c] *Herbert Irving Comprehensive Cancer Center, Columbia University, NY*

slides and processed for immunohistochemical analysis. The intensity of nuclear staining for γH2AX and pChk2 were quantified and averaged from 50 randomly selected cells using a soft ware system (Becton Dickinson).

**Results**

There was a statistically significant increase in the levels of expression for γH2AX and pChk2 after the radiation exposure. The mean intensity for pChk2 before the radiation treatment was 0.114 (SD= 0.035) and after the radiation was 0.139 (SD= 0.038). For γH2AX, the mean intensity before the radiation was 0.105 (SD= 0.033) and after the radiation was 0.125 (SD=0.052). A paired t-test showed $p< 0.001$ for pChk2 and $p<0.001$ for γH2AX.

**Conclusion**

pChk2 and γH2AX are promising biomarkers and show increased expression in oral cells exposed to ionizing radiation. Based on this proof-of-concept study, in a future investigation, we can assess the time course for these biomarkers and define a dose and time range that yield the highest sensitivity. ■

# Radiation-Induced Mitochondrial DNA Damage: A Dosimeter for Radiation Exposure

*Hongning Zhou, Michael Partridge, Sarah Huang, Yu-Chin Lien and Tom K. Hei*

There is an urgent need for a rapid, high throughput screening test to identify individuals exposed to radiation in the event of a radiological "dirty bomb" incident. Radiation exposure can damage nuclear DNA (nDNA), as well as mitochondria (mtDNA), which encodes a subset of the proteins involved in the electron transport chain. It is well established that radiation increases the level of reactive oxygen species (ROS) in the cell, and DNA polymerase-γ, the polymerase responsible for the replication and repair of mtDNA, is susceptible to oxidative damage. Radiation has been shown to change the copy number of mtDNA, and induce a unique large deletion in the mtDNA sequence in a dose dependent manner. Importantly, radiation-induced deletions as well as changes in the amount of mtDNA can be detected using a PCR-based assay, a technique which can be easily automated and is therefore capable of analyzing large numbers of samples. Consequently, measuring the damage to mtDNA after radiation exposure could potentially be adapted for use as a high-throughput radiation biodosimeter.

**Hypothesis and Specific Aims:**

Hypothesis: the changes in the amount of mtDNA, or the incidence of common deletion (CD) in mtDNA, can be used as a biodosimeter to detect radiation exposure in human cells.

To answer this question, two specific aims are proposed in this pilot project. The first is to establish *in vitro* PCR amplification conditions utilizing whole cell suspensions as template to simulate protocols using cells from a mouth swab or finger prick of blood in the field, and using real-time PCR, to detect the changes in mtDNA-nDNA ratio and/or common deletion >24 hours after radiation exposure. The second is to establish whole animal models for detecting, by real-time PCR, radiation-induced changes in mtDNA copy number or in common deletion incidence.

**Research Methods and Results:**

Our first goal was to establish that whole cell suspensions could be used as a template in the PCR reaction without employing time-consuming DNA extraction protocols. As indicated before, the fragment can be amplified from the D-loop region even when as few as 10 cells were added to the PCR as template.

Next we determined whether we could detect changes in the incidence of CD after irradiation of human cell cultures using real time PCR. First, we established standards using mtDNA from a patient homoplasmic for CD and serially diluted this with wild type mtDNA. Figure 1 shows the determination of the cycle "threshold" (Ct) for the standards. Ct is the cycle number for each sample where the output fluorescence (ΔRn, a quantification of the PCR product) is identical. The CD incidences in control and irradiated samples were then calculated based on these standards.

Normal human lung fibroblasts (NHLF) were irradiated with 1, 3 and 6 Gy of γ-radiation and grown for 24 or 48

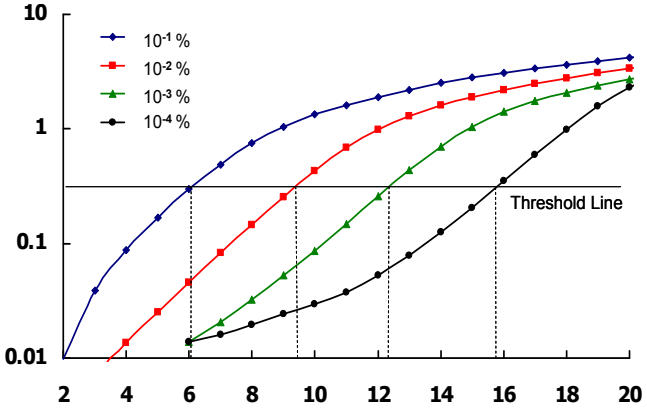


**Fig. 1.** Quantification of human mtDNA common deletion in WT DNA by Real-time PCR.

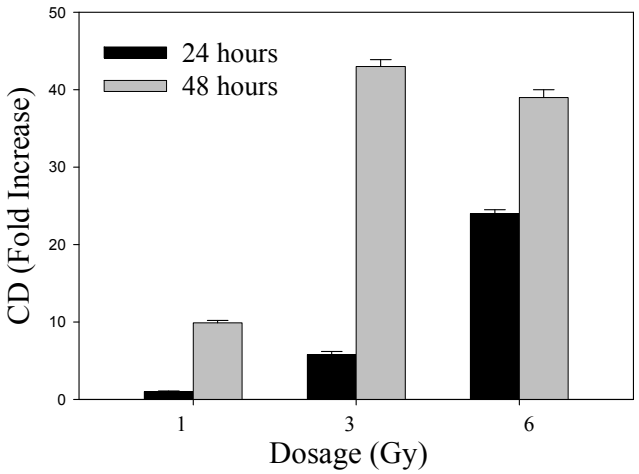


**Fig. 2.** Real-time PCR detection of a dose dependent increase in mtDNA common deletion (±SD) after γ-irradiation in NHLF.

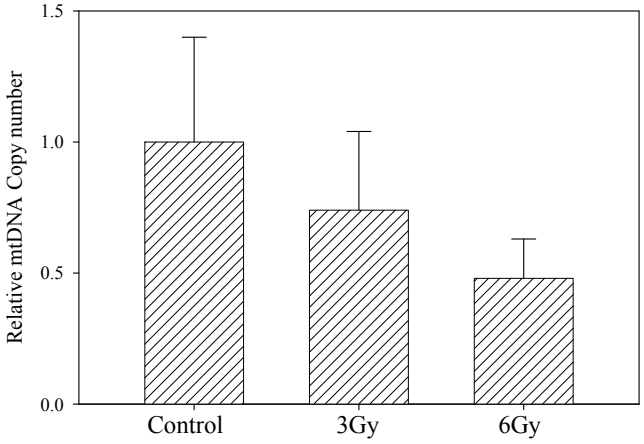


**Fig. 3.** Real-time PCR detection of changes in mtDNA-nDNA ratio (±SEM) in blood obtained from γ-irradiated mice.

hours. DNA was prepared from whole cell suspensions and the mtDNA amount in each sample was normalized. The incidences of CD were then quantified by real-time PCR using identical amounts of template. As shown in Figure 2, a clear dose-response effect was detected in cells 24 hours after radiation exposure. Furthermore, after 48 hours, γ-irradiation induced a ~43 fold increase in the common deletion in human fibroblasts after exposure to 3Gy. Importantly, even at doses as low as 1Gy, a 10-fold increase in the CD incidence was detected after 48-hours. This is important as it is highly likely that individuals will request screening two or more days after a terrorist incident occurs. These results suggest that in cultured cells, radiation exposure induces a dose-dependent increase in the incidence of CD, and that even at relatively modest doses, the CD could be an effective radiation dosimeter.

The estimated LD50 (50% lethal dose) for radiation exposure in humans is between 3-4 Gy. However, prompt medical attention, including antibiotic treatment to prevent infection, isolation, blood transfusions and, as a final resort, bone marrow transplants, can raise the LD50 to ~7 Gy. Consequently, a rapid and precise screening test to identify individuals exposed to between1-7 Gy, and thus ensure treatment is administered in a timely manner, could save a significant number of lives. Finally, in an attempt to more faithfully mimic testing biological material obtained from humans after a radiological incident, we wanted to establish whether we could use real-time PCR to detect changes in mtDNA from samples obtained from radiation exposed animals. Specifically, we wanted to determine whether we could detect alterations in mtDNA copy number in radiation exposed animals. To accomplish this, we irradiated mice and 48 hours later obtained blood**,** from which DNA was extracted by light alkali treatment as described for cultured cells. Figure 3 shows real-time PCR analysis of the ratio of mtDNA-nDNA in blood from animals irradiated with 3 and 6 Gy compared to controls. After 48 hours, the mtDNA copy number decreased in exposed cells in a does-dependent manner. Importantly, this result demonstrates that real-time PCR can effectively be used to detect changes in biological samples obtained from whole animals, in addition to cell culture samples.

Results from this study demonstrate that the changes in the amount of mtDNA, or the incidence of common deletion (CD) in mtDNA, can be used as a potential biodosimeter after radiation exposure. ■

# Remodeling of Interphase Chromosome Domains In Response to Radiation Damage

*Michael N. Cornforth*[a]

**Hypothesis and Specific Aims**

Chromosomes (which normally are visible as such only at mitosis) exist as semi-compact globular structures (domains) during interphase. Our overall proposal is based on a published report the radiation-induced translocations – again, normally visible only at mitosis, several hours/days after irradiation – could be visualized during interphase almost immediately after exposure via a "splitting" of individual domains. This approach potentially allows for a relatively non invasive method of detecting dose-dependent rearrangements in cells exposed to radiation. Specific Aims follow.

**Aim 1**. Several parameters likely to affect the visualization/quantitation of domain disruption will be examined in association with a single fixed dose of $^{137}$Cs gamma rays. For this aim we plan to use two experimental cell systems, cultured human fibroblasts, and later, lymphocytes from venous blood. Considerable effort will be spent investigating the best way to obtain reproducible high-quality images of interphase chromosome domains in fibroblasts and lymphocytes. These include the optimum cell fixative and the type and tonicity of the buffer used to swell nuclei, factors known to affect the quality of preparations (J.R.K. Savage, personal communication). We will explore the use of Calyculin A (e.g., in conjunction with p34$^{cdc2}$/cyclin B kinase and ATP) to augment the visualization of domains, particularly in unstimulated lymphocytes. With fibroblasts, we will look at differences in cultures that are fixed while attached to glass coverslips, as compared to those fixed following trypsinization. For lymphocytes, we will determine whether PHA-stimulation of $G_1$ cells improves the quality/ reproducibility of preparations. Ideally, conventional 2D fluorescence microscopy will be adequate to quantify domain remodeling, but we will investigate the use of image deconvolution (3D image reconstruction) to see whether the added resolution this approach brings to mapping the topology of chromosome domains is justified in terms of the additional cost and turnaround time this procedure would entail under a high throughput scenario. We predict that $G_0/G_1$ stages of the cell cycle will provide the best opportunity to visualize interphase chromosome domains, but plan to examine briefly S phase cells as well. Once the above parameters are optimized, we will develop objective criteria for scoring domains, and then ascertain the time course for the development of domain remodeling/splitting for up to a few days following a single fixed dose. The parameters under consideration include:

a. optimum methods of specimen preparation;
b. phase(s) of the cell cycle in which domains are suitable for scoring;
c. time course for the development of domain disruption;
d. the potential use of confocal or deconvolution imaging techniques;
e. substrate attachment status (fibroblasts);
f. PHA-stimulated blast formation (lymphocytes);
g. objective criteria for identifying disrupted domains.

**Aim 2**. Following optimization of the above parameters, more detailed dose responses will be constructed for both cell types following exposures to gamma rays ranging from 1 to 10 Gy. Such dose responses will be examined for the purposes of determining the:

a. sensitivity of the system;
b. inter-experimental variation;
c. inter-individual variation;
d. dose dependency of the time course for the development of domain disruption;
e. correlation between the frequency of disrupted domains and that of rearrangements in metaphase cells receiving the same dose.

**Aim 3**. Modifications to the system will be implemented to make it more amenable to realistic situations of biodosimetric triage, including:

a. smaller blood samples; finger-stick instead of venous puncture;
b. automatic image thresholding and pixel classification.

**Aim 4**. Consistent with the overall objectives of the HTMIB program, we plan to investigate the use of premature chromosome condensation (PCC) as a method of observing mitotic-like chromosomes in interphase cells.

**Research Methods**

Following either fixed or graded doses of gamma rays, cells from *in vitro* cultures will be either fixed immediately, or returned to a cell culture incubator and thereafter fixed at regular intervals postirradiation. After fixation interphase cells will be subjected to fluorescence (FISH) whole chromosome painting probes for the largest chromosomes (e.g., chromosomes 1,2,3,4) since they are more likely to receive the radiogenic breakage required to produce chromosome interchanges, as compared to smaller chromosomes. Cells will be visualized by fluorescence microscopy to determine the number of apparent painted chromosome "domains". Portions of Aim 1 provide additional detail. More specifi-

[a] *Department of Radiation Oncology, The University of Texas Medical Branch, Galveston, TX*

cally, and in the context of overall aims we plan, if funded for a continuation, to do the following:

1. Continue to experiment with other postirradiation treatment parameters in order to increase the resolution of the system, this time focusing effort on the effects of phosphatase inhibitors, in combination with $p34^{cdc2}$/cyclin B kinase and ATP, to enhance resolution of chromosome domain disruption in unstimulated peripheral lymphocytes. [We have IRB approval to work with human blood lymphocytes specifically as it relates to this grant]

2. Carry on currently stalled efforts aimed toward robotically controlled optical scanning, first concentrating on the development of algorithms for image thresholding and pixel classification for use in computer-assisted pattern recognition of interphase domains. Initial studies will employ fibroblasts; later studies to include lymphocytes.

3. Use image deconvolution and/or confocal microscopy to render 3D images of normal and radiation-disrupted interphase chromosome domains. These studies will concentrate on lymphocytes which, owing to their spherical nuclear shape, will require such an approach.

4. Use PCC, in conjunction with 24-color whole chromosome painting to study the dose and time dependence of exchange-type aberrations, such as translocations and dicentrics in unstimulated interphase (i.e., G0-phase) lymphocytes and fibroblasts. In this method, an unirradiated mitotic cell is fused with an irradiated interphase cell. This has the result of forcing the chromatin of the interphase cell into a "pseudo mitosis" allowing interphase chromosomes to be viewed more-or-less like the chromosomes of mitotic cells. We plan to use PCC, in conjunction with 24-color whole chromosome painting (mFISH), to visualize translocations and other rearrangements between different chromosomes within irradiated interphase cells; such rearrangements form within minutes to a few hours post irradiation. Our lab has years of experience with both PCC and mFISH, which we can bring to bear on the project.

**Research Results**

In our original proposal we argued, based largely on preliminary data published from the Harwell group, that radiation-induced translocations and dicentrics show a separation of interphase domains within minutes to hours following radiation exposure, while still in G1. Thus, this approach showed promise for high-throughput, minimally invasive dose reconstruction for irradiated human populations. On the basis of single color whole chromosome painting, for a single dose, and two time points, we found a time-dependent increase in the "splitting" of chromosome domains for two particular chromosomes, consistent with kinetics previously published. Subsequently, we began first steps toward assessing the feasibility of automating such an analysis. A confocal imaging system was used to assess domain separation of chromosome #1 domains in cells containing a clonal 1:5 translocation (using cells from clone F4 that are homogeneous for the 1:5 translocation; i.e. same translocation in each cell of the clone F4). From these experiments we observed the ratio of normal cells carrying the expected two domains (one from each homologue) to that of cells carrying three distinct chromosome #1 domains was about 0.5, whereas this ratio for clone F4 was about 0.8. We concluded, whereas this approach was sufficiently sensitive to distinguish between normal and translocation-bearing cells, the signal, compared to background was too low to be of practical value except for very high doses. More recently, we decided to revisit the issue of signal/noise, returning to the use of con-

**Table 1.** The effects of radiation dose and calyculin on interphase domain splitting

| Dose Radiation | Dose Calyculin | Cells Observed | Chromo. 1 Domains per Cell | Chromo. 5 Domains per Cell | Prop with ≥3 Chromo 1. Domains | Prop with ≥3 Chromo 5. Domains |
|---|---|---|---|---|---|---|
| With Calyculin | | | | | | |
| 0 Gy | 25 nM; 5 min. | 393 | 1.79 ± 0.07 | 1.78 ± 0.07 | 0.006 ± 0.004 | 0.018 ± 0.006 |
| 4 Gy | 25 nM; 5 min. | 372 | 1.86 ± 0.07 | 1.89 ± 0.07 | 0.035 ± 0.010 | 0.035 ± 0.010 |
| Without Calyculin | | | | | | |
| 0 Gy | 0 nM N/A[1] | 315 | 1.87 ± 0.08 | 1.91 ± 0.08 | 0.038 ± 0.011 | 0.051 ± 0.013 |
| 4 Gy | 0 nM 0.5 hr PI[2] | 300 | 1.86 ± 0.07 | 1.91 ± 0.08 | 0.040 ± 0.012 | 0.050 ± 0.013 |
| 4 Gy | 0 nM 4.0 hr PI | 374 | 1.86 ± 0.07 | 1.90 ± 0.07 | 0.048 ± 0.011 | 0.048 ± 0.011 |
| 4 Gy | 0 nM 6.0 hr PI | 348 | 1.95 ± 0.07 | 1.97 ± 0.08 | 0.066 ± 0.014 | 0.083 ± 0.015 |
| 8 Gy | 0 nM 4.0 hr PI | 302 | 1.85 ± 0.08 | 1.88 ± 0.08 | 0.026 ± 0.009 | 0.033 ± 0.010 |

**Note:** [1]not applicable; [2]PI refers to the number of hours post-irradiation.

ventional microscopy, in which chromosomes 1 and 5 were stained with differently colored fluorochromes. The results, for an uncloned, irradiated population of fibroblasts, are shown in the table 1, in which the time course, as well as the effect of Calyculin was used, in an attempt to further accentuate the visualization of split interphase chromosome domains following irradiation. The results appear to be somewhat encouraging as regards the overall objectives of this aim. Whereas it does appear that 25nM Calyculin did enhance significantly the signal to noise ratio (rows 1 and 2; columns 6 and 7), the remaining data do not show a clear dose or time course dependency. We will continue to experiment with other postirradiation treatment parameters in order to increase the resolution of the system, but, in the mean time we are considering shifting emphasis to the use of 24-color premature chromosome condensation as an alternative approach (Aim 4).

**Potential Products**

The "splitting" of individual domains, we propose, represents an ideal minimally invasive biodosimeter to estimate doses received by an exposed person or persons, particularly if lymphocytes could eventually serve as the target cell. Since previous studies have shown that the maximum frequency of chromosome domain splitting occurs in about 6 hours before leveling off, the analysis is, realistically, unaffected by the time interval from sample collection to analysis. In addition, such an approach would appear to lend itself to high throughput (automation), once samples are prepared. ■

# Minimally Invasive High-Throughput Radiation Biodosimetry Using a Finger Prick Blood Cytokinesis-Block Micronucleus Assay Microculture System

*Michael Fenech*[a]

**Hypothesis and specific aims**

The cytokinesis-block micronucleus Cytome (CBMN Cyt) assay is one of the most reliable and rapid methods for biological dosimetry of ionising radiation exposure.[1-3] We hypothesized that the CBMN Cyt assay could be performed using 50µl whole blood and that results with this assay for blood obtained by finger prick would be similar to those obtained for venous blood from the arm using a vacutainer.

The following report outlines our research outcomes for the development of a whole blood micro-culture system that enables at least 1000 cytokinesis-blocked binucleated lymphocytes to be transferred to a slide and scored. This entailed:

1. Development of a finger prick blood collection system.
2. Development of a whole blood CBMN microculture method.
3. Performing a pilot study to compare the CBMN assay results for the microculture method using finger prick blood obtained using a lancet versus venous blood from the arm obtained by venepuncture using a vacutainer.

**Research methods**

**1. Finger prick blood collection system for whole blood microculture protocol**

i. Hands are washed with soap and rinsed and then held under running warm tap water for 2-5 minutes to increase blood flow.
ii. The hand is held in the biohazard hood.
iii. Finger tip is swabbed with ethanol and allowed to air dry in the biohazard cabinet.
iv. Finger tip is pricked with a 1.5mm lancet close to the corner of the nail bed.
v. First blood drop is wiped away with a sterile tissue.
vi. 100 to 200µl of blood is then collected with a sterile funnel into a 1ml sterile eppendorf tube containing 10µl heparin (250IU/ml).
vii. Tube is tapped several times to ensure blood and heparin is thoroughly mixed.

**2. Whole blood CBMN Cyt microculture assay method**

The following protocol was developed so that the CBMN Cyt microculture assay could be carried out to obtain a minimum of 1000 binucleated cells from a 50µl sample of sterile finger prick blood: Finger prick blood was collected as described above. 0.5ml (500µl) whole blood microcultures were then set up in 48-flat bottom well plates with 50µl finger prick blood and 450µl RPMI medium per culture with phytohaemagglutinin as mitogen. The standard CBMN Cyt assay whole blood protocol was then carried out as per Figure 1. After harvesting of cells onto slides and fixing and staining with Diff Quik, the slides were scored for the various DNA damage and cytotoxicity biomarkers using established criteria described previously.[1, 2]

[a] *Nutritional Genomics and DNA Damage Diagnostics Laboratory, CSIRO Human Nutrition, Australia*

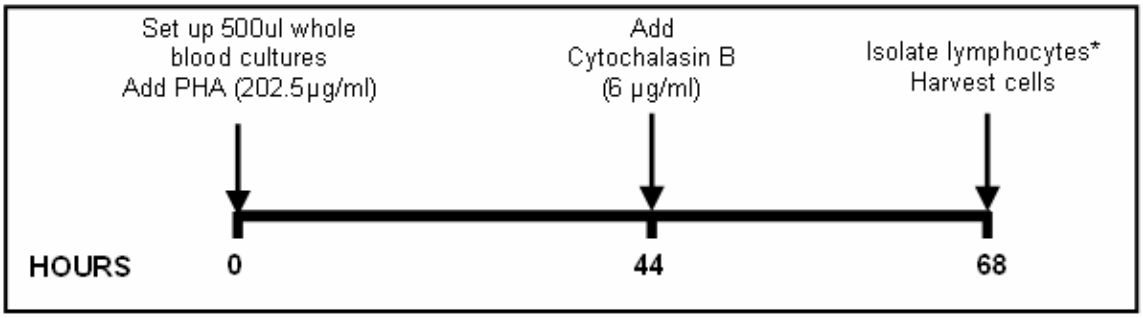


**Fig. 1. Schematic protocol of the whole blood CBMN Cyt assay.**
* lymphocytes were isolated from the whole blood cultures by underlaying the cultures with Ficoll using a syringe and the plates centrifuged at 400g for 30 minutes at room temperature. Lymphocytes were collected from the Ficoll-medium interface.

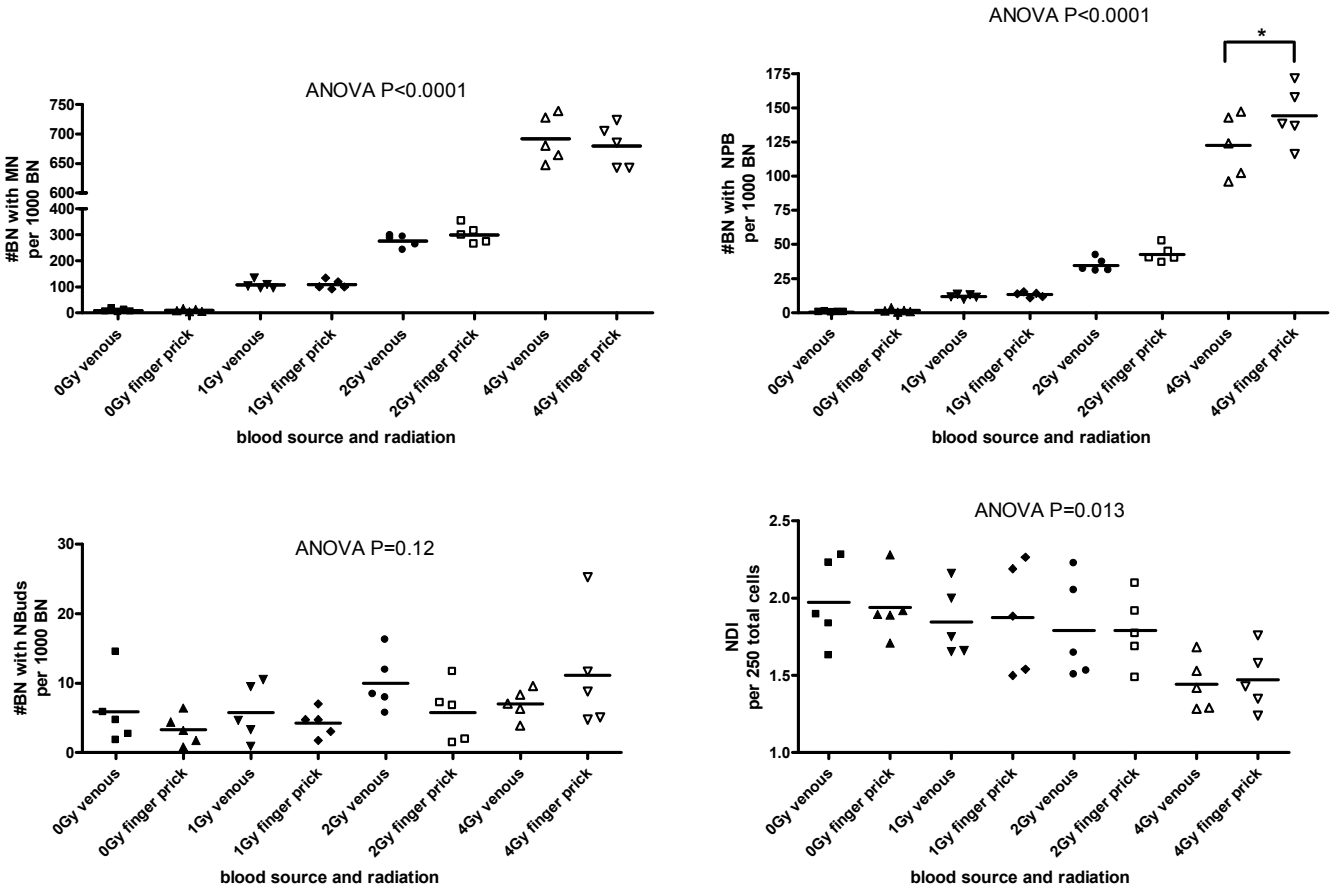


**Fig. 2. Comparison of radiation dose response of venous vs finger prick whole blood microcultures from 5 different healthy individuals.** Whole blood microcultures were set up as per Figure 1 for venous blood from the arm and finger prick blood. DNA damage biomarkers of chromosome breakage or loss (micronuclei, MN), asymmetrical chromosome rearrangement (nucleoplasmic bridges, NPB), gene amplification (nuclear buds, NBud) and cytostatic effects (Nuclear Division Index, NDI) were measured. Results shown as mean ± SEM. Significance accepted at $P<0.05$.

## Research results

In preliminary studies (not shown) we ascertained that the ionising radiation dose-response effects for γ-rays with the CBMN Cyt assay were the same for conventional venous blood 5ml cultures and 0.5ml venous blood microcultures for blood collected from the arm by venepuncture. We then tested whether results for 0.5ml microcultures were the same for finger prick blood collected by lancet and venous blood collected from the arm using a vacutainer. The results for tests on blood from five different healthy subjects (Fig. 2) exposed to increasing doses of ionising radiation (0, 1, 2, 4Gy γ-rays) showed good agreement between micro-cultures using both sources of blood with respect to the induced levels of binucleated (BN) cells with micronuclei (MN), nucleoplasmic bridges (NPB), nuclear buds (Nbuds) and for nuclear division index (NDI) with the exception that frequency of BN cells with NPB which tended to be slightly higher at 4Gy in the finger prick blood.

**Potential products**

Results from this project indicate that the CBMN Cyt whole blood microculture assay can be efficiently and reproducibly performed using 50µl of blood sourced from a finger prick blood sample and used for the purpose of radiation exposure biodosimetry. The results suggest that the system can reliably detect an exposure of 1Gy or greater doses. The micro-culture system is practical to use and is likely to be amenable to automation and the development of a minimally invasive high-throughput biological dosimetry system.

**Acknowledgments**

Sasja Beetstra, Bianca Benassi and Jing Wu contributed to the laboratory work for this project. Jing Wu carried out all experiments outlined in this report. Bianca Benassi analysed the data and assisted with writing the final report. Michael Fenech provided scientific direction and supervision of the entire project.

**References**

1. Fenech M. Cytokinesis-block micronucleus cytome assay. *Nat Protoc* **2**:1084-104, 2007.
2. Fenech M, Chang WP, Kirsch-Volders M, Holland N, Bonassi S and Zeiger E. HUMN project: detailed description of the scoring criteria for the cytokinesis-block micronucleus assay using isolated human lymphocyte cultures. *Mutat Res* **534**:65-75, 2003.
3. Thomas P, Umegaki K and Fenech M. Nucleoplasmic bridges are a sensitive measure of chromosome rearrangement in the cytokinesis-block micronucleus assay. *Mutagenesis* **18**:187-94, 2003. ■

# miRNA Based Dosimetry for Irradiation Exposure

*Lubomir B. Smilenov*

**Goal**

The goal of the current proposal was to show that miRNA expression profiles in peripheral blood could be used as a biodosimeter.

**Phase I** of the proposal was aimed to test this idea by measuring miRNA expression profiles after whole body irradiation in mice. A potential **Phase II** of the proposal was supposed to develop miRNA based markers for radiation exposure in human blood.

What we achieved is 1) The development of reliable methodology for miRNA profiling in whole blood and 2) The confirmation that miRNA profiles in mouse PBMC could be used as biodosimeter.

Due to delays with developing of reliable methodology for miRNA expression profiling of whole blood and delays with the release of mouse miRNA expression arrays by Applied Biosystems, Phase I was completed late which prevented us for applying for funding for Phase II. Nevertheless by conducting unplanned for phase I experiments we prove in principle that miRNA expression signatures in human peripheral blood are radiation specific.

Here is a brief explanation of the results of our work:

**Overall results**

**1. Based on a commercially available kit a simple and reliable method for purification of RNA from blood was developed.**

Briefly the methodology involves:

- Drawing 250ul blood directly in lysis solution minimizing changing of any blood mRNA parameters
- High quality blood RNA purification (RIN: 9.6)

**2. miRNA expression signatures in mice are radiation specific**

Whole blood miRNA expression profiles show distinctive miRNA expression signatures for irradiated and non irradiated mice.

**Unplanned experiments**

**1. miRNA expression profiles of human peripheral blood irradiated *ex vivo* are radiation specific.** These experiments were done to show that in principle miRNA can be detected in human peripheral blood and they may reflect radiation events. Blood was collected from donors, irradiated *ex vivo* and miRNA expression profiles were measured in PBMC. The results show quantitative changes in miRNA expression in irradiated cells 6 hours after irradiation. The expression of 12% of miRNA were altered by radiation.

**2. miRNA expression profiles in patients undergoing radiation therapy are radiation specific.** These experiments were done to show the principal possibility for detection of miRNA distinctive signatures in directly irradiated people. Blood was collected from a patient undergoing radiation therapy before irradiation and 3 hours and 27 hours after irradiation with 1.5Gy. PBMC were isolated and miRNA expression profiles were measured. The results show 11 miRNA differentially expressed in comparison with the control ( 7miRNA in the 3 hrs time point, 7 miRNA in the 24 hrs time point; in those numbers 3 miRNA were expressed in both time points)

**3. Designing of a method for miRNA profiling without the need for RNA purification.** It is clear that fast screening for miRNA expression will be significantly complicated by RNA purification steps which are difficult to be automatized. We developed a very short procedure for

miRNA expression profiling without RNA purification which involves:

(1) Separation of the PBMC from the RBC fraction by passing of whole blood samples through LeucoLock filters (Ambion)
(2) Lysis and elution of the retained PBMC cells from the filters
(3) Direct RT reaction for converting of the miRNA to cDNA in the lysis solution followed by miRNA specific TaqMan PCR.

The results show that this methodology could be used in miRNA profiling of whole blood and that it could be easily automated and used for mass screening.

**Overall Conclusions**

1. We proved in principle that miRNA profiling of blood could be valuable tool in biodosimetry.

2. More miRNA profiling of patients on radiotherapy are needed in order to determine the accurate miRNA expression signatures in humans applicable to biodosimetry.

**Potential Product**

After additional data collection from radiotherapy patients, a methodology consisting of fast depletion of RBC and direct RT PCR without the need for RNA purification is a product that may satisfy the needs of high-throughput minimally-invasive radiation biodosimetry. ■

# Development of a Button-Type Personal Dosimeter

*Stephen A. Marino*

**Hypothesis and specific aims**

In radiological emergency situations, such as a "dirty bomb" incident or nuclear reactor accident, large numbers of people might be exposed to radioactive materials dispersed in the area, especially that on skin and clothing, which could result in significant whole body doses. It would be of great use in such situations if the dose to those affected or suspected of being affected could be determined quickly. If the general public wore inexpensive personal dosimeters, the doses received could be quickly determined without using biological dosimetry. It is much easier to read dosimeters rapidly than process blood or other biological samples for large numbers of people and it requires less sophisticated equipment.

The specific aim of this proposal was to develop a prototype personal thermoluminescent dosimeter (TLD) for the general public in the form of a clothing button or similar item. The main purpose of the dosimeter would be to provide whole body gamma-ray dose estimation for radiological emergency situations, such as "dirty bomb" incidents or nuclear reactor accidents. The system might be able to be extended to include measurement of skin and neutron dose.

**Research methods**

The TLD materials chosen for testing were LiF:Mg,Ti (TLD100) and LiF:Mg,Cu,P (TLD100H) because of their lower cost and more widespread use. A Harshaw 3500 TLD manual TLD reader was purchased and set up along with a personal computer for control of the reader and data acquisition.

Prototype buttons of polyethylene fabricated in the machine shop at the Center for Radiological Research (CRR) were filled with salt and heat-sealed. The buttons were attached to shirts and subjected to two cycles of home machine washing and drying, and hand ironing. Testing also was done by sending shirts to a commercial laundry where they were twice dry cleaned and ironed by pressing machines.

To check the TLD system, bare TL chips 1/8" x 1/8" x 0.035" and square rods 1 mm x 1 mm x 6 mm of both TLD100 and TLD100H from Harshaw (Thermo Scientific) were irradiated with 250 kVp X rays using a Thoreaus filter (0.44 mm Sn, 0.25 mm Cu, 1.0 mm Al) to harden the beam. The TLD100 and TLD100H chips were given doses from 3 mGy to 0.6 Gy. TLD100 and TLD100H rods were given doses from 0.05 to 2.0 Gy. All TLD materials were read and then annealed between irradiations using the TLD reader according to the procedures recommended by Harshaw.

TLD chips of both types were placed inside unsealed buttons made of polycarbonate and irradiated with 10 to 80 mGy of 250 kVp X rays as above simultaneously with bare chips of the same type to demonstrate that the plastic would not modify the TLD response.

TLD 100H square rods were sealed in polycarbonate buttons and TLD100 square rods were sealed in acrylic buttons. The "buttons" were made in two pieces: the upper, thin part was 0.042" thick; the bottom part was 0.083" thick and had 3 recesses machined in it to hold the rod TLDs. A thin layer of epoxy (2 Ton brand, ITW Devcon) was applied to the upper part using a small roller in order to seal the two parts together. The assembled buttons were 0.438" in diameter and 0.125" thick, about the size of a common men's shirt button. One acrylic button was sealed with solvent. A small groove was made at the joint of the two parts of the buttons so that the two pieces could be separated by a sharp edge to access the TLDs for reading. One button of each type containing 3 rods was given a dose of 0.5, 1.0 or 2.0 Gy to determine if the epoxy would affect the TLD response. Bare rods of the same types were irradiated simultaneously for comparison.

**Research Results**

The salt did not clump or dissolve in the test buttons subjected to the home washing or commercial dry cleaning, indicating that the buttons remained waterproof and the sealing method was successful. However, when TLD chips were placed in similar buttons, the polyethylene closed up around the chips and there was no way to free them to do measurements. Since polyethylene is very difficult to bond except by heat and it melts at a temperature far below what is necessary to read the TLDs without removing them, it was abandoned as a potential button material.

The bare TLDs chips showed a quite linear relationship with dose over the range tested without individual calibration. The standard deviation of the light output for 3-4 chips was typically 1-6%, averaging 3-4%. The light output square rods also showed a linear relationship but had a larger variation in response. The standard deviation in readings for TLD100 rods was typically 1-8%, averaging ~6%, and for TLD100H rods it was 5-11%, averaging ~8%. The weights of the TLDs varied with a standard deviation of 1-2.5% for batches of 20 except for the TLD100H rods, which had standard deviations of 4 and 9% for the two batches. If this is a problem with the manufacturing process for this material/shape combination, it would explain the greater variance in response and make these rods a poor choice to place in the dosimeters.

As expected, tests of the TLDs in unsealed polycarbonate buttons resulted in no net affect. The ratios for bare chips and those in the buttons differed from unity by ~0.5% with a standard deviation of 5-6%.

A test of sealed buttons was somewhat problematic. The acrylic button sealed with solvent sealed too well and could not be opened by the same method as the other buttons. Also, it appeared that small amounts of the TLD material may have adhered to the epoxy on the top part (lid) of the two-part button. Nevertheless, the average responses of the TLDs in the buttons were within 1-2% of the bare TLDs. The TLD100H material had a much wider variation in relative response (14% s.d.), again possibly due to the wider variation in mass.

TLD chips (1/8" x 1/8" x .035") seem sturdier and seem to have less response variation in response than the square rods (1 mm x 1mm x 6 mm), particularly those made with LiF:Mg,Cu,P (TLD100H), possibly because there was less variation in weight, and therefore in dimensions, at least for the batches received from Harshaw.

**Potential product**

The potential product for this project is a personal dosimeter clothing "button" for the general public. Exposed clothing buttons come in a wide variety of sizes, shapes and colors. This makes it difficult to fabricate buttons that would not be conspicuous and detract from the garment. A button of a single size, shape and color would likely be less expensive to manufacture because of the economy of scale and could be placed readily in an inconspicuous area on shirts, blouses and other clothing (Men's shirts, e.g., often have spare buttons attached near the bottom hem). Two TLD chips could be incorporated into the button if a back-up measurement is desired since reading a TLD removes most of the signal. ■

# Stability of Expression of Endogenous Controls in Single and Multiple Cells by qRT-PCR

*Brian Ponnaiya, Sally A. Amundson, Shanaz A. Ghandhi, Lubomir B. Smilenov, Charles R. Geard and David J. Brenner*

Given the increasing awareness of the complexity and multiple relationships between cellular processes, there is a growing appreciation for the power of analyzing cellular responses on a cell-by-cell basis.[1-3] One of the logical extensions of the microbeam's ability to target individual cells is the analysis of single cells. For example, single-cell gene expression analysis holds great promise, but the methodology to process these samples in a reproducible, quantitative, and parallel fashion remains challenging.

We have previously quantified alterations in gene expression in individual microbeam-irradiated and bystander cells.[4] Single cells were isolated using a micromanipulator (Narashige) fitted with a microcapillary attached to a microsyringe (Narashige) and alterations in CDKN1A (p21/WAF1/Cip1) were measured using Reverse Transcription Polymerase chain reaction (RT-PCR). One of the main limitations of such an approach is the non-quantitative nature of the measurements made and the small number of gene products that can be assayed in any given cell. Another issue is variable losses of material during manual processing, which can be especially problematic for single cell analysis.

To overcome some of the limitations discussed above, we have developed a protocol to increase the number of genes that can be assayed from individual irradiated cells. This approach uses low-density TaqMan real-time PCR arrays that require only a very small amount of material for amplification and quantitative measurement of up to 48 genes in a single cell. TaqMan real-time PCR is an extremely sensitive and reproducible method for detecting gene expression. However, many factors may affect the

analysis of the data, including the selection of the endogenous control genes. To date there has been little effort to examine the variation of endogenous controls among individual cells. Presumably the best endogenous control would be one that is expressed in all cells at the same level regardless of the experimental conditions. However, experimental evidence suggests that some of the most commonly used control genes (eg. GAPDH and 18S) are not stably expressed across different cell types or experimental conditions.[5-7] Therefore, to achieve any accuracy in gene expression analyses it is important that a careful selection of endogenous controls be conducted. In single cell analyses this becomes even more crucial.

In preliminary experiments, IMR90 cells were irradiated with 1 Gy X-rays and 4 hours post-irradiation, 100, 10 and single cell samples were isolated into wells of 96-well plates using the flow cytometry facility at the Columbia University Medical Center. After lysis and reverse-transcription (Cells to Ct kit, Applied Biosystems), the cDNA product was pre-amplified using target-specific primers (Pre-Amp Kit, Applied Biosystems). Samples were then loaded onto Human Endogenous Control TLDAs (Applied Biosystems) that have triplicates of 16 genes, which are routinely used as normalization controls (18S, ACTB, B2M, GAPDH, GUSB, HMBS, HPRT1, IPO8, PGK1, POLR2A, PPIA, RPLPO, TBP, TFRC, UBC and YWHAZ). Baseline and threshold values were automatically determined for all samples using the SDS version 3 software (Applied Biosystems). The obtained data were analyzed using geNorm, version 3.5,[8] to determine the most stably expressed endogenous control genes, and these are presented in Figure 1.

As can be seen, within the 100 cell analyses all genes except 18S had M values of less than 1.5, and would be considered stably expressed and appropriate normalization controls for qRT-PCR. When the numbers of cells were reduced to 10, M values of 3 genes (YWHAZ, TBP and HPRT1) were above 1.5 which would make them unsuitable endogenous controls. When numbers of cells were reduced to single cells, 10 of the genes rose above a 1.5 M value. The other trend observed is that, regardless of the number of cells being assayed, some genes such as YWHAZ, 18S, TBP and HPRT1, tend to be variably expressed, that is, their M values tend to be among the highest for that particular group of cells. Further, with two exceptions (18S and HPRT1), increasing the number of cells being assayed increased the stability of a particular gene. For example, the most stably expressed gene among single cells, RPLPO had an M value of 1.387, 0.988 and 0.328 in single cell, 10 cell and 100 cell samples respectively. This is expected, that for some genes there would be more variation across 10 single cells as compared to a pool of 10 cells or 100 cells. Additionally, other genes such as B2M, PPIA and GAPDH tended to be among the more stably expressed across all three groups.

In conclusion, we have demonstrated a thorough analysis of the stability of endogenous genes used to normalize qRT-PCR, which is an absolute requirement for the accurate analysis of gene expression. Further, the data presented here speak to the sensitivity of qRT-PCR to detect small changes in gene expression profiles and together with single cell analyses provides a powerful approach to investigate the complexity of cellular responses to ionizing radiation and many other applications where gene expression patterns in individual cells may be of interest.

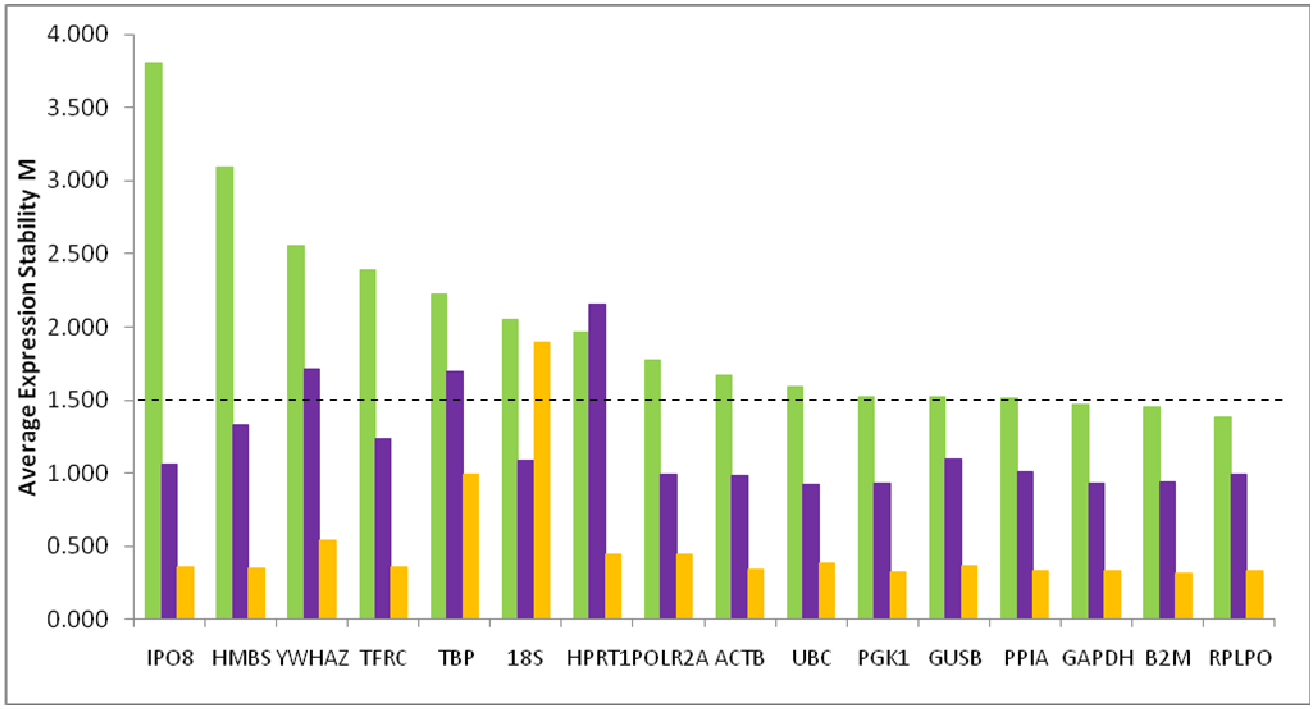


**Fig. 1.** Comparisons of average expression stability (M, as generated by geNorm) of 16 control genes on the endogenous control arrays between samples of single cells (green), 10 cells (purple) and 100 cells (yellow). The dashed line indicates an M value of 1.5 below which genes are considered to be stable when assayed in populations. Genes are ranked by stability in single cells with the most variable on the left and the most stable on the right.

## References


1. Marcy Y, Ishoey T, Lasken RS, Stockwell TB, Walenz BP, Halpern AL, Beeson KY, Goldberg SM and Quake SR. Nanoliter reactors improve multiple displacement amplification of genomes from single cells. *PLoS Genet* **3**:1702-8, 2007.
2. Zhang W, Ding J, Qu Y, Hu H, Lin M, Datta A, Larson A, Liu GE and Li B. Genomic expression analysis by single-cell mRNA differential display of quiescent CD8 T cells from tumour-infiltrating lymphocytes obtained from in vivo liver tumours. *Immunology* **127**:83-90, 2009.
3. Zhong JF, Chen Y, Marcus JS, Scherer A, Quake SR, Taylor CR and Weiner LP. A microfluidic processor for gene expression profiling of single human embryonic stem cells. *Lab Chip* **8**:68-74, 2008.
4. Ponnaiya B, Jenkins-Baker G, Randers-Pherson G and Geard CR. Quantifying a bystander response following microbeam irradiation using single-cell RT-PCR analyses. *Exp Hematol* **35**:64-8, 2007.
5. Glare EM, Divjak M, Bailey MJ and Walters EH. beta-Actin and GAPDH housekeeping gene expression in asthmatic airways is variable and not suitable for normalising mRNA levels. *Thorax* **57**:765-70, 2002.
6. Suzuki T, Higgins PJ and Crawford DR. Control selection for RNA quantitation. *Biotechniques* **29**:332-7, 2000.
7. Thellin O, Zorzi W, Lakaye B, De Borman B, Coumans B, Hennen G, Grisar T, Igout A and Heinen E. Housekeeping genes as internal standards: use and limits. *J Biotechnol* **75**:291-5, 1999.
8. Vandesompele J, De Preter K, Pattyn F, Poppe B, Van Roy N, De Paepe A and Speleman F. Accurate normalization of real-time quantitative RT-PCR data by geometric averaging of multiple internal control genes. *Genome Biol* **3**:RESEARCH0034, 2002. ■


2008 Maurice Lenz Lecture was on July 17, 2008. Speaker Professor Lester J. Peters (left) came from Peter MacCallum Cancer Institute, Australia, and Professor Eric J. Hall (right).

Seminar speaker, Dr. Max Costa (left), Professor and Chairman of the Department of Environmental Medicine, School of Medicine, NYU, and Professor Tom Hei (right).

# On-Line Breath Gas Analysis for Non-Invasive High-Throughput Radiation Biodosimetry

*Uwe Oeh,[a] Lothar Keck,[a] Claudia Brunner,[a] Mattia Fredrigo[a] and Herwig G. Paretzke[a]*

**Hypothesis and specific aims**

In the event of a radiological incident, the extent of the ionizing radiation exposure to individuals has to be detected in order to react with adequate medical and therapy treatment. For a large-scale incident, such a biodosimetry technique must necessarily be applicable as a high-throughput method. Additionally it should be easy to handle and minimally-invasive.

Breath gas analysis is a non-invasive investigation method. Volatile organic compounds (VOCs) being exhaled by breath are mainly blood born and therefore enable to monitor physiological processes in the body.

At the Helmholtz Zentrum München (formerly known as GSF) human breath gas analysis has been established using a Proton Transfer Reaction Mass Spectrometry (PTR-MS) system. PTR-MS allows highly sensitive, rapid and on-line measurements and is therefore well suited for high-throughput application.

The aim of this proposal was to prove the feasibility of breath analysis for retrospective radiation exposure assessment. When radiation interacts with biologically important molecules, the principal molecular target is DNA but also membrane lipids and proteins are affected, whereas in the latter cases inflammatory processes play a major role. The products of such inflammatory processes are released into the blood, reach the lung and the volatile compounds of them are exhaled via breath, and thus, may act as biomarkers for diagnostic radiation assessment.

The specific aims were as follows:

1. In a first step, human in vitro cultured cells were used to test the hypothesis in an in vitro cell system
2. In a further step, the hypothesis was tested directly on human subjects.

**Research methods**

**1. Irradiation of *in vitro* cells**

For the in vitro tests two different cell lines, retinal pigment epithelium cells hTERT-RPE1 and lung epithelium cells A-549, were irradiated with gamma radiation at doses of 4 Gy and 8 Gy. Subsequently, the VOCs in the headspace of the cell culture flasks were analyzed by PTR-MS and the mass spectra were compared for cells before, during and after irradiation.

**2. Measurements applied on human subjects**

The measurements applied on human subjects were performed in collaboration with the University Hospital "Rechts der Isar" in Munich. Patients undergoing radiation therapy (partial body radiotherapy) were asked to spend breath gas before and after irradiation.

2.1 Then the VOC spectra were analysed by PTR-MS and compared for both situations. From this information specific VOC biomarkers might be identified and then be used for diagnostic radiation assessment.

2.2 In order to additionally investigate VOCs which are not detectable by PTR-MS running with $H3O^+$ primary ions, breath samples collected in Teflon bags from patients immediately before and after radiotherapy were analysed with a remote laser based photoaccustic spectrometer (EDT 300, Sensor Sense) especially to look for ethylene.

**Research results**

**1. Irradiation of in vitro cells**

PTR-MS was used to search for radiation induced changes in the composition of volatile organic compounds in the headspace of in vitro cultured cells. To enable online-measurements, first an appropriate experimental setup had to be developed. Therein, two different cell lines, retinal pigment epithelium cells hTERT-RPE1 and lung epithelium cells A-549, were irradiated with gamma radiation at doses of 4 and 8 Gy. Pilot experiments showed that the reaction of the experimental setup on the gamma rays, the diffusion through the medium and the adsorption of VOCs on the inner walls of the culture flasks were not a problem for the measurements. Furthermore, a simulation of the deposited dose was calculated, which proved that more than enough radiation was used to induce radiation effects in all cells. The concentrations of the VOCs in the headspace of the cells were analyzed for changes immediately after irradiation as well as for changes appearing up to four days later. The experiments showed that immediately after the irradiation of the cells a small but distinct number of VOCs exhibited relative changes in their concentrations compared to non-irradiated cells. In particular, these changes were dependent on the dose. However, no long-term radiation induced effects could be found in the composition of the VOCs in the headspace of the cells.

**2. Measurements applied on human subjects**

Altogether 149 breath gas samples together with isochronal room air samples were collected and analysed. The set comprises samples from 11 leukaemia patients exposed to total body dose of 2-12 Gy of γ-rays, (ii) 18 lung cancer patients where the thorax was exposed to a total tumor dose of 12-75 Gy, (iii) 6 other cancer patients, (iv) 35 control persons and (v) 91 room air samples. Table 1 summarizes the split-up of the samples. The total dose was normally ap-

[a] *Helmholtz Zentrum München - German Research Center for Environmental Health (GmbH), Neuherberg, Germany*

**Table 1.** Collected samples

| Sample type | | Number of samples |
|---|---|---|
| Room air samples | | 91 |
| Non-irradiated people | Controls' samples | 84 |
| | Patients' samples before radiotherapy | 15 |
| | Total | 99 |
| Irradiated people | Patients' samples during/after radiotherapy | 50 |

plied in 1-7 fractions on consecutive days. In the ideal case 8 samples were collected from an individual patient, the first one at the day before the first dose and the last one three days after the last dose.

2.1 PTR-MS measurements

The samples were collected in Teflon bags and the volatile organic compounds (VOCs) were measured by PTR-MS. Unfortunately no unique striking marker for the exposure to radiation could be detected with PTR-MS.

However, statistical tests indicated significant differences associated with the radiation therapy. A new ansatz for the analysis of high dimensional breath sample mass spectra was developed. The ansatz consists in preconditioning the data by extracting logarithms and normalising with respect to the room air, then extract a significant mass subset and finally construct a simple linear test on the subset. Three parameters representing noise level, dimension and distortion allow to tune the test for a better performance. Figure 1 shows the scores of the weighted scalar product (WSP) approach applied to a test sample subset data aggregated into irradiated and non-irradiated groups. The first results are very encouraging and show that both groups (irradiated and non-irradiated people) can be separated.

In Figure 2 the results are plotted in a Receiver Operating Characteristic (ROC) curve. The training sets are also included as a further reference, and the results are repeated for the LDA and the WSP strategies. With a test family on seven different sample subset partitions, masses 45, 46, 59, 60, 63 and 73 pop up for most of the partitions, the first four typically associated to Acetaldehyde (45,46) and Acetone (59,60) respectively. Acetone appears to be critical for the test quality, results are significantly worse when it is masked out.

There is a lot of space for development both in the statistical analysis and on the operative side. Among others we ignored correlation between masses and the use of non-linear tests. More stringent sample collection protocols are needed in order to reduce dependence from some of the many sources of unwanted sample variation.

2.2 Laser based photoacoustic spectroscopy of ethylene in breath gas samples

For the measurements $CO_2$ and water were removed from the breath gas with KOH and CaCl scabbers in the breath stream line (mass flow 2l/h) between the bag and the ethylene analyser. An additional following cold trap (<40°C) was used to hold back interfering volatiles e.g. methanol with higher boiling points.

It was found that after a bronchial treatment with a dose

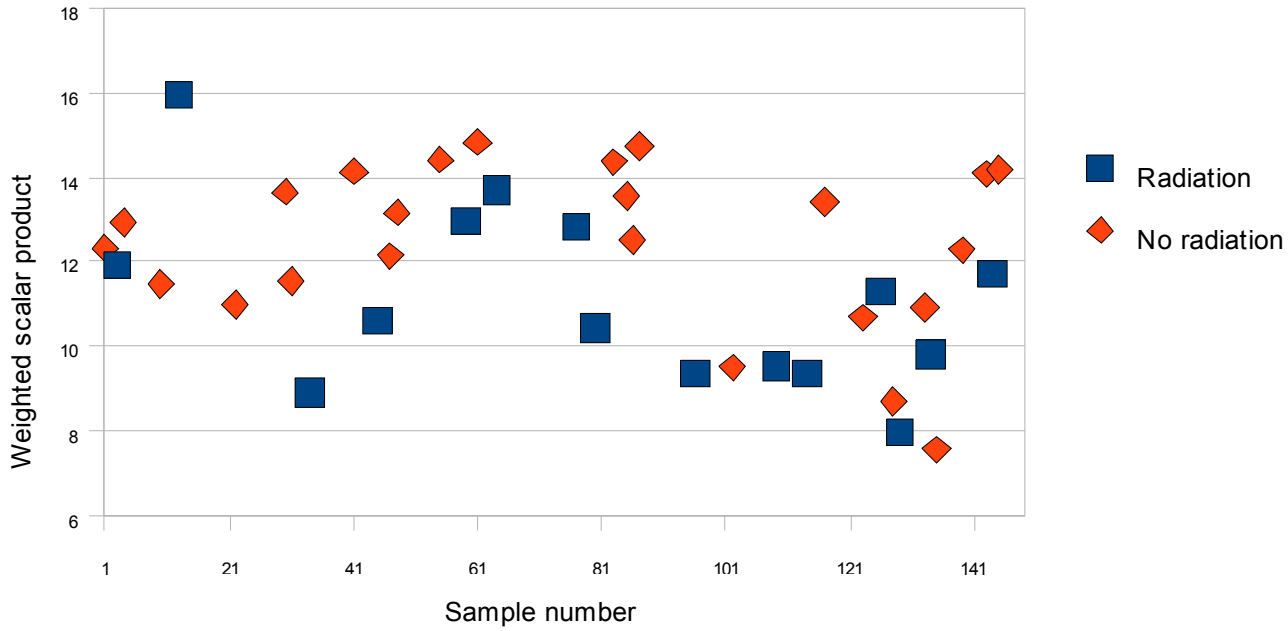


**Fig. 1.** Scoring of the weighted scalar product test based on a non-overlapping training partition subset.

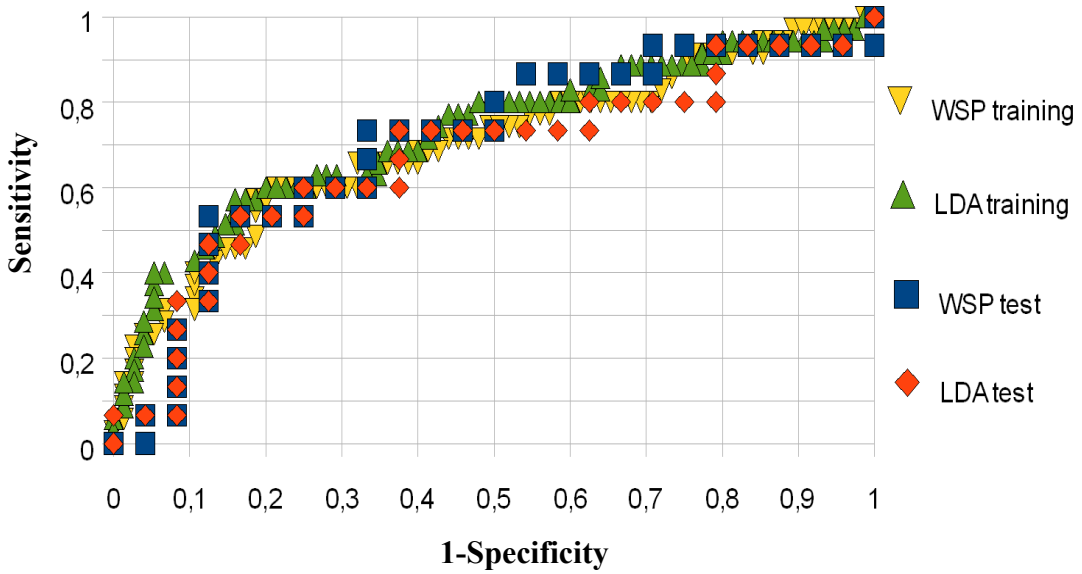


**Fig. 2.** ROC curves for the separation between irradiated and non-irradiated people.

of 1.8Gy the ethylene concentration in the breath increased in two independent samples from 2.5 and 3 ppbv by 13% and 21%, respectively. In other two cases after lung treatment the increase was 2- and more than 3-fold. But we frequently found strong background signals dependent on the therapy and waiting areas which interfere with the ethylene signal. Online fieldwork in measuring ethylene at the therapy- and waiting areas may in time reduce the interferences. Nevertheless the results show that ethylene might be a candidate for a radiation induced biomarker.

**Potential products**

A specific PTR-MS breath gas analyzing system optimized for high-throughput radiation biodosimetry might be a potential product, but has not been yet developed, since more and detailed research still has to done first. ■

# Human DNA Repair Variation and Radiation Exposure Biomarkers

*Bruce Demple*[a]

**Hypothesis and specific aims**

The overall hypothesis was that individual variation in repair capacity for radiation damage in DNA would be detectable at the level of specific excision and repair products.

Aim 1: Develop methods for detecting specific repair products in cells.

Aim 2: Determine whether common polymorphisms in repair genes affect these products.

As detailed below, we made progress toward the analytical goals of Aim 1 as originally planned. In the meanwhile, because increased information is available on the subject, we re-focused Aim 2 more toward mitochondrial DNA (mtDNA). In addition to its demonstrated roles in both normal metabolism and apoptosis, mtDNA presents a much simpler analysis target (16,569 bp in humans) than does the human nuclear genome (~3 x $10^9$ bp), and mtDNA is present in multiple copies, 100-10,000 per cell. Note also that mtDNA, surrounded by oxidative metabolism, may be more susceptible to oxidative DNA damage than the nuclear genome. The overall goal remained to identify DNA repair-related products that could be used to monitor cellular damage as a result of exposure to ionizing radiation, and whether individual variations in repair capacity could be used to help identify individuals at greater risk.

**Research methods**

The initial effort under Aim 1 was centered on two products, 3'-phosphoglycolate esters (3'-PG) at oxidative strand breaks, and 2-deoxyribonolactone (dL) residues at sites of alkaline lability. Each of these products is expected to be a major component among the ~100 different known radiation

[a] *Department of Genetics and Complex Diseases Harvard School of Public Health, Boston, MA*

lesions. Biologically, 3'-PG are important as groups that block the activity of DNA polymerases and other enzymes, while dL residues can both block replication forks and, during attempted repair, form stable covalent cross-links to DNA polymerases involved in abasic site excision. The methods used involved cellular exposure to ionizing radiation or other oxidative agents, recovery of the DNA, and quantification of general lesion types using a primer activation assay,[1] followed by mass spectrometry for specific lesions. We have also been developing an assay for protein-DNA crosslinks formed during attempted repair of dL; this measure would be the converse of repair, but it would also be a potential reporter of limitations in normal DNA repair.

**Results**

We first attempted to apply the primer activation assay to bacterial genomic DNA following gamma irradiation. That effort indicated that even this sensitive assay experienced considerable interference from other lesions formed by irradiation. We therefore used chemical oxidants as a more efficient way to generate single-strand breaks; that effort confirmed the study published in 1986. We then collaborated with Peter Dedon at MIT to demonstrate that 3'-PG accumulated specifically in the chromosomal DNA of repair-deficient *E. coli* treated with hydrogen peroxide. The cells were treated with $H_2O_2$ under conditions allowing for repair, then the DNA was extracted to analyze by mass spectrometry. The strain BW528 lacks both of the known enzymes that excise 3'-PG, while AB1157 is repair-competent. It can be seen (Fig. 1) that 3'-PG levels are normally quite low, and that $H_2O_2$ treatment made the level only moderately higher in the repair-competent strain. In contrast, unrepaired 3'-PG persisted in the repair-deficient strain following $H_2O_2$ treatment. The measured 3'-PG values for $H_2O_2$-treated BW528 were very close to the number of DNA single-strand breaks estimated for these cells, which further substantiates the analysis and indicates that virtually all the unrepaired strand breaks accumulating under these conditions contain 3'-PG as the blocking groups.

The results provide sufficient data to plan for improvements in the method. These would include using the key bacterial repair enzyme, endonuclease IV, as a reagent for this analysis. The current protocol employs generalized degradation enzymes, but the much higher specificity of endonuclease IV (in addition to its activity under conditions that suppress most other enzymes) should increase the sensitivity of the analysis. With such improvements, it may be possible to apply the procedure to human cells, in which suppression of the main 3'-PG excision enzyme Ape1 is expected to compromise repair of this critical lesion.

Progress under Aim 2 now benefits from new information showing dL repair in mitochondria. For nuclear DNA, attempted base excision repair of dL can lead to covalent cross-links between the Ape1-incised dL and DNA polymerase beta; this problem can be avoided by activation of a long-patch pathway dependent on the flap endonuclease Fen1.[2] Our recent work demonstrated that the mitochondrial DNA polymerase gamma also undergoes mechanism-based crosslinking to dL,[3] and that the long-patch repair pathway also occurs in mitochondria, where it depends partly on the flap endonuclease Fen1. We also showed the importance in long-patch base excision repair of another structure-specific nuclease, Dna2.[4]

These studies provide important background for developing assays for radiation risk biomarkers. We reasoned that quantification of crosslinks between dL and DNA polymerase beta or DNA polymerase gamma would give information on the limits of repair for the nuclear or the mitochondrial genome, respectively. We have carried out the initial stages to develop a labeling method for specific protein-DNA crosslinks. The general procedure involves the isolation of the chromosomal DNA, the isolation from that of particular proteins linked to the DNA, and finally labeling of the DNA to which they are attached. While this required more effort than anticipated, our initial reconstruction efforts show that this approach is feasible, and that we can post-label crosslinks specifically. Indeed, this approach might be generalized to quantify all protein-DNA crosslinks, or specific categories of them. It may be that a more comprehensive assay for multiple types of crosslinks may give more useful information on the overall repair capacity of cells and tissues.

**Potential products**

While we have made significant progress toward the analytical goals of this work, it is premature to propose specific

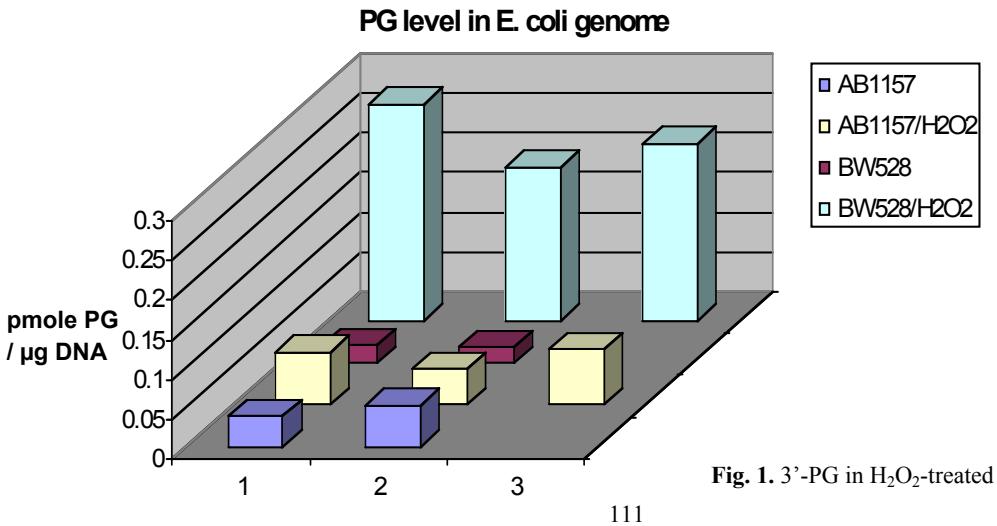


**Fig. 1.** 3'-PG in $H_2O_2$-treated *E. coli* chromosomal DNA.

product applications deriving from it. That said, microfluidic devices can be envisioned that would in principle provide for the necessary reactions to carry out an automated analysis.

### References


1. Demple B, Johnson A and Fung D. Exonuclease III and endonuclease IV remove 3' blocks from DNA synthesis primers in H2O2-damaged Escherichia coli. *Proc Natl Acad Sci USA* **83**:7731-5, 1986.
2. Sung JS, DeMott MS and Demple B. Long-patch base excision DNA repair of 2-deoxyribonolactone prevents the formation of DNA-protein cross-links with DNA polymerase beta. *J Biol Chem* **280**:39095-103, 2005.
3. Liu P, Qian L, Sung JS, de Souza-Pinto NC, Zheng L, Bogenhagen DF, Bohr VA, Wilson DM, 3rd, Shen B and Demple B. Removal of oxidative DNA damage via FEN1-dependent long-patch base excision repair in human cell mitochondria. *Mol Cell Biol* **28**:4975-87, 2008.
4. Zheng L, Zhou M, Guo Z, Lu H, Qian L, Dai H, Qiu J, Yakubovskaya E, Bogenhagen DF, Demple B, *et al.* Human DNA2 is a mitochondrial nuclease/helicase for efficient processing of DNA replication and repair intermediates. *Mol Cell* **32**:325-36, 2008. ■


# Integrated Microfluidic Visualization on a Microchip for Ultrahigh-Throughput Low-Cost Radiation Biodosimetry

*Robin Muller,[a] Michael Grad,[b] Chee Wei Wong,[b] Samuel K. Sia[c] and Daniel Attinger[b]*

**Hypothesis and Specific Aims**

For micro-biofluidic assays, a key limitation to high throughput visualization and scalability is the detection technology. For example, large fluorescence microscopes are used to evaluate the assay, which is a paradox with respect to the miniaturization of the microfluidic chip.

The purpose of the pilot project is to integrate a portable microscope with a flow-through microfluidic chip to do visualization of flowing cells for radiation biodosimetry. The whole setup is to be actuated from a notebook computer.

**Research Methods**

A GpA-fluorescence tagging method will allow radiation biodosimetry of red blood cells (Fig. 1). Glychophorin A (GpA) is a human glycoprotein on the surface of erythrocytes that determine the M and N blood group variant. γ-radiations induce mutations in the stem cells which can be detected by the failure of an erythrocyte to express an allelic form of GpA (MØ or NØ). Studies have shown that the mutation frequency can be related to the dose of radiation received.[1] Limitations for this method are a high interindividual variation, and the facts that only MN variant blood group is eligible for the assay (50% of the population), that MØ and NØ mutation variant frequency is low (in the order of 104-106) and that a radiation dose lower than 1 Grey cannot be detected. Advantages are that this method requires a small amount of blood (< 10uL), can be transported to points of care and is inexpensive. Cells are fixed, tagged with fluorescent FITC antibodies-M, and suspended in a buffer solution. Mutated cells are detected as they express half the intensity of healthy cells. The developed prototype investigates the ability to detect a simple or double intensity of FITC tagged erythrocytes.

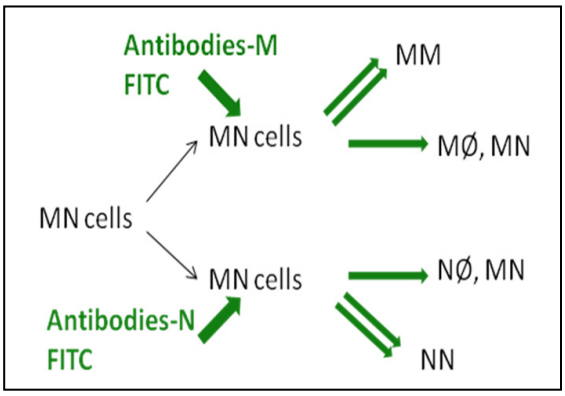


**Fig. 1.** Strategy to detect simple or double intensity of FITC tagged erythrocytes.

The optical part (Fig. 2) is made of a focalized blue high power LED (5W), a bandpass blue filter, a 20x microscope objective (N.A. 0.4), a bandpass green filter and a CCD Peltier cooled camera. Filters are needed to separate the FITC excitation light (peak at 490nm) from the FITC emission light (peak 518nm).

Injection of the samples is performed using a standard syringe. Flow in the microfluidic chip is driven by gravity, which is reliable and does not require power. A simple washing procedure using water and a syringe has been inte-

[a] *Department of Microtechnologies, Ecole Polytechnique de Lausanne, Switzerland*
[b] *Department of Mechanical Engineering, Columbia University, NY*
[c] *Department of Biomedical Engineering, Columbia University, NY*

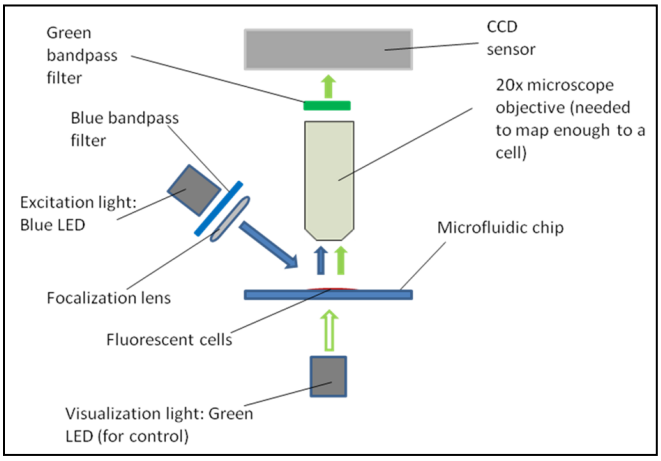


**Fig. 2.** Optical part design.

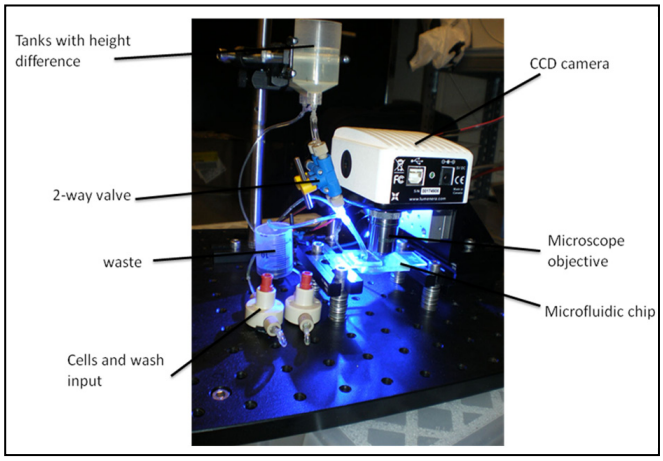


**Fig. 3.** Picture of the prototype.

grated to make the device re-usable. A PDMS microfluidic chip where cells flow through under the microscope has been manufactured using photolithography method in the Columbia University cleanroom. A critical requirement is to have an identical exposure time for all the cells flowing in the channel, which means to have an identical velocity. This has been achieved using the same pressure in both channels and designing a low height/width cross section ratio of the channels, according to the study.[2] Experiments have shown a very good flow control correlation between simulations and experiments.

An in-house controlling software has been developed using the software Matlab (Mathworks, Inc.), which allows computer LED and camera control, automatic particle detection and tracking along the channel, automatic suppression of uninteresting particles (e.g. stuck to chip walls) and fluorescence intensity detection.

## Research Results

Results with the prototype in Figure 3 have shown that the fluorescent detection performance of the prototype is on the same order than an IX71 Olympus fluorescence microscope with a filtered mercury lamp source and a 10x objective with 0.3 NA.

The tagging efficiency was investigated by comparing the fluorescence of the cells to the fluorescence of a known quantity of labeled antibodies. Two calibration curves were derived from separate experiments: first the signal to noise ratio of different antibody concentrations was found for a constant exposure time (Fig. 4A), and second the exposure time required to yield a signal to noise ratio of 2.5 was found for the same antibody concentrations (Fig. 4B).

The tagging efficiency was found for the direct staining procedure to be approximately 30%. The directly tagged cells are shown on the graphs in figure 4, and the required exposure time for a signal to noise ratio of 2.5 is ~250ms. This exposure time is the limiting factor for the throughput, because in order to visualize a cell it cannot move more than its diameter during the time of exposure. The throughput is therefore estimated as ~2000 cells per minute.

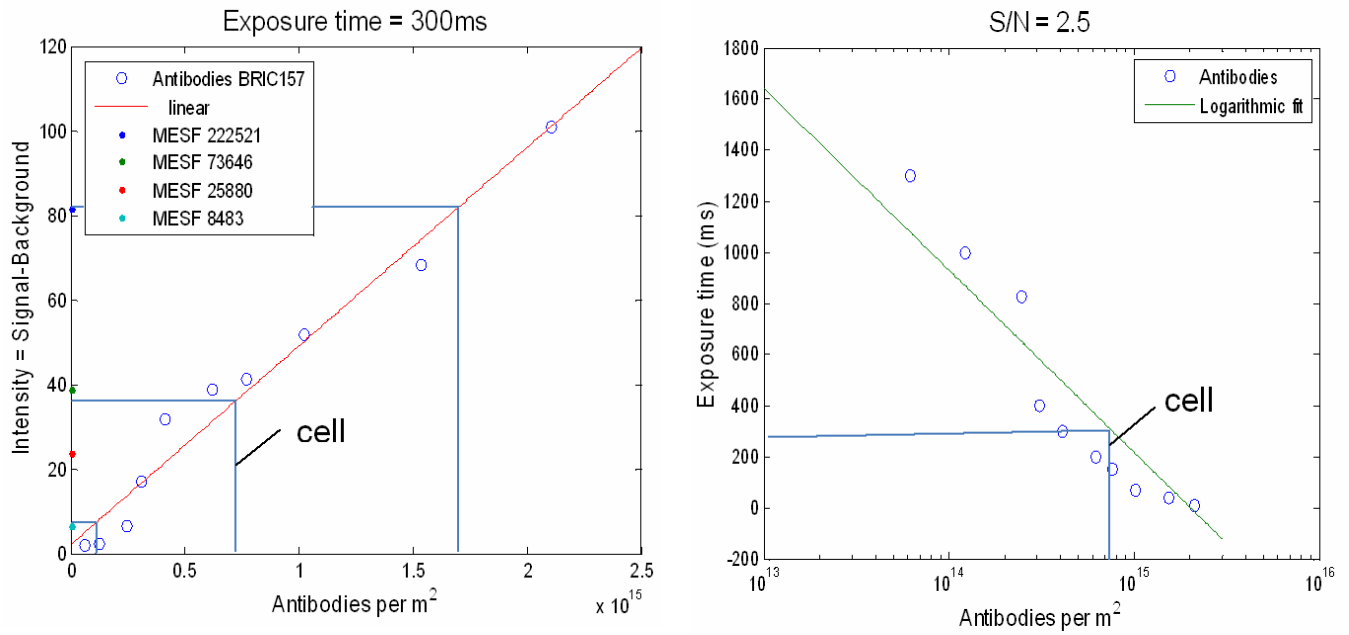


**Fig. 4. A (left)**, Calibration curve for constant exposure time; **B (right)**, Calibration curve for constant S/N.

**Potential Products**

A low cost, portable flow through fluorescence microscope with a throughput of ~2000 cells per minute has been built that can replace a traditional expensive fluorescence microscope for point-of-care analysis. The prototype (excluding the camera) was built for under $1000 while traditional fluorescence microscopes can be upwards of $20k.

**References**

1. Langlois RG, Bigbee WL, Kyoizumi S, Nakamura N, Bean MA, Akiyama M and Jensen RH. Evidence for increased somatic cell mutations at the glycophorin A locus in atomic bomb survivors. *Science* **236**:445-8, 1987.
2. Brody JP, Yager P, Goldstein RE and Austin RH. Biotechnology at low Reynolds numbers. *Biophys J* **71**:3430-41, 1996. ■

# Potential Application of γ-H2AX and TUNEL Assays in Hair Follicle Cells for High-Throughput Minimally-Invasive Biodosimetry in the 2-8 Gy Dose Range

*Yuanlin Peng*[a] *and Joel S. Bedford*[a]

**Introduction and Hypotheses**

Radiation induced changes in hair follicle cells and its hair has been studied and recognized for some 40 years for potential use in biodosimetry. Some of these include changes, with time after irradiation, in pigmentation, the width of individual hairs, and the number of cells in the medullary region of the forming hair. We have carried out preliminary experiments measuring the appearance of the phosphorylated form of the H2AX histone variant (γ-H2AX) in cells in the hair root by a fluorescence immunocytochemical assay carried out 24 hours after *ex vivo* irradiation of plucked hair.

An example of these preliminary results is illustrated in Figure 1, and shows large and diffuse amounts of γ-H2AX in a fraction of cells in irradiated (panel A, 8Gy + 24h) but not unirradiated (panel B, 0Gy) hairs at this time. This observation suggests that a process occurring after a day or so (perhaps apoptosis involving massive DNA degredation) swamps the initial production and disappearance of small discrete γ-H2AX foci arising from DNA DSBs by irradiation.

Hypotheses and Aims: For the present proposal, we suggested that 1) for hair follicle cells and assay times after irradiation pertinent to the CMCR concerns, the proportions of cells with massive DNA fragmentation, likely due to apoptosis, will be a more robust and sensitive index of dose than the residual discrete γ-H2AX foci per cell remaining from the initial exposure at these later times, and 2) the proportion of apoptotic cells will be a sensitive index of dose. Few, if any, procedures could be as "minimally invasive" as an assay using hair follicle cells from plucked hairs. A further requirement for a high-throughput minimally invasive assay is that it needs to be sufficiently sensitive and robust for the

[a] *Environmental and Radiological Health Sciences, Colorado State University, Fort Collins, CO*

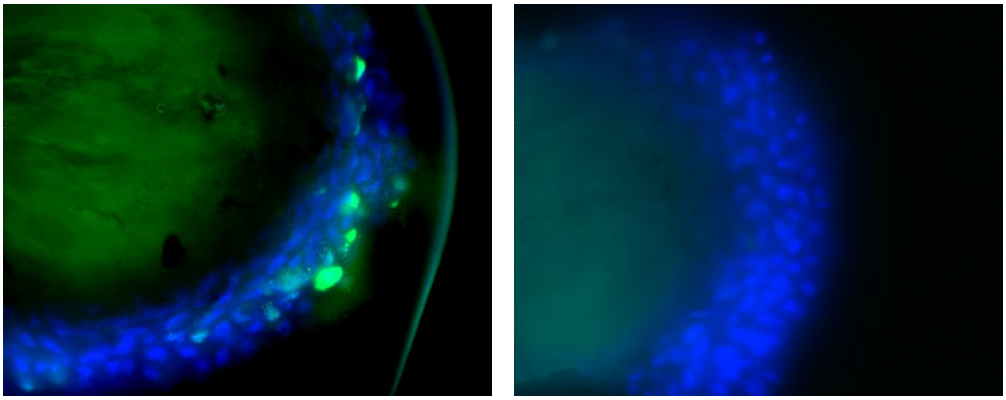

**Panel A** **Panel B**

**Fig. 1. Panel A.** Hair root cells 24 hours after 8Gy, (DAPI and FITC anti-γH2AX staining); **Panel B.** Hair root cells 24 hours after 0Gy, ( DAPI and FITC anti-γH2AX staining).

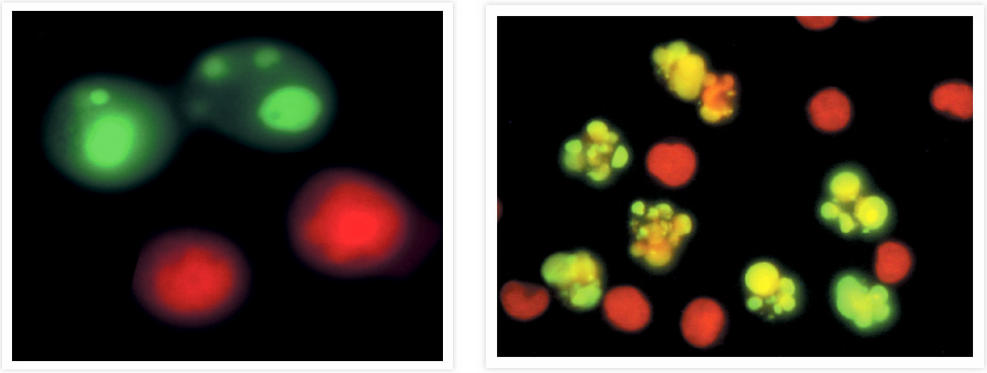

**Panel A** **Panel B**

**Fig. 1. Panel A.** Example from Molecular Probes of their Vybrant *Apoptosis Assay.* Apoptotic cells are labeled green and necrotic cells red; **Panel B.** Example from Molecular Probes of their APO-BrdU TUNEL Assay. Cells with DNA strand nicks (apopt) are labeled green while other cells are labeled red.

limited numbers of cells that would be available using such procedures. The aim is to test the hypotheses.

**Research Methods**

A standard immunofluorescence assay, such as illustrated in Figure 2 by the *Molecular Probes* Vybrant Apoptosis Assay (panel A) and their APO-BrdU TUNEL assay (panel B) was used. For our experiments the latter (APO-BrdU TUNEL) assay was chosen. In the example from Molecular Probes the cells were human Jurkat lymphoma cells treated with campothecin for a time that gives maximum expression of apoptosis.

**Research Results**

In the early stage of this study we showed in plucked hairs from irradiated mice that the appearance of the massive γ-H2AX yields 24 hours after irradiation did correspond to cells experiencing apoptosis, as determined by a TUNEL assay.

We then determined dose responses for numbers of such apoptotic cells in plucked hairs at 1 or 2 days after irradiation of mice with doses of 0, 2, 4, 6, and 8 Gy of gamma-rays.

Figure 3 shows a plot of the proportion of cells in mouse hair root cells that were positive in the TUNEL assay 24 or 48 hours after the various doses. It should be noted that not all plucked hairs displayed cells undergoing apoptosis, but this was expected because not all hairs are in a growth phase at any one time. For this study only those hair roots showing evidence of some apoptosis were scored.

For sampling at 24 hours the response appears to increase linearly with dose at a rate of about 7%/Gy For sampling at 48 hours after irradiations the dose response was steeper with the proportion increasing at least initially at a rate of about 16%/Gy but then the proportion saturated for doses exceeding 4Gy. One possible explanation for this is that (1) apoptotic cells are not rapidly eliminated and their numbers accumulate with increased time, and (2) even in growing hairs not all cells are cycling, and cycling is necessary for cells to undergo apoptosis. For such a scenario a maximum would be reached to include essentially all cycling cells. It is noteworthy that in some of the hairs, presumably those that were not in the growing state, virtually no apoptotic cells were ever seen for any dose.

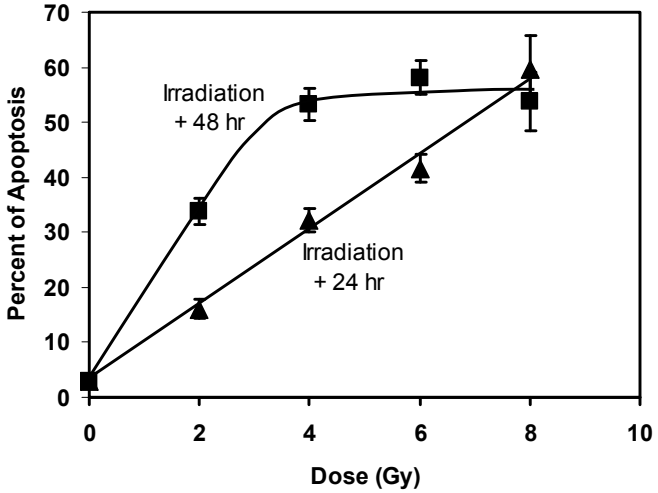


**Fig. 3.** A plot of the proportion of cells in mouse hair root cells that were positive in the TUNEL assay 24 or 48 hours after the various doses.

**Potential Products**

This pilot project provides data to support further development of a rapid assay for fluorescence due to apoptosis in human hair follicle cells at times of 24 hours, 48 hours, and perhaps longer after irradiation. The levels of total fluorescence per hair root might be measured for several plucked hairs in a small portable instrument and the average reading would presumably be proportional to the number of cells undergoing apoptosis per hair root. This, in turn, would be proportional to radiation dose to the hair follicle, and would be much, much faster and could be done on many more exposed individuals than a chromosomal aberration assay from peripheral blood lymphocytes. Though the hair assay would not be nearly so accurate as a chromosomal aberration assay it would be far superior for the mass screening and triage purposes that would be required following a ground level nuclear detonation in a large city, where perhaps a million people would need to know their radiation doses within a very few days. ■

# Quantitative Microarray Flow-Channel Assay for Use With a Hand-Held Fluorescent Reader

*Matthew Coleman* [a]

**Hypothesis and specific aims**

Hypothesis: Since it is unlikely that the amount of exposure will be known for each individual and since different individuals are likely to respond differently to radiation exposure, it will be critical to quantify the protein levels and profile responses of an individual's body to the dose received (bio-dosimeters), so that proper medical care can be administered in a timely manner. Immuno-based assays can be designed for candidate biomarkers in response to ionizing radiation exposures. The device employed can be inexpensive, rapid, easy-to-use and capable of identifying individuals with whole body exposure to IR exceeding 2Gy.

**AIM 1. Develop and test biodosimetry lateral flow array and prototype reader using spiked in antigens.** Aim 1 will deliver an integrated sample collection, preparation and microarray flow-channel prototype that has been tested using antibodies for characterizing protein responses. This will use proteins known to be IR responsive as well as controls (gamma-H2AX, amylase, BAX, GADD45A and controls IgG, GAPDH) spiked in to solutions to assess the sensitivity of the microarray flow-channel and fluorescent reader.

**AIM 2. Validate device prototypes by establishing the baseline protein biomarkers in *ex vivo* irradiated blood samples.** Aim 2 will validate data using our device for discriminating different IR exposure using *ex vivo* irradiated human blood samples. The experiments will evaluate the ability of each candidate biodosimeter used in AIM 1 to measure responses between normal human cells that are unexposed and irradiated *ex vivo* to 2 Gy, 4 Gy or 6 Gy and higher. Time after exposure will be an important component of these experiments (1, 4, 24 and 48 hours post-exposure).

**Research methods**

This grant relied upon multiple techniques related to antibody-based detection to include lateral flow strips and a flow microarray. Antibody-based affinity reagents were commercially purchased for selected candidate biomarkers and evaluated for their ability to multiplex within our microarray flow-channels. Imaging of data relied on the development of a hand-held microarray reader that was built as part of this project. Proteins were evaluated for levels of expression and variability in unexposed samples, consistency of dose-response, and ability to discriminate among dose levels relevant for triage binning (0-2, 2-4, >4 Gy). Statistical comparison of the biomarker levels used both a t-test and a linear mixed effect model to account for biological and technical variability. All studies involving human subjects were reviewed and approved by the appropriate Institutional Review Boards, at LLNL and UC Davis Medical Center.

**Research Results**

**Progress on AIM 1:** We have designed several flow arrays to test antibody-antigen interactions for gamma-H2AX, amylase, BAX, GADD45A and controls IgG, GAPDH. We decided to also include ATM, C-reactive protein, Vascular endothelial growth factor, Herceptin -2 receptor and matrix metallopeptidase 2 antibodies in this process because they were readily available. The protein microarrays were tested for proper IgG recognition and detection over three logs of antigen concentration to determine specificity (Fig. 1). These antibodies are now available as paired combinations to ensure the specificity and the needed limits of detection (ng/mL). This process has also allowed us to validate our stock antibodies to be used for device development. The following antibody pairs gamma-H2AX, amylase, BAX, GADD45A and controls IgG, GAPDH, C-reactive protein have been adapted to lateral flow assays for use in relevant samples (saliva and blood-related cells). Of future interest will be translating the passive flow devices to cancer detection.

This project also piloted the development of a device for fluorescent-based microarray flow-channel assays capable of assessing levels of ionizing radiation (IR) exposures in human-derived samples. The prototype device is potentially suitable for utilization in a clinical or triage setting. This work was carried-out by a graduate student Deanna Thompson at U.C. Davis and co-funded by the NSF Center for Biophotonics Sciences at UCD. The device was designed to

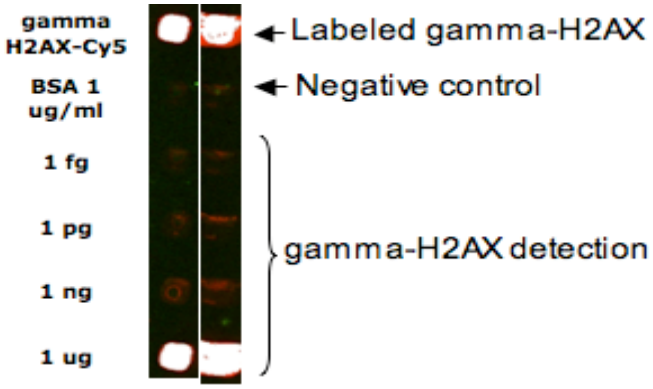


**Fig. 1.** A false color image of replicate microarray flow channels. The detection is based on gamma-H2AX antigen detection using specific antibodies. The strips show a dramatic drop in detection from 1 ug/mL to 1 ng/mL for gamma-H2AX.

[a] *Physics and Life Sciences Directorate, LLNL, L-448, Livermore, CA*

monitor multiple biomarkers for better sensitivity as once single biomarker may be entirely insufficient for accurate quantitative diagnosis. As shown in Figure 2, this portable device uses LEDs for image analysis of the arrays that are currently printed on glass slides. This demonstrates a simple hand-held device for multiplexed measurements of protein biomarkers.

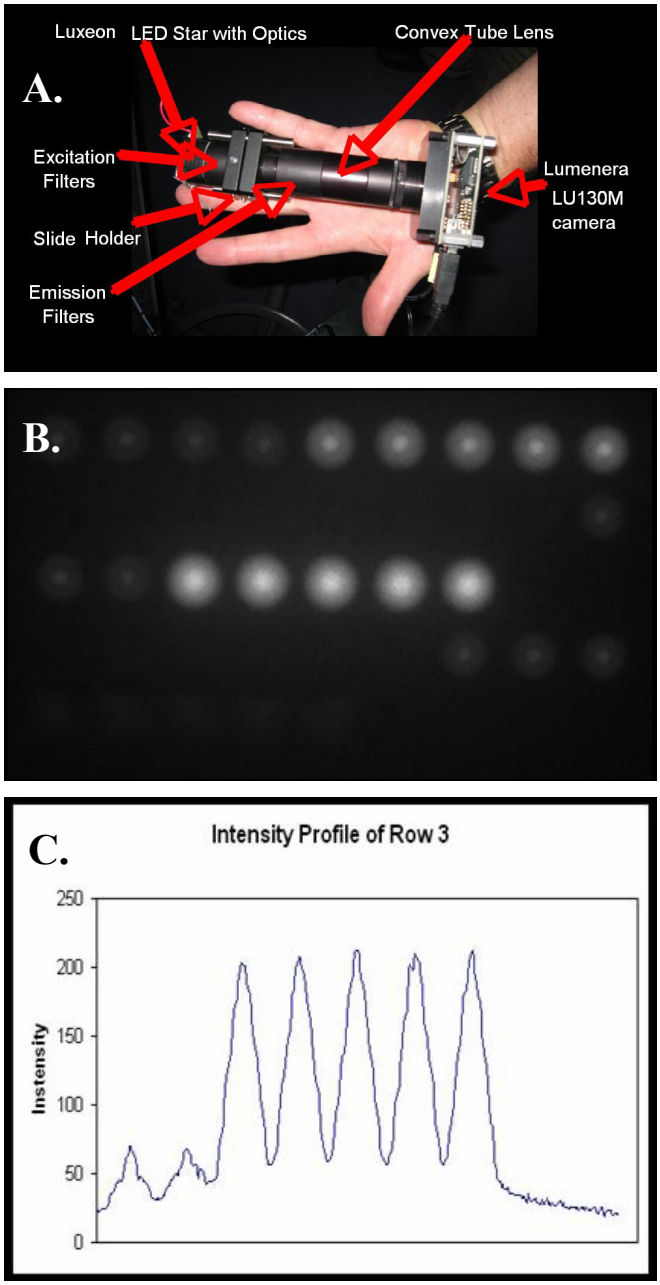


**Fig. 2.** A Hand-held array reader. (**A**) shows the 8" long device without the attached batteries that sit along side the convex tube lens. (**B**) 10 x 5 array containing different levels of labeled antibodies to demonstrate the sensitivity and dynamic range of the system. The image was integrated over a 200 milisecond time frame (**C**) Histogram of row 3 from the array image shown in B (statistical data analysis is ongoing).

**Progress on AIM 2:** As part of this process we have renewed our IRB protocol for another year. Blood samples were the primary samples we used to validate selected IR responses for time and dose of known IR responsive proteins and determine the feasibility of screening people using our microarray flow device.

We have tested previously frozen samples of blood irradiated *ex vivo* from three individuals for testing on conventional lateral flow assay strips. This was done to gauge the shelf life of antibody assays that made use of previously prepared test strips. The data showed that we were able to detect an IR response for both C—reactive protein, gamma-H2AX and BAX. For an example see Figure 3. Interestingly, BAX also showed a response in serum samples obtained after 30 minutes of IR exposure of 200 cGy. The C-reactive protein was responsive in both our *ex vivo* and radiotherapy patient samples.

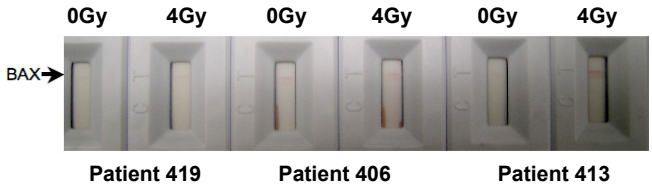


**Fig. 3.** Lateral flow strip test assays using lymphocytes. Whole blood sham or irradiated ex vivo at 400 cGy and sampled 24 after the exposure. Data from three individuals is shown.

## Potential products

This project provided the following deliverables: i) Development of a rapid novel immunoassay platform for clinical and triage biodosimetry in the form of a lateral flow test strip and microarray. ii) A hand-held reader prototype for future development. iii) Identification of potential commercial partners for future assay and device refinement and manufacturing to include Arista Biologicals, www.aristabiologicals.com, and Merlin Labs Inc., www.merlinlabs.com. The project also shared findings with the BioDesign Institute for designing future microfluidics platforms for assay development. ■

# RARAF – Table of Contents



# RARAF PROFESSIONAL STAFF

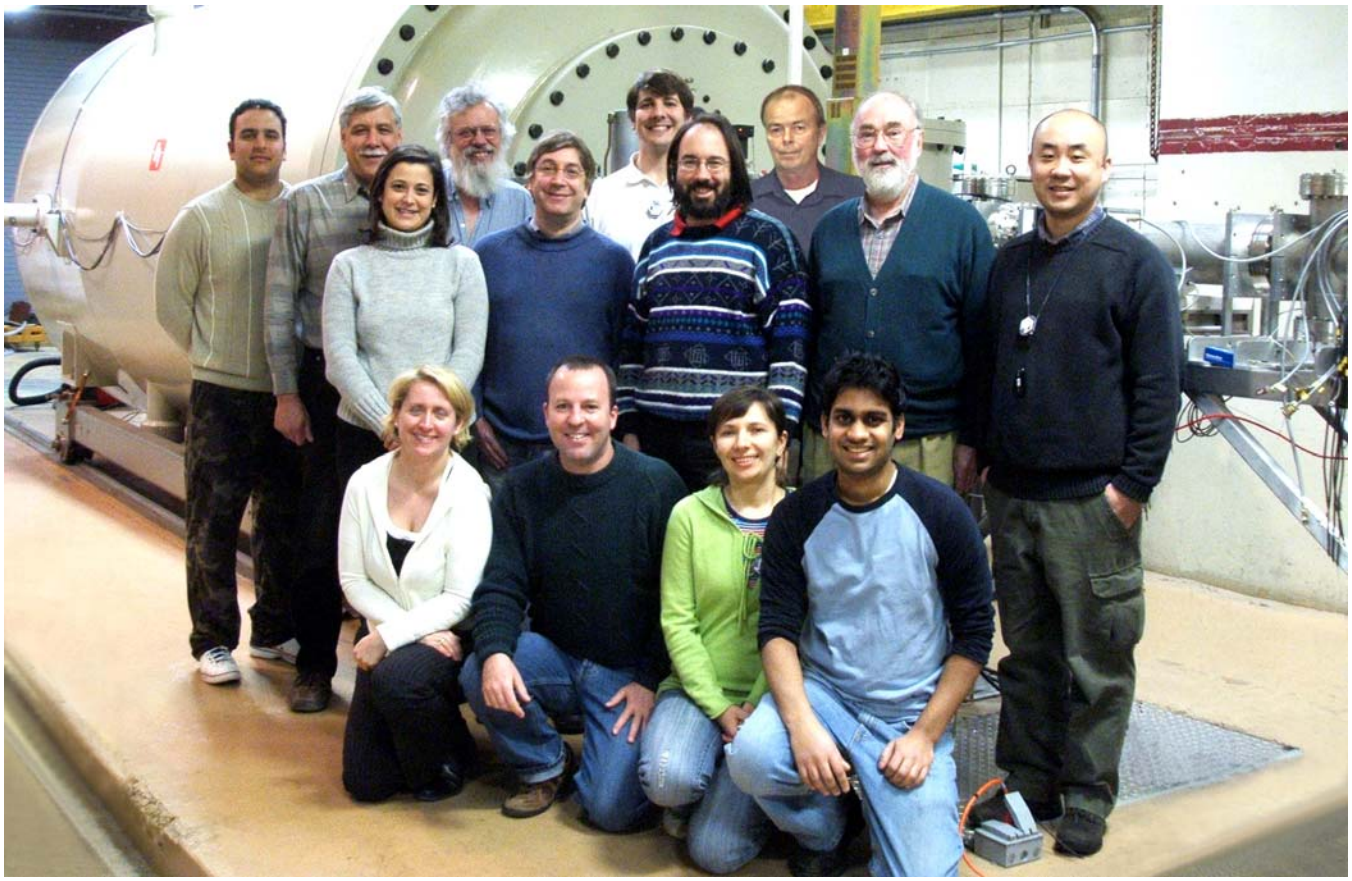

**RARAF Staff** *(l–r)*: *Front row*: Helen Turner, Alan Bigelow, Sasha Lyulko and Bharat Patel; *2nd* row: Antonella Bertucci, David Brenner, Guy Garty, Charles Geard and Yanping Xu; *3rd row*: Abel Bencosme, Stephen Marino, Gerhard Randers-Pehrson, Andrew Harken and Gary Johnson. Not shown: Brian Ponnaiya, Kenichi Tanaka and Gloria Jenkins-Baker.

**David J. Brenner**, Ph.D., D.Sc. **–** CRR Director**,** RARAF Director
**Stephen A. Marino**, M.S. **–** RARAF Manager
**Gerhard Randers-Pehrson**, Ph.D. **–** RARAF Associate Director, Chief Physicist
**Charles R. Geard**, Ph.D. – Senior Biologist
**Alan Bigelow**, Ph.D. – Associate Research Scientist
**Brian Ponnaiya**, Ph.D. – Associate Research Scientist
**Guy Y. Garty**, Ph.D. – Associate Research Scientist
**Andrew D. Harken**, Ph.D. – Post-Doctoral Research Scientist
**Kenichi Tanaka**, Ph.D. – Post-Doctoral Research Scientist
**Yanping Xu**, Ph.D. – Post-Doctoral Research Scientist
**Oleksandra Lyulko**, – Pre-Doctoral Research Scientist
**Bharat Patel**, B.S., B.A. – Technician B

# The Radiological Research Accelerator Facility

**AN NIH-SUPPORTED RESOURCE CENTER – WWW.RARAF.ORG**

*Director: David J. Brenner, Ph.D., D.Sc.*
*Associate Director: Gerhard Randers-Pehrson, Ph.D.*
*Manager: Stephen A. Marino, M.S.*

## Introduction

There have been several notable accomplishments at RARAF this year:

- The achievement of a sub-micron focused charged particle beam.
- Completion of the installation and upgrading of the two-color multiphoton system on the Microbeam Facility, the first multi-photon system installed on a microbeam for biological irradiations.
- Microbeam irradiation of small animals (C. elegans nematodes), including the first vertebrate irradiations (Japanese medaka embryos).
- A record amount of use of the accelerator for radiobiology and also for on-line development of facilities and procedures.

## Research using RARAF

The "bystander" effect, in which cells that are not irradiated show a response to radiation when in close contact with or even only in the presence of irradiated cells, continues to be the main focus of the biological experiments at RARAF. Almost every biology experiment run this year, including those involving animals, examined this effect. The emphasis of the present experiments is to determine the mechanism(s) by which the effect is transmitted primarily for direct gap junction communication through cell membrane contact. Both the Microbeam and the Track Segment Facilities continue to be utilized in various investigations of this phenomenon. The single-particle Microbeam Facility provides precise control of the number and location of particles so that irradiated and bystander cells may be distinguished, but is somewhat limited in the number of cells that can be irradiated. The Track Segment Facility provides broad beam irradiation that has a random pattern of charged particles but allows large numbers of cells to be irradiated.

A special type of track segment dish is being used to investigate cell-to-cell communication in the bystander effect using the Track Segment Facility. "Strip" dishes consist of a stainless steel ring with thin (6-μm) Mylar foil glued to one side in which a second dish is inserted. The Mylar foil glued to the inner dish has alternate strips of the Mylar removed. Cells are plated over the combined surface and are in contact. The Mylar on the inner dish is thick enough (38 μm) to stop the charged particles ($^4$He ions) and the cells plated on it are not irradiated.

Interest in irradiation of 3-D systems continued this past year, with tissue samples irradiated using either helium ions or protons. Imaging systems for the Microbeam Facility have been developed to enable observation and targeting of cells that are not in monolayers. Two animal systems have been irradiated using the Microbeam Facility this year: *C. elegans* nematodes and Japanese medaka embryos. In addition, cultured human tissue samples are being irradiated using the Track Segment Facility.

The experiments performed at RARAF from January 1 through December 31, 2008 and the number of days each was run in this period is listed in Table I. Fractional days are assigned when experimental time is shared among several users (e.g., track segment experiments) or experiments run for more or less than an 8-hour shift. Use of the accelerator for experiments was 56% of the regularly scheduled time (40 hours per week), about 85% higher than last year and the highest use we have attained at Nevis Labs. Thirteen different experiments were run during this period. Eight experiments were undertaken by members of the CRR, supported by grants from the National Institutes of Health (NIH), the National Aeronautics and Space Administration (NASA), and the Department of Energy (DoE). Five experiments were performed by outside users, supported by grants and awards from the Department of Defense (DoD), NASA, and DoE. Brief descriptions of these experiments follow.

Exposure to ionizing radiation may induce a heritable genomic instability that leads to a persisting enhanced frequency of genetic and functional changes in the progeny of irradiated cells. Burong Hu and Charles Geard of the CRR continued their investigation into whether cytoplasmic irradiation or the bystander effect can also lead to delayed genomic instability (Exp. 103). The charged-particle Microbeam Facility was used for precise nuclear or cytoplasmic irradiation of normal human lung fibroblasts using 6 MeV $^4$He ions. Their results show that the fraction of metaphase cells involving human chromosome 11 changes (including chromosome 11 rearrangement, entire chromosome 11 deletion and duplication) was significantly higher than that of the controls, not only after nuclear irradiation but also after cytoplasmic irradiation and in the bystander cell group. mBAND chromosome analyses of 15 clonal 1 isolates from each of the control, nuclear and cytoplasmic irradiations as well as the bystander cell group were conducted. The results show that unstable clones involving human chromosome 11 rearrangements arose in three irradiated groups. Clones from the control group remained stable. Further analyses showed there was no large change in the number of unstable clones over the time in culture in each irradiated group. The stability of the individual clones, however, changed with time in culture in some clones from the control and the irradiated groups. These results suggest that genomic instability fol-

**Table 1. Experiments Run at RARAF, January 1 - December 31, 2008**

| Exp. No. | Experimenter | Institution | Exp. Type | Experiment Title | No. Days Run |
|---|---|---|---|---|---|
| 103 | B. Hu<br>C. R. Geard | CRR | Biology | Damage induction and characterization in known hit versus non-hit human cells | 14.8 |
| 106 | B. Ponnaiya<br>C. R. Geard | CRR | Biology | Track segment alpha particles, cell co-cultures and the bystander effect | 0.3 |
| 110 | H. Zhou<br>M. Hong<br>T. K. Hei | CRR | Biology | Identification of molecular signals of alpha particle-induced bystander mutagenesis | 55.7 |
| 113 | A. Miller | AFRRI | Biology | Role of alpha particle radiation in depleted uranium-induced cellular effects | 0.2 |
| 114 | M. Suzuki<br>(H. Zhou) | NIRP, Japan | Biology | Bystander response in primary human bronchial epithelial cells using the G2PCC technique | 2.3 |
| 133 | S. Ghandhi<br>B. Yaghoubian<br>S. Amundson | CRR | Biology | Bystander effects in primary cells | 7.3 |
| 136 | A. Mezentsev<br>S. Amundson | CRR | Biology | Bystander effects in 3D tissues | 8.8 |
| 139 | S. Amundson | CRR | Biology | Signal transduction in cytoplasmic irradiation | 9.8 |
| 140 | L. Han<br>(T. K. Hei) | Shanghai Medical University | Biology | Study of the mechanism of radiation-induced inactivation of the FHIT gene by single cell microbeam irradiation | 19.1 |
| 141 | D. Chen,<br>A. Asaithamby | Univ. of Texas Southwestern Medical Center | Biology | Visualization of recruitment of DNA damage markers to the sites of DNA damage induced by microbeam irradiation | 7.3 |
| 142 | W. Dynan,<br>W. Kuhne<br>(A. Bertucci) | Medical College of Georgia | Biology | Proton irradiation of Japanese medaka embryos *in vivo* | 5.5 |
| 143 | W. Dynan,<br>W. Kuhne | Medical College of Georgia | Biology | Accumulation of PSF p54 (nrb) at sites of human cells *in vitro* | 1.5 |
| 144 | A. Bertucci | CRR | Biology | Microbeam irradiation of *C. elegans* | 8.0 |

**Note**: Names in parentheses are members of the CRR who collaborated with outside experimenters.

lowing ionizing radiation exposure is not dependent on direct damage to the cell nucleus.

Brian Ponnaiya and Charles Geard of the CRR continued another study investigating the bystander effect (Exp. 106). The Track Segment Facility was used for broad-beam charged particle irradiations with 125 keV/μm $^4$He ions to examine genomic instability in irradiated and bystander htert immortalized human bronchial epithelial cells (HBEC-3kt). These cells were cultured on standard single-sided Mylar track segment dishes and irradiated with half the dish covered by a thin metal shield. Cells on the non-covered portion of the dishes were irradiated with $^4$He ions, while cells on the covered portions of the dishes were bystander cells. Irradiated and bystander populations from each dish were separated and set up in culture. At various times post irradiation G2-PCCs were prepared from each culture. The chromosomes were analyzed by both Giemsa staining (for gross chromosomal aberrations) and mFISH for more subtle alterations (e.g. translocations).

Efforts to identify the cell-to-cell signaling transduction pathways involved in radiation-induced bystander responses (Exp. 110) were continued by Hongning Zhou, Mei Hong and Tom Hei of the CRR. Using the Microbeam Facility to produce a focused 6 MeV $^4$He beam, they have found that oxidative stress as well as lipid peroxidation is induced after cytoplasmic irradiation. The product of lipid peroxidation, 4-hydroxynonenal, may be able to induce downstream activation of MAPK pathway(s) and, in turn, expression of cyclooxygenase-2. Using the Track Segment Facility for irradiation with 125 keV/μm $^4$He ions, they have found that PKC is translocated from cytosol to membrane both in directly-irradiated and bystander cells. In addition, free fatty acid content is elevated in both irradiated and bystander cells. Since fatty acids have been shown to induce translocation of PKC from cytosol to membrane, they may serve as possible signal molecules mediating bystander effects. In other experiments, several different human and rodent cell lines were irradiated using both irradiation facilities. The preliminary data indicate that mitochondrial function is critical for the radiation-induced bystander effect.

Exposure to depleted uranium (DU) during military operations or a terrorist attack is a concern for military personnel and civilians. The long-term health effects of low-dose high-LET radiation exposures are not well known. Furthermore, development of pharmacological countermeasures to low-dose radiological contamination is important for the health and safety of both military and civilian populations. Alexandra Miller of the Armed Forces Radiobiological Research Institute (AFFRI) continued studies using 125 keV/μm $^4$He ions from the Track Segment Facility to evaluate low-dose radiation- or DU-induced carcinogenesis using *in vitro* and *in vivo* models and to test safe and efficacious medical countermeasures (Exp. 113). A third goal of this study is to identify biomarkers of both exposure and disease development. New approaches in her laboratory have enabled her to add an additional goal, which is to identify the mechanisms involved in these processes. These experiments include survival, neoplastic transformation, mutagenicity, genomic instability, and genotoxicity studies. Recently she has begun to evaluate the effect of LET on radiation-induced leukemia.

Masao Suzuki of the National Institute of Radiological Science, Japan in collaboration with Hongning Zhou of the CRR resumed a study to determine whether alpha particle irradiation in the cytoplasm can induce a bystander response in primary human bronchial epithelial cells using the G2PCC technique (Exp. 114). A fraction of the cells were irradiated in the nucleus with 6 MeV $^4$He ions using the Microbeam Facility. The cells were then accumulated in the G2 phase of the cell cycle and the process of premature chromosome condensation was used to observe chromatin aberrations.

A group led by Sally Amundson of the CRR continued three experiments concerning radiation-induced gene expression profiles in primary human fibroblast and epithelial cell lines using cDNA microarray hybridization and other methods. The first experiment, performed by Shanaz Ghandhi and Benjamin Yaghoubian, involved use of the Track Segment Facility for comparison of gene expression responses to direct and bystander irradiation (Exp. 133). Human fibroblast cells (IMR90) and epithelial cells: (HBEC-3KT and SAEC) were plated on "strip" dishes (described above) for direct-contact bystander irradiations. The cells were irradiated with 0.5 Gy of 125 keV/μm $^4$He ions and assayed for micro-nucleus formation. Using the fibroblast model, they have identified potential genes and pathways that are being validated by real-time PCR. They continue to work on the identification of potential genes of interest in epithelial cells from microarray studies.

The second experiment (Exp. 136), performed by Alexandre Mezentsev, involved irradiation of artificial human tissue samples using the Track Segment Facility. Tissue model Epi-200 (MatTek) precisely imitates the structure of the epidermis. It is composed of ~20 layers of cells, which represent keratinocytes at different stages of differentiation. The goal of this project is to reproduce tissue response to ionizing radiation *ex vivo* (e.g. for biodosimetry) and characterize the effects of low and high doses. The tissues were irradiated with protons having an initial LET of ~10 keV/μm or $^4$He ions having an initial LET of ~73 keV/μm, either over the entire tissue surface or in a narrow line (~25 μm) across the diameter. The tissue samples are grown on membranes on the end of cylindrical plastic holders. Plastic discs have been constructed that fit in the dish openings in the irradiation wheel and have small holes to provide precise alignment of the feet that are around the bottom edges of the tissue holders. A hole in the middle of each disc is fitted with two stainless steel half-discs that have a precise 0.001" (25 μm) space between them and are thick enough to stop the charged particles. This provides a narrow line of irradiation across the center of the entire sample. Two types of procedures were performed: isolation of total RNA and immunohistochemistry. The RNA provides quantification of gene expression by Microarray analysis and validation by quantitative real-time PCR. Microarray results are analyzed by computer. The analysis includes gene ontology procedures and network analysis, which normally has a graphical output representing the specific responses to the ionizing radiation. Tissue samples are also fixed in formalin, embedded in paraffin, and sectioned parallel to the line of irradiation for immunohistochemistry and counterstaining. This provides characterization of proteins of interest and describes their role in post-irradiation events, such as transcriptional regulation, contribution to cell signaling mechanisms and gap junction signaling.

In the third experiment, Sally Amundson used the Microbeam Facility to irradiate either the nuclei or the cytoplasm of normal human fibroblasts with 6 MeV $^4$He ions and extracted RNA with the goal of performing global gene expression profiling in order to gain a better understanding of the cell signaling that arises from radiation damage to the cytoplasm, and which damage response pathways require direct damage to DNA (Exp. 139). She has had initial success in amplifying and labeling small quantities of RNA (from about 2000 cells per sample) and has hybridized this amplified RNA from microbeam experiments to whole genome microarrays. This work is continuing in order to obtain a sufficient number of biological repeats for meaningful data analysis. She is beginning to validate the microarray results for individual genes using quantitative real-time PCR.

Ling Han of the Second Military Medical University, Shanghai, China, in collaboration with Dr. Tom Hei of the CRR, completed an experiment to determine the expression, injury and signal transduction of the FHIT (Fragile Histidine Triad) gene (Exp. 140). The Microbeam Facility was used to irradiate cells in the nucleus, the cytoplasm or the culture medium with 6 MeV $^4$He ions. In other irradiations, only a fraction of the cells were irradiated and the co-cultured unirradiated (bystander) cells were examined. FHIT gene function was studied at different stages over 50 generations after irradiation and the role FHIT plays in cell transformation was examined in any transformed cells detected.

David Chen and Aroumougame Asaithamby of the University of Texas Southwestern Medical Center initiated an experiment to observe the responses of cells after microbeam irradiation (Exp. 141). HT1080 human fibrosarcoma cells expressing different types of DNA damage sensing and repair factors were irradiated in the nucleus with 6

MeV $^4$He ions. The cells contain a red fluorescent protein (RFP) reporter attached to the 53BP1 gene and a green fluorescent protein (GFP) attached to the XRCC1 gene. Cells were irradiated singly and observed for up to 2 hours to monitor the recruitment of the DNA damage sensing and repair factors to the sites of DNA damage.

William Dynan and Wendy Kuhne of the Medical College of Georgia conducted the first vertebrate irradiations using the RARAF Microbeam Facility (Exp. 142). Japanese medaka fish embryos were selected because of their small size (~1.2 mm D) and their optically clear chorion, which makes them easy to view on the microbeam endstation. Fertilized embryos were collected from CAB wild-type breeding adults and shipped to RARAF. At the time of irradiation embryos were at Stage 27-28 (representing the 24 – 30 somite stage). 4.5 MeV protons were delivered at fluences of 10,000 or 20,000 protons to areas of the brain using beam diameters of 25, 50 and 100 μm. The protons have a range of only ~280 μm and stop in the embryos. The embryos were then subjected to a fluorescent *in situ* terminal deoxynucleotidyl transferase-mediated dUTP nick-end labeling (TUNEL) assay to detect DNA fragmentation, which is characteristic of apoptotic cells. A confocal laser scanning microscope was used to collect images using a 3 μm step size. Three-dimensional renderings of the Z-stack images were created and analyzed for the presence of TUNEL-positive cells. The average number of TUNEL-positive cells for the 50 μm beam treatment group was 62±16 for embryos irradiated with 10,000 protons, and 185±36 for embryos irradiated with 20,000 protons. Statistical analysis conducted using a t-test indicates that the difference between the 20,000-proton group and the other two (including controls) were significant ($p<0.01$). Similar analyses will be completed for the treatments using a 25 and 100 μm beam diameter. Future work will address response using later stage embryos and incorporate the use of histological sectioning and staining to investigate the presence of a peak of tissue damage corresponding to the proton Bragg peak. Additionally, cellular and DNA damage effects will be investigated in neighboring regions not traversed by the charged particle beam.

In another experiment, William Dynan of the Medical College of Georgia irradiated the nuclei of two human cell lines using the Microbeam Facility (Exp. 143). The purpose of this experiment was to investigate the role of polypyrmidine tract binding protein-associated splicing factor (PSF) and p54(nrb) in the repair of radiation-induced DNA damage. PSF and p54(nrb) each contain tandem RNA-recognition motifs (RRMs) and interact to form a stable complex, which has multiple functions in RNA biogenesis. The PSF p54 complex enhances DNA end-joining in vitro, suggesting that these proteins might also be involved in DNA double-strand break repair. HeLa and HCT 116 cells transfected with mCherry-Ku80 (positive control), PSF-dsRed and p54-AcGFP were irradiated in the nucleus with 100 and 200 6-MeV $^4$He ions. Using fluorescent microscopy, the mobilization of the PSF and p54 to the site of DNA double-strand breaks can be monitored.

The first animal irradiations using the Microbeam Facility were performed for an experiment by Antonella Bertucci of the CRR (144). For this project the strain SJ4005 zcls4 hsp-4::gfpV was used, which has a transcriptional reporter for the hsp-4 gene. Under normal conditions, the green fluorescent protein (GFP) expression is most prominent in the spermatheca, the tail and pharynx. Transcription of the hsp-4 gene is induced in the gut and in the hypodermis upon endoplasmic reticulum (ER) chemical stress. Young adult *C. elegans* were exposed to a 3 MeV proton microbeam with a 1μm diameter beam spot. Animals were placed in specially designed microbeam dishes under anesthesia and irradiated with different numbers of particles. Each worm was exposed in one or more anatomical regions (tail, pharynx or spermatheca). Samples were collected after exposure and re-cultured for GFP expression evaluation at 24 hours. Initial analysis of the results indicates that worms exposed to proton microbeams delivered at precisely targeted regions elicit a distal bystander effect characterized by a GFP over-expression after 24 hours.

**Development of Facilities**

This year our development effort continued on a number of extensions of our facilities:

- Development of focused accelerator microbeams
- Non-scattering particle detector
- Advanced imaging systems
- Targeting of cells
- Focused X-ray microbeam
- Neutron microbeam

*Development of focused accelerator microbeams*

In April, the compound electrostatic quadrupole triplet lens system installed at the end of 2006 was used to produce a sub-micron diameter focused $^4$He ion beam at RARAF for the first time! A beam diameter of ~0.8 μm can now be obtained routinely. The beam can be used to target sub-nuclear structures in cells. The major goal of the focused lens development now has been achieved.

The original quadrupole triplet lens used for the microbeam from 2003 to 2007 and another quadrupole triplet that was assembled in December have been inserted in a second lens alignment tube. This tube has been modified for the installation of the deflection coil for the Point and Shoot system and will replace the existing lens system in February, 2009. The point and Shoot system, will direct the microbeam to the target position rather than moving the cells to the beam, greatly decreasing the time required.

The permanent magnet microbeam (PMM) uses a compound quadrupole triplet lens made from commercially available precision permanent magnets. It is similar to the one designed for the sub-micron microbeam, the major difference being that it uses magnetic rather than electrostatic lenses. Because the magnet strengths are essentially fixed, only a single energy (5.3 MeV) proton or $^4$He ion beam can be focused.

The quadrupole magnet strengths used to focus the beam have been adjusted to produce the minimum beam spot diameter using micrometric screws to retract and extend the individual magnets of each quadrupole. Using a phase space "sweeper" and an object aperture 0.3 mm in diameter, a

beam of 5.3 MeV $^4$He ions has been focused into a spot 5 μm in diameter (a demagnification of x60, compared to the theoretically attainable x100). A miniature Hall probe will be used to map the magnetic fields of the lenses to look for aberrations and determine the octupole moment of the lenses, both of which would interfere with focusing.

The end station for the PMM has been tested and is ready to be used. The PMM will be used primarily for cell irradiations when the electrostatic system is unavailable because of development or repair and was used to test the Point and Shoot system.

*Non-scattering particle detector*

Currently the RARAF microbeam irradiator delivers a precise number of particles to thin samples by counting the particles traversing them using a gas proportional placed immediately above the cells. To irradiate samples thicker than the range of the incident ions, a completely non-scattering particle detector is necessary upstream of the samples. The Lumped Delay Line Detector ($LD^2$) is a novel particle detector consisting of 250 silver cylinders, each 3 mm long with a 2.2 mm inside diameter, connected by inductors and capacitively coupled to ground. If the capacitance is set such that the propagation velocity of the pulse equals the projectile velocity, the pulses capacitively induced in all segments by the passage of a single charged particle will add coherently, resulting in a fast electron pulse at each end of the delay line.

The detector constructed at the end of 2007 was placed in a horizontal beam line for testing with a $^4$He ion beam. The noise in the Amptek low-noise pre-amplifier is still large enough that the signal pulse, which consists of only 125 electrons, cannot easily be seen. In addition, there are reflections when an electronic pulse is provided to the detector, indicating a mismatch between the impedance of the detector and the input of the preamplifier.

Efforts are being made to cool the input FET on the detector amplifier to reduce the inherent thermal noise and enhance the signal-to-noise ratio. Calculations using the computer program AIMSPICE to simulate the electronic behavior of the $LD^2$ are underway to determine the best termination system for the signal from the detector in order to reduce "ringing" and signal loss. One of the prototype detectors will be taken to the Edwards Accelerator Laboratory in Athens, Ohio in March to be tested with a pulsed particle beam. A single nanosecond pulse will contain more than 1,000 protons and provide a signal at least 500 times larger than will be produced by a single $He^{++}$ ion, making it much easier to tune the signal termination and determine the signal amplitude.

After the full-length detector is tested, it will be mounted between the two electrostatic lenses in the electrostatic microbeam and become the standard detector for all microbeam irradiations.

*Advanced imaging systems*

Development continued on new imaging techniques to view cells without using stain and to obtain three-dimensional images of unstained cells.

The immersion-based Mirau interferometric (IMI) objective has been designed to function as an immersion lens using standard interferometric techniques by acquiring successive images at four positions with sub-wavelength separations using the vertical motion of the microbeam stage. It uses 540 nm (green) light for imaging and therefore does not induce UV damage in the cells. A custom Mirau objective was constructed in our shop in 2007 and several beamsplitters of different reflectivity (5-85%) were combined with spot mirrors into separate modules so that they can easily be interchanged in the lens.

Interferometry is very sensitive to vibrations, even as small as a fraction of a wavelength. A vibration-free environment provides usable images with this system; however on the Microbeam II endstation vertical motions due to vibrations in the building greatly reduce the image quality. Passive and active systems to reduce the vibrations were unsuccessful. A Fourier technique was investigated to remove the effects of the vibrations, but did not improve the images sufficiently.

The feasibility of a new approach using Simultaneous Immersion Mirau Interferometry has been demonstrated to overcome the vibration problem. Polarized light is split into equal components in the x and y planes, one of which undergoes a phase shift of 90º using a λ/8 waveplate. A polarization beam splitter is used to send the x and y components to form iterferograms on two separate cameras. Since the images are taken simultaneously, there is no effect from the vibration.

A multi-photon microscope was developed for and integrated into the microscope of the single-particle Microbeam Facility in 2007 to detect and observe the short-term molecular kinetics of radiation response in living cells and to permit imaging in thick targets, such as tissue samples. Two photons delivered closely together in space and time can act as a photon with half the wavelength (twice the energy). This method has the advantages that: the longer wavelength of the light beam allows better penetration into the sample while still being able to excite the fluorophor at the focal volume and less damage is produced in the portion of the sample not in the focal volume.

Initially a Chameleon (Coherent Inc.) tunable titanium sapphire laser was the source for the multi-photon excitation. This year the laser was upgraded to a Chameleon Ultra II, which has a wider range of wavelengths (680 to 1080 nm), increasing the available range of effective wavelengths for the two-photon effect so that red fluorescent protein (RFP) can be imaged. The light available from the laser can penetrate to depths of about 100 microns in a biological sample by varying the Z-position of the specimen stage. Light emitted from the specimen is selectively deflected by a series of dichroic mirrors to an array of photomultiplier tubes (PMTs). The system has been used to observe a GFP-tagged XRCC1 DNA single-strand break repair protein in real time for the experiments by David Chen (exp.141).

A housing that enables use of two PMTs, and therefore the acquisition of simultaneous images from two fluorophors, has been constructed and mounted on the microbeam microscope. Two PMTs allows investigation of fluorescence resonance energy transfer (FRET). Molecules labeled with two fluors normally widely separated can change their con-

formation by phosphorylation, positioning the two fluors near each other. In this close proximity, the emission from one fluor can excite the other, changing the ratio of emissions from the two fluorophors, giving a measure of the amount of phosphorylation in the sample. Initial experiments to observe FRET initiated by microbeam irradiation have begun.

Another potential use for the multi-photon system is fluorescent recovery after photobleaching (FRAP). Foci that are formed in a cell nucleus can be "erased" by extended exposure from the multiphoton laser, which bleaches the fluorophors. The cells can then be observed to determine the time course of foci reforming.

The multiphoton system can also be used as a laser "microspot" to induce UV damage in the focal volume of the laser spot, a capability that some users have requested.

*Targeting of cells*

During irradiation, cells to be irradiated are moved to the beam position using the microbeam stage. When a collimated microbeam was being used, this was necessary but relatively time-consuming. A focused microbeam is not restricted to a single location on the beam exit window and therefore can be deflected magnetically or electrostatically to any position in the field of view of the microscope used to observe the cells during irradiation much faster than moving the stage.

We are developing a "Point and Shoot" targeting system for microbeam irradiation based on a wide-field magnetic split-coil deflector system from Technisches Büro Fischer (Ober Ramstadt, Germany). This magnet system has been used for the microbeam facility at Gesellschat für Schwerionenforschung (GSI), Darmstadt, Germany. Two Kepco BOP power amplifiers are used to drive the coils. A short section of beam line was constructed around which the coil was placed and the assembly was mounted just below the upper quadrupole triplet on the PMM for preliminary testing. The deflection of the beam is linear with coil current and does not affect the beam spot size. A similar coil has been mounted in the lens tube for a second compound electrostatic quadrupole triplet, just below the second lens, and will be installed in the Microbeam II beamline in February.

*Focused X-ray microbeam*

We are developing an X-ray microbeam to provide characteristic $K_\alpha$ X rays generated by proton-induced emission (PIXE) from Ti (4.5 keV). Higher X-ray energies are not feasible due to Compton scattering; we are limited to X-ray energies where the predominant mode of interaction is photoelectron absorption. Charged particle beams can generate nearly monochromatic X rays because, unlike electrons, they have a very low bremsstrahlung yield.

At the suggestion of one of the members of our Advisory Committee, in 2007 we changed from a transmission design, in which the X rays used are emitted in the direction of the proton beam, to a reflection design, in which the X rays used are emitted at 90° to the proton beam direction. This eliminated several problems inherent in the previous design. The system has been mounted on its own horizontal beam line on the 1st floor of RARAF and the X-ray beam is oriented vertically, so that the geometry of the microscope and stage is the same as for our other microbeam systems.

A small X-ray source (~20 μm D) will be produced by bombarding a Ti target with high-energy protons using the quadrupole quadruplet lens used for our first focused microbeam, reducing the requirements on the subsequent X-ray focusing system. A zone plate will be used to focus the X-ray source to a beam spot 1-2 μm in diameter. The zone plate has a radius of only 120 μm, an outmost zone width of 50 nm and a demagnification factor of ~11.

The zone plate has been received and assembled in its mounting structure. Preliminary measurements were performed using a proton beam in Microbeam II focused to 10 μm to produce X rays from a thin Ti foil. The zone plate structure was mounted above the foil and scanned with an aperture to determine the X-ray beam spot size. A beam spot ~14 μm in diameter was measured, which was expected for the test geometry.

The beam line, including the electrostatic lens, has been assembled and initial tests of the focusing of the proton beam are underway. The microscope and micropositioning stage have been assembled and will soon be put in place. A focused X-ray beam should be available this spring.

*Neutron microbeam*

Calculations and preliminary measurements have been undertaken for a neutron microbeam.

Neutrons produced by the $^7Li(p,n)^7Be$ reaction are emitted only in a forward conical volume when the proton energy is just above the reaction threshold (1.881 MeV). The half-angle of this cone is dependent on the proton energy and increases with increasing energy. Thin samples placed very close to the thin, neutron-producing target layer will be irradiated by neutrons in a restricted area. A focused proton microbeam 5 μm in diameter will be incident on a 1 μm thick lithium target. The backing material will be Au or Pt, ~15-17 μm thick. Using a 1.890 MeV proton beam, thin samples in contact with the target backing should be exposed to a beam of neutrons 10-12 μm in diameter.

Initial measurements using CR-39 track etch plastic and, in collaboration with Mark Akselrond and Jeff Sykora of Landauer, Inc., fluorescent nuclear track detectors (FNTDs) are being performed to demonstrate the restricted nature of the neutron emission.

**Singletron Utilization and Operation**

Table 2 summarizes accelerator usage for the past year. The Singletron is started at 7 to 7:30 a.m. on most days from September through June and by 9 am the rest of the year. It is often run well into the evening, frequently on weekends, and occasionally 24 hours a day for experiments, development and repair. This has resulted in a total use that far exceeds the nominal accelerator availability of one 8-hour shift per weekday (~250 shifts per year).

Accelerator use for radiobiology and associated dosimetry was about 85% higher than last year and was the highest level of use since RARAF has been at Nevis Labs, about 20% higher than the previous record. About 74% of

**Table 2. Accelerator Use, January–December 2008**
**Usage of Normally Scheduled Days**

| | |
|---|---|
| Radiobiology and associated dosimetry | 56% |
| Radiological physics and chemistry | 0% |
| On-line facility development and testing | 62% |
| Safety system | 2% |
| Accelerator-related repairs/maintenance | 3% |
| Other repairs and maintenance | 2% |
| Off-line facility development | 30% |

the use for all experiments was for microbeam irradiations and 26% for track segment irradiations. Demand for the Microbeam Facility has increased because it enables selective irradiation of individual cell nuclei or cytoplasm, making it essential for many of the experiments examining the bystander effect. Because of the relatively low number of cells that can be irradiated in a day, microbeam experiments usually require significantly more beam time than broad beam (track segment) irradiations to obtain sufficient biological material, especially for low probability events such as mutation and bystander effects.

Use of the Track Segment Facility was 22% of the experiment time, about the same as last year. Irradiation times for individual samples are usually 30 seconds or less, so that multiple experimenters, as many as 5, can be run in a single shift, sometimes using different LETs and even different types of ions in the same day. Because the facility is used so efficiently, cell irradiations typically are scheduled one day every other week.

For the first time since 2000, there was no utilization of the accelerator for radiological physics. The experiment of last year by Elenea Aprile examining the response of a liquid xenon detector has likely finished and the irradiations of TLDs by Yigal Horowitz have paused for the time being.

On-line facility development and testing surged to 62% of the available time, a new record, 40% higher than last year and 30% higher than the previous record. This includes development and testing of the electrostatically focused microbeam, development of the PMM, the Point and Shoot system, the LD2, the X-ray microbeam, the neutron microbeam and development of new biological techniques (e.g. FRET).

Approximately 26% of the experiment time was used for studies proposed by outside users, about 30% less than what was used last year and 25% less than the average for the last five years.

Online development use increased by about 40% over last year and was at a record level, about 30% higher than the previous record. In addition to beam tests and development of the electrostatically focused microbeam, considerable effort was expended on minimizing the beam spot diameter for the permanent magnet microbeam (PMM) and developing the X-ray microbeam.

There were only 8 shifts of Singletron maintenance and repair time this year, less than 2/3 that of last year. This is equal to the lowest it has been in the last 20 years. We reinstalled the GVM that was sent at the end of 2007 to the manufacturer, High Voltage Engineering Europa (HVEE), for repair. There was also a replacement of some of the column resistors and diodes damaged by a vacuum excursion that occurred when a microbeam exit window broke. The accelerator charging power supply is so stable that we continue to run without terminal voltage regulation by setting the charging current to obtain the desired terminal voltage. The ion source has run very reliably and required no maintenance this year.

Because the beam energy acceptance is so narrow for the electrostatic microbeam and the PMM, beam intensity decreases rapidly as the terminal potential changes by less than a kilovolt. In 2007 a remote computer terminal was installed in the Microbeam II lab to allow the accelerator terminal voltage to be controlled from both the console and the lab. This year a remote computer terminal was installed for the PMM.

**The Use of Wikis for Scientific Dissemination at RARAF**

Much dissemination of information today involves electronic media, for example, online journals (including electronic publication of new articles), WIKIs, blogs, and web sites. The RARAF web site is already a significant repository of information about our microbeam and the technology we are developing. The content of our website is continually updated to reflect the current state of the research at RARAF and to answer questions our users may have. We offer useful information such as the current month's accelerator schedule, keep users apprised of the status of new developments at RARAF through our New Developments section, and also offer a list of papers detailing research performed at RARAF and published in peer-reviewed journals (many available in PDF format free). While we continue to keep the website up-to-date, as discussed below, we plan to expand significantly our online information dissemination program.

A wiki is a page or collection of web pages on a topic designed to enable anyone who accesses it to contribute or modify content. Wikis can be used to create collaborative websites. Our goal is to disseminate information about microbeam technology to the general public and to the microbeam community through Wikipedia, an online encyclopedia. We have already created an encyclopedic entry for "microbeam," (Fig. 1) and we will continue to add content to the microbeam wiki topics of interest to the microbeam community. Our hope is to encourage others to take up the mantle as well.

Some terms that do not exist or have only very limited entries in Wikipedia, but would be useful, include:

- Bystander effect
- RARAF
- Center for Radiological Research
- *In vitro* oncogenic transformation
- Mutagenesis
- Chromosomal aberration
- Mirau optics
- Multiphoton microscopy

Creative use of online media can improve exposure of our field, aid in recruitment of new scientists, train those

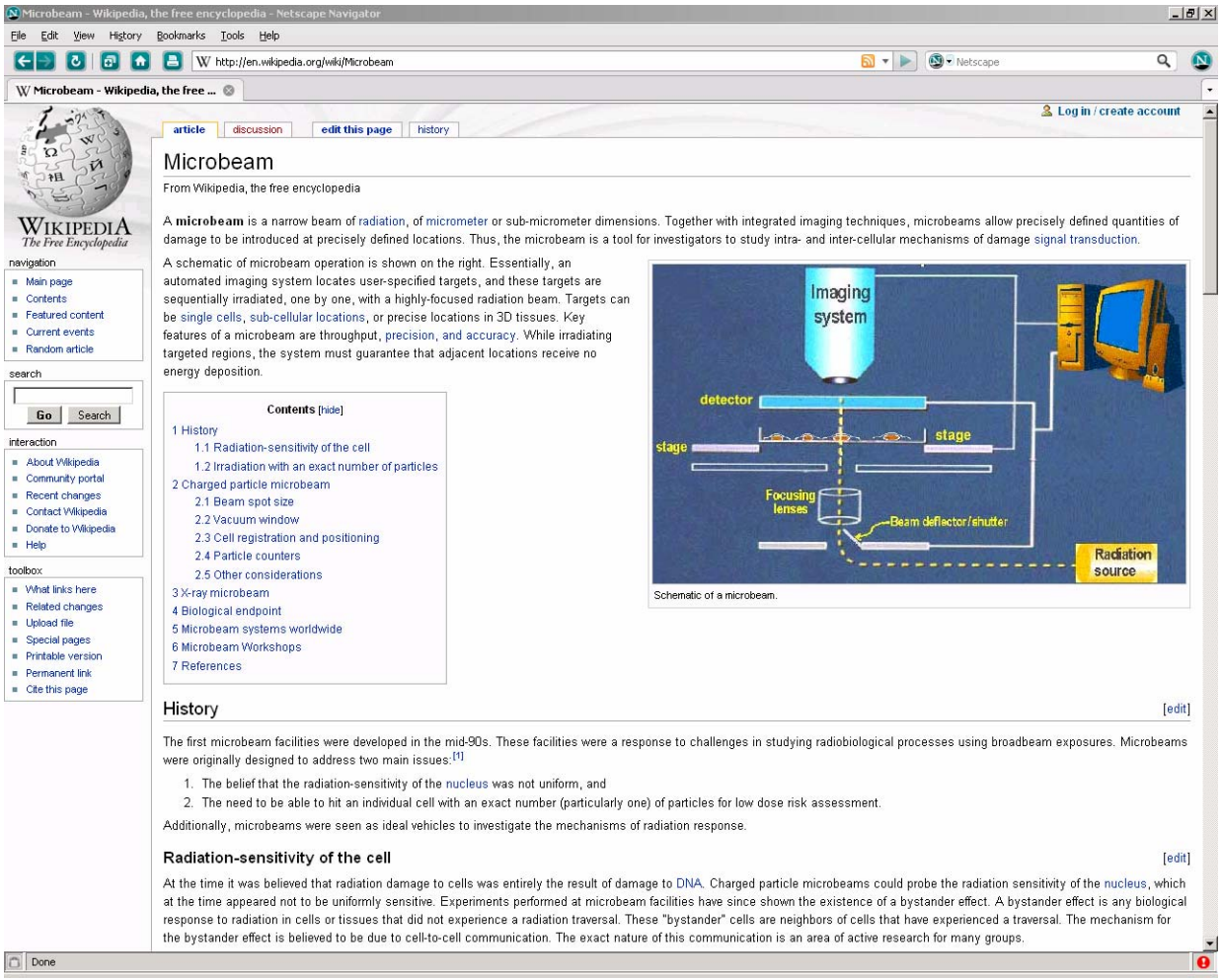


**Fig. 1.** Encyclopedic entry for "microbeam" from Wikipedia.

already in the field, and rapidly disseminate information to accelerate the pace of new discoveries.

## Training

This summer we again participated in the Research Experiences for Undergraduates (REU) project in collaboration with the Columbia University Physics Department. Students attend lectures, work on a research project and present an oral report on their progress at the end of the 10-week program. Andrew Durocher from Wheaton College in Massachusetts worked with Gerhard Randers-Pehrson on a procedure to unfold the energy spectrum of an intense pulsed X-ray microbeam from the piled-up pulses in a gas proportional counter.

## Personnel

The Director of RARAF is Dr. David Brenner, the Director of the Center for Radiological Research (CRR). The accelerator facility is operated by Mr. Stephen Marino, the manager, and Dr. Gerhard Randers-Pehrson, the Associate Director of RARAF.

Dr. Charles Geard, the former Associate Director of the CRR and the Senior Biologist for the P41 grant that is the major support for RARAF, continues to spend most of each day at RARAF.

Dr. Alan Bigelow, an Associate Research Scientist, continues the development of the multiphoton microscopy system that uses a fast Ti-sapphire laser for three-dimensional imaging and as a "microspot" irradiation facility.

Dr. Guy Garty, an Associate Research Scientist, is developing an inductive detector ($LD^2$) for single ions and the permanent magnet microbeam (PMM). He spends about half his time working on the National Institute of Allergy and Infectious Diseases (NIAID) project, for which he is the project manager.

Sasha Lyulko, a graduate student in the Physics Department at Columbia University, is involved in developing methods to image cells without stain and spends about half her time working on the NIAID project.

Dr. Andrew Harken, a Postdoctoral Fellow, is developing the X-ray microbeam and the Point and Shoot targeting system and is working with Guy Garty on the PMM.

Dr. Yanping Xu, a Postdoctoral Fellow, has been working on the development of a neutron microbeam. He is also working on the NIAID project, developing a method for the determination of the number of lymphocytes in blood samples using light absorption and scattering.

Several biologists from the CRR have office space at the facility and use the RARAF biology laboratories to perform experiments:

- Dr. Brian Ponnaiya is an Associate Research Scientist performing experiments using the Track Segment irradiation facility. He now spends much of his time at the CRR.
- Dr. Alexandre Mezentsev, an Associate Research Scientist, is working with cultured tissue systems and spends some of his time at RARAF.
- Dr. Helen Turner, an Associate Research Scientist, is working on the NIAID project and spends about half her time at RARAF. She is also working on the development of FRAP and FRET capabilities for the Microbeam Facility.
- Dr. Antonella Bertucci, a Postdotoral Fellow, arrived in March and spends about half her time at RARAF. She has been working with Helen Turner on the NIAID project and is performing microbeam experiments using *C. elegans* nematodes.

Kenichi Tanaka, a Staff Associate who arrived in August, 2007 from Hiroshima University, Japan for a one-year visit, worked with Gerhard Randers-Pehrson on the detection of explosives. He terminated his visit in March in order to accept a position at the University of Hokkaido.

Julia Schaefer, an undergraduate student from Berufsakademie Karlsruhe (the University of Cooperative Education), Germany, arrived at the end of December for a three-month visit. She is working with Helen Turner on part of the NIAID high-throughput biodosimetry program. She will submit a 25-page report to her university on her learning experience at RARAF.

**Recent Publications of Work Performed at RARAF**


1. Aprile E, Baudis L, Choi B, Giboni KL, Lim K, Manalaysay A, Monzani ME, Plante G, Santorelli R and Yamashita M. New measurement of the relative scintillation efficiency of xenon nuclear recoils below 10 keV. *Phys. Rev. C* **79**, id. 045807, 2009.
2. Bailey SM. Michael Fry Research Award lecture: Telomeres and double-strand breaks - all's well that "ends" well. *Radiat Res* **169**:1-7, 2008.
3. Bertucci A, Pocock RD, Randers-Pehrson G and Brenner DJ. Microbeam irradiation of the *C. elegans* nematode. *J Radiat Res (Tokyo)* **50 Suppl A**:A49-54, 2009.
4. Bigelow AW, Brenner DJ, Garty G and Randers-Pehrson G. Single-particle / single-cell ion microbeams as probes of biological mechanisms (Review article). *IEEE T. Plasma Sci.* **36**: 1424-31, 2008.
5. Bigelow A, Garty G, Funayama T, Randers-Pehrson G, Brenner D and Geard C. Expanding the question-answering potential of single-cell microbeams at RARAF, USA. *J Radiat Res (Tokyo)* **50 Suppl A**:A21-8, 2009.
6. Bigelow AW, Geard CR, Randers-Pehrson G and Brenner DJ. Microbeam-integrated multiphoton imaging system. *Rev Sci Instrum* **79**:123707, 2008.
7. Ghandhi SA, Yaghoubian B and Amundson SA. Global gene expression analyses of bystander and alpha particle irradiated normal human lung fibroblasts: Synchronous and differential responses. *BMC Med Genomics* **1**:63, 2008.
8. Hei TK, Zhou H, Ivanov VN, Hong M, Lieberman HB, Brenner DJ, Amundson SA and Geard CR. Mechanism of radiation-induced bystander effects: a unifying model. *J Pharm Pharmacol* **60**:943-50, 2008.
9. Horowitz YS, Horowitz A, Oster L, Marino S, Datz H and Margaliot M. Investigation of the ionisation density dependence of the glow curve characteristics of LiF:Mg,Ti (TLD-100). *Radiat Prot Dosimetry* **131**:406-13, 2008.
10. Randers-Pehrson G, Johnson GW, Marino SA, Xu Y, Dymnikov AD and Brenner DJ. The Columbia University sub-micron charged particle beam. *Nucl. Instr. Meth. A* (submitted 2008).
11. Zeitlin CJ, Maurer RH, Roth DR, Goldsten JO and Grey MP. Development and evaluation of the combined ion and neutron spectrometer (CINS). *Nucl. Inst. Methods B* **267**: 125-38, 2009.
12. Zhou H, Ivanov VN, Lien YC, Davidson M and Hei TK. Mitochondrial function and nuclear factor-kappaB-mediated signaling in radiation-induced bystander effects. *Cancer Res* **68**:2233-40, 2008. ■

# RSO – TABLE OF CONTENTS



Above. *Standing (l-r):* David Park, David Rubinstein, Salmen Loksen, Igor Kravchuk, Moshe Friedman, Bithi Roy; *sitting:* Jillian Sacheli, Pantea Kadkhodazadeh, Shira Abraham.

Right. *Standing:* Tom Juchnewicz, Salmen Loksen; *sitting:* Shira Abraham, Jennifer Curiel.

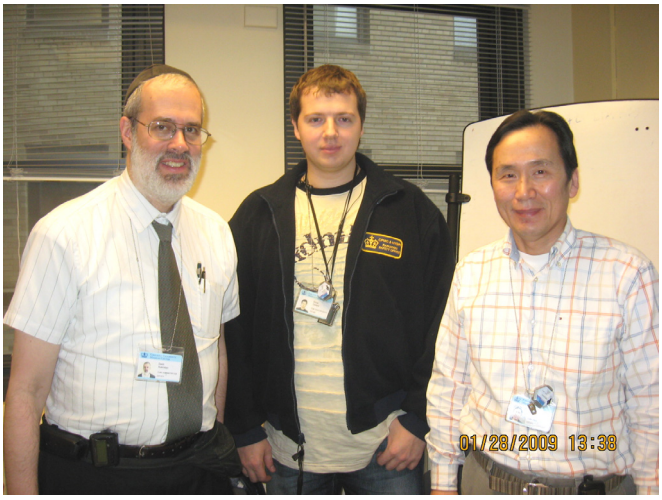


David Rubinstein, Roman Tarasyuk and David Park.

Jillian Sacheli and Dae In Kim.

# RADIATION SAFETY OFFICE STAFF


**RSO Staff** *(l-r) front row*: James Donlan, Shira Abraham, Bithi Roy, Maria Taveras, Jillian Sacheli and Roman Tarasyuk; *back row:* Thomas Cummings, David Rubinstein, Salmen Loksen, Thomas Juchnewicz, Igor Kravchuk and Moshe Friedman; *not shown:* Bruce Emmer, Dae In Kim, David Park Pantea Kadkhodazadeh and Jennifer Curiel.

## PROFESSIONAL STAFF

**Salmen Loksen**, CHP, DABR; Director, Radiation Safety Officer
**Ahmad Hatami**, DABR, DABMP; Assist. Dir., Assist. Radiation Safety Officer (left 12/2008)
**Thomas Juchnewicz**, DABR; Assist. Radiation Safety Officer
**Bruce Emmer**, DABMP, DABR; Physicist
**Dae In Kim**, MS, Health Physicist
**Shinkyu (David) Park**, MS, Radiation Protection Supervisor
**Charles Geraghty**, BS, Assist. Physicist (left 6/2008)
**James Donlan**, DABR, Assistant Physicist
**Pantea Kadkhodazadeh**, BS, Assistant Physicist
**Thomas Cummings**, BS, Assistant Physicist

## TECHNICAL STAFF

**David Rubinstein**, BS, Senior Technician
**Jaclyn Marcel**, MS, Technician B (left 6/2008)
**Shira Abraham**, BS, Technician B
**Igor Kravchuk**, MS, Technician B
**Bithi Roy**, BA, Technician B
**Roman Tarasyuk**, Technician B

## ADMINISTRATIVE & OFFICE SUPPORT STAFF

**Moshe Friedman**, BRE, Office Administrator
**Jillian Sacheli**, BA, Administrative Aide
**Maria Taveras**, BA, Senior Clerk
**Jennifer Curiel**, BS, Clerk B

During the July 15, 2008 CAMPEP visit to the CUMC campus (see page 141), Salmen Loksen, David Park with Edward A. Christman, CHP, Ph.D., Columbia University Consultant in Health Physics and Occupational Health & Safety.

# RADIATION SAFETY OFFICE

## INTRODUCTION

Grayson L. Kirk, President of Columbia University, distributed a memo, dated May 19, 1957, entitled "Directive to All University Departments Having a Source of Ionizing Radiation," advising all parties of the expanded function of the Radiation Safety Committee.

A notice entitled "Radiation Safety Guide for Columbia University," dated February 10, 1959, named Philip M. Lorio as Health Physics Officer for University Departments and Laboratories other than the College of Physicians & Surgeons, where Dr. Edgar Watts was named Health Physics Officer. Dr. Gioacchino Failla chaired the Radiation Safety Committee and initiated the Radiological Research Laboratory in Columbia University's Department of Radiology.

By agreement between Columbia University and New York Presbyterian Hospital in 1962, the Radiation Safety Office was established as an autonomous unit for the purpose of maintaining radiation safety. The Joint Radiation Safety Committee (JRSC), appointed by the Medical Board of the New York Presbyterian Hospital and the Vice President for Columbia University's Health Sciences Division, was charged with the responsibility of defining and ensuring enforcement of proper safeguards in the use of sources of ionizing radiation.

Dr. Harald H. Rossi, Director of the Radiological Research Laboratory, was appointed Chairman of the Joint Radiation Safety Committee. Under his direction this committee developed a "Radiation Safety Code & Guide," which is administered by the Radiation Safety Officer. In 1984 Dr. Eric J. Hall became the next Director of the Radiological Research Laboratory, subsequently renamed the Center for Radiological Research, and also followed as JRSC Chairman. In 2008, after Dr. Hall's his retirement from these roles, Dr. David J. Brenner succeeded him as Director of the Center for Radiological Research and JRSC Chairman.

The present Joint Radiation Safety Committee of Columbia University Medical Center, New York Presbyterian Hospital and New York State Psychiatric Institute came into existence through an agreement made on February 12, 1991 between the three institutions. The agreement combined several overlapping clinical and educational programs, including all programs for ensuring radiation safety. The current Director of the Radiation Safety Office and Radiation Safety Officer, Salmen Loksen, CHP, DABR, was appointed on December 16, 1996.

The Radiation Safety Office reports to and advises the Joint Radiation Safety Committee, which meets on a quarterly basis. At the present time the Radiation Safety Officer reports on professional and technical matters to Dr. David Brenner, Chair of the JRSC, and on budgetary matters to Dr. Robert S. Kass, Vice Dean for Research, who represents Dr. Lee Goldman, Dean of Columbia University Medical Center. In addition, the Radiation Safety Office participates in the review of research protocols for the Radioactive Drug Research Committee (RDRC) under the jurisdiction of the U.S. Food and Drug Administration.

Radiation Safety Office staff are Columbia University employees. The Radiation Safety Office is funded by a cost sharing arrangement between Columbia University, New York Presbyterian Hospital and New York State Psychiatric Institute.

## OVERVIEW OF RESPONSIBILITIES

Collectively, Columbia University Medical Center, New York Presbyterian Hospital and New York State Psychiatric Institute form a large health sciences complex with extensive teaching, research, and clinical facilities. The basic goal of the Radiation Safety Office is to ensure implementation of all protective measures necessary to guarantee that doses from ionizing radiation to patients, visitors, students, faculty and staff on campus, as well as to the community at large, remain "as low as reasonably achievable" (ALARA). Major entities supported by Radiation Safety Office services include:

- Columbia University Medical Center
- New York Presbyterian/Columbia Center
- New York State Psychiatric Institute
- New York Presbyterian/Allen Pavilion
- New York Presbyterian/Morgan Stanley Children's Hospital (CHONY)
- Kreitchman PET Center Radiopharmacy
- CUMC Integrated Imaging Center
- Dental facilities on the CUMC/NYPH/NYSPI campus and elsewhere (as described on page 145 of this report).

The projected completion of several additional buildings, as well as the Columbia University Medical Center Integrated Imaging Center will add to the responsibilities of the Radiation Safety Office in the near future. For the purposes of this report, this collection of entities will hereafter be referred to as CUMC/NYPH/NYSPI.

Reporting to the Joint Radiation Safety Committee of CUMC/NYPH/NYSPI, the Radiation Safety Officer and the staff of the Radiation Safety Office are responsible for obtaining and maintaining licenses authorizing the possession and use of radioactive materials and obtaining and maintaining registrations and permits for the operation of radiation producing equipment. In addition, the Radiation Safety Office is responsible for obtaining and maintaining permits necessary for the safe disposal or controlled release of research and medical wastes containing radioactivity.

The Radiation Safety Office ensures that authorized users of radioactive materials and radiation producing equipment comply with all governmental regulatory requirements and guidelines by means of training, education, consultation, and by a program of internal audits, as well as the inspections of facilities. Regulatory agencies charged with over-

seeing the possession, use, or disposal of radioactive materials or radiation producing machines include:

- United States Environmental Protection Agency (EPA)
- United States Food and Drug Administration (FDA)
- United States Nuclear Regulatory Commission (NRC)
- New York State Department of Environmental Conservation (NYS DEC)
- New York State Department of Health (NYS DOH)
- New York City Department of Health & Mental Hygiene (NYC DOHMH), Office of Radiological Health

New York City Department of Health & Mental Hygiene, New York State Department of Environmental Conservation, and United States Food and Drug Administration conduct periodic inspections and audits of CUMC/NYPH/NYSPI facilities operating under their licenses or permits. The Radiation Safety Office works continuously to prevent regulatory violations and swiftly implements any regulatory recommendations.

The Radiation Safety Office also ensures compliance with institutional policies and procedures published in the "Radiation Code & Guide of Columbia University Medical Center, New York Presbyterian Hospital & New York State Psychiatric Institute."

## SUMMARY OF OPERATIONS 2008

A summary of activities performed and services provided by the Radiation Safety Office is presented below. While inclusive of most major activities and services, the summary is by no means exhaustive, however, it is intended to provide a representative overview of departmental operations. An unabridged compilation of Radiation Safety Office activities and services may be found in the Minutes of the Quarterly Meetings of the Joint Radiation Safety Committee of CUMC/NYPH/NYSPI.

Statistical data presented are from the calendar year, January 1, 2008 through December 31, 2008. Activities are covered through the beginning of 2009.

### ***New York City Department of Health & Mental Hygiene, Office of Radiological Health – Maintenance of Licenses, Registrations, Permits, and Audits and Inspections***

A primary activity of the Radiation Safety Office is the continued maintenance of City of New York Radioactive Materials Licenses, Certified Linac Registrations and X-Ray Permits. Currently this includes:

- Radioactive Materials License No. 75-2878-01 – Broad Scope Human Use
- Radioactive Materials License No. 74-2878-03 – Broad Scope Non- Human Use
- Radioactive License No. 52-2878-04 – PET Cyclotron Facility in the Milstein Building
- Radioactive Materials License No. 52-2878-06 – the new Integrated Imaging Center PET Cyclotron Facility
- Radioactive Materials License No. 93-2878-05 – Gamma Knife
- Columbia-Presbyterian Hospital Radiation Installation Permit H96 0076353-86 – Broad Scope X-ray Permit
- Therapeutic Radiation LINAC Unit Certified Registration No. 77-0000019 – New York Presbyterian Hospital, 622 W. 168th Street, New York, NY 10032.
- Columbia-Presbyterian–Allen Pavilion Radiation Installation Permit H96 0076383 86 – Allen Pavilion, 5141 Broadway, New York, NY 10032
- X-ray Permit H91 1292556-84 – CUMC Dental Associates Faculty Practice, 100 Haven Ave, New York, NY 10032.
- Columbia University Radiation Installation Permit H98 1005495-72 – Baker Field Gymnasium, Morningside Campus, 500 West 120th Street, New York, NY 10027.
- Columbia University Radiation Installation Permit H98 1295353-78 – Baker Athletic Complex, 533 W. 218th Street, New York, NY 10034.
- Columbia University Physicians Metabolic Diseases Unit, Bone Density Permit H98-1162695 76 – Harkness Bldg. 9th fl., 180 Ft. Washington Ave., NY, NY 10032

Activities performed in 2008 to maintain the City of New York Licenses, Registrations and Permits included:

**Human Use License amendment:** An application to amend NYC DOHMH Broad Scope Human Use License No. 75-2878-01 was completed and submitted to the NYC DOHMH on June 23, 2008. The amendment application is limited to adding several new radioactive sources and a description of the new CUMC Integrated Imaging Center PET Imaging Facility to the existing Human Use License, to authorize the possession of certain Ga/Ge 68 sealed sources for use the in new PET/CT Scanners in the CUMC Integrated Imaging Center. At the beginning of 2009 the Radiation Safety Office was still awaiting NYC DOHMH's reply.

In the interim, Siemens shipped the new sources with the scanners on the basis of the general possession limits for Ga/Ge 68 in the existing Human Use License.

**Human Use License amendment – SIR Spheres:** On September 28, 2008 a quorum of the JRSC voted to approve an Amendment to NYC DOHMH Radioactive Materials License No. 75-2878-01 (Human Use) requesting authorization for the possession and use of 32 Gigabecquerals of Yttrium-90, as SIR Spheres® sealed sources. SIR Spheres® are used for the treatment of unresectable hapatocelluar carcinoma. The Radiation Safety Office submitted this amendment request to the NYC DOHMH.

On March 16, 2009 the Radiation Safety Office received Amendment No. 27 to NYC DOHMH Radioactive Materials License No. 75-2878-01 authorizing possession and use of SIR Spheres brachytherapy sources.

**Human Use inspection:** From October 2, 2008 through October 21, 2008 the City of New York Department of Health and Mental Hygiene conducted an audit of records and inspection of activities conducted under Broad Scope Human Use License No. 75-2878-01 at New York Presbyterian Hospital and Columbia University Medical Center. This audit and inspection included such Departments as: Nuclear Medicine, Nuclear Cardiology, Transfusion Services, and brachytherapy activities of the Department of Radiation Oncology. On November 17, 2008 the City Inspector conducted an exit interview with Andria Castellanos, Vice

President and COO, New York Presbyterian Hospital, and informed her that the Departments appeared to be in full compliance with City regulatory requirements and license conditions. At the beginning of 2009 the Radiation Safety Office was still awaiting NYC DOHMH's written report.

**Non-Human Use inspection:** Starting on March 3, 2008 the New York City Department of Health and Mental Hygiene, Office of Radiological Health conducted an inspection of Radioactive Materials License #74-2878-03, which authorizes the extensive activities at CUMC and NYSPI that involve the non-human use of radioactive materials. The NYC DOHMH inspector randomly audited about 50 research laboratories throughout the CUMC and NYSPI campus for compliance with the regulations for the use of radioisotopes as set forth in RCNY Article 175 and audited the facilities, records and policies of the Radiation Safety Office. On April 18, 2008 the Radiation Safety Office received the written report of the NYC DOHMH inspection dated April 16, 2008. The report stated that: "*At the time of inspection, it was found that your facility was in compliance with the requirements of Article 175 of NYC Health Code and the conditions of your license*."

**Cyclotron License renewal:** On October 23, 2007 the Radiation Safety Office submitted to the New York City Department of Health and Mental Hygiene a completed Application for the renewal of NYC DOHMH Radioactive Materials License No. 52-2878-04 and on the same day received from the NYC DOHMH a Letter of Timely Renewal. License No. 52-2878-04 authorizes the operations of the CUMC Cyclotron Radiopharmacy and Radioligand Laboratory. On February 5, 2008 the Radiation Safety Office received a five-year renewal of the above License, with expiration date of October 31, 2012.

**License for new CUMC Integrated Imaging Center:** On April 23, 2008 a first draft of the Radioactive Materials License Application for the CUMC Integrated Imaging Center (NYSTAR) was submitted for review and approval of the NYC DOHMH. On July 25, 2008 the Radiation Safety Office received City of New York Radioactive Materials License No. 52-2878-06, dated June 18, 2008, with an expiration date of July 31, 2013.

The new License for the CUMC Integrated Imaging Center authorizes the possession and use of up to: 296 Gigabecquerals of Carbon-11, 29.6 Gigabecquerals of Nitrogen-13, 296 Gigabecquerals of Oxygen-15 and 444 Gigabecquerals of Flourine-18. The new facility, located in the basement and 1st Floor level of the Allan Rosenfield Building at 722 West 168th Street (Mailman School of Public Health Building), includes: two Siemens RDS-111 Eclipse HP Cyclotrons, each with two beam lines and six targets, a Radiopharmacy, a GMP Laboratory and a Radioisotope Research Laboratory.

**Gamma Knife License renewal:** On October 22, 2007 the Radiation Safety Office submitted to the New York City Department of Health and Mental Hygiene a completed Application for the renewal of NYC DOHMH Radioactive Materials License No. 93-2878-05 and on the same day received from NYC DOHMH a Letter of Timely Renewal. License No. 93-2878-05 authorizes the operation by the New York Presbyterian Hospital Department of Radiation Oncology Gamma Knife. On February 5, 2008 the Radiation Safety Office received a five-year renewal of the above License, with expiration date of October 31, 2012.

**Gamma Knife inspection:** From October 22, 2008 through October 23, 2008 the New York City Department of Health and Mental Hygiene conducted an audit of records and inspection of activities conducted under Radioactive Materials License No. 92-2878-05 which authorizes the operation of the Gamma Knife in the Department of Neurosurgery, New York Presbyterian Hospital. On November 17, 2008 the City Inspector conducted an exit interview with Andria Castellanos, Vice President and COO, NYPH, and informed her that the Department appeared to be in full compliance with City regulatory requirements and license conditions. At the beginning of 2009 the Radiation Safety Office was still awaiting NYC DOHMH's written report.

**New York Presbyterian Hospital Linac Registration amendments and renewal:** On June 21, 2007 a quorum of the JRSC voted to approve an amendment of City of New York Therapeutic Radiation Linac Unit Certified Registration No. 77-0000019 to remove the Varian Associates Clinac 2100C/D listed on the Registration and authorizes replacement by a Varian Associates Trilogy 2300TX. On December 19, 2007 the Radiation Safety Office submitted to the New York City Department of Health and Mental Hygiene the completed Amendment Application for Therapeutic Radiation Linac Unit Certified Registration No. 77-0000019. On March 3, 2008, the Radiation Safety Office received Amendment No. 6 to the Registration. Registration No. 77-0000019 with an expiration date of August 31, 2008. The Trilogy 2300TX was placed into patient service.

On July 15, 2008 the Radiation Safety Office filed an application for the renewal of the City of New York Therapeutic Linac Unit Certified Registration. The renewal application requested that the NYC Department of Health & Mental Hygiene allow the continued operation of three therapeutic linear accelerators in New York Presbyterian Hospital, Department of Radiation Oncology for an additional five-year period. On September 18, 2008 the Radiation Safety Office received City of New York, Therapeutic Linac Unit Certified Registration No. 77-0000019, Amendment No. 7, dated July 30, 2008, with an expiration date of August 31, 2013, authorizing operation of the therapeutic linear accelerators for the requested five year period. Another modification of the Registration, Amendment #8, dated October 29, 2008, was received. The Registration has an expiration date of August 31, 2013.

**CUMC/NYPH Broad X-ray Permit inspection:** Beginning on January 15, 2008 New York City Department of Health and Mental Hygiene conducted a biannual inspection of CUMC/NYPH/NYSPI X-Ray Permit No. H96 0076353 86. The inspection was concluded on January 29, 2008 with an exit interview in Dr. Alderson's Office. On March 17, 2008 the Radiation Safety Office received the written report of the NYC DOHMH inspector dated February 14, 2008. The report stated that: "*Radiological equipment inspection*

*performed on 1/29/2008 disclosed No violations of Article 175 of NYC Health Code*." No recommendations were made.

**CUMC/NYPH Broad X-ray Permit renewal:** On October 28, 2008 the Radiation Safety Office received the renewal of the CUMC/NYPH Broad X-ray Permit No. H96 0076353 86 that covers all the x-ray facilities in the Medical Center campus. The renewed X-ray Permit will expire on October 31, 2010.

**Allen Pavilion X-ray Permit renewal:** On December 16, 2008 the Radiation Safety Office received the renewal of NYC DOHMH X-ray Permit No. H96 0076383 86 that covers x-ray facilities at the NYPH-Allen Pavilion, 5141 Broadway, New York, NY. The renewed X-ray Permit will expire on December 31, 2010.

**Web-based RAM inventory:** New York City Department of Health and Mental Hygiene Office of Radiological Health launched its Web-based Radioactive Material Inventory Tracking System in early September 2007. The NYC DOHMH Material Inventory Tracking System requires that: Licensees receiving, possessing, using, storing or transferring more than 500 mCi (18.5 GBq) of radioactive material submit an accurate electronic inventory to the Office of Radiological Health on a quarterly basis.

The Radiation Safety Office compiled inventory records for hospital and research areas, and completed the required first quarter 2008 data entry. Since that time the requirement for this Web-based reporting was suspended pending system updating and improvement.

**Emergency radiation equipment – area monitors and policy:** As reported previously, the Radiation Safety Office and Emergency Departments of New York Presbyterian Hospital, Allen Pavilion, and Morgan Stanley Children's Hospital of New York were awarded three grants from NYC DOHMH's Hospital Radiation Equipment Project.

The Radiation Safety Office oversaw the distribution and installation of the radiation monitoring equipment, in coordination with IT, Facilities and Security personnel. It is planned that information generated will be logged on computers in the NYPH Security Department and in the Radiation Safety Office. The Radiation Safety Office developed a policy and procedure document for the Area Radiation Detection Systems, and initiated a training program for Hospital end-users.

On February 14, 2008, in order to assess the current status of hospital radiation preparedness and to assist participating hospitals in achieving this goal, staff from New York City Department of Health & Mental Hygiene's Healthcare Emergency Preparedness Program and Office of Radiological Health conducted a site visit to the Allen Pavilion, met with staff involved in radiation preparedness, and reviewed the installation of area radiation detectors and the facility's response plans to alarms from any of the area monitors.

On March 14, 2008 the NYPH Environment of Care Council, at its regularly scheduled meeting, approved area radiation detection system policy and procedure that establishes guidelines for responding to area monitor alarms, and for treatment and management of potentially contaminated persons identified by the area monitors. This policy and procedure was produced through a joint effort of the Radiation Safety Offices of NYPH/Columbia and NYPH/Cornell.

At the end of 2008 area monitors had been installed in: Energy Court Security Desk, NYPH Pediatric Walk-In Entrance, NYPH Adult Walk-In Entrance, VC Ambulance Bay Entrance, CHONY Ambulance Bay Entrance, CHONY Lobby Security Desk, and Milstein Lobby Security Desk. The area monitors have the capability of detecting contaminated patients during a radiation 'event.'

**Increased Controls regulations:** US NRC regulations for Increased Controls affect Columbia University activities under NYC DOMHM Radioactive Materials Licenses #74-2878-03 (Columbia University Medical Center, 168th Street, New York, NY), and #74-0303-01 (Columbia University Morningside Campus, 116th Street, New York, NY), CUMC and New York Presbyterian Hospital activities under NYC DOMHM Radioactive Materials License #75-2878-01 and New York Presbyterian Hospital activities under NYC DOMHM Radioactive Materials License #93-2878-05.

**NYC DOHMH Symposium on Increased Controls regulations and Hospital Radiation Detection Program:** On February 28, 2008, the Radiation Safety Officer received an e-mail communication from the Office of Radiological Health of the New York City Department of Health and Mental Hygiene informing the RSO of a symposium on the Physical Security of Radioactive Sources and Implementation of USNRC Increased Control to take place April 1, 2008 at the NYU Kimmel Center. The e-mail communication indicated that Radiation Safety Officers and Security Directors should attend. Salmen Loksen, Radiation Safety Officer and staff attended. Topics discussed included: Malicious Uses of Radiation Sources; Physical Security of Radioactive Sources; Implementation of the Increased Control Requirements – Fingerprinting Requirements.

A separate afternoon session focused on the NYC DOHMH Hospital Radiation Area Detection Program. Salmen Loksen, RSO, delivered a presentation on the installation of the emergency equipment at New York Presbyterian/Columbia Center and highlighted how our institution is resolving networking issues for the area monitors, with lessons that apply throughout New York City.

**Increased Controls – fingerprinting requirements:** On May 7, 2008 the Radiation Safety Office received NYC DOHMH Information Notice ORH 2008-01, Fingerprinting and Criminal History Check Requirements for Individuals Having Unescorted Access to Radioactive Materials of Concern, dated April 25, 2008, which when implemented will add to the requirements set forth in the Order Of The Commissioner To Licensees Possessing Certain Radioactive Materials In Quantities Of Concern In The City Of New York, dated November 30, 2005.

Specifically, licensees are required to enhance their increased controls programs by submitting to the NRC fingerprints of each individual the licensee wishes to permit unescorted access to certain radioactive material. The NRC will forward the fingerprints to the FBI for a criminal history record check. The information will be returned from the FBI

to the NRC, which forwards it to the licensee. Licensees are required to appoint Trustworthiness and Reliability (T&R) Officials, with responsibility to review information returned by the FBI/NRC, and determine the trustworthiness and reliability of individuals requiring unescorted access privileges to radioactive materials of concern. The T&R reviews are to be based on NRC guidelines attached to Information Notice ORH 2008-01 and potential future Notices.

On March 13, 2008 the Radiation Safety Officer met with the new CUMC Director of HR, Louis Lemieux for a general discussion of the requirements of Increased Controls regarding Unescorted Access to certain radioactive sources by CUMC employees.

**Increased Controls – meetings & follow up:** The Radiation Safety Office organized a meeting for those individuals at CUMC with responsibility for implementing increased controls. The meeting took place on June 18, 2008 with representation from Human Resources, Faculty Affairs, Public Safety, Legal Counsel and EH&S, to discuss the development of the new regulations, when they would become legally binding, and the compliance deadlines.

Also discussed were matters pertaining to the fingerprinting process. Mr. Loksen met with James Verdicchio, CUMC Public Safety in order to contact the NRC to discuss the possibility of taking fingerprints internally, in-house with our own security departments. Subsequently Mr. Loksen discussed this issue with Richard Irizarry, Director, and Dan Lord, Manager of Operations, NYPH Security. Mr. Loksen also discussed the in-house fingerprinting option with Tobias Lickerman, NYC DOHMH, and Doug Broaddus, Sr. Project Manager, NRC.

At the meeting it was tentatively decided that the Trustworthiness & Reliability (T&R) Officials for Columbia University, for both CUMC and Morningside campuses, would be a team of CUMC HR Representatives, who would work together with CU Legal Counsel to clarify any questions concerning the Trustworthiness & Reliability determination and how to respond to the FBI criminal report information received. A similar plan was accepted by New York Presbyterian/Columbia Center, that the T&R Officials would be HR Representatives, who would work together with the NYPH Legal Counsel for clarification of any questions.

At the meeting it was agreed that a letter would be generated and sent to all individuals currently approved for unescorted access privileges informing them of the new fingerprinting regulations. Regulations require that employees who are to be fingerprinted must receive a copy of Information Notice ORH 2008-01.

A second meeting concerning Increased Controls for Columbia University and NYPH was held on July 1, 2008. Attending this meeting were representatives from Human Resources, Faculty Affairs, Public Safety, Security, Legal Counsel and EH&S from the respective institutions.

Salmen Loksen, Director, RSO, reported that in a phone conversation on September 17, 2008 Tobias Lickerman, Director, Radioactive Materials Section, NYC DOHMH, confirmed that the Final Rule had been adopted by the Board of Health as scheduled on September 17, 2008 and that the effective date of the new law would be on or about October 22, 2008. Mr. Lickerman indicated that variances for extensions may be granted on a case by case basis.

On October 27, 2008 the Radiation Safety Office received City of New York Dept. of Health & Mental Hygiene Information Notice ORH 2008-04, dated October 17, 2008 regarding *Fingerprinting Requirements For Individuals Having Unescorted Access To Radioactive Materials Of Concern*. The Information Notice describes the steps taken to revise New York City Health Code, Article 175 (Radiation Control) to incorporate the new NRC regulations. Information Notice ORH 2008-04 provides a detailed timetable for implementation, with a final date of April 23, 2009.

The New York City Department of Health and Mental Hygiene Fingerprinting Compliance Timeline requires that a fingerprinting program be in place and Trustworthiness and Reliability (T&R) Officials be certified by January 23, 2009; and that fingerprints have been submitted and FBI criminal history records have been reviewed for all individuals authorized to have unescorted access by April 23, 2009.

**Certification of trustworthiness & reliability officials:** In compliance with the above NYC DOHMH and USNRC requirements CU Morningside, CUMC and NYPH completed the process of certifying Trustworthiness and Reliability (T&R) Officials.

On behalf of Columbia University activities under NYC DOMHM Radioactive Materials Licenses #74-2878-03 (Columbia University Medical Center, 168th Street, New York, NY), and #74-0303-01 (Columbia University Morningside Campus, 116th Street, New York, NY), three individuals will serve as T&R Officials: Louis Lemieux, Chief Human Resources Officer, CUMC & Executive Director, Christine DeAbreu-Henriquez, Director, HR Operations, CUMC Human Resources, and Inez Ruiz, CUMC HR Operations Representative.

On behalf of New York Presbyterian Hospital activities under NYC DOMHM Radioactive Materials Licenses #75-2878-01 and #93-2878-05 two individuals will serve as T&R Officials: Stacie Williams, Director, Labor Employee Relations, Human Resources, and Shawn McCollister, Manager, Labor Relations, Human Resources.

**Communication with CU Morningside, CUMC and NYPH employees regarding fingerprinting compliance:** The Radiation Safety Office forwarded copies of New York City Department of Health and Mental Hygiene Information Notices 2008-01 and 2008-04, pertaining to the new fingerprinting requirements for unescorted access to Radioactive Sources of Concern, to the management of the concerned research labs, Transfusion Services and the Gamma Knife. With the guidance of CU Legal Counsel the Radiation Safety Office prepared an authorization form for unescorted access users to certify their receipt of the Information Notice requiring fingerprinting and their consent for the fingerprinting process. For CUMC employees the Radiation Safety Office distributed a notice from James Verdicchio, CUMC Public Safety, informing individuals who need to be fingerprinted the preferred days and times scheduled by CUMC Public Safety for processing fingerprints. NYPH employees

were referred to NYPH Security Department. Radiation Safety Office staff met with management and employees of the research labs, Transfusion Services and the Gamma Knife to review and implement the new requirements.

**NYS DOH facility inspection:** On January 22, 2008 Radiation Safety Office staff attended a meeting in preparation for the New York State Department of Health, Metropolitan Area Regional Office, pre-opening survey for the new Trilogy 2300 TX Linac installation in the NYPH Department of Radiation Oncology. The NYS DOH MARO survey was conducted on January 29, 2008. The survey consisted of an audit for compliance with New York State required safety regulations for major new hospital installations. This audit included a review of: shielding design for the linear accelerator facility, radiation safety surveys of the linear accelerator facility and actions taken with regard to amending the NYC DOHMH Certified Linac Registration to authorize operation of the facility. During an exit interview with Sylvia Esteves, NYPH administrator of the Department of Radiation Oncology, the NYS DOH inspector indicated that the facility appeared to be in compliance. On February 21, 2008 Herbert Pardes, M.D., President/CEO NYPH, received a written report from Patricia Jones, R.N., M.N., Deputy Regional Director, NYS DOH MARO, that approval was granted to utilize the linear accelerator.

**NYS DOH licensing for practice of nuclear medicine:** The Radiation Safety Office reminded members of the JRSC that after January 1, 2009 only individuals licensed by the New York State Department of Health will be permitted to practice nuclear medicine technology. Individuals who hold certificates from the Nuclear Medicine Technology Board or the American Registry of Radiologic Technologists should automatically qualify for the new License. It is the understanding of the Radiation Safety Office that the Licensing of Nuclear Medicine Technologists may allow them, after appropriate training, to be credentialed to operate PET/CT imaging equipment.

**US NRC concern about cesium-137 chloride:** The Radiation Safety Office received from the US NRC a Request for Comments on the Security and Continued Use of Cesium-137 Chloride Sources and Notice of Public Meeting [NRC-2008-0419], dated July 24, 2008.

This document provided notice of a public meeting and solicited comments regarding the use of Cesium Chloride (CsCl) in licensed irradiators. Such irradiators are typically used for research and to process blood transfusion products. Issues for discussion included: alternatives to the use of CsCl sources; the use of other chemical and physical forms of Cs-137; the use of other isotopes; alternative technologies; the possible phase out of CsCl sources; and the associated regulatory changes and impact on industry and manufacturers. The public meeting was scheduled for September 29-30, 2008. Comments to the US NRC were to be submitted by September 30, 2008.

On December 12, 2008 the Radiation Safety Office received an e-mail document from the US NRC, titled NRC News, No. 08-223 NRC Staff Recommends Security Over Replacement Of Cesium Chloride Radiation Sources, dated December 12, 2008. The document states: *"The Nuclear Regulatory Commission staff has recommended a continued emphasis on improving the security of cesium chloride radiation sources instead of replacing or banning them, citing their beneficial uses in medicine and industry and the lack of effective alternatives at the present time."*

**Annual report 2007:** NYC Article 175.03(b)(1)(iv), requires that the radiation safety committee "shall oversee all uses of radiation-producing equipment and radioactive materials within the facility, shall review the activities of the radiation safety officer, and shall review the radiation safety program at least annually." NYC Article 175.03(b)(1)(ix) requires that the committee shall "review the radiation protection program content and implementation at intervals not to exceed twelve months."

In addition, City of New York Department of Health, Office of Radiological Health License Guide 10.8 Revision 2 requires that the committee shall *"review at least annually the RSO's summary report of the entire radiation safety program to determine that all activities are being conducted safely, in accordance with regulations and the conditions of the license, and consistent with the ALARA program and philosophy. The review must include an examination of records, reports from the RSO, results of Bureau of Radiological Health inspections, written safety procedures, and the adequacy of the management control system*."

In accordance with this the Radiation Safety Officer submitted the 2007 annual summary report of the Radiation Safety Program, with a representative summary of activities and services provided. While inclusive of most major activities and services, the summary is by no means exhaustive, but is intended to provide an overview of radiation safety operations. Additional information with regard to Radiation Safety activities and services may be found in the Quarterly Reports of the Radiation Safety Office and the Minutes of the Joint Radiation Safety Committee.

***New York State Department of Environmental Conservation – Maintenance of Permits, and Audits & Inspections***

Another primary activity of the Radiation Safety Office is the continued maintenance of New York State Department of Environmental Conservation Radiation Control Permit No. 2-6201-00056/00006. This year has seen unprecedented activities due to the construction and startup of the new CUMC Integrated Imaging Center, and receipt of its associated NYS DEC Radiation Control Permit No. 2-6201-00056/00008.

CUMC/NYPH/NYSPI conducts medical research and clinical activities that discharge limited and controlled quantities of radioisotopes to the atmosphere and to sewage systems as per the Conditions of the Radiation Control Permit and in compliance with New York State 6 NYCRR Part 380, Rules and Regulations for Prevention and Control of Environmental Pollution by Radioactive Materials.

The institutions served by the Radiation Safety Office are situated within a densely populated urban area. The quantities of radioisotopes discharged and the resulting public radiation dose are closely regulated by the New York

State Department of Environmental Conservation. Radiation doses to the general public resulting from atmospheric discharges of radioisotopes may not exceed the USNRC Constraint Limit of 10 mrem per year. This amounts to only a fraction of the annual naturally occurring background radiation level.

CUMC/NYPH/NYSPI is currently permitted a total of 16 atmospheric emission points for discharge of radionuclides to the atmosphere. A major continuing activity of the Radiation Safety Office is monitoring, analyzing, reporting, and minimizing discharges from these emission points, in order to ensure compliance with the Conditions of the Radiation Control Permit. Activities performed in 2008 to maintain the NYSDEC Radiation Control Permit included:

**Permit modification – C-11:** On April 4, 2008 the Radiation Safety Office received the revised Radiation Control Permit in which the Permit Annual Limit for C-11 discharges from the Radioligand Laboratory was increased from 12 Curies to 17 Curies. The Permit modification document is dated October 30, 2007.

**Annual report of 2007 discharges:** On March 5, 2008, the Radiation Safety Office, in accordance with the requirements of 6 NYCRR 380-9.1, submitted to the New York State Department of Environmental Conservation an Annual Report for Year 2007 summarizing atmospheric discharges authorized by Radiation Control Permit No. 2-6201-00005/00006. The Report included calibration information on the PET effluent stack monitoring systems. In summary, all atmospheric discharges of radionuclides for the Calendar Year 2007 were within Permit Annual Limits and the calculated radiation dose to the general public from these discharges is within the NYS DOH 10 mrem per year limit.

The NYS DEC year 2008 annual report and calibration for CUMC Kreitchman PET Center Radiation Control Permit No. 2-6201-00056/00006, will be submitted before the March 31, 2009 due date. Atmospheric discharges for Year 2008 for all radionuclides from all emission points are within the Permit Annual Limits.

**Quarterly audits:** Audits of records and inspections of facilities and operations for the Cyclotron Radiopharmacy, Radioligand Laboratory and PET Imaging Suite are completed on a quarterly basis. No violations were reported for any of the facilities inspected.

**Filter changes:** On Saturday, June 21, 2008 the Radiation Safety Office cleared 36 filters for the Cyclotron and Radioligand stacks on the Milstein Hospital building roof for filter replacements. RSO staff performed wipe tests and surface surveys, reported no radioactive contamination, and the filter change process was completed smoothly.

**Kreitchman PET Center Radiopharmacy – shutdown of operations:** December 12, 2008 was the last day for the production of F-18 FDG and N-13 Ammonia radiopharmaceuticals at the Milstein Cyclotron Radiopharmacy. However, the Radioligand Laboratory in the Milstein basement continues to operate the cyclotron in the Milstein basement and continues to produce C-11 and F-18 radionuclides for research use. This usage is projected to extend into at least the 2nd Quarter of 2009. Radiation Safety support, including discharge monitoring, analysis and reporting, continues for the Milstein Cyclotron and Radioligand Laboratory.

Beginning in the month of December 2008, and continuing through February 2009 Radiation Safety Office staff performed facilities and equipment surveys and clearances for the Milstein Cyclotron Radiopharmacy and assisted with relocation of radiation equipment from the old Milstein facility to the new CUMC Integrated Imaging Center.

**Routine annual inspection by NYS DEC:** The New York State Department of Environmental Conservation, Radiation Section, informed the Radiation Safety Office that they would conduct an audit and inspection of activities under NYS DEC Radiation Control Permit No. 2-6201-00056/00006 starting on January 8, 2009. This Permit authorizes current activities of the Kreitchman PET Center at the Milstein Hospital Building.

**CUMC Integrated Imaging Center site visit:** On January 8, 2008 representatives of the New York State Department of Environmental Conservation visited the site of the CUMC Integrated Imaging Center (NYSTAR Project) under construction at 722 West 168$^{th}$ Street, New York, NY 10032. CUMC representatives and consultants gave a presentation with regard to the design and construction of facilities, the installation of the two new cyclotrons and the installation of a PET imaging center. On February 8, 2008 the Radiation Safety Office received a letter from the NYSDEC dated January 29, 2008 reporting their impression of the site visit. The letter states*: "The major aspects of exhaust system design and emission control, as currently postulated, disclosed no foreseeable difficulties in regard to CUMC's ability to meet the requirements of 6 NYCRR Part 380 regulations. We understand the CUMC is nearing its decision regarding the selection of an effluent monitoring system."*

The letter from the NYS DEC dated January 29, 2008 also contained recommendations that CUMC ensure: timely submission of a new radiation control permit application; deployment of pre-operational environmental dosimetry; deployment of a meteorological station; and adequate professional staffing in the Radiation Safety Office.

**Correspondence regarding DEC recommendations:** The Radiation Safety Officer submitted a letter of response to the NYS DEC dated March 7, 2008 which addressed the recommendation made in a NYS DEC letter dated December 19, 2008 and the four recommendations (noted in the previous item) made in the NYS DEC letter dated January 29, 2008. On March 17, 2008 the Radiation Safety Office received an e-mail communication from Markus Spivak, Radiation Control Specialist, NYS DEC stating: *"Your responses to the recommendations, proposed actions, and the schedules for their completion are adequate. The implementation and effectiveness of these actions will be evaluated during the next inspection of your facility."*

**CUMC Integrated Imaging Center – draft Permit application:** On April 22, 2008 a draft application for a New York State Department of Environmental Conservation Radiation Control Permit for the CUMC Integrated Imaging Center was sent for technical review by the NYS DEC Radiation Control Section. During a telephone conversation

on June 16, 2008 with the NYS DEC Radiation Control Section, Markus Spivak, Environmental Specialist, indicated that the technical review was being completed and the application would be sent to the NYS DEC Region 2, Division of Environmental Permits for issuance.

**CUMC Integrated Imaging Center – pre-permitting inspection:** The second pre-permitting inspection of the CUMC Integrated Imaging Center (NYSTAR Project) under construction at 722 West 168th Street, New York, NY 10032 occurred on July 24, 2008. On August 15, 2008 the Radiation Safety Office received a letter from the New York State Department of Environmental Conservation, Radiation Section, dated August 11, 2008 stating: *"Within the scope of our inspection, we noted no incompatibilities or problems between our current understanding of the Part 380 permit application and implementation of construction and emission monitoring plans."*

The inspection report went on to recommend: *"Adequate Radiation Safety Office staff will be assigned to support the CUMC Integrated Imaging Center Discharge Minimization program and a further commitment to ensure appropriate training in cyclotron, radiopharmacy and radiochemistry operations to the individuals assigned responsibilities in these areas."*

NYS DEC requested submission by Sept. 22, 2008 of a list of required training and an implementation schedule.

**CUMC Integrated Imaging Center – final Permit application:** Following the July 24, 2008 pre-permitting inspection by the NYS DEC Radiation Control Permit Section, on July 28, 2008 the Radiation Safety Office submitted a Final Draft of the Application for the NYS DEC Radiation Control Permit for the CUMC Integrated Imaging Center to the NYS DEC Division of Environmental Permits, Region 2.

**Reply to NYS DEC letter of August 11, 2008:** In a letter dated September 18, 2008, Salmen Loksen, Director, Radiation Safety Office answered the specific questions raised by the NYS DEC in their August 11, 2008 letter. With regard to the issue of adequate staffing, Mr. Loksen's reply identified recent promotions and new hires within the Radiation Safety Office that enhanced the Department's ability to provide the expanded radiation safety support required by the new CUMC Integrated Imaging Center. With regard to the issue of appropriate training, Mr. Loksen's reply identified both completed training attended by Radiation Safety Office staff and training scheduled to take place in the immediate future. This training includes: PET/CT physics and applications; Eclipse Cyclotron systems; operation of and data analysis with the ROTEM MediSmarts stack monitoring system; and Siemens Eclipse Cyclotron operations.

**CUMC Integrated Imaging Center – receipt of new NYS DEC Radiation Control Permit No. 2-6201-00056/00008:** On November 13, 2008 the Radiation Safety Office received the new NYS DEC Radiation Control Permit. The Permit number is No. 2-6201-00056/00008, and authorizes the following annual atmospheric discharges from the Columbia Integrated Imaging Center cyclotron, radiopharmacy, radioisotope laboratories and PET imaging suites: C-11 – 24 Curies; N-13 – 4 Curies; O-15 – 8 Curies; and F-18 – 8 Curies.

A letter accompanying the new Permit also contained notification of a change of the previously existing Permit number, from No. 2-6201-00005/00006 to No. 2-6201-00056/00006.

**Stack monitoring issues:** New York State Department of Environmental Conservation Part 380 Regulations and relevant Radiation Control Permit Conditions require continuous monitoring of atmospheric discharges of radionuclides by a data logging stack monitoring system. At the Milstein Cyclotron Radiopharmacy and Radioligand Lab this was performed by a Bicron stack monitoring system. As the Bicron system is no longer supported by the manufacturer's successor corporation, the NYSTAR Construction Group decided to install a MediSmarts stack monitoring system manufactured by Rotem at the new facility.

On November 11, 2008 Dan Conaster, Rotem Sales Engineer, provided training in the operation of the Rotem MediSmarts stack monitoring system to Radiation Safety Office and CUMC Integrated Imaging Center professional and technical staff.

On December 15, 2008 the installation of the MediSmarts stack monitoring system at the CUMC Integrated Imaging Center was complete.

CUMC Integrated Imaging Center management is responsible for ensuring that cyclotron and chemistry staff utilizes the stack monitoring system as required by the conditions of the Radiation Control Permit and the instructions of the Radiation Safety Office.

The Radiation Safety Office provides professional expertise to assist with quantitative analysis of discharges, and reporting discharges to the NYS DEC, and calibration of the stack monitoring system.

### ***Radioactive Material Administration: Receipt, Distribution and Radioactive Waste Disposal***

A major program of the Radiation Safety Office is the centralized administration of all authorized radioactive materials used at CUMC/NYPH/NYSPI. The use of radioisotopes by individual investigators is authorized by the Joint Radiation Safety Committee and controlled by the Radiation Safety Office. Human Use of radioactive materials is carried out by Authorized User Physicians. Authorized User status is granted following a review of credentials and a majority vote by a quorum of the Joint Radiation Safety Committee. Non-Human Use of radioactive materials by Responsible Investigators is granted after a review of applications and written permission of the Chairman of the Joint Radiation Safety Committee and the Radiation Safety Officer. In 2008 four new Responsible Investigators were reviewed and approved for non-human use of radioactive materials, and 30 current Responsible Investigators received renewals and amendments of their authorizations.

Activities in 2008 to administer, receive, distribute, and dispose of radioactive materials included:

**Monitoring incoming radioactive shipments:** In ac-

cordance with RCNY Article 175 and 10CFR Part 20.205 of the Nuclear Regulatory Commission regulations pertaining to the receiving of radioactive shipments, during 2008 the Radiation Safety Office reviewed and approved 834 purchase orders and monitored 1190 incoming shipment packages within three hours of receipt (in addition to direct radiopharmaceutical shipments to the Departments of Nuclear Medicine and Nuclear Cardiology). Monitoring included an external survey of the package and wipes to detect loose surface contamination. All packages were found to be within acceptable limits. The Radiation Safety Office maintains inventory control of all radioactive materials received and distributed through the use of a computerized database. The orders resulted in the purchase of a total of approximately 1131 milliCuries of activity. $^{35}S$, $^{3}H$, and $^{32}P$ and $^{125}I$ were the isotopes purchased with the highest activities.

**Radioactive waste shipment:** On February 20, 2008 the RSO shipped a total of 97 drums of Dry Active Waste (two 55-gallon metal drums, fifty 30-gallon metal drums and forty-one 30 gallon plastic drums) for disposal by Envirocare of Utah via GTS Duratek Super-Compaction. The same day, the Radiation Safety Office shipped a total of 4 fiber drums of solid animal carcasses for incineration at Envirocare of Utah. The total volume of animal carcasses shipped was 16.07 cubic feet, weighing 160 pounds and containing 74.1 mCi of tritium (H-3). The total volume of the dry shipment was 269.2 cubic feet, weighting 3,812 pounds. The total activity shipped was 205.50 mCi, of which 201.7 mCi was H-3, 3.86 mCi was carbon-14. The waste originated from several locations, including the New York State Psychiatric Institute Building #5 and the P&S Building.

On June 17, 2008 the RSO shipped twenty-seven 30-gallon drums of liquid scintillation vials (LSV) for disposal by NSSI Source & Services of Texas via Radiac Research Corp. The total volume of the LSV shipment was 108.27 cubic feet, weighting 2,700 pounds. The total activity shipped was 0.671 mCi, of which 0.595 mCi was H-3, and 0.076 mCi was other isotopes.

On October 24, 2008 the Radiation Safety Office shipped eleven drums of LSV radioactive waste through our vendor Radiac Research Corp. The shipment totaled 1,050 pounds, 44.11 cubic ft. in volume. Total activity was 0.52 mCi, with 0.512 mCi of H-3, and 0.008 mCi of C-14.

**Sewer discharge statistics:** On January 30, 2008 the Radiation Safety Office performed a controlled release of aqueous material to the sewer. Approximately 33 mCi (0.04 mCi of P-32, 10.3 mCi of H-3, 0.225 mCi of I-125, 24.7 mCi of S-35) was released to the sewer from the radioactive material storage room in the P&S building. For the entire first quarter of 2008 the controlled releases through sewer systems amounted to approximately 1,280 liters of low-level aqueous radioactive waste, containing 62.081 mCi of H-3, 3.804 mCi of C-14, 1.196 mCi of P-32, 28.616 mCi of S-35, and 1.284 mCi of I-125.

In August 2008 a controlled release of approximately 450 liters of low level aqueous radioactive waste was disposed of to the sewer. Approximately 36.8 mCi (21.9 mCi of H-3, 4.9 mCi of S-35) was released to the sewer from the Irving Cancer Research Center building.

In October 2008 the RSO performed a controlled release of 1,260 liters of low level aqueous radioactive waste through the sewer. Approximately 117.2 mCi (97.6 mCi of H-3, 5.2 mCi of S-35, 2.5 mCi of P-32, 2.5 mCi of I-125, 9.2 mCi of C-14, 0.2 mCi of Na-22) was released from the Hammer Health Sciences Center, Physicians & Surgeons, NYS Psychiatric Institute and Russ Berrie buildings.

**Sewer discharges – NYS DEC review:** As required by 6 NYCRR Part 380 and the conditions of NYS DEC Radiation Control Permit No. 2-6201-00056/00006, the Radiation Safety Office reviewed records of controlled sewer disposal of aqueous radionuclides throughout CUMC/NYPH/NYSPI. All quarterly sewer discharges in 2008 were well below the concentration limits of 6 NYCRR Part 380-11.7 Table II.

**LLRW annual report:** On February 29, 2008 the Radiation Safety Office filed an annual report with the New York State Energy Research and Development Authority for 2007 Low-Level Radioactive Waste.

**Short-lived radioactive liquid mixed wastes:** Short-lived radioactive liquid mixed wastes are held in storage in the laboratories for decay. When the radioactivity has decayed to background levels, the wastes are transferred to the Environmental Health and Safety Office for disposal as non-radioactive hazardous waste.

**Patient waste collection:** During 2008 the Radiation Safety Office collected 262 black bags. Black bags are collected from incontinent patients who have undergone nuclear medicine procedures.

**Research lab waste container collection:** During 2008 the Radiation Safety Office waste section picked up 675 full waste containers from research labs and distributed about an equal number of empty waste containers.

**EPA mock audit:** The Radiation Safety Office participated in an EPA Mock Audit arranged by the CUMC Environmental Health and Safety Office on October 27, 2008. The EPA Mock Audit was conducted by a consulting firm, and focused on waste storage areas and research labs. Radiation Safety Office and EH&S staff accompanied the auditors on a walk-through of waste storage rooms and research labs.

***Personnel Dosimetry, Bioassay and Area Monitoring***

In accordance with regulatory requirements, the Radiation Safety Office maintains an ALARA Program to ensure that the radiation doses resulting from operations at CUMC/NYPH/NYSPI are within the regulatory limits and "as low as reasonably achievable" (ALARA). The principal methods of monitoring radiation dose include the assignment of personnel radiation dosimeters to individuals, the use of area and environmental dosimeters, and the control of all discharges of radioactive materials.

Immediate action is taken, as appropriate, in response to unusual or high dosimeter readings. Quarterly ALARA reports are prepared and submitted to the Joint Radiation Safety Committee. These reports present the following: a) the doses of individual workers that exceeded ALARA I limits; b) summaries of investigations of doses to individual workers that exceeded ALARA II limits; and c) discussions

of trends within departments that have a history of high individual doses. The Quarterly Environmental ALARA report presents the quantities of radionuclides discharged to the atmosphere and the sewer system and the resulting dose to the general public.

In 2008 all annual radiation doses received by individual workers were below the regulatory limits specified in RCNY Article 175, Radiation Control. All radiation doses to the general public resulting from atmospheric discharges of radionuclides were below the USNRC constraint limit of 10 mrem per year.

Activities performed in 2008 to maintain the ALARA Program included:

**Personnel radiation dosimetry:** The Radiation Safety Office distributed approximately 10,000 personnel radiation dosimeters each quarter, including both monthly and quarterly badges. A total of approximately 40,000 dosimeters were distributed and collected in 2008. To maintain dosimetry records, the Radiation Safety Office uses dedicated computers with internet and direct modem access to the database of the dosimeter supplier, Landauer Inc.

The Radiation Safety Office received Annual Occupational Exposure Reports (NRC Form 5) from Landauer Inc. for the year 2007 and reviewed and forwarded these reports to all Supervisors and PI's of CUMC, NYSPI and NYPH, to be distributed to the corresponding workers, as required by the New York City Department of Health regulations.

Based on the badge reports by Landauer Inc., in 2008 the Radiation Safety Office reported 94 ALARA Level I notifications and 51 ALARA Level II notifications. Each Level II reading is investigated by RSO staff. Particular attention is paid to occupational groups that typically exceed the ALARA limits, i.e., the Cyclotron Facility, Angiography, the Cardiac Cath Lab, and the PET Imaging Suite.

**Bioassay testing:** In 2008 the Radiation Safety Office performed a total of 87 bioassays on radiation workers who either supported radiopharmaceutical therapy or in the laboratory used 10 mCi or more of volatile radioactivity, consisting of mostly I-131, but also some I-125 and P-32 radioisotopes. An additional 21 bioassays were performed on lab workers using 1 to 10 mCi of I-125. All bioassays were within regulatory limits and no action was necessary.

**Counseling pregnant workers:** The Radiation Safety Office provided all workers who declared pregnancy with health physics counseling concerning the risk factors of exposure to radioactivity. Additional monitoring of the fetus during the gestation period was provided, and personnel radiation exposure reports were closely followed. Work environments were evaluated and modified if necessary.

**Dosimetry program – contract renewal:** In 2008 the Radiation Safety Office renewed its contract with Landauer Inc. for personnel and environmental dosimetry services. Another major vendor for dosimetry services is Global Dosimetry. On June 5, 2008 Global Dosimetry presented the details of their services at a meeting in the Radiation Safety Office. A meeting with the Landauer Inc. representative for contract renewal negotiations was held on July 15, 2008. The representative discussed advantages of Landauer's service, including a number of technological upgrades now available.

The Radiation Safety Office received a written two year service contract from Landauer, dated from October 1, 2008, with significant cost reduction over previous contracts. Included in the contract are a new MicroStar reader, dots and badges, which are able to be read immediately in-house, as well as many programming and support upgrades.

***Routine Radiation Safety Compliance – Internal Inspections, Audits and Surveys***

A major activity of the Radiation Safety Office is the performance of facility inspections and audits of records at clinical departments and research labs to ensure compliance with regulatory requirements as well as with the guidelines and policies of the Joint Radiation Safety Committee.

Routine internal compliance activities in 2008 included:

**Quarterly inventories of sealed sources:** The Radiation Safety Office conducted quarterly inventories of sealed sources located in the following departments: Nuclear Cardiology, Nuclear Medicine-Milstein, Nuclear Medicine-Allen Pavilion, PET Imaging Suite, Cyclotron Radiopharmacy, Radioligand Laboratory and Kreitchman PET Center.

**Biannual leak testing:** Biannual leak testing was performed for all radioactive sources located in the following facilities: Milstein Hospital Nuclear Medicine, Milstein Hospital Nuclear Cardiology, Kreitchman PET Suite, Radioligand and Cyclotron facilities, Allen Pavilion Nuclear Cardiology, Allen Pavilion Nuclear Medicine, and CUMC laboratories. Leak Test Certificates were generated and issued. All sealed sources were found to be in compliance with RCNY Article 175 regulations.

**Quarterly inspections and audits of clinical facilities:** The Radiation Safety Office conducted quarterly inspections and audits of CUMC and NYPH clinical facilities using radioactive materials. The audits and inspections are to ensure compliance with City of New York Radioactive Materials License conditions and with RCNY Article 175, Radiation Control. The facilities audited include: Milstein Hospital Nuclear Cardiology, Milstein Hospital Nuclear Medicine, Allen Pavilion Nuclear Cardiology, Allen Pavilion Nuclear Medicine, PET Imaging Suite, Cyclotron Radiopharmacy, and Radioligand Laboratory.

**Unannounced laboratory inspections:** The Radiation Safety Office conducts unannounced laboratory inspections for the purpose of reinforcing CUMC policies prohibiting food from labs, and requiring rooms containing radioisotopes be locked when unattended. Radiation Safety Office personnel conduct periodic walkthroughs of research areas including Irving Cancer Research Center, Russ Berrie Building, College of Physicians & Surgeons, Black Building, Hammer Health Sciences Center, Kolb Building, and the New York State Psychiatric Institute. Observed violations were documented by digital photography. Labs found in violation were contacted by the Radiation Safety Office and corrective actions were required. The RSO followed up to ensure that deficiencies were corrected. Compliance with these regulations was emphasized in the monthly training

and refresher courses the RSO gave to radiation users.

**Routine statistics:** In 2008, 630 routine radiation safety inspections and audits were performed in Columbia University Medical Center and New York State Psychiatric Institute research labs, and results communicated to the Responsible Investigators. A total of 217 labs were cited for minor deficiencies and were reinspected to ensure compliance.

In 2008, the Radiation Safety Office performed a total of 149 equipment clearance and laboratory exit/entry surveys.

In 2008, the Radiation Safety Office measured airflow rates in 86 fume hoods in areas where volatile radioactive materials are used. In all rooms where radioactive gases or aerosols are used, ventilation rates were measured, and spill gas clearance times were calculated and posted. Adjustments were made as required to air supply and exhaust systems to obtain negative pressure conditions. Researchers whose hoods did not meet safe flow rate standards were instructed to have their hoods repaired or replaced. Follow-up audits confirmed that corrective actions were taken.

In 2008, the Radiation Safety Office performed 215 live animal and carcass surveys, in order to identify potential contamination in animal facilities and cages, protect animal care staff, and ensure proper disposal of animal carcasses containing radioactivity.

In 2008, calibration and maintenance services were provided for 153 radiation survey instruments used throughout CUMC/NYPH/NYSPI. The Radiation Safety Office maintains a supply of portable survey instruments available for loan to Responsible Investigators. These portable survey instruments are also available for emergency response.

***Radiation Safety Training***

Pursuant to Article 175 of the New York City Health Code, the Radiation Safety Office provides initial radiation safety training to all new employees of CUMC/NYPH/NYSPI prior to beginning work with radiation equipment or radioactive materials. The Radiation Safety Office then provides annual refresher training as well. The Radiation Safety Office also provides training in the general area of Emergency Response Preparedness. In 2008 the following radiation safety courses and training sessions were presented:

- Monthly initial training for individual researchers.
- Monthly annual refresher training for researchers.
- Monthly training for the Nursing Staff of NYPH.
- Monthly training sessions for the new animal irradiator located in Irving Cancer Research Center.
- Annual refresher training for Nuclear Cardiology, Nuclear Medicine, PET Suite, Cyclotron, and Radiation Oncology.
- Training for all clinical departments, such as Radiology, Anesthesiology, Cardiology, Endoscopy, Nuclear Medicine, Oncology, Pathology, PET Suite and Urology.
- Training for Dental School residents and assistants.
- Training for various Research departments.
- Training for the Facilities departments.
- Training for Public Safety and Security departments
- Greater New York community, including science teachers and high school students.

Employees who are unable to immediately attend the regularly scheduled classes, are administered a self-study program, conducted by the Radiation Safety Office. A passing grade on a subsequently administered online quiz (www.rascal.columbia.edu) qualifies an employee working in Non-Human Use applications to be issued a radiation monitoring badge. If the individual's employment involves human use of radioactive material, a passing grade on the quiz results in obtaining a temporary badge until the next regularly scheduled new employee training session. Individuals who complete their training online must provide a copy of their training certificate to the Radiation Safety Office prior to being issued a personal radiation dosimeter.

**Annual badge coordinator meetings:** The Radiation Safety Office held two Annual Badge Coordinator Meetings on March 6, 2008 and on April 3, 2008 for the review of badge procedures, exposure history, pregnant employee policies and other issues. These meetings were attended by Principle Investigators, Supervisors, Badge Coordinators and Lab Representatives in order to coordinate the Dosimetry Badge Program in an effective manner. The presentation included an explanation of how badges are distributed to each department; how badge coordinators should document changes and inform the Radiation Safety Office when such changes occur; how ALARA reports should be signed and returned to the RSO; the importance of the prompt return of badges and how to decrease the number of unreturned badges for each department. RSO Dosimetry Program forms, and contact information were distributed, and questions were entertained from the participants.

The Badge Coordinator meetings help set clear expectations, explain Radiation Safety rules, and result in significant improvements to the Personnel Radiation Dosimetry Program. The 2008 meetings had a high attendance rate. Seventy five people attended the March 6, 2008 meeting and 85 people attended the April 3, 2008 meeting.

Since the meetings the percentage of timely badge return has improved dramatically. Badge Coordinators have become more aware of the requirements of the Personnel Radiation Dosimetry Program. There is greater cooperation with the Radiation Safety Office. In 2009, the Radiation Safety Office will continue to improve communication with Departmental Badge Coordinators.

***Professional Medical Health Physics Support Services***

The Radiation Safety Office provides professional medical health physics consultation and support to clinical departments and research laboratories.

Examples of professional medical health physics support provided by the Radiation Safety Office in 2008 included:

**Joint Commission inspection:** The Joint Commission (formerly JCAHO) campus-wide unannounced inspection of New York Presbyterian Hospital, started August 18, 2008 and was finished August 22, 2008. One focus of the inspection was Harkness Pavilion, 10th floor, Dr. Henry Ginsberg's lab. The auditor met with Radiation Safety Office staff and

inquired with regard to procedures for disposing of radioactive waste. The Radiation Safety Office responded to all of the auditor's questions. Andria Castellanos, Vice President, Operations, New York Presbyterian Hospital, commended the Radiation Safety Office staff for their contributions to the successful Joint Commission inspection.

**CAMPEP evaluation of the Columbia University medical physics program:** The Commission on Accreditation of Medical Physics Educational Programs, Inc. (CAMPEP) is a non-profit organization that reviews and accredits education programs in medical physics. CAMPEP is sponsored by the American Association of Physicists in Medicine, American College of Medical Physics, American College of Radiology and the Canadian College of Physicists in Medicine. The American Board of Radiology implemented a requirement that candidates for board certification in medical physics must complete a CAMPEP accredited clinical training program as of 2012.

On July 15, 2008, as part of CAMPEP's evaluation of the Columbia University Medical Physics Program for accreditation, CAMPEP reviewers paid a site-visit to the Radiation Safety Office on the CUMC campus. A significant portion of the Radiation Safety staff is composed of graduate medical physics students who gain much of their clinical experience in medical health physics under the supervision and tutelage of the Department's ABR Board Certified professionals. Other medical physics graduate students elect to take practicums in the Radiation Safety Office.

The Radiation Safety Office was informed by Edward A. Christman, CHP, Ph.D., Consultant in Health Physics & Occupational Health & Safety, that the CAMPEP reviewers had decided to recommend the Columbia University Medical Physics Program for accreditation for a period of three years starting from January 2009, and thanked everyone for the hard work that made this possible.

**Construction of CUMC Integrated Imaging Center – professional support:** The Radiation Safety Office provided continuous professional medical physics and health physics consulting services to the ongoing Columbia University Medical Center Integrated Imaging Center (NYSTAR Construction Project). The Radiation Safety Office provided professional support in the areas of: cyclotron vault design; PET and PET/CT facility radiation shielding; technical purchasing assistance for a radioactive exhaust stack monitoring system; preparation and submission of necessary New York City and New York State radioactive materials licenses and permits.

The Radiation Safety Office reviewed proposed modifications to radiation shielding drawings and specifications presented by Radiation Shielding Systems, Inc. These modifications principally involve shielding of the pneumatic tube system, the diverter and radioactive gas distribution lines. The Radiation Safety Office inspected and documented all shielding as it was installed.

Original radiation shielding recommendations for the cyclotron vault included the shielding of ducts and penetrations in the vault walls to minimize the transmission of neutron and X-ray radiation to adjacent and overlying areas. On August 13, 2008 the Radiation Safety Office provided a scope of work, including a draft shielding design to J.A. Jennings for the duct and penetration shielding, and as of September 8, 2008 the Radiation Safety Office reviewed and signed off on revised drawings. On September 15, 2008 the installed shielding was inspected and found satisfactory.

The Radiation Safety Office provided regulatory guidance and recommendations regarding specifications for connecting individual hot cells, hoods and isolators to the radioactive exhaust system. The Radiation Safety Office inspected and documented all the radioactive exhaust system components, including the exhaust stack, during installation.

The Radiation Safety Office provided recommendations with regard to the installation of the ROTEM MEDISmarts Stack Monitoring System, the location of ROTEM radiation detectors in the radioactive exhaust system and of the ROTEM stack monitoring computer displays within the CUMC Integrated Imaging Center.

Members of the Radiation Safety Office professional and technical staff attended on-site manufacturer's training for operation of and data analysis with the ROTEM MediSmarts stack monitoring system, and operation of the Siemens Eclipse HP Cyclotron.

At the request of the NYSTAR Construction Group the Radiation Safety Office, in collaboration with Peter Esser, Ph.D., performed radiation shielding analysis for the PET


PET production cyclotrons installed in the new CUMC Integrated Imaging Center.

Remote manipulators for handling radiopharmaceuticals in the new CUMC Integrated Imaging Center.

Imaging facility.

Based on the shielding recommendations made in the May 14, 2007 shielding report, the calculated public radiation dose for uncontrolled areas adjacent to and above the PET Imaging facility meet the regulatory requirements of RCNY 175.03(d)(1), not to exceed 100 mrem in a year. The average calculated increase above background calculated for ten locations on the second floor was: 36 mrem/yr, with a high of 86 mrem/yr and a low of 0.3 mrem/yr. The methodology of calculation used is conservative and it is likely that the measured radiation dose will be less than the calculated radiation dose. A radiation dose of thirty-six (36) mrem is comparable to the effective dose equivalent received from one (1) chest X-ray.

On January 8, 2008 the New York State Department of Environmental Conservation in the course of a site-visit to the CUMC Integrated Imaging Center, under construction in the Alan Rosenfield Building, 722 W. 168th Street, made verbal recommendations to institute pre-operational background environmental radiation monitoring at that facility. The recommendation of the NYS DEC was repeated in writing in a letter dated, January 29, 2008.

On January 17, 2008, in response to the NYS DEC recommendation, Radiation Safety Office staff installed twenty-one (21) environmental radiation monitors at suitable sites within, on and adjacent to the Mailman School of Public Health Building, including three dosimeters in the second floor Biostatistics area.

**CUMC Integrated Imaging Center – communication and education:** A number of occupants of the Allan Rosenfield Building expressed their concern with the potential for increased background radiation from the operations of the CUMC Integrated Imaging Center under construction on the basement and 1st Floor of that building. On February 21, 2008 the Radiation Safety Officer was forwarded an e-mail received by David Brenner, Chair, JRSC from Joseph Graziano, Ph.D., Assoc. Dean, Environmental Health Science, regarding the concerns raised by Bruce Levin, Ph.D., Chairman, Biostatistcs. On August 13, 2008 the Radiation Safety Office was requested by Kelly Roska, Administrator, Division of Biostatistics to at some point schedule a meeting on this issue. On September 15, 2008 W. Ian Lipkin, M.D., Director, Center for Infection and Immunity, expressed his concerns regarding atmospheric discharges from the new facility to members of the Radiation Safety Office staff.

The Radiation Safety Officer responded with an e-mail reply to Dr. Brenner stating that the calculated public radiation dose for uncontrolled areas adjacent to and above the PET Imaging facility meet the regulatory requirements of RCNY 175.03(d)(1), not to exceed 100 mrem in a year. The average calculated increase above background calculated for ten locations on the second floor was 36 mrem/yr, with a high of 86 mrem/yr and a low of 0.3 mrem/yr. Conservative methodology was used for the calculation and it is likely that the measured radiation dose will be less than that.

Radiation Safety Office professional staff have reviewed the shielding calculations and have not identified any errors. Further verification of radiation exposure in the vicinity of the CUMC Integrated Imaging Center will be performed by a formal radiation safety survey and continuous area monitoring of radiation levels.

On September 22, 2008 Salmen Loksen, Director, Radiation Safety Office, met with W. Ian Lipkin, M.D., to discuss the potential atmospheric discharges from the Center. On November 20, 2008 the Radiation Safety Office conducted an informational meeting for management and staff of CUMC and NYSPI departments located on the First Floor of the Allan Rosenfield Building above the CUMC Integrated Imaging Center regarding radiation shielding design and installation and Radiation Safety Office oversight and surveys for regulatory compliance by the Center. The presentation was followed by questions and discussion. At least one additional informational meeting, that will address questions raised at the November 20, 2008 meeting, will be scheduled in 2009. Completion of the radiation safety surveys and report should provide quantitative confirmation of the facility radiation shielding design.

New York City Department of Health & Mental Hygiene regulations require that all shielding installation in radiation facilities be subject to a radiation safety survey to determine compliance with the requirements of RCNY 175.03(d)(1) that radiation dose to an individual member of the public does not exceed 100 mrem in a year and RCNY 175.03(c)(1) states that the occupational dose to any individual adult does not exceed 5 rem in one year.

**CUMC Integrated Imaging Center – radiation safety surveys:** From November 3, 2008, as radiation equipment was been installed, Radiation Safety Office staff have been performing radiation safety surveys in all areas adjacent to and overlying the cyclotron vault and PET imaging center. Source terms include: X-ray and neutron radiation from the operation of the two cyclotrons; 511 KeV annihilation photons from PET radiopharmaceutical preparation, administration and scanning; and scattered CT X-rays from PET/CT imaging. These surveys include measurement of natural background radiation and the installation of Luxel© monitors at fixed locations to provide isodose mapping information. Preliminary measurements tend to indicate that annual radiation exposure in both public and controlled areas can be expected to be well within regulatory limits. Upon completion of the radiation safety survey a report of the survey will be submitted to the NYC DOHMH and made available to CUMC employees.

**CUMC Integrated Imaging Center – establishment of a radiation safety program:** The Radiation Safety Office is presently establishing and implementing a Radiation Safety Program for CUMC Integrated Imaging Center. The Radiation Safety Office will organize quarterly audits and inspections of the Cyclotron Radiopharmacy, the GMP Lab, the Radioisotope Lab and the PET Imaging Suites. The Radiation Safety Office will report on compliance to the facility management, the PET Subcommittee and the JRSC. In addition, the Radiation Safety Office will perform ALARA investigation and analysis of personnel radiation dosimeters worn by cyclotronradiopharmacy, GMP, radioisotope lab and PET imaging staff. The RSO will provide ALARA

reports to the facility management, the PET Subcommittee and the JRSC. The Radiation Safety Office will also perform quarterly source inventories and leak testing.

On November 13, 2008 the Radiation Safety Office conducted a "NYS DEC Communications Meeting" with the management of the CUMC Integrated Imaging Center. Attendance included Dileep Kumar, Manager, Mike Sanfillipo, Radiopharmacy Manager, and Chitra Saxena, PET Manager. Discussion included: receipt of the NYC DOHMH Radioactive Materials License and NYS DEC Radiation Control Permit; License and Permit Conditions; radiation safety surveys; radiation exhaust system measurements; quantitative measurement and reporting of atmospheric discharges of radionuclides; appropriate and adequate radiation survey instruments; required signage.

**Milstein cyclotron decommissioning timeline for reassignment of space:** The Radioligand Laboratory and the Cyclotron rooms located in the Milstein Hospital building are to be decommissioned after the new cyclotrons are commissioned in the Allen Rosenfield Building Basement.

December 12, 2008 was the last day for the production of clinical F-18 FDG and N-13 Ammonia radiopharmaceuticals at the Milstein Cyclotron Radiopharmacy, which is being replaced by the new Integrated Imaging Center. The Radioligand Laboratory in the Milstein basement continues in operation and the cyclotron in the Milstein basement will continue to produce C-11 and F-18 radionuclides for research use. This period is projected to extend into the first two quarters of 2009. Radiation safety support, including discharge monitoring, analysis and reporting, will continue.

Radiation Safety Office staff assisted Kreitchman PET Center personnel with the clearance of equipment and facilities at the Milstein Radiopharmacy. The Radioligand Laboratory and the Cyclotron located on the basement level of the Milstein Hospital Building will be removed from service and decommissioned after the new dual cyclotron facility, radiopharmacy, GMP radiopharmaceutical laboratory and radioisotope research laboratory are placed into service on the basement level of the Allan Rosenfield Building. The movement of equipment other than the cyclotron itself out of Milstein Basement now appears to be projected for the 1st and 2nd Quarters 2009. However, the progress of construction of the CUMC Integrated Imaging Center remains subject to changing variables and unpredictable factors which may cause delay in the project completion time and delays in the decommissioning of the existing facility.

**ICRC Mark I irradiator repair:** A JL Shepherd & Associates representative, Brad Olson, serviced the Institute of Comparative Medicine animal irradiator, MK I-30 S/N 1172, on February 6, 2008. The irradiator is now functioning properly. The representative adjusted the door latch, correcting the problem (difficulty opening the door) which led to the call to JL Shepherd. In addition, annual preventative maintenance and a leak test were performed. Documentation of the work was given to Veronica Ifill, Supervisor, ICRC, the Institute of Comparative Medicine, and Radiation Safety Office. Experiments using the irradiator are resuming.

**ICRC Mark I irradiator security upgrade:** In connection with the Increased Control requirements, the US Department of Energy is undertaking a program for upgrading security, in the form of field retrofits, for Mark I Irradiators. CUMC's Mark I irradiator in the ICRC building requires sanding, grinding, welding, and touch up painting to meet these security upgrades. Radiation Safety Office staff discussed the issue with Mr. Leejerris Jamel, ICRC Asst. Plant Superintendent, and it appears upgrades can be performed on the irradiator in its present location. The Radiation Safety Office corresponded with DOE and JL Shepherd & Associates to comply with the upgrades.

**Professional support for Department of Radiation Oncology – draft shielding design for expansion:** On November 8, 2008 Radiation Safety Office staff provided, at the request of David Wicklow, New York Presbyterian Hospital, and Cheng-Shie Wuu, Ph.D., a report reviewing proposed radiation shielding for the Radiation Oncology Expansion under the Garden at West 168th Street. The proposed construction is to be underneath the area bounded by: New York Presbyterian Hospital, CHONY North and South and the Service Building.

The proposed radiation shielding was presented in drawings from the architect Perkins Eastman dated August 29, 2008 and October 29, 2008. Due to space constraints for this new clinical facility, in addition to standard concrete, the proposed shielding design utilized approximately 450,000 pounds of lead to meet regulatory requirements for public and occupational radiation dose.

The Radiation Safety Office recommended that rather than using standard concrete and lead shielding; baryte or ilmenite concretes which typically have a density of 4.0 g $cm^{-3}$ to 4.4 g $cm^{-3}$ (275 lb $feet^{-3}$) be used in the construction of this facility. Although such heavy concrete is more costly than standard concrete, its use would eliminate the requirement for lead and likely reduce the total cost of the project. In addition, the use of heavy concrete would result in an addition of approximately 130 square feet of floor space to the Linac vaults and generally lower public and occupational radiation doses.

At the Radiation Oncology Expansion Construction Meeting on November 19, 2008 the Department of Radiation Oncology indicated that due to cost of heavy concrete they would continue with the original shielding design.

The Radiation Safety Office continues to support this project. Current issues include shielding design for doors and vault penetrations, and X-ray and neutron radiation safety surveys.

**Professional support for Columbia Manhattanville expansion – review of draft architectural drawings:** November 20, 2008 the Radiation Safety Office received an e-mail from Fanny Gong and Robert Read of AVP Design Management, Manhattanville Development. The e-mail stated that Columbia EH&S informed them that it is likely that the CUMC Radiation Safety Office will be responsible for management of radioactive materials at Manhattanville. The e-mail requested Radiation Safety Office review of Manhattanville Schematic Design Documents in appropriate

areas and the Radiation Safety Office initially received a set of drawings for the proposed Mind, Brain and Behavior Building. On December 12, 2008, after review of these drawings, the Radiation Safety Office replied with a series of questions regarding the planned use of radioactive materials and medical diagnostic equipment in the building. In a telephone conversation on December 16, 2008 Fanny Gong informed the Radiation Safety Office that they would be receiving additional documentation for the MB&B project and be requested to attend Manhattanville construction meetings.

**Human Use protocol application review:** Radiation Safety Office Board Certified and NYS Licensed medical physics professional staff review CUMC and NYSPI IRB Research Protocols involving administration of radioactive materials or application of X-rays to human subjects for accuracy and completeness of human radiation dosimetry.

In 2008 the Radiation Safety Office received 92 JRSC and 6 RDRC Applications for Use of Radioactive Agents in Research Involving Human Subjects and for Use of X-ray Equipment in Research Involving Human Subjects. In addition to reviewing research protocols for accuracy and completeness of human radiation dosimetry, subject consent statements for appropriateness and accuracy with regard to radiation risk, and reporting to the JRSC/RDRC, Radiation Safety Office professional staff are consulted by researchers with regard to references and materials providing information on dosimetry, including: medical internal radiation dosimetry for radiopharmaceuticals; entrance skin exposures, organ doses, equivalent doses or CTDIs for typical diagnostic studies; and guidance on the correct uses of committed dose, effective dose and organ weighting factors.

The Radiation Safety Office reviews are forwarded to the Chairman, JRSC/RDRC. The reviews are performed by NYS Licensed and Board Certified professional staff. Full reviews of the Applications for Use of Radioactive Agents in Research Involving Human Subjects and for Use of X-ray Equipment in Research Involving Human Subjects are subsequently performed by Salmen Loksen, Director, Radiation Safety Office, as a member of the Executive Committee of the JRSC. Mr. Loksen's approval or disapproval of the protocol is reported to the Executive Committee.

**JRSC/RDRC RASCAL system access developments:** Radiation Safety Office staff met a number of times with Halayn Hescock, Project Manager, Columbia University Information Technology, and Maggie Berryman, RASCAL consultant, to implement incorporating JRSC and RDRC research protocols review into the RASCAL system. The "look and feel" will be similar to the IRB review process. It was agreed to work in phases toward accomplishing this goal. David J. Brenner, Ph.D., JRSC Chair, has been personally involved in this project.

Phase 1 of the development, already accomplished, grants viewing access to JRSC/RDRC committee and administration members. JRSC/RDRC access is granted if the PI user selects "Radioisotopes" and/or "X-Ray, Fluoroscope." The Radiation Safety Office has provided feedback and suggestions with regard to the system structure and formatting, and is performing testing of the prototype system. The Radiation Safety Office has also already provided most of the texts for the help fields to assist PIs complete the JRSC/RDRC forms.

The JRSC and Radiation Safety Office provided a list of JRSC approved RIs/Authorized Users to compare to the RIs/Authorized Users entered on the Applications. It was agreed that it would be desirable that certain uniform fields, such as the project title and personnel, remain constant to facilitate exporting information from the IRB forms to the JRSC forms. There was also discussion of what needs to be done differently for NYSPI protocol integration into the RASCAL system, since the NYSPI has an independent IRB. In the past quarter several scheduled meetings with the RASCAL programmers were postponed. The Radiation Safety Office is looking forward to completing this project.

**Patient treatment support:** In 2008 the Radiation Safety Office conducted surveys of 63 inpatients and outpatients treated with $^{131}$I by the Nuclear Medicine Department and 12 surveys of patients treated with $^{137}$Cs, $^{192}$Ir or $^{103}$Pd implants by the Radiation Oncology department.

In 2008 the Radiation Safety Office interviewed 31 outpatients who were being considered for treatment with Iodine-131 for cancer of the thyroid by the Department of Nuclear Medicine. Records of interviews are on file in the Radiation Safety Office.

**NYS DOH CRESO certification:** New York State Department of Health requires individuals who perform inspections of radiation equipment in dental, veterinary and podiatric installations in most New York counties to be approved by the State as Certified Radiation Equipment Safety Officers (CRESO). Radiation Safety Office physicists James Donlan and Bruce Emmer applied for and received NYS CRESO Certifications. Other RSO professional staff are in the process of applying for CRESO certifications.

**Consulting medical physicists:** In accordance with the policy discussed and approved at JRSC meetings, the Radiation Safety Office in cooperation with CUMC/NYPH medical physicists has identified additional consulting physicists who may be available to assist researchers with the preparation of applications to the JRSC. In line with the JRSC approved policy, when researchers contact the Radiation Safety Office for dosimetry support, the JRSC/RSO refers them to the appropriate in-house medical physics group. The JRSC/RSO informs the researcher that there may be a fee involved for this service. If in-house consultants are unable to provide support the JRSC/RSO will refer the researcher to outside consulting medical physicists approved in accordance with JRSC policy.

***Radiation Safety and Technical Support Services***

The Radiation Safety Office investigates spills, misadministrations, and other incidents involving radioactive materials and sources of radiation. The Radiation Safety Office ensures that, when required, timely notice of reportable incidents is made to the New York City Department of Health, Office of Radiological Health. The Radiation Safety Office responded to a few incidents in 2008 which are on

file in the Radiation Safety Office and may also be found in the Radiation Safety Office's quarterly reports to the JRSC.

The Radiation Safety Office provides continuing radiation safety support for the Columbia University Cyclotron Facility and the Columbia University Radioligand Laboratory for production and synthesis of PET imaging radiopharmaceuticals. This support includes maintenance of licenses and permits, basic radiation safety services, personnel dosimetry, area radiation monitoring and quantitative measurement and ALARA analysis of radioisotope releases to the atmosphere, review of Authorized User credentials, and review of system modifications.

Specific examples of such technical support provided by the Radiation Safety Office in 2008 include:

**Audits for food in labs:** The Radiation Safety Office maintains a rigorous, ongoing inspection program, including photo documentation, in which every lab licensed to use radioactive material is randomly inspected at least every two months for compliance with food/drink regulations and for locking rooms containing radioisotopes when unattended. A summary of the compliance results is forwarded to the JRSC and/or IHSC as necessary. This ensures that CUMC's past record of NYC DOHMH inspections of research laboratories without any reported violations continues in the future.

Radiation Safety Office staff walk through all research areas including Irving Cancer Research Center, Russ Berrie Building, College of Physicians & Surgeons, Black Building, Hammer Health Sciences Center, Kolbe Building, and the New York State Psychiatric Institute. Any lab found in violation is contacted by the Radiation Safety Office to implement corrective actions. The Radiation Safety Office revisits the deficient laboratories to ensure that the problems that were identified are corrected. The concern for compliance with regulations pertaining to food in the labs and keeping labs locked when not in use is emphasized in the monthly training and refresher courses that the RSO gives to radiation users.

**Face velocity measurements:** During the year 2008 the Radiation Safety Office performed face velocity measurements on approximately 86 fume hoods in which radioisotopes were used or stored. Researchers whose hoods did not meet flow rate standards were instructed to have their hoods repaired. The Radiation Safety Office ensures that repairs are performed in a timely manner. Ventilation was measured in all rooms using radioactive gases or aerosols, and spill gas clearance times were calculated and posted.

**Inventory and leak testing:** During the year 2008 the RSO performed the required quarterly inventory and leak testing for all radioactive sealed sources located in the following facilities: Milstein Nuclear Medicine; Allen Pavilion Nuclear Medicine; Cyclotron; Radioligand Laboratory; PET Imaging Suite; Division of Functional Brain Mapping; and Columbia University Health Sciences (VC-11, Irradiators, ICRC Animal Irradiators, etc.). Leak test Certificates were generated and issued for each of the above sealed sources. All sealed sources were found to be in compliance with Article 175 regulations.

***Professional Radiation Safety and Medical Physics Support for Non-Radiology X-ray Activities***

**Dental QA program:** The dental quality assurance program is designed to optimize the radiological safety and clinical quality of dental radiography. This program is based on recommendations for quality assurance promulgated by a number of professional organizations, including the National Council on Radiation Protection & Measurements (NCRP), the Bureau of Radiological Health of the Food & Drug Administration, the American College of Radiology (ACR), and the American Academy of Dental Radiology Quality Assurance Committee. In this program, the Radiation Safety Office has primary responsibility for preliminary radiation safety shielding evaluation, acceptance testing, diagnostic quality assurance, and radiation safety surveys on all dental x-ray units installed at the following locations:

- Ambulatory Care Networked Corporation (ACNC): 4 intraoral units and 1 panoramic/cephalographic unit.
- Babies Hospital OR: 1 portable intraoral unit.
- Columbia Eastside: 5 intraoral units and 1 panoramic/cephalographic unit.
- Columbia North: 5 intraoral units and 1 panoramic unit.
- Dental Facility in the Bard Haven Towers: 8 intraoral units and 1 panoramic/cephalographic unit.
- Dentcare Clinic at Intermediate School 143: 1 intraoral unit.
- Harlem Children's Health Initiative Dental Facility: 1 intraoral unit.
- Irving Institute for Clinical & Translational Research: 1 intraoral units and 1 panoramic unit.
- Mannie L. Wilson Health Care Center: 5 intraoral units and 1 panoramic unit.
- Mobile Dental Facility: 2 intraoral units.
- Morningside Dental Associates (2 locations): 9 intraoral units and 1 panoramic/cephalographic unit.
- Odyssey House Dental Clinic: 3 intraoral units.
- Pediatric Dentistry: 6 intraoral unit and 1 panoramic/cephalographic unit.
- Project Renewal Dental: 2 intraoral units and 1 panoramic unit.
- Vanderbilt Clinic Teaching and Research Areas: 2 panoramic unit, 1 panoramic/cephalographic unit, 23 intraoral units, and 1 intraoral–cephalographic unit.

**Dental facility installation at I.S. 164:** On November 21, 2008 Radiation Safety Office staff visited the dental facility installation located at Intermediate School 164 to perform an integrity survey of the shielding. Using a low energy and low activity gamma source it was determined that the lead shielding was installed correctly, with no loss of integrity throughout the installation, and that it is adequately shielded for dental work. Follow up visits are planned for 2009.

**X-ray permits audit program:** In agreement with the New York Presbyterian Hospital, the Joint Radiation Safety Committee has assigned the Radiation Safety Office responsibility for Radiation Safety and Medical Physics support for those clinical facilities outside the Department of Radiology that use x-ray equipment. The Radiation Safety Office and

the Department of Radiology Medical Physics staff jointly run the audit program for these facilities. This program is conducted in accordance with the conditions of the CUMC/NYPH/NYSPI New York City X-ray Permits, as specified in Article 175 of the New York City Health Code. In this audit program, the Radiation Safety Office is primarily responsible for ensuring that each site follows the proper QA procedures, safety practices and keeps proper records, while the Department of Radiology Medical Physics is responsible for performing all technical tests. The following locations are audited under this program:

- Cardiac Care, Milstein 5th Floor: 1 C-arm unit
- Cystoscopy Suite, Milstein 4th Floor: 3 radiographic/fluoroscopic units
- Endoscopy Department, Atchley 13th Floor: 3 C-arm fluoroscopy units
- Harkness Pavilion 9th Floor: 4 bone densitometery units, 1 Xtreme CT.
- Pain Management, Presbyterian Hospital 5th Floor: 1 C-arm unit
- Spine Center, Neurological Institute, 5th Fl: 1 C-arm unit
- Sports Medicine, Dodge Fitness Center/Bakers Field: 1 mini C-arm unit
- Urology Department, Atchley Pavilion 11th Floor: 1 fluoroscopy unit

**NYC DOHMH biannual X-ray inspection:** On January 15, 2008 the New York City Department of Health and Mental Hygiene began its biannual inspection of CUMC/NYPH/ NYSPI X-Ray Permit No. H96 0076353 86. The inspection was concluded on January 29, 2008 with an exit interview in Dr. Alderson's Office. On March 17, 2008 the Radiation Safety Office received the written report of the NYC DOHMH inspector dated February 14, 2008. The report stated that: "*Radiological equipment inspection performed on 1/29/2008 disclosed No violations of Article 175 of NYC Health Code*." No recommendations were made.

The quality assurance program is based on recommendations for quality assurance that have been promulgated by a number of professional organizations, including the National Council on Radiation Protection and Measurements (NCRP), the Bureau of Radiological Health of the FDA, the American College of Radiology (ACR), and the American Academy of Dental Radiology Quality Assurance Committee. The Radiation Safety Office performed all required Quality Assurance testing in a timely manner.

## ***Radiation Safety Office Personnel, Meetings, Communications, and Professional Training***

**Administrative assignment change:** In July 2008 the Radiation Safety Office was administratively reassigned by Columbia University from the Health Sciences Division to the Medical School Administration. Accordingly the Columbia University department number for the Radiation Safety Office has been changed from 500-60 to 501-60. In addition, at the end of 2008 the administrative assignment of the Radiation Safety Office was passed from Dr. Robert Lewy, Sr. Associate Dean for Health Sciences, to Dr. Robert S. Kass, Vice Dean for Research.

**Personnel changes:** On December 20, 2007, Salmen Loksen, Director, Radiation Safety Office and Dae-In Kim, Health Physicist agreed to continue an arrangement where Dae-In Kim would be employed three mornings each week as a cyclotron operator and on Thursday and Friday he would work full days at his position, as a Health Physicist in the Radiation Safety Office. This arrangement continued throughout 2008. In addition, Dae-In Kim continued to operate the cyclotron in support of large primate research.

In June 2008 the Radiation Safety Office hired James Donlan for an Assistant Physicist position. Also in June 2008 Charles Geraghty, Assistant Physicist, and Jaclyn Marcel, Technician B, left to assume positions in other institutions. To fill these positions Pantea Kadkhodazadeh, a Technician B in the Radiation Safety Office, was hired for an Assistant Physicist position, and Shira Abraham, previously a part-time student casual in the Radiation Safety Office, was hired for the position vacated by Pantea Kadkhodazadeh.

At the beginning of July 2008 Tom Cummings, B.S., Radiation Safety Office Technician B, was promoted to Assistant Health Physicist. Mr. Cummings' primary responsibilities now include quantitative analysis of discharges to the environment from the current and future cyclotron facilities and the performance of routine audits of the cyclotron, radiochemistry and PET facilities for compliance with radiation safety requirements.

In September 2008 the Radiation Safety Office hired Ms. Bithi Roy, B.A., and Mr. Igor Kravchuk, M.S., as another Technician B's.

Ms. Abraham, Ms. Roy, Mr. Cummings and Mr. Kravchuk are graduate students in Columbia University's Medical Physics program. They assist with radiation safety surveys and air flow measurements in the new cyclotron, radiopharmacy and PET imaging facility.

At the end of 2008 Ahmad Hatami ended his tenure as Assistant Radiation Safety Officer.

**Emergency response meetings:** The Radiation Safety Office staff attends regularly scheduled meetings with the departments of Environmental Health & Safety, Public Safety and Security, and Emergency Room staff to discuss and train for emergency response to potential emergencies.

**IACUC animal care protocol review committee:** The Radiation Safety Office participates as a member of the IACUC Animal Care Protocol Review Committee by reviewing all procedures that utilize radionuclides in animal research and reviewing other animal protocols.

**NYPH safety committee meetings:** The Radiation Safety Office participates in monthly Safety Committee meetings of New York Presbyterian Hospital/Columbia and New York State Psychiatric Institute. In addition, the Radiation Safety Office participates in frequent Emergency Preparedness Sub-Committee meetings for NYPH and NYSPI.

**NYPH-NYPrepares executive emergency preparedness coordinating council meetings:** The Radiation Safety Office participates in monthly meetings of the NYPrepares Executive Emergency Preparedness Coordinating Council of

New York-Presbyterian. This is a combined committee of NYP/Columbia, NYP/Weill Cornell Medical Center, NYP/Allen and NYP/CHONY. In addition, the Radiation Safety Office participates in frequent Emergency Preparedness Sub-Committee meetings.

**NYPH emergency preparedness disaster drill:** Radiation Safety Office staff participated in a NYPH Emergency Preparedness Disaster Drill on December 9, 2008. This was a non-radiation involved drill, but radioactivity needed to be ruled out. A dozen or so 'victims' were brought through to 'Area B' of the ED before being checked for hazmat or radioactivity. The RSO staff checked them in this area, gave the all clear of radioactive contamination. These drills are helpful in identifying areas of concern and lead to quicker and more efficient response in cases of actual emergency.

**RCRA training:** On July 16, 2008 four RSO staff members attended RCRA training presented by Environmental Resource Center.

**Integrated Imaging Center meetings:** The Radiation Safety Office has been participating in weekly construction meetings regarding the CUMC Integrated Imaging Center.

**RSO staff professional training:** Radiation Safety Office staff completed and/or scheduled to attend the following training with regard to cyclotron, radiopharmacy and radiochemistry operations:

From June 25, 2008 through June 27, 2008, Thomas Juchnewicz, Assistant Radiation Safety Officer attended an AAPM sponsored program: The Physics and Applications of PET/CT Imaging, at the Baylor College of Medicine, Houston, Texas. This program included: PET production cyclotron physics and chemistry; radioligand chemistry and research methodology; and PET facility shielding and discharge minimization.

Salmen Loksen, Director, Radiation Safety Office, attended the AAPM Conference from July 28, 2008 through August 1, 2008.

From August 25, 2008 through September 5, 2008, Dae-In Kim, Health Physicist attended a manufacturer's course, Introduction to Eclipse Systems at the Siemens factory in Knoxville, Tennessee. Topics included: safety/radiation hazard avoidance; system overview and component identification; automatic operation; control system fundamentals; support systems; vacuum system components; ion source theory; RF system theory; targetry system theory; cyclotron engineers tasks, responsibilities support services; manual single and dual beam operation.

On November 18, 2008 Radiation Safety Office staff attended training in Rotem MediSmarts stack monitoring system operation.

On December 12 and December 15, 2008 Radiation Safety Office staff attended training in Siemens Explora F-18 FDG Chemistry box operation.

On December 15 through December 17, 2008 Radiation Safety Office staff attended training in Siemens Eclipse cyclotron operations.

**Internal technical staff training:** The Radiation Safety Office program of monthly internal technical staff training sessions continued throughout 2008, for officers and technicians to discuss current radiation safety issues. Topics have included: review of RSO policy for distributing radioactive "Yellow-II" labeled packages; to quickly respond to researchers' concerns about evaluation of radiation exposures and testing for contamination; how to prepare for a broad scope license inspection and interact with researchers and inspectors; an overview of the new online Service Request form for faster and better request processing; review of set-up and clean-up procedures for rooms of patient receiving Iodine-131 treatment, removal of sources dislodged from patient during brachytherapy treatment; the Radiation Safety Office waste disposal log system; review of procedures for Clearance of Labs, operation of emergency equipment and emergency response, remote monitor installations were reviewed, survey equipment selection and use, and the new increased controls regulations. Also, several Radiation Safety training videos have been converted from tapes to DVD and made available on the newly purchased dedicated server for the Radiation Safety Office.

**RSO-EH&S cross-training sessions:** The Radiation Safety Office and the Office of Environmental Health & Safety conduct joint training sessions in order to review fume hood certification, increased controls for radioactive materials in quantities of concern, record keeping requirements and the CUMC mixed waste program.

A joint Radiation Safety Office and Environmental Health & Safety Cross-Training Meeting was held on March 19, 2008 in the Judith Jansen Memorial Conference Room adjacent to the RSO suite. Topics included: New Lab Equipment Clearance Policy, US Department of Homeland Security policies and procedures for chemicals of interest, how CUMC and NYPH are meeting enhanced security requirements, Security Clearance Background Checks, Contingency Plan and DOT Security Plan, and mixed waste (chemical and radioactive combined) policies and procedures.

On November 5, 2008 the Radiation Safety Office and the CUMC Environmental Health and Safety Office held another cross-training session. Topics of discussion included: shipping, radiation safety at Lamont, mixed waste policy and inspections, Public Safety personnel training, disposal of liquid radioactive and chemical waste, and security clearance background checks.

**Morningside campus meetings:** As recommended by Dr. David Brenner, Chairman, JRSC, the CUMC Radiation Safety Office is now attending Radiation Safety Committee meetings at the Morningside Campus, and vise versa. This participation is expected to continue.

**Outlook for 2009:** The Radiation Safety Office is projecting an increased work load in year 2009, and is committed to the goal of providing the best possible radiation safety support services to Columbia University Medical Center, New York Presbyterian Hospital, New York State Psychiatric Institute and the adjacent community.

# Publications


1. Ahuja AK, Barber RC, Hardwick RJ, Weil MM, Genik PC, **Brenner DJ** and Dubrova YE. The effects of Atm haploinsufficiency on mutation rate in the mouse germ line and somatic tissue. *Mutagenesis* **23**:367-70, 2008.
2. **Amundson SA**. Functional genomics in radiation biology: a gateway to cellular systems-level studies. *Radiat Environ Biophys* **47**:25-31, 2008.
3. **Amundson SA**, Do KT, Vinikoor LC, Lee RA, Koch-Paiz CA, Ahn J, Reimers M, Chen Y, Scudiero DA, Weinstein JN*, et al.* Integrating global gene expression and radiation survival parameters across the 60 cell lines of the National Cancer Institute Anticancer Drug Screen. *Cancer Res* **68**:415-24, 2008.
4. Baskar R, **Balajee AS**, **Geard CR** and Hande MP. Isoform-specific activation of protein kinase c in irradiated human fibroblasts and their bystander cells. *Int J Biochem Cell Biol* **40**:125-34, 2008.
5. **Bertucci A**, Pocock RD, **Randers-Pehrson G** and **Brenner DJ**. Microbeam irradiation of the C. elegans nematode. *J Radiat Res (Tokyo)* **50 Suppl A**: A49-54, 2009.
6. **Bigelow A**, **Brenner DJ**, **Garty G** and **Randers-Pehrson G**. Single-particle/single-cell ion microbeams as probes of biological mechanisms. *IEEE Trans Plasma Sci* **36**:1424-31, 2008.
7. **Bigelow AW**, **Geard CR**, **Randers-Pehrson G** and **Brenner DJ**. Microbeam-integrated multiphoton imaging system. *Rev Sci Instrum* **79**:123707, 2008.
8. **Bigelow A**, **Garty G**, Funayama T, **Randers-Pehrson G**, **Brenner DJ** and **Geard CR**. Expanding the question-answering potential of single-cell microbeams at RARAF, USA. *J Radiat Res* **50**: Suppl., A21-8, 2009.
9. **Brenner DJ**. Effective dose: a flawed concept that could and should be replaced. *Br J Radiol* **81**:521-3, 2008.
10. **Brenner DJ**. Should computed tomography be the modality of choice for imaging Crohn's disease in children? The radiation risk perspective. *Gut* **57**:1489-90, 2008.
11. **Brenner DJ**. The linear-quadratic model is an appropriate methodology for determining isoeffective doses at large doses per fraction. *Semin Radiat Oncol* **18**:234-9, 2008.
12. **Brenner DJ** and **Hall EJ**. Secondary neutrons in clinical proton radiotherapy: a charged issue. *Radiother Oncol* **86**:165-70, 2008.
13. **Brenner DJ** and Huda W. Effective dose: a useful concept in diagnostic radiology. *Radiat Prot Dosimetry* **128**:503-8, 2008.
14. **Calaf GM**, Echiburu-Chau C, **Zhao YL** and **Hei TK**. BigH3 protein expression as a marker for breast cancer. *Int J Mol Med* **21**:561-8, 2008.
15. **Calaf GM** and Roy D. Cell adhesion proteins altered by 17beta estradiol and parathion in breast epithelial cells. *Oncol Rep* **19**:165-9, 2008.
16. **Garty G**, Chen Y, Salerno A, **Turner H**, Zhang J, **Lyulko OV**, **Xu Y**, Wang H, Simaan N, **Randers-Pehrson G**, Yao YL, **Amundson SA** and **Brenner DJ**. The RABIT: A Rapid Automated Biodosimetry Tool for radiological triage. *Health Physics* (in press).
17. **Ghandhi SA**, **Yaghoubian B** and **Amundson SA**. Global gene expression analyses of bystander and alpha particle irradiated normal human lung fibroblasts: Synchronous and differential responses. *BMC Med Genomics* **1**:63, 2008.
18. **Hall EJ**. Is There a Place for Quantitative Risk Assesment. *J. Radiol. Prot.* **29** A171-84 , 2009.
19. **Hall EJ**. Protons for radiotherapy: a 1946 proposal. *Lancet Oncol* **10**:196, 2009.
20. **Hall EJ**. Radiation biology for pediatric radiologists. *Pediatr Radiol* **39 Suppl 1**:S57-64, 2009.
21. **Hall EJ** and **Brenner DJ**. Cancer risks from diagnostic radiology. *Br J Radiol* **81**:362-78, 2008.
22. **Hei TK**, Ballas LK, **Brenner DJ** and **Geard CR**. Advances in radiobiological studies using a microbeam. *J Radiat Res (Tokyo)* **50 Suppl A**:A7-A12, 2009.
23. **Hei TK**, **Zhou H**, **Ivanov VN**, **Hong M**, **Lieberman HB**, **Brenner DJ**, **Amundson SA** and **Geard CR**. Mechanism of radiation-induced bystander effects: a unifying model. *J Pharm Pharmacol* **60**:943-50, 2008.
24. Hu Z, Liu Y, Zhang C, Zhao Y, He W, Han L, Yang L, **Hopkins KM**, Yang X, **Lieberman HB** and Hang H.. Targeted deletion of *Rad9* in mouse skin keratinocytes enhances genotoxin-induced tumor development. *Cancer Res* **68**:5552-61, 2008.
25. **Ivanov VN**, **Partridge MA**, Johnson GE, **Huang SX**, **Zhou H** and **Hei TK**. Resveratrol sensitizes melanomas to TRAIL through modulation of antiapoptotic gene expression. *Exp Cell Res* **314**:1163-76, 2008.
26. **Ivanov VN**, **Zhou H**, **Partridge MA** and **Hei TK**. Inhibition of ataxia telangiectasia mutated kinase activity enhances TRAIL-mediated apoptosis in human melanoma cells. *Cancer Res* **69**:3510-9, 2009.
27. Johnson GE, **Ivanov VN** and **Hei TK**. Radiosensitization of melanoma cells through combined inhibition of protein regulators of cell survival. *Apoptosis* **13**:790-802, 2008.
28. Li H, **Balajee AS**, Su T, Cen B, **Hei TK** and Weinstein IB. The HINT1 tumor suppressor regulates both gamma-H2AX and ATM in response to DNA damage. *J Cell Biol* **183**:253-65, 2008.
29. **Lieberman HB**. DNA damage repair and response proteins as targets for cancer therapy. *Curr Med Chem* **15**:360-7, 2008.
30. Liu YX, Wang J, Guo J, Wu J, **Lieberman HB** and **Yin Y**. DUSP1 Is Controlled by p53 during the Cellular Response to Oxidative Stress. *Mol Cancer Res* **6**:624-33, 2008.
31. **Meador JA**, Zhao M, Su Y, Narayan G, **Geard CR** and **Balajee AS**. Histone H2AX is a critical factor for cellular protection against DNA alkylating agents. *Oncogene* **27**:5662-71, 2008.
32. **Partridge MA**, **Huang SX**, Kibriya MG, Ahsan H,

Davidson MM and **Hei TK**. Environmental mutagens induced transversions but not transitions in regulatory region of mitochondrial DNA. *J Toxicol Environ Health A* **72**:301-4, 2009.

33. **Paul S** and **Amundson SA**. Development of gene expression signatures for practical radiation biodosimetry. *Int J Radiat Oncol Biol Phys* **71**:1236-44, 2008.
34. Sakamoto-Hojo ET and **Balajee AS**. Targeting Poly (ADP) Ribose Polymerase I (PARP-1) and PARP-1 Interacting Proteins for Cancer Treatment. *Anticancer Agents Med Chem* **8**:402-16, 2008.
35. Shah JN, Shao G, **Hei TK** and **Zhao Y**. Methylation screening of the TGFBI promoter in human lung and prostate cancer by methylation-specific PCR. *BMC Cancer* **8**:284, 2008.
36. Shao G, **Balajee AS**, **Hei TK** and **Zhao Y**. p16INK4a downregulation is involved in immortalization of primary human prostate epithelial cells induced by telomerase. *Mol Carcinog* **47**:775-83, 2008.
37. Straume T, **Amundson SA**, Blakely WF, Burns FJ, Chen A, Dainiak N, Franklin S, Leary JA, Loftus DJ, *et al*. NASA Radiation Biomarker Workshop, September 27-28, 2007. *Radiat Res* **170**:393-405, 2008.
38. **Wen G**, **Calaf GM**, **Partridge MA**, Echiburú-Chau C, **Zhao Y**, **Huang S**, **Chai Y**, Li B, **Hu B** and **Hei TK**. Neoplastic transformation of human small airway epithelial cells induced by arsenic. *Mol Med* **14**:2-10, 2008.
39. **Wen G**, **Partridge MA**, **Calaf GM**, **Meador JA**, **Hu B**, Echiburu-Chau C, **Hong M** and **Hei TK**. Increased susceptibility of human small airway epithelial cells to apoptosis after long term arsenate treatment. *Sci Total Environ* **407**:1174-81, 2009.
40. Xu A, **Chai Y**, Nohmi T and **Hei TK**. Genotoxic responses to titanium dioxide nanoparticles and fullerene in gpt delta transgenic MEF cells. *Part Fibre Toxicol* **6**:3, 2009.
41. **Yin Y**. Nuclear PTEN at the center of the stage. *Oncogene* (invited review) 2008.
42. **Yin Y** and **Shen WH**. PTEN: a new guardian of the genome. *Oncogene* **27**:5443-53, 2008.
43. Zhang Y, **Wen G**, Shao G, Wang C, Lin C, Fang H, **Balajee AS**, Bhagat G, **Hei TK** and **Zhao Y**. TGFBI deficiency predisposes mice to spontaneous tumor development. *Cancer Res* **69**:37-44, 2009.
44. **Zhou H**, **Hong M**, **Chai Y** and **Hei TK**. Consequences of cytoplasmic irradiation: studies from microbeam. *J Radiat Res (Tokyo)* **50 Suppl A**:A59-65, 2009.
45. **Zhou H**, **Ivanov VN**, Lien YC, Davidson M and **Hei TK**. Mitochondrial function and nuclear factor-kappaB-mediated signaling in radiation-induced bystander effects. *Cancer Res* **68**:2233-40, 2008.
46. **Zhu A**, Zhang CX and **Lieberman HB**. Rad9 has a functional role in human prostate carcinogenesis. *Cancer Res* **68**:1267-74, 2008. ■

The reception at the inauguration of the Dr. Chu Chang's Professorship was held on December 2nd, 2008. (Sitting): Dr. Chu Chang. (L-r): Dr. Eric Chang, Dr. Clifford Chao, Dr. Tom Hei, Dr. David Brenner, Dr. Charles Geard and Mrs. Bee Chang.

Dr. Howard Lieberman (left) and Mr. Gary Johnson (right) are at the reception at the inauguration of the Dr. Chu Chang Professorship.

Center for Radiological Research 2008 Departmental Picnic. (L-r): Ms. Gertrude Maina and Ms. Lilian Oling, Dr. Shanaz Ghandhi and Dr. Antonella Bertucci.

Center for Radiological Research 2008 Departmental Picnic. (L-r): Dr. Alexander Kofman and Dr. Alexandre Mezentsev.

Center for Radiological Research 2008 Departmental Picnic. CRR members are playing soccer.

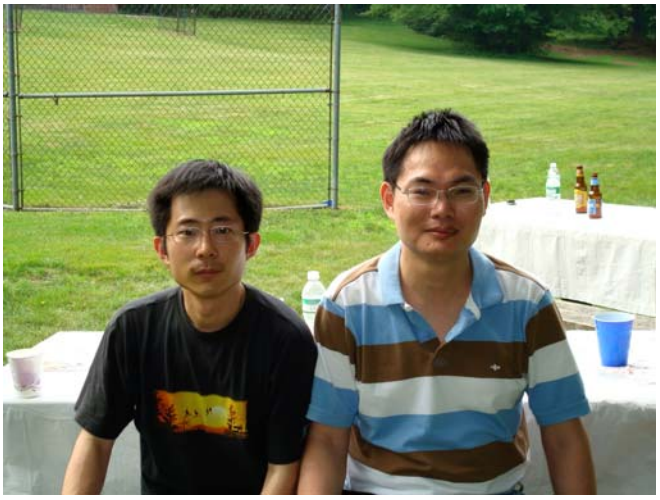

Center for Radiological Research 2008 Departmental Picnic. (L-r): Mr. Yunfei Chai and Dr. Chuanxin Huang.

Center for Radiological Research 2008 Departmental Picnic. (L-r): Dr. Corinne Leloup, Dr. Guy Garty and Mr. Bill Amundson.

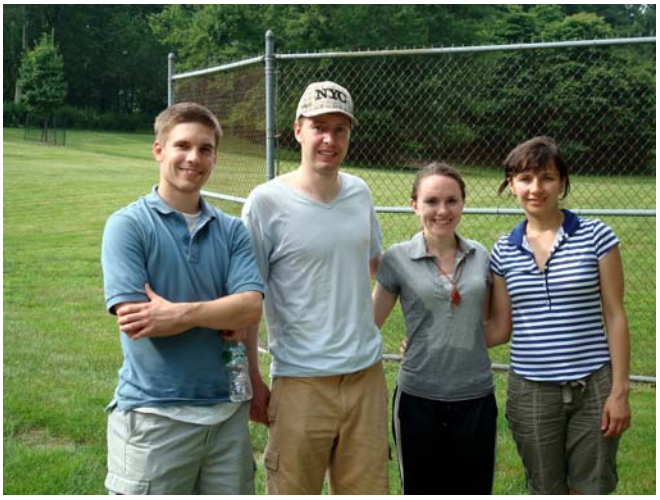

Center for Radiological Research 2008 Departmental Picnic. (L-r): Mr. Andreas Maerki, Dr. Thomas Templin, Ms. Jennifer Maerki and Ms. Oleksandra Lyulko.